

Efficient and High Precision Momentum Bias Attitude Control for Small Satellite

vorgelegt von
M.Kom.
Mohammad Mukhayadi
ORCID: 0000-0003-1089-8654

an der Fakultät V – Verkehrs- und Maschinensysteme
der Technischen Universität Berlin
zur Erlangung des akademischen Grades

Doktor der Ingenieurwissenschaften
– Dr.-Ing. –

genehmigte Dissertation

Promotionsausschuss:

Vorsitzender: Prof. Dr.-Ing. U. von Wagner

Gutachter: Prof. Dr.-Ing. K. Brieß

Gutachter: Prof. Dr.-Ing. U. Renner

Gutachter: Prof. Dr.-Ing. S. Montenegro

Tag der wissenschaftlichen Aussprache: 28. September 2020

Berlin 2021

Acknowledgment

Foremost, I would like to express my sincere gratitude to my supervisors Prof. Dr.-Ing. K. Brieß and Prof. Dr.-Ing. U. Renner for the continuous support of my doctoral studies and research, for their patience, motivation, enthusiasm, and immense knowledge. Their guidance helped me in all the time of research and writing of this thesis. It was a great honor to finish my studies under their supervision. Besides my supervisors, I would like to thank the rest of my doctoral committee: Prof. Dr.-Ing. U. von Wagner and Prof. Dr.-Ing. S. Montenegro, for their encouragement, insightful comments, and hard questions.

My sincere gratitude also goes to the Boards of Indonesian National Institute of Aeronautics and Space (LAPAN), especially Prof. Dr. Thomas Djamaluddin (Chairman), Prof. Dr. Erna Sri Adiningsih (Prime Secretary), Dr. Rika Andiarti (Deputy Chairman for Aerospace Technology Affairs), and Ir. Christianus R. Dewanto, M.Eng (Head of Bureau for Cooperation, Public Relations, and General Affairs), whose administration and policies strongly supported me to complete my doctoral degree by research related to the satellite technology development program at LAPAN.

Immeasurable appreciation and deepest gratitude to the Management of Satellite Technology Center of LAPAN: Ir. Mujtahid, M.T. (Director), Wahyudi Hasbi, M.Sc (Dissemination Coordinator), Abdul Karim, M.T. (Program and Facility Coordinator), Rinto Ferdian, M.M. (Administration Coordinator), Rinto Andri Wiendarto, S.T. (Finance and State Property Sub-Coordinator), and Sujati, M.Si. (Human Resource Administration Sub-Coordinator), that fully contribute to my doctoral studies and research activities with the funding, resources, and use of the services and facilities at the Satellite Technology Center.

I would like to thank my labmates in LAPAN's Satellite Assembly, Integration and Test Facility: Eriko N. Nasser, M. Arif Saifudin, Tri Mediansyah, M. Farid Huzain, A Hadi Syafruddin, Supia, Deddy El Amin, Nayla Najati, Widya Roza, and Rosza Madina, for the stimulating discussions, for the sleepless nights we were working together before satellites launch, and for all the fun we have had in the last ten years. I would also like to acknowledge my colleagues in Satellite Operations: Patria Rahman Hakim, Satria Utama, Rizki Permala, Ade Putri Septi Jayani, Annisa Sarah, and Kamirul for a great collaboration in the experiment and operation of the LAPAN satellites. In particular, I am grateful to Nurati Fidaus and Doni Susanto who have helped me a lot in administrative matters.

Last but not the least, I would like to thank my family: my mother, my sister, my brother, and my beloved wife and children, for never-ending love and support throughout my life.

Abstract

The fast-growing of small satellite technology gives advantages and opportunities for developing country with little or no experience in space technology to enter the field of space technology and its application. The ongoing reduction in mission complexity and the costs associated with management, as well as the possibility of launching it as an auxiliary payload on the launcher, have made the small satellite become interesting for the current and future space mission. Indonesian National Institute of Aeronautics and Space, LAPAN, started the small satellite program by developing LAPAN-A satellite series as a strategic approach. The program was arranged by design to cost approach to produce a cost-effective small satellite for several missions such as Earth observation, communication, scientific mission as well as technology demonstration and academic training. Small satellite development could take full advantage of the ongoing technology developments and advances of micro technology for sensors and instruments that lead to further miniaturization of engineering components for dedicated mission.

To ensure the success of small satellite mission, the design of attitude control system is very critical and indispensable. Within the small satellite philosophy that is characterized by low mass, small dimensions, low energy consumption, high reliability and less complexity, the attitude control system of LAPAN-A satellite series must work in both equatorial and inclined orbit. These LAPAN-A satellite series implement a momentum bias method to obtain efficient and high precision attitude control. It required the development of a highly integrated pair of three fiber optic gyros and three reaction wheels in the body-fixed axes of the spacecraft to control the spacecraft angle and angular velocity while the star sensor and magnetic coils will responsible for determining and controlling the angular momentum vector. The experiment performed that the attitude control system has met several important aspects in achieving high precision pointing to support current and future advanced mission such as surveillance, remote sensing, celestial object imaging, and the LEO constellation of communications by using momentum bias technique. The reliability and efficiency of the LAPAN-A satellite series attitude control system has been demonstrated by the inclusion of appropriate measurement data discussed in this research paper.

Zusammenfassung

Das schnelle Wachstum der Kleinsatellitentechnologie bietet Entwicklungsländern mit wenig oder keiner Erfahrung in der Weltraumtechnologie Vorteile und Möglichkeiten für den Einstieg in das Gebiet der Weltraumtechnologie und ihrer Anwendung. Die fortlaufende Reduzierung der Missionskomplexität und der mit dem Management verbundenen Kosten sowie die Möglichkeit, sie als zusätzliche Nutzlast mit Trägerraketen zu starten, haben die kleinen Satelliten für aktuelle und zukünftige Weltraummission interessant gemacht. Das Indonesische Nationale Institut für Luft- und Raumfahrt, LAPAN, startete das Kleinsatellitenprogramm mit der Entwicklung der LAPAN-A-Satellitenserie als strategischen Ansatz. Das Programm wurde so konzipiert, dass ein kostengünstiger kleiner Satellit für verschiedene Missionen wie Erdbeobachtung, Kommunikation, wissenschaftliche Mission sowie Technologiedemonstration und akademische Ausbildung hergestellt werden kann. Die Entwicklung kleiner Satelliten könnte die laufenden technologischen Entwicklungen und Fortschritte der Mikrotechnologie für Sensoren und Instrumente voll ausnutzen, die zu einer weiteren Miniaturisierung der technischen Komponenten für spezielle Aufgaben führen.

Um den Erfolg einer Kleinsatellitenmission sicherzustellen, ist der Entwurf eines Lageregelungssystems sehr kritisch und unverzichtbar. Innerhalb der Kleinsatellitenphilosophie, die sich durch geringe Masse, kleine Abmessungen, geringen Energieverbrauch, hohe Zuverlässigkeit und geringere Komplexität auszeichnet, muss das Lageregelungssystem der LAPAN-A-Satellitenserie sowohl in der äquatorialen als auch in der geneigten Umlaufbahn arbeiten. Diese LAPAN-A-Satellitenserien implementieren eine Drallstabilisierung, um eine effiziente und hochpräzise Lageregelung zu erhalten. Es erforderte die Entwicklung eines hochintegrierten Paares von drei faseroptische Kreisel und drei Reaktionsrädern in den körperfesten Achsen des Raumfahrzeugs, um den Winkel und die Winkelgeschwindigkeit des Raumfahrzeugs zu steuern, während der Sternsensor und die Magnetspulen für die Bestimmung und Steuerung des Drallvektors verantwortlich sind. Das Experiment ergab, dass das Lageregelungssystem mehrere wichtige Aspekte bei der Erzielung einer hochpräzisen Ausrichtung erfüllt hat, um aktuelle und zukünftige fortgeschrittene Missionen wie Überwachung, Fernerkundung, Bildgebung von Himmelsobjekten und die LEO-Konstellation der Kommunikation mithilfe der Drallstabilisierung zu unterstützen. Die Zuverlässigkeit und Effizienz des Lageregelungssystems der Satellitenserie LAPAN-A wurde durch die Einbeziehung geeigneter Messdaten demonstriert, die in diesem Forschungsbericht erörtert wurden.

Contents

| | | |
|-------|---|-----|
| 1 | Introduction | 1 |
| 1.1 | Small Satellite Advanced Mission | 3 |
| 1.2 | Scope and Objective of the Research | 6 |
| 1.3 | Project of LAPAN-A Satellite Series | 7 |
| 2 | State of the Art | 10 |
| 2.1 | Performance Parameter of Attitude Control System | 15 |
| 2.2 | Momentum Bias Attitude Control in GSO | 20 |
| 2.3 | Momentum Bias Attitude Control in LEO | 27 |
| 3 | Improvement of the State of the Art by LAPAN-A Satellite Series | 40 |
| 3.1 | Momentum Bias Attitude Control of LAPAN-A Satellite Series | 41 |
| 3.2 | Momentum Bias Establishment and Disturbance Torque Compensation | 49 |
| 3.3 | Full Performance and Efficient Attitude Control | 51 |
| 3.4 | High Precision and Accuracy | 54 |
| 3.5 | Higher Reliability | 56 |
| 4 | Attitude Geometry and Dynamics | 58 |
| 4.1 | Coordinate Systems | 58 |
| 4.1.1 | Spacecraft-Centered Coordinates | 59 |
| 4.1.2 | Nonspacecraft-Centered Coordinates | 62 |
| 4.1.3 | RPY (Roll, Pitch, Yaw) Coordinates | 65 |
| 4.2 | Coordinate Transformation | 66 |
| 4.3 | Mapping and Pointing Budget | 69 |
| 4.4 | Mission Planning Software | 71 |
| 4.5 | Attitude Dynamic | 83 |
| 5 | Attitude Control System of LAPAN-A Satellite Series | 87 |
| 5.1 | Momentum Bias Strategy | 87 |
| 5.1.1 | Nadir Pointing Mode | 89 |
| 5.1.2 | Slew and Hibernation Mode | 93 |
| 5.1.3 | Contingency Operations | 95 |
| 5.2 | Advantages and Disadvantages of Momentum Bias | 98 |
| 5.3 | Attitude Hardware | 104 |
| 5.3.1 | Fiber Optic Gyro | 106 |
| 5.3.2 | Solar Cells as Sun Sensor | 107 |
| 5.3.3 | Star Sensor | 110 |
| 5.3.4 | Magnetic Field Sensor | 112 |
| 5.3.5 | Reaction Wheel and Wheel Drive Electronics | 113 |

| | | |
|-------|---|-----|
| 5.3.6 | Air Coil | 116 |
| 5.4 | Acquisition Phase of Momentum Bias..... | 118 |
| 5.4.1 | Disturbance Torque Characterization..... | 118 |
| 5.4.2 | Raising Angular Momentum..... | 122 |
| 5.5 | Momentum Bias in Equatorial Orbit..... | 123 |
| 6 | Flight Result | 127 |
| 6.1 | Nadir Pointing Mode..... | 127 |
| 6.1.1 | Maintaining Angular Momentum..... | 127 |
| 6.1.2 | Nutation Damping | 134 |
| 6.1.3 | Controlling the Direction of Angular Momentum | 139 |
| 6.2 | Slew Mode | 146 |
| 6.2.1 | Pointing Calibration | 147 |
| 6.2.2 | Off-Nadir Pointing | 150 |
| 6.3 | Hibernation Mode | 157 |
| 6.4 | Discussion | 160 |
| 7 | Summary and Outlook | 163 |
| 7.1 | Summary | 163 |
| 7.2 | Outlook..... | 164 |
| | References..... | 167 |
| | Appendix..... | 172 |

List of Figures

| | |
|--|----|
| Figure 1.1: Development Approach of LAPAN-A Satellite Series..... | 8 |
| Figure 1.2: Roadmap of Satellite Technology by LAPAN | 9 |
| Figure 2.1: Classification of Momentum-based Attitude Stabilization | 11 |
| Figure 2.2: Various Momentum-based ACS | 14 |
| Figure 2.3: Typical Spacecraft Momentum Requirements | 20 |
| Figure 2.4: Spin-stabilized Communication Satellites..... | 21 |
| Figure 2.5: Mechanically Despun Antenna on INTELSAT III Spacecraft | 22 |
| Figure 2.6: Spin-stabilized Satellites with A Mechanically Despun Antenna | 22 |
| Figure 2.7: Dual Spinner Satellites | 23 |
| Figure 2.8: The Predecessor of Three-axis Stabilized Communication Satellites | 25 |
| Figure 2.9: Earlier Generation of Three-axis Momentum Bias Stabilized Satellites in GSO . | 27 |
| Figure 2.10: Simplified Schematic of <i>Stabilite</i> and Its Control Elements..... | 29 |
| Figure 2.11: The Schematic of WHECON Attitude Control | 30 |
| Figure 2.12: SEASAT On-Orbit Control Hardware..... | 31 |
| Figure 2.13: Combination of Gravity Gradient and Momentum Bias Stabilization on Small Satellite | 33 |
| Figure 2.14: Reconstitution of Star Data on TUBSAT-A | 35 |
| Figure 2.15: DLR-TUBSAT Satellite | 37 |
| Figure 2.16: System Architecture of DLR-TUBSAT's Attitude Control System | 38 |
| Figure 2.17: MAROC-TUBSAT Satellite and Its Star Sensor | 38 |
| Figure 2.18: KITSAT-3 Operation Mode | 39 |
| Figure 3.1: Precession and Nutation of Spinning Satellite | 40 |
| Figure 3.2: Flight Configuration Design of LAPAN-A2 Equatorial Satellite | 42 |
| Figure 3.3: Layout Design of LAPAN-A2 Attitude Control System | 43 |
| Figure 3.4: Orbital Section of LAPAN-A2 Satellite Where No Attitude Information Available | 43 |
| Figure 3.5: Power Switch Button on The Ground Station Software..... | 44 |
| Figure 3.6: Magnetic Coil Controller and Telemetry on The Ground Station Software..... | 45 |
| Figure 3.7: Wheel - Gyro Telemetry and Real Time Estimation of Total Angular Momentum | 45 |
| Figure 3.8: Star Sensor Telemetry and Real Time Estimation of Attitude Deviation from Target | 46 |
| Figure 3.9: Stability of the Spinning Satellite Related to the Mass Distribution and the Spin Axis | 48 |
| Figure 3.10: Layout Optimization of LAPAN-A3 Satellite | 48 |

| | |
|--|-----|
| Figure 3.11: Precession of the Angular Momentum | 50 |
| Figure 3.12: Nominal Pitch Rotation of LAPAN-A Satellite Series..... | 51 |
| Figure 3.13: A Slew Rotation About Z Axis in Inertial Space | 52 |
| Figure 3.14: Illustration of Moon Parallax | 55 |
| Figure 3.15: Difference of Moon Position Based on Observer Location | 55 |
| Figure 4.1: Spacecraft-Fixed Coordinate System | 60 |
| Figure 4.2: Celestial Coordinates..... | 61 |
| Figure 4.3: Celestial Coordinates..... | 63 |
| Figure 4.4: Local Horizontal Coordinates | 65 |
| Figure 4.5: Roll, Pitch, and Yaw (RPY) Coordinate System | 66 |
| Figure 4.6: Sequence of 3-2-1 Euler Angles | 67 |
| Figure 4.7: Main Payload of LAPAN-A Satellite Series | 70 |
| Figure 4.8: Classical Plot of the Satellite Ground Track | 71 |
| Figure 4.9: Hi-Res Image of Cloudy Abidjan Port, Ivory Coast by SPACECAM of LAPAN-A2 Satellite | 72 |
| Figure 4.10: Ground Station Geometry | 76 |
| Figure 4.11: Flowchart of the Mission Planning Software | 77 |
| Figure 4.12: User Interfaces of the Mission Planning Software..... | 77 |
| Figure 4.13: Orbit and Schedule Menus in the Main Interface..... | 78 |
| Figure 4.14: 2D Earth Map Interface..... | 79 |
| Figure 4.15: Placing KML File Code in A Text File..... | 80 |
| Figure 4.16: Plotting the Ground Track of LAPAN-A2 Satellite in the Google Earth | 81 |
| Figure 4.17: Plotting the Ground Track of LAPAN-A3 Satellite in the Google Earth | 81 |
| Figure 4.18: Measuring Distance of the Target from Satellite Ground Track in the Google Earth | 82 |
| Figure 4.19: Cones Motion of Axisymmetric Body..... | 83 |
| Figure 4.20: Local Earth's Magnetic Field Direction of Polar Orbiting Satellite | 86 |
| Figure 5.1: Satellite's Flight Configuration | 88 |
| Figure 5.2: Angular Momentum Direction | 90 |
| Figure 5.3: Magnetic Torque and Angular Momentum of Polar Orbiting Satellite..... | 91 |
| Figure 5.4: Angular Momentum Monitoring on the LAPAN-A3 Satellite Telemetry | 92 |
| Figure 5.5: Slew Capability of LAPAN-A1 Satellite..... | 93 |
| Figure 5.6: Roll Maneuver for Off-Nadir Pointing Mode | 94 |
| Figure 5.7: Right Ascension Precession of LAPAN-A1 due to Bias Current Setting of Y Coil | 96 |
| Figure 5.8: Declination (DE) Drift of Angular Momentum Viewed from Video Camera..... | 97 |
| Figure 5.9: Attitude Control System Testing on Single Axis Air Bearing Platform | 99 |
| Figure 5.10: Measurement of Magnetic Dipole of Reaction Wheel | 101 |
| Figure 5.11: Cable Routing of Solar Panel | 102 |
| Figure 5.12: The Measurement of the Magnetic Field on the Li-ion Batteries | 103 |
| Figure 5.13: Attitude Control System Assembly of LAPAN-A1 Satellite..... | 104 |

| | |
|--|-----|
| Figure 5.14: Decentralized Attitude Control System..... | 105 |
| Figure 5.15: LITEF μ FORS Fiber Optic Gyroscopes and its Rotation Axis | 106 |
| Figure 5.16: Placement of Solar Cells/ Panels on the LAPAN-A1 Satellite..... | 108 |
| Figure 5.17: Geometry of Sun Illumination on the Solar Cell..... | 108 |
| Figure 5.18: Sun Angle Calculation on the Ground Station Software of LAPAN-A1 Telemetry | 109 |
| Figure 5.19: Flight Configuration and Star Sensor Placement on LAPAN-A Series | 110 |
| Figure 5.20: CMOS Star Tracker | 111 |
| Figure 5.21: Reference Frame Definition of Star Sensor | 111 |
| Figure 5.22: Magnetic Field Sensor (MFS) | 113 |
| Figure 5.23: Block diagram of the Wheel Drive Electronic with Motor | 115 |
| Figure 5.24: Reaction Wheel, Gyro, and WDE | 115 |
| Figure 5.25: Air Coil Assembly on LAPAN-A1 Satellite's Main Structure..... | 116 |
| Figure 5.26: Gyro Reading during Free Tumbling Condition | 119 |
| Figure 5.27: Wheel Speed for External Torque Compensation | 120 |
| Figure 5.28: Free Tumbling Condition with the Maximum Current Setting on Y Coil | 121 |
| Figure 5.29: The Gravity Gradient Torque of a Constant Pitch Orientation..... | 122 |
| Figure 5.30: Increasing of Angular Momentum | 123 |
| Figure 5.31: The Earth's Magnetic Vector with Respect to the Spacecraft Axis of LAPAN-A2 Satellite | 125 |
| Figure 5.32: Magnetic Torque and Angular Momentum of Equatorial Orbiting Satellite..... | 126 |
| Figure 5.33: Zenith Monitoring on the LAPAN-A2 Satellite Telemetry | 126 |
| Figure 6.1: Block Diagram of the Spacecraft Angular Velocity Control | 129 |
| Figure 6.2: Block Diagram of the Spacecraft Angle Control | 130 |
| Figure 6.3: Block diagram of the Wheel Speed Control | 130 |
| Figure 6.4: Motion in Pitch Axis in the Angular Velocity Control and Wheel Speed Control | 131 |
| Figure 6.5: Angular Momentum Increment of LAPAN-A2 Satellite due to Bias Coil Current | 134 |
| Figure 6.6: Various Nutation Damping Applied on LAPAN-A Satellite Series | 135 |
| Figure 6.7: Nutation Damping by Reaction Wheel in Angular Velocity Mode | 135 |
| Figure 6.8: Nutation Damping by Reaction Wheel in Angle Mode..... | 136 |
| Figure 6.9: Nutation Damping by Magnetic Coil | 137 |
| Figure 6.10: Nutation Growth in the Single Wheel Operation Mode..... | 138 |
| Figure 6.11: Attitude Movement of LAPAN-A3 Satellite Observed by Star Sensor..... | 139 |
| Figure 6.12: Attitude Movement in the Single Pitch Wheel Operation | 141 |
| Figure 6.13: Right Ascension Drift of Angular Momentum due to Bias Current on Y-Coil . | 142 |
| Figure 6.14: Earth's Magnetic Field Dipole Model and Quarter Orbit Region Definition .. | 143 |
| Figure 6.15: Declination Precession in A Quarter Orbit due to Deviation of Y-Coil Bias Current | 143 |
| Figure 6.16: Declination Precession due to Deviation of Y-Coil Bias Current | 144 |

| | |
|---|-----|
| Figure 6.17: Imaging Mission over Indonesian Territory Using Momentum Bias Attitude Control | 145 |
| Figure 6.18: Attitude Movement of Nadir Pointing Satellite in the Equatorial Orbit..... | 145 |
| Figure 6.19: The Moon and Mars Imaging by LAPAN-A1 Satellite..... | 147 |
| Figure 6.20: Angular Relationship between Star Sensor, Spacecraft, and Moon | 147 |
| Figure 6.21: 1st Acquisition Result of Moon Image | 149 |
| Figure 6.22: Ground Track of Mombasa Imaging Mission | 151 |
| Figure 6.23: Momentum Distribution in the Off-Nadir Pointing | 152 |
| Figure 6.24: Declination (<i>DE</i>) Coordinate of LAPAN-A2 Satellite's Recorded Telemetry .. | 152 |
| Figure 6.25: Images of Mombasa Port and Ships Resulted by Off-Nadir Pointing | 154 |
| Figure 6.26: Angle Control Maneuver for Off-Nadir Pointing Mode | 155 |
| Figure 6.27: Lombok Earthquake on July 29th, 2018 | 156 |
| Figure 6.28: Satellite Ground Track in the Imaging of Lombok Island..... | 156 |
| Figure 6.29: Off-Nadir Imaging of Mount Rinjani | 157 |
| Figure 6.30: Circles of Cones Motion in the Single Spinner Mode..... | 158 |
| Figure 6.31: Oscillation around Pitch Axis in the Constant Wheel Speed Mode | 160 |
| Figure 6.32: Measurement of Magnetic Field on the Li-Ion Batteries | 162 |
| Figure 7.1: Constellation of 9 Small Satellites in Equatorial Low Earth Orbit | 165 |
| Figure 7.2: Concept of LEO Communication Satellites in Constellation..... | 166 |

List of Tables

| | |
|--|-----|
| Table 2.1: Typical Spacecraft Control Modes and Requirements | 15 |
| Table 2.2: Effects of Pointing Accuracy Requirements on Sensor Selection and ACS Design | 16 |
| Table 2.3: Comparison of Attitude Control Actuators | 17 |
| Table 2.4: Slewing Requirements and Control Actuator Selection | 18 |
| Table 2.5: Attitude and Orbit Determination Sensors Onboard UoSAT-12 | 34 |
| Table 2.6: Attitude and Orbit Control Actuators Onboard UoSAT-12 | 34 |
| Table 2.7: Overview of the TUBSAT Program..... | 36 |
| Table 3.1: Power Consumption of LAPAN-A1 Satellite | 53 |
| Table 4.1: Common Coordinate Systems Used in Space Application | 59 |
| Table 4.2: Azimuth and Elevation Coordinates in Several Spherical Coordinate System..... | 61 |
| Table 4.3: Mapping and Pointing Budget of LAPAN-A Satellite Series | 70 |
| Table 4.4: The Orbital Elements in the NORAD -TLE | 72 |
| Table 5.1: Right Ascension (RA) Drift of Angular Momentum Viewed from Video Camera. | 96 |
| Table 5.2: Inertia Tensor of LAPAN-A Satellite Series | 100 |
| Table 5.3: Technical Specification of Fiber Optic Gyroscopes..... | 107 |
| Table 5.4: Technical Specification of Magnetic Field Sensor..... | 113 |
| Table 5.5: Technical Specification of Reaction Wheel | 114 |
| Table 5.6: The Technical Specification of Air Coil..... | 117 |
| Table 5.7: Gravity Gradient Torque and Solar Pressure Torque | 119 |
| Table 6.1: Wheel Speed Fluctuation Due to Disturbance Torque | 132 |
| Table 6.2: Conserving Angular Momentum of LAPAN-A3 Satellite | 132 |
| Table 6.3: Conserving Angular Momentum of LAPAN-A2 Satellite | 133 |
| Table 6.4: Amplitude and Period of Nutation Measured by Star Sensor | 140 |
| Table 6.5: Amplitude and Period of Precession Measured by Star Sensor | 140 |
| Table 6.6: Imaging Requirements of LAPAN-A3's Multispectral Pushbroom Imager for 5% Overlap..... | 140 |
| Table 6.7: Controlling Right Ascension of Angular Momentum | 142 |
| Table 6.8: Attitude Correction on LAPAN-A2 Satellite | 146 |
| Table 6.9: Lunar Ephemeris and the 1st Acquisition Setup | 148 |
| Table 6.10: Lunar Ephemeris and the 2nd Acquisition Setup | 149 |
| Table 6.11: Result of the 2nd Acquisition of Moon Image | 150 |
| Table 6.12: Interpolation of Attitude Information for Off-Nadir Maneuver..... | 153 |
| Table 6.13: Measurement of Body Cone and Nutation Angles in the Single Spinner Mode | 158 |

| | |
|--|-----|
| Table 6.14: Principal Moments of Inertia and Its Direction Cosines Matrices..... | 159 |
| Table 6.15: Magnetic Field Magnitude of Li-ion Batteries | 162 |

List of Abbreviations and Symbols

Abbreviations

| | |
|-------|--|
| ACS | Attitude Control System |
| AIS | Automatic Identification System |
| ADS-B | Automatic Dependent Surveillance-Broadcast |
| AWS | Automatic Weather System |
| CCD | Charge Coupled Device |
| COTS | Commercial off-the-shelf |
| CMG | Control Moment Gyro |
| CMOS | Complementary Metal Oxide Semiconductor |
| DAC | Digital-to-Analog Converter |
| DLR | German Aerospace Center |
| ESA | European Space Agency |
| FOV | Field of View |
| GEO | Geosynchronous Equatorial Orbit |
| GG | Gravity Gradient |
| GMST | Greenwich Mean Sidereal Time |
| GS | Ground Station |
| HD | High Definition, a substantially higher resolution of image |
| IoT | Internet of Things |
| JAXA | Japan Aerospace Exploration Agency |
| KML | Keyhole Markup Language, a file format used to display geographic data and visualization within internet-based |
| LAPAN | Indonesian Institute of Aeronautics and Space |
| LEO | Low Earth Orbit, an altitude between 200 and 2000 km |
| LEOP | Launch and Early Orbit Phase |
| M2M | Machine to Machine |
| MFS | Magnetic Field Sensor |
| NASA | National Aeronautics and Space Administration |
| NORAD | North American Aerospace Defense Command |
| OBDH | On-Board Data Handling |
| PCDH | Power Control and Data Handling, an integration between Power Control Unit and On-Board Data Handling |
| PID | Proportional–Integral–Derivative, a control loop mechanism employing feedback |
| RCS | Reaction Control System, a system that uses thrusters to provide attitude control |
| RTU | Remote Terminal Unit |
| SAR | Synthetic Aperture Radar |
| TEWS | Tsunami Early Warning System |

| | |
|----------|--|
| TLE | Two Line Elements, the satellite orbit properties which is noted in a two lines format |
| TTC | Tracking, Telemetry and Command |
| TUBSAT | Technische Universität Berlin Satellit |
| UNISPACE | United Nations Conference on the Exploration and Peaceful Uses of Outer Space |
| UTC | Universal Time Coordinated |
| WDE | Wheel Drive Electronic |

Symbols

| | |
|-----------------|--|
| AZ, DE, RA | Azimuth, declination, right ascension |
| B | Magnetic field strength |
| C_d | Drag coefficient |
| c_m | Center of mass |
| c_{pa} | Center of aerodynamic pressure |
| C_{sp} | Solar pressure constant |
| D | Magnetic dipole moment |
| H | Angular momentum |
| I | Inertia tensor |
| i | Orbital inclination |
| K_D | Derivative gain factor of controller |
| K_I | Integral gain factor of controller |
| K_M | Motor constant |
| K_P | Proportional gain factor of controller |
| L | Slant range |
| M | Orbital mean anomaly |
| M_e | External disturbance torques |
| M_f | Friction moment |
| M_w | Moment of the flywheel |
| n | Mean Motion |
| r | Orbital radius |
| R_E | Radius of the Earth |
| T_{rot} | Rotational kinetic energy |
| α | Spacecraft azimuth angle from horizon |
| β | Angular distance |
| δ | Spacecraft elevation angle from horizon |
| \varnothing_M | Moon's angular diameter |
| Ω | Right ascension of ascending node |
| γ | Body cone angle |
| ε | Eccentricity |
| η | Nadir angle |
| θ | Pitch angle, nutation angle |
| Θ_G | Greenwich hour angle of the Vernal Equinox |
| λ | Elevation coordinate, spacecraft's longitude |

| | |
|-------------|---|
| μ | Earth gravitation constant |
| ρ | Atmospheric density |
| τ_a | Atmospheric drag torque |
| τ_{gg} | Gravity gradient torque |
| τ_m | Magnetic field torque |
| τ_{sp} | Solar pressure torque |
| φ | Spacecraft's latitude |
| ψ | Yaw angle |
| ω | Orbital argument of perigee, angular velocity |
| ϕ | Azimuth coordinate, roll angle |

1 INTRODUCTION

In the early 1990s, small satellites were mainly designed and built by governments, universities, private companies, and research centers for experimental application and technology demonstration. But currently a growing number of large space institution such as ESA, NASA, the French space agency (CNES), Japan Aerospace Exploration Agency (JAXA) and several world big companies are using small satellites not only as technology demonstrators but also for operations. For many years big satellites are the mainstay of the space industry, but smaller spacecraft missions are increasing as a growing number of customers are discovering that small satellites are reliable, affordable and capable of performing many jobs.

There is no universally accepted definition of a “small satellite”. UNISPACE III 1998 gave an upper limit of about 1,000 kilograms, NASA defined that small satellite focus on spacecraft with a mass less than 180 kilograms and about the size of a large kitchen fridge, while more researchers and satellite developers set 500 kg as a maximum weight. Below that limit, satellites over 100 kilograms are frequently called “minisatellites”, between 10 and 100 kilograms “microsatellites”, between 1 and 10 kilograms “nanosatellites” and below 1 kilogram “picosatellites”. The development of small satellites has also given rise to the new term "CubeSat", a class of nanosatellites that use a standard size and form factor. The standard CubeSat size uses a "one unit" or "1U" measuring 10×10×10 cm and is extendable to larger sizes; 1.5, 2, 3, 6, and even 12U.

Small satellites with current and emerging technologies offer valuable missions for all fields of science and applications as well as technology demonstration and academic training. Especially for developing countries, small satellites give them opportunity for accessing space missions, applications and spin-off technologies. Together with reduced size and mass, costs, and development times of the spacecraft and their more manageable proportions, small satellites become attractive ways to develop a national expertise in the space technology utilization and its application to address solutions for the national problems. The small satellite has greatly increased the range of possible space missions, thereby lowering the cost threshold for emerging countries in space technology to access to space [1].

In the early days of space exploration, most space missions were small, primarily because of small launch capability. As the launchers grew, so did the satellites. The advancements of technology have made the space missions return to the small satellite. With current achievement,

small satellites could not only for technology demonstrator, but also allowed completely new applications in environmental monitoring, remote sensing, communications, and even advanced scientific mission into deep space exploration.

The small satellite technology is growing fast because supported by the following trends [2]:

- **Electronics advancements and miniaturization**

Improvements in electronics technology have made many devices become smaller, lighter, more efficient and generally cheaper. Advance in digital electronics is closely related to Moore's law which observed and projected that the number of transistors in integrated circuits would double in every two years. Moore's prediction that described in 1965 has guided the semiconductor industry to set targets of long-term planning for research and development which had an influence on the continuous improved performance of microprocessors, memory capacity, sensors and even the number and size of pixels in digital cameras. These improvements affect for most satellite equipment. Commercial off the shelf or mass production of electronic components that generally non-space-qualified has driven technological developments to be successfully flown on small satellite missions to replace bulky devices.

- **Affordable launch**

The Russian Federation has introduced smaller launcher by promoting the use of modified military missiles to launch small satellites. Many launch service providers offer the possibility of launching to orbit as an auxiliary payload on launch vehicle which are often referred to as "piggyback". It yielded a major influence along the small satellite market owing to the high reliability, large stockpile and low price of such launchers. In the market the cost of small satellite launches fell as more launch capacity entered the marketplace. Matured launch vehicle such as Long March China and PSLV India enhanced its capability of placing multiple missions into orbit by using multi-payload adaptors in the payload fairing. Soon, the new capacity from commercial small launchers: Rocket Lab, Virgin Orbit, Vector Launch, Firefly and a few new Chinese small launch vehicles would surge the launch market and put more pressure on the price. That plentiful of small launcher development is stimulated by growing demand for small satellites as well as an interest in dedicated launch services versus auxiliary payload on larger vehicles. The surge of launch capacity gives advantage for small satellite to purchase custom launch dates and orbit in obtaining better performance of the mission.

- **Mission complexity and independence**

The bigger cost and complexity of the space missions oftentimes rise the constraints and the management layers associated with those missions, so traditionally the end-users had less control over the mission and considerably more time to wait for the results. The small satellite mission could conduct qualifying and demonstrating new components and systems in orbit cheaply and deliver valuable results in a short time. It would offer an affordable

manner for many countries to establish independent space mission capability, without relying on inputs from the major space-faring nations. Together with reduced development times and the inherent reduction in launch due to smaller size and mass, the mission that fully under nation's direct control have made small satellite concept becomes an attractive solution to serving the needs of the developing countries to have access to space missions, applications and the relevant technologies.

- **Availability of spacecraft systems and their components in the market**

The rapid development in small satellite technology has resulted many flight proven systems and components, so did emerged new providers of spacecraft systems and components. NASA has released the updated report of Small Spacecraft Technology State of the Art in 2015 that emphasizes new technologies developed by various vendors complete with its technology readiness level metric [3]. The availability of flight proven systems and components in the market within its various technology readiness levels will make newcomers in space technology easily build customized missions, so that the number of small satellite missions would be increased rapidly soon.

1.1 Small Satellite Advanced Mission

Smaller satellites do not imply low technology and short durability, instead, they may mean highly advanced technology, offering a greater payload mass ratio in relation to the entire mass of the spacecraft. Even with today's technology, small satellites offer valuable missions for science and applications, as well as for education and training. Several small satellites have been targeted at state of the art missions such as surveillance, remote sensing, astronomical observations, and communications constellations in low Earth orbit.

Small satellites have been expanding their roles in Earth observation. In the field of video surveillance technology on small satellite, Technical University of Berlin has introduced DLR-TUBSAT and LAPAN-TUBSAT which used analog color video within the ground resolution about 5 m. Nowadays, after a decade, Google SkySat and SSTL Carbonite have been realizing high-definition resolution video of Earth in around 1 m ground resolution from about 500 km altitude. SkySat acquires HD video in its panchromatic channel covering 2.0 km x 1.1 km at 30 frame/s with duration of up to 90 seconds while the spacecraft always keeps looking the target by slew compensation maneuver. This satellite also covers four multispectral channels of the Blue 450-515, Green 515-595, Red 605-695 and Near Infrared 740-900 nm in obtaining a multispectral resolution of 2 m at nadir with a swath width of 8 km [4].

In the remote sensing area, SSTL has been starting early by establishing the Disaster Mitigation Constellation in 2005 which is consists of a number satellite that operated for the British,

Nigerian, Algerian, Turkish and Chinese government. The latest generation of DMC-3 satellites carries very high-resolution pushbroom imager with resolution of <1 m panchromatic and <4 m multispectral in 23 km swath width from nominal reference altitude of 630 km. The spacecraft has capability for real-time imaging and broadcasting data to the licensed ground stations, hence it could deliver a fast and straightforward of an accurate image acquisition request to the customer [5].

Earth observation mission using small satellites in this decade also becomes more attractive by the launch of the first under 100 kilograms synthetic aperture radar (SAR) satellite of the Finnish company, Iceye, in early 2018. Iceye plans to develop a constellation of 18 small satellites to provide SAR imagery of any place on the Earth within a few hours. The first 70-kilogram satellite, Iceye-X1, inserted into 500 km orbit altitude by PSLV C40 India has become successful proof-of-concept of SAR imagery on small satellite. In this area, JAXA/ISAS, University of Tokyo, and Keio University have also been developing an X-band compact synthetic aperture radar (SAR) system that is compatible with 100kg class satellite [6].

In the space science and exploration, small satellite had a long history to be used for astronomical observation. The astrophysics observatories have used smaller satellite since 1970 by launch 142.8 kg Small Astronomical Satellite 1 (SAS-1), the first earth-orbiting mission dedicated entirely to celestial X-ray astronomy observation. Scientists hypothesized that X-rays came from astronomical objects that contain extremely hot gases that related to the existence of compact stars, such as neutron stars or black holes. Since most X-rays and gamma rays are absorbed by Earth's atmosphere, so the instrument or detector must be placed in high altitude by sounding rocket, balloon, or satellite. One of an active small satellite for astrophysical studies today is Agile weighs 350 kg, which is operated by the Italian Space Agency (ASI).

To study an exoplanet, ESA develop a mini satellite weighing 290 kg called CHEOPS (Characterizing ExOPlanets Satellite). Exoplanet is defined as a planet outside the Earth solar system and would be seen when a planet passes in front of a star as viewed from the observer, the event is called a “transit”. Through high-precision monitoring of the star's brightness, scientists will look for signs of transit when a planet passes briefly on its face. In the similar area, a team of UK scientists is working together with SSTL to develop a small satellite mission called Twinkle for exoplanet research. The satellite would be placed into Sun synchronous orbit in the attitude range of 600 to 700 km with dawn-dusk operating time (6 hrs and 18 hrs local).

To give contributions to astronomy, NAOJ (National Astronomical Observatory of Japan) collaborated with JAXA have established JASMINE (Japan Astrometry Satellite Mission for INfrared Exploration) mission for astrometric survey that follow previous ESA mission, Hipparcos (1989) and Gaia (2013). This mission would consist of three satellites as pathfinder series with increasing size and capability: Nano-JASMINE weighs 35 kg that carries a 5.25 cm telescope, Small-JASMINE with a 30 cm telescope, and JASMINE with an 80 cm telescope. As a precursor mission, Nano-JASMINE observed stars brighter than magnitude 7.5 at near-

infrared spectrum of 0.6 – 1.0 μm for easier observation toward the center of the Milky Way. It is planned to operate for more than 90% of 2 years mission duration to acquire astrometry data of the entire celestial globe [7].

Small satellites have existed in spreading area of communication from simple experimental communication until a high data rate of digital communication. In the early years of small satellite technological exploration, most of small satellites were doing amateur communication missions such as an analog voice repeater, digital short message repeater, and store and forward messages as a data collection platform. In the decade of the 1980s and 1990s, a civilian digital store and forward transponder began to be carried by microsatellites. UoSat-2 (1984) and UoSAT-3 (1990) of the University of Surrey, FO-12 (1986) of the Japan Amateur Radio League, Inc, (JARL) and TUBSAT-A (1991) of the Technical University of Berlin are counted as the predecessor of small satellites that performed digital store and forward mission.

Following the growth of capabilities and demand, a data collection platform small satellite is currently expanding its function and roles to become connected devices and vehicles for the Internet of Things (IoT), Machine to Machine (M2M), and traffic monitoring (AIS or ADS-B) that's mostly based on a constellation approach to give better and faster delivery services to the user. ORBCOMM as the leading of global IoT provider operates a small satellite network 100% dedicated to M2M has launched 18 of new generation IoT satellites named OG2 from 2010 to 2015 to update its network and capability. It provides communication solutions for tracking, monitor, and controlling fixed and mobile assets including transportation, maritime, oil and gas, heavy equipment, and government utilities. OG2 also equipped by Automatic Identification System (AIS) payloads to receive and report transmissions from AIS-equipped maritime vessels for tracking ship activity, navigational purposes, as well as for maritime surveillance by coast guards and government agencies. In the upcoming years, there are also many startups in the space industry that want to apply a small satellite constellation for expanding Internet of Things (IoT) system.

In the broadband communication area, the launch of small satellites is expected to exhibit the most substantial growth from 2017 to 2026. Four satellite constellations from hundreds to thousands of small satellites deployment are promising internet service from low earth orbit, they are OneWeb (648 satellites), SpaceX Starlink (4,425 satellites), Boeing (2,956 satellites) and Telesat (117satellites). Besides launching the satellite into a low Earth orbit is the simplest and cheapest way, they especially would take advantage of low earth orbit to provide high bandwidth in a low communication time lag or latency.

1.2 Scope and Objective of the Research

The attitude control system plays an essential role in satellite on-orbit operation which could greatly affect the satellite's performance. A few simple missions carry payloads, devices or sensors which are characterized as omnidirectional do not require any strict orientation and allow the spacecraft in the tumbling condition. Some of the payload or instrument has toroidal direction that constrains spacecraft to direct one of its axes to certain orientation and allowing rotation on that axis. But most of the missions containing imager or directional instrument require three-axis stabilization and must be stabilized in a high accuracy. A small satellite for remote sensing expect the attitude control accuracy of 8×10^{-3} to 5.5×10^{-4} deg/s depends on the field of view and ground resolution of the imager [8]. An astrometry dedicated small satellite that has to accurately estimate the positions of stars and to update star catalogues should control its angular velocity within accuracy of 2.5×10^{-5} deg/s to satisfy the mission requirements [9]. If the satellite attitude is unstable, the obtained images are blurred and not crisp.

Controlling the small satellite may be accomplished in several ways: atmospheric drag control, gravity gradient, magnetic stabilization, spin stabilization, or three-axis stabilization. Three-axis stabilization is typically needed for applications requiring better than 0.10 deg of pointing accuracy. Many requirements influence attitude control system design, but the primary drivers are requirements of pointing knowledge, control stability, and maneuvering. Previously, many studies have focused on precise attitude control for conventional standard-sized satellites. These methods are now being applied to small satellites. However, some of them are unsuitable for small satellites because of constraints such as power consumption, mass, and space requirements. This study clarifies these constraints and problems and proposes new efficient methods to solve some of these problems with the objective of realizing high precision attitude control for small satellites by using a momentum bias method.

In the case of conventional standard-sized satellites, many satellites can achieve precise attitude stabilization. But since nowadays the small satellites are as considerably used for sophisticated missions as standard-sized satellites, therefore, they also expect precise attitude stabilization that generally needs three-axis stabilization to meet the requirement. The development of small satellite requires an attitude control system that is inexpensive, light-weight, meanwhile with small volume and low power consumption. Therefore, magnetic coils and momentum or reaction wheel have been adopted as the most popular actuators. Running a pitch bias momentum wheel is the simplest way to accomplish the three-axis stabilization control. This method establishes the attitude stabilization in roll and yaw directions by the momentum wheel which is nominally spinning at a fixed rate in the pitch direction of the satellite. Many previous satellites operating in the orbit subject to this control strategy because of its efficiency. However, establishing high precision of attitude control of small satellite that carrying a line scanner

imager or a high-resolution camera for remote sensing or a narrow beam transponder for communications is very challenging.

Many constraints since the design phase until selecting the operation strategy have to be considered to provide both efficient and high precision attitude control method. Together with the compliance to the small satellite requirements and constraints, the attitude control system must conduct the standard mode of the operation such as nadir pointing mode, slew pointing mode, as well as hibernation mode. Although the hibernation mode is not directly related to the payload operation, choosing the right strategy for hibernation will shorten the satellite recovery time from the power deficit and prepare for the next mission.

To support the small satellite that requires high pointing accuracy of imaging or advanced communications mission, then the key research question and objectives of this study will focus on how to establish the momentum bias capability for a small satellite class with limited electric power, mass and space to realize the efficient and high precision of attitude control. Since then, this research will explore the designing of attitude control, testing it on the ground and in orbit operation to prove the aforementioned objectives. The scope of research will include the following activities:

1. Designing the spacecraft mass properties to support its attitude control method.
2. Pre-launch testing of the attitude control system.
3. Characterizing and handling of the disturbance torque in both polar and equatorial orbits.
4. Performance analysis of the attitude control to satisfy the mission requirement in the standard of satellite operation mode such as nadir pointing, inertial pointing and target pointing.
5. Recommendation for future small satellite attitude control operation.

1.3 Project of LAPAN-A Satellite Series

The LAPAN-A satellite series program began with development of capabilities that focus on acquiring knowledge, skills and experience in integration, testing, launch and satellite operations. In the second phase, satellite development was targeted for proving the ability of satellites built in the country in carrying out remote sensing missions. Furthermore, in the third stage, the development of LAPAN-A satellite series will be directed to a dedicated mission as well as the exploration of new missions. The development approach of LAPAN-A satellite series can be seen in Figure 1.1.

In the Satellite Technology Center – LAPAN's roadmap as seen in the Figure 1.2, LAPAN-A satellite series become the baseline of satellite technology development. The first phase of LAPAN-A satellite series program was started by developing LAPAN-A1 (LAPAN-TUBSAT)

that carried a high-resolution video camera for surveillance and attitude control demonstration technology in Sun synchronous polar orbit. The following satellite, LAPAN-A2 (LAPAN-ORARI), has been inserted into near-equatorial orbit to provide maximum orbit access over Indonesia for disaster mitigation, amateur radio communication, and maritime surveillance. The third satellite, LAPAN-A3 (LAPAN-IPB) that carried pushbroom multispectral imager, has been launched into Sun synchronous orbit and proved remote sensing mission of agricultural observation and the global maritime monitoring.

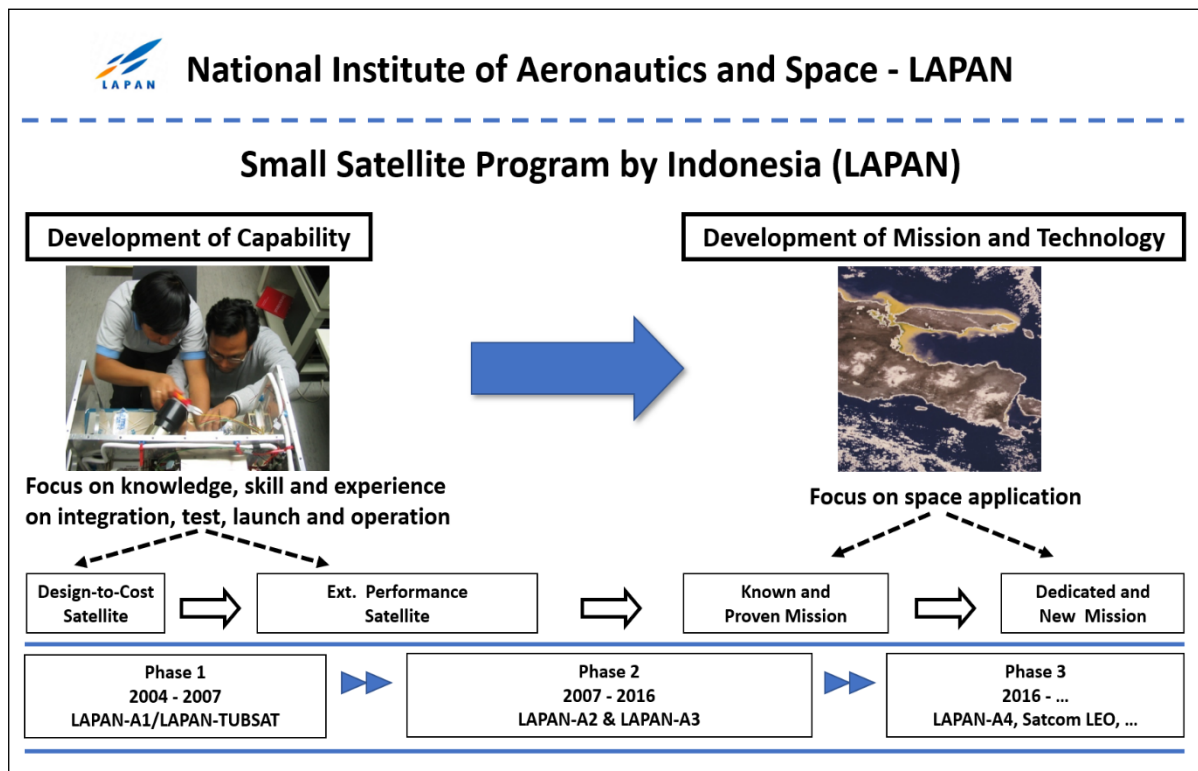


Figure 1.1: Development Approach of LAPAN-A Satellite Series

The next mission of LAPAN-A4 will continue and improve LAPAN-A3 mission by carrying a higher resolution of the multispectral imager payload in addition of its medium resolution which is double LAPAN-A3 swath-width to be 200 km. The development of more advanced satellites with dedicated missions also important to address the national needs of communication and synthetic aperture radar (SAR) missions. Communication missions are needed to connect between islands and remote areas with no terrestrial networks as well as for the disaster early warning system. The next strategic satellite development is defining new mission of SAR on the small satellite platform. SAR mission is important to provide a near real-time solution of Earth observation over Indonesia. It would overcome the cloud cover problem to monitor the rapidly changing of land cover and environment that related to deforestation, agricultural cycle, infrastructure development or even the impact of disaster.

Establishing the baseline technology for the next satellite development, LAPAN-A satellite series will use the proven platform, including the attitude control system that has been used since LAPAN-A1 (LAPAN-TUBSAT) with continuous improvement resulted in every single mission. The attitude control of LAPAN-A satellite series employs three pairs of wheel-gyro that is placed in the orthogonal axis as main actuator and sensor while the star sensor and the air coil type of magnetic torquers are used for controlling the angular momentum.

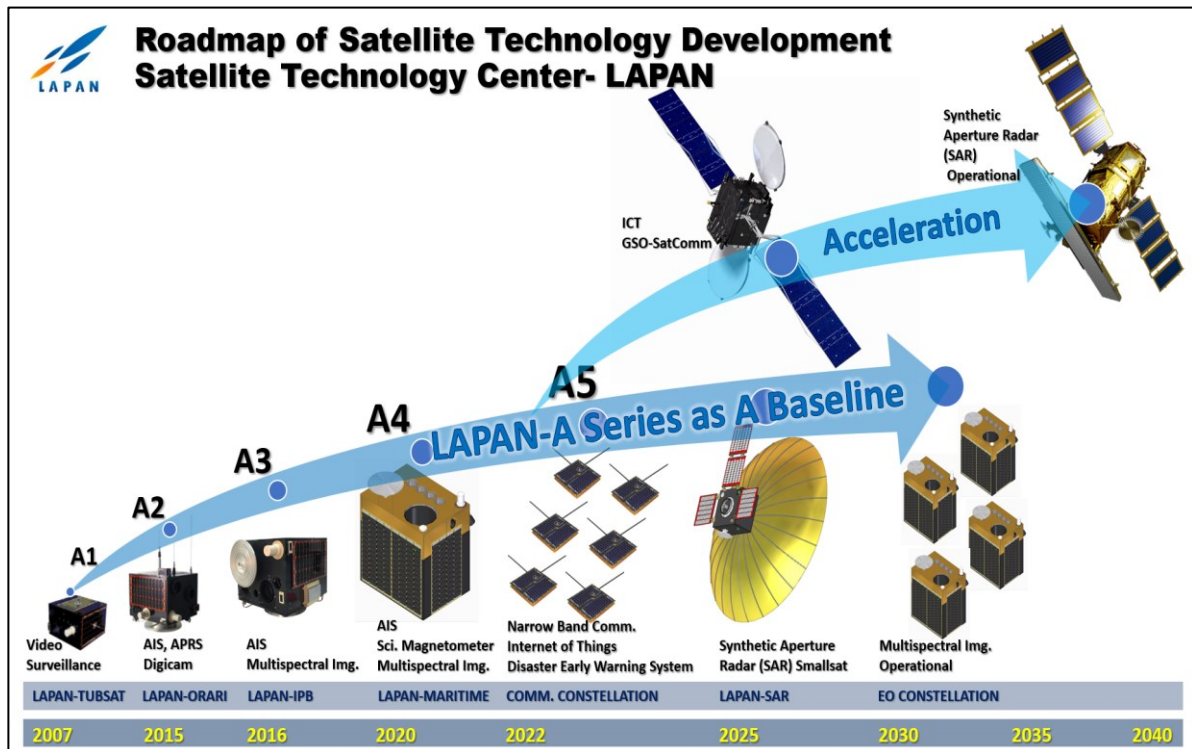


Figure 1.2: Roadmap of Satellite Technology by LAPAN

2 STATE OF THE ART

Nowadays the small satellites are as considerably used for sophisticated missions as standard-sized satellites, therefore, they also expect precise attitude stabilization that generally needs three-axis stabilization to meet the requirement. Small three-axis stabilized satellites are expected to accurately pinpoint their instruments to specific objects or regions of space. Also, small communication satellites, especially those employing multiple narrow-beam antennas, require tight pointing accuracies to ensure adequate antenna gain. Therefore, attitude control system technologies developed for larger satellites are being utilized to meet increasingly stringent pointing requirements. At present, pointing accuracies of 1 degree or less are quite common for both spin and three-axis stabilized small satellites.

To stabilize the spacecraft in three-axis, there are two methods of momentum exchange could be implemented, momentum bias and zero momentum. The term of momentum refers to the angular momentum of the spacecraft, “bias” (or offset) indicates large and “zero” means small. The spacecraft stabilized by momentum bias could spin the whole of its body called “single spinner” or spin a part of its body while the other part stays fixed to certain reference called “dual spinner” but now it frequently uses a subsystem named momentum wheel that is always spinning at a very high speed to make the spacecraft resistant to changing its attitude. Instead of retaining, the spacecraft that implements a zero momentum always dump the momentum using thruster or another torquer to keep it low and employs the reaction wheel that is spun up or down to create the torque against the disturbance and force the vehicle to rotate. Figure 2.1 shows the classification of spacecraft stabilization based on momentum exchange method.

Besides momentum wheel and reaction wheel, there is a device that also could support momentum exchange technique named control moment gyro (CMG) as kind of a hybrid of the two. It spins at high speed to stabilize the spacecraft, but it also has gimbals that could rotate the axis of the wheel to create maneuver torques. As an example of the momentum exchange technique in the famous missions, Hubble Space Telescope and Kepler Space Telescope use momentum/ reaction wheels while the International Space Station (ISS) employs CMGs. The selection of an attitude control system (ACS) is a function of many factors, including mission objectives, orbit, and available system budgets. Stabilization systems using momentum and reaction wheels as control torque sources are well-suited to small satellite applications due to their proven performance, relative simplicity, versatility, and capability of providing high accuracy pointing control [10].

Considering the momentum devices for use in small satellite attitude control systems has shown their advantage for the following reasons:

- concepts are flight-proven
- operation is independent of orbit and environment
- they permit high pointing accuracies
- they reduce (or eliminate) expendables
- components can be mixed and matched to suit specific requirements
- components have relatively low mass, power, and volume requirements

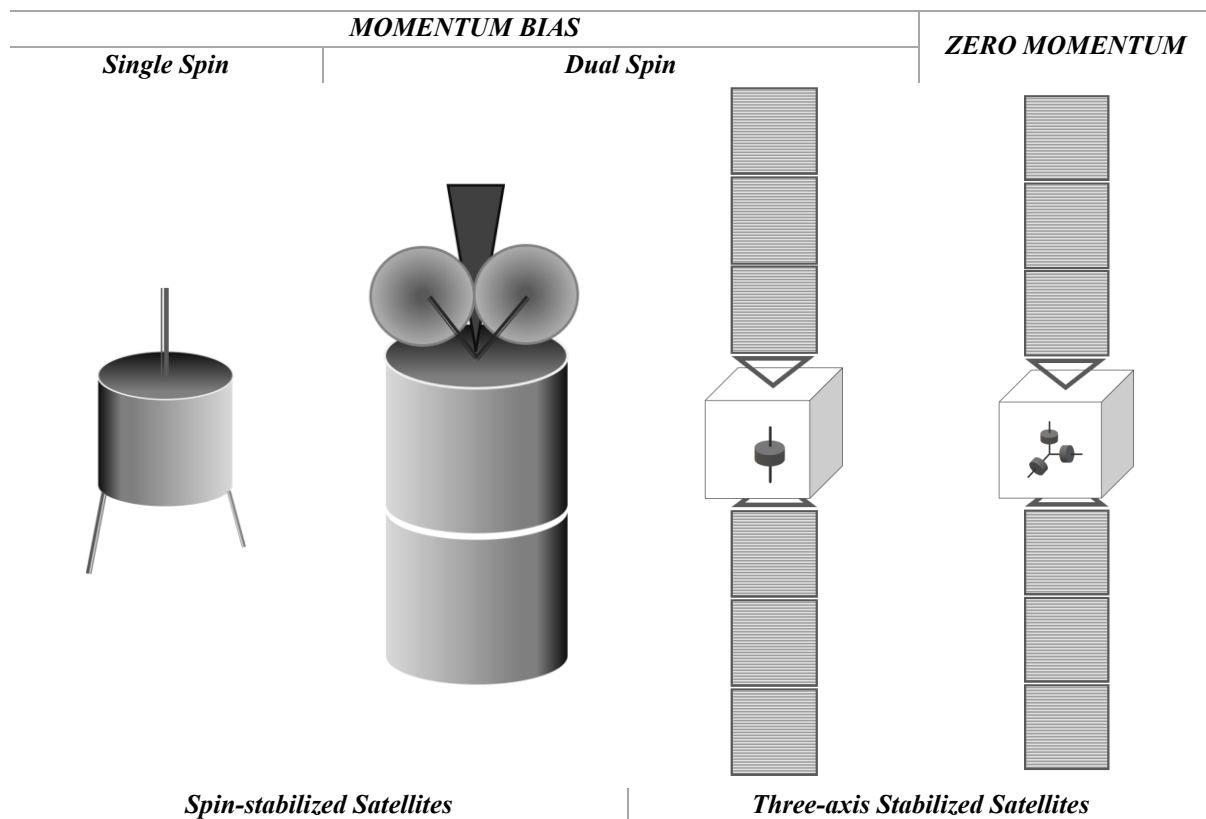


Figure 2.1: Classification of Momentum-based Attitude Stabilization

When momentum-based systems are used to stabilize and control the attitude of a satellite. An auxiliary torqueing system is included to desaturate the wheels. The auxiliary torqueing system can employ thrusters, gravity gradient, solar pressure, or magnetic torquers. Secular torques acting on a spacecraft cause the wheel speed to increase until it reaches its upper operating or saturation limit. At tills point, an external torque must be used to restore the wheel speed to its nominal operating value so that the wheel is maintained in its torque-producing range. The two most common techniques used for desaturation are magnetic torqueing and mass expulsion torqueing. Electromagnetic actuation systems are quite common and have been discussed and analyzed in several papers and report. Three types of magnetic torquer systems, currently being

used, are permanent magnets, air-core torquing coils, and iron-core torquing coils. However, due to the weight of permanent magnets, their use is limited. In most systems, a set of three mutually perpendicular coils is used.

In a magnetic desaturation system, momentum dumping is exercised when the wheel speed exceeds a specified threshold. The commands are generated either manually from a ground station or automatically by an on-board computer. The magnetic torquers are energized at predetermined orbit locations and remain on until wheel speed returns to its nominal value. The onboard magnetic desaturation systems also require a three-axis magnetometer and signal processing electronics. The magnetometer sensors detect Earth's magnetic field components along each of the satellite axes. The corresponding signals are amplified and used to drive the coils [11], [12].

The magnetic coil system is an attractive method of desaturation for low Earth orbit (LEO) satellites due to the relatively high magnetic field intensity at lower elevations. This system also has high reliability since it includes only simple static devices (a magnetometer, a signal processor, and three coils). Other advantages are that it does not depend on a fuel supply and is much lighter than the simplest low specific impulse thruster system. Disadvantages of this system are that it may require significant amounts of power at higher altitudes. Also, coil commands may last over a large fraction of the orbit (or over several orbits) to reach desaturation. Magnetic systems may also interfere with the operation of certain payloads.

The other well-known technique used for desaturation are mass expulsion torquing. Thrusters are usually used to desaturate the momentum storage systems. In operation, a jet is fired to produce a torque opposite to the direction of the accumulated angular momentum while the satellite is commanded to maintain its attitude. This results in a wheel acceleration that counteracts the applied torque. For a desaturation system using body-fixed offset roll/yaw thrusters, the efficiency of the system can be defined as the ratio of the daily secular momentum increase to the angular impulse provided by the thruster. A reasonable design value for the efficiency is about 80 percent [13].

The duration of the desaturation impulse is a function of the amount of momentum to be dumped. This is typically about one percent of nominal wheel momentum [10]. The number of thruster cycles expected over the lifetime of the satellite is a potentially limiting item. Another concern is that a wheel system will tend to exhibit a nutation when within the thruster deadbands. The amplitude of this nutation is dependent on the minimum impulse bit from the thruster. Reducing the impulse bit to decrease the nutation amplitude will increase thruster cycles.

Thruster systems typically include a few solenoid valves, nozzles, high-pressure tanks and lines, as well as fuel heaters and pressure transducers. The complexity of these systems reduces reliability and increases weight. Thrusters for momentum desaturation also need to be rated at

a few millipounds of thrust to avoid significant disturbances to the wheel system. In high altitude orbits, however, mass expulsion systems are the only viable means for desaturation due to the low magnetic field intensity at higher elevations [14].

Various momentum-based ACS configurations have been used for three-axis stabilized satellites. Control system actuators typically consist of a combination of momentum and/or reaction wheels, thrusters, and magnetic control components. Thrusters and magnetic coils are typically used in both desaturation and active control capacities, depending on the exact configuration. Following are the configuration alternatives of three-axis stabilization systems based on momentum exchange method:

- single momentum wheel
- pitch momentum wheel/yaw reaction wheel
- pitch momentum wheel/thruster
- double-gimbal momentum wheel
- single-gimbal momentum wheel
- three reaction wheels
- canted scan wheel momentum bias

A reaction wheel is sometimes operated as a momentum wheel by operating it at a constant rotation speed to saturate a spacecraft with a large amount of stored angular momentum. Doing so alters the spacecraft rotational dynamics so that disturbance torques perpendicular to one axis of the satellite, i.e. the axis parallel to the wheel's spin axis, do not result directly in spacecraft angular motion. Instead produce an angular motion in the same axis, the disturbance torque result in generally smaller angular motion which is called precession that is perpendicular to the spacecraft axis. This has the effect of tending to stabilize that spacecraft axis to point in a nearly-fixed direction, allowing for a less-complicated attitude control system [10]. Satellites usually using this momentum bias by orienting the momentum wheel's axis toward the orbit-normal vector, therefore this configuration is also called pitch momentum bias.

The implementation of momentum bias method by running a pitch bias momentum wheel is the simplest way to accomplish the three-axis stabilization control. This method establishes the attitude stabilization in roll and yaw directions by the momentum wheel which is nominally spinning at a fixed rate in the pitch direction of the satellite. Many previous satellites operating in the orbit subject to this control strategy because of its efficiency. Nowadays the fixed rate momentum wheel generally replaced by a reaction wheel which could also control the rotation in the pitch axis so the three-axis stabilization basically could achieve by implementing single wheel operation. Nevertheless, performing a high precision attitude control of small satellite to support an advanced mission payload such as line scanner imager, high-resolution remote sensing camera, or narrow beam communications transponder requires special provision. While reaction wheel could control the pitch rotation precisely, the small residual oscillating motion in roll and yaw directions would naturally occur in the gyroscopic motion. This oscillation is usually called nutation could be managed by additional actuator called nutation damper.

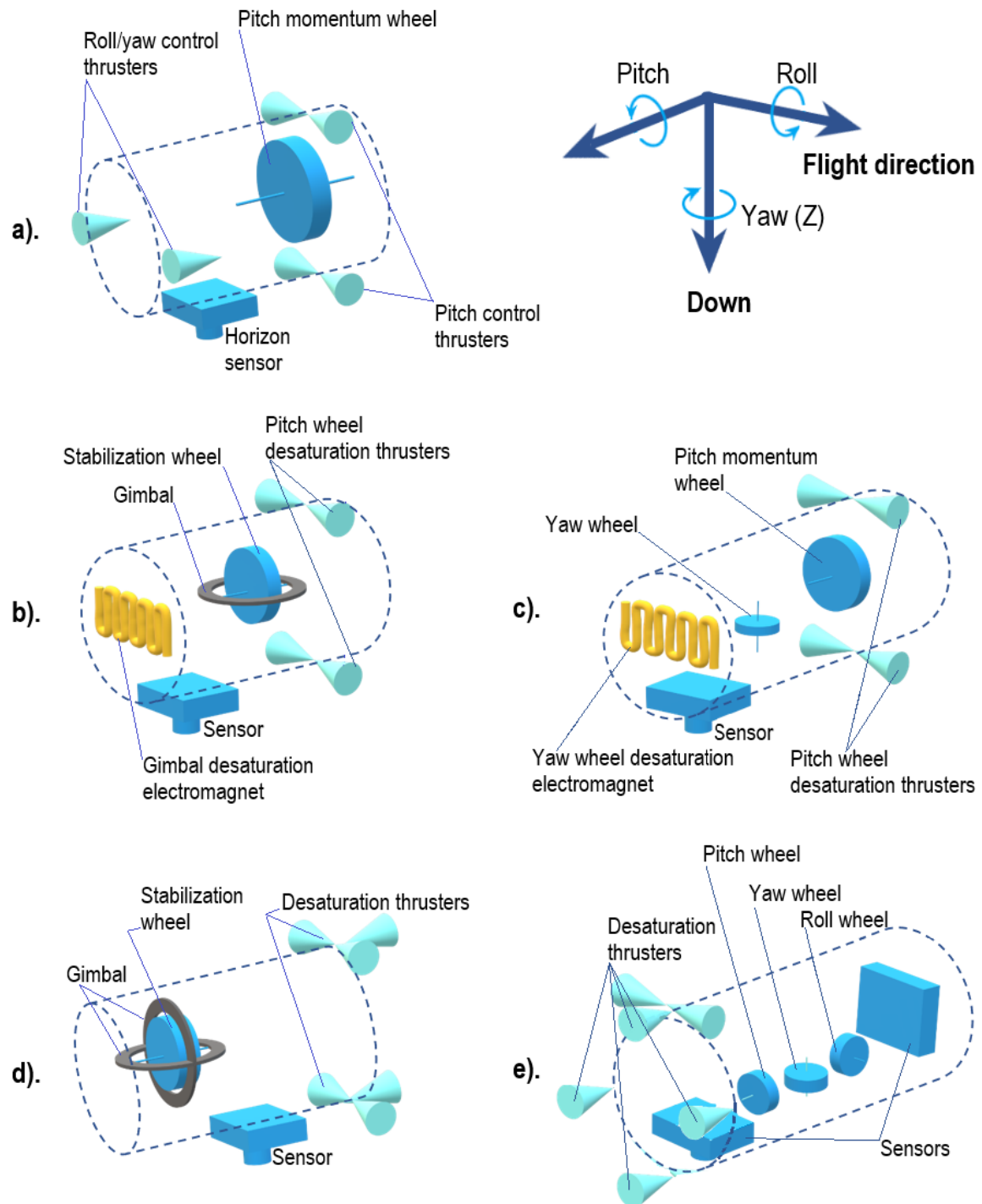


Figure 2.2: Various Momentum-based ACS [10]

2.1 Performance Parameter of Attitude Control System

The attitude control system (ACS) design process has to define guiding requirements based on mission goals. Since the mission goals often require more than one mode of operating a spacecraft, the guiding requirements generally begin with a description of the control modes the ACS is expected to execute to meet those goals. Many constraints since the design phase until selecting the operation strategy have to be considered to provide both efficient and high precision attitude control method. Typical control modes and requirements of the spacecraft are described in Table 2.1.

Table 2.1: Typical Spacecraft Control Modes and Requirements [15]

| Attitude Control Requirements | | Description |
|---|------------------------------------|--|
| M O D E | Orbit Insertion | Period during and after boost while spacecraft is brought to final orbit. Options include no spacecraft control, simple spin stabilization of solid rocket motor, and full spacecraft control using liquid propulsion system. May drive certain aspects of ACS design. |
| | Acquisition | Initial determination of attitude and stabilization of vehicle for communication with ground and power generation. Also may be used to recover from power upsets or emergencies. |
| | Normal/Nominal Mission, On-Station | Used for the vast majority of the mission. Requirements for this mode should drive system design. |
| | Slew | Reorienting the vehicle when required. |
| | Contingency or Safe | Used in emergencies if regular mode fails or is disabled. Will generally use less power or fewer components to meet minimal power and thermal needs. |
| | Special | Requirements may be different for special targets or time periods, such as when the satellite passes through a celestial body's shadow, or umbra. |
| C R I T E R I O N | Accuracy | Knowledge of and control over a vehicle's attitude relative to a target attitude as defined relative to an absolute reference |
| | Range | Range of angular motion over which determination & control performance must be met |
| | Jitter | Specified bound on high-frequency angular motion |
| | Drift | Limit on slow, low-frequency angular motion |
| | Transient Response | Allowed settling time or max attitude overshoot when acquiring new targets or recover from upsets |

For many missions the ACS must control spacecraft attitude during the firing of large liquid or solid rocket motors for orbit insertion or management. Large motors can create large disturbance torques, which can drive the design to larger actuators than may be needed for the rest of the mission. Once the spacecraft is on-station, the payload pointing requirements usually dominate. These may require planet-relative or inertial attitudes and fixed or spinning fields of view. Table 2.2 explain the effects of control accuracy requirements on sensor selection and ACS design, while Table 2.3 presents a comparison of attitude control actuators.

Table 2.2: Effects of Pointing Accuracy Requirements on Sensor Selection and ACS Design [15]

| Required Accuracy (3σ) | Effect on Spacecraft | Effect on ADCS |
|---------------------------------|---|---|
| $>5^\circ$ | <ul style="list-style-type: none"> - Permits major cost savings - Permits gravity-gradient (GG) stabilization | <p>Without attitude determination</p> <ul style="list-style-type: none"> - No sensors required for GG stabilization - Boom motor, GG damper, and a bias momentum wheel are only required actuators <p>With attitude determination</p> <ul style="list-style-type: none"> - Sun sensors & magnetometer adequate for attitude determination at $\geq 2^\circ$ - Higher accuracies may require star trackers or horizon sensors |
| 1° to 5° | <ul style="list-style-type: none"> - GG not feasible - Spin stabilization is feasible if stiff, inertially fixed attitude is acceptable - Payload needs may require despun platform on spinner - 3-axis stabilization will work | <ul style="list-style-type: none"> - Sun sensors and horizon sensors may be adequate for sensors, especially a spinner - Accuracy for 3-axis stabilization can be met with RCS deadband control but reaction wheels will save propellant for long missions - Thrusters and damper adequate for spinner actuators - Magnetic torquers (and magnetometer) useful |
| 0.1° to 1° | <ul style="list-style-type: none"> - 3-axis and momentum-bias stabilization are feasible - Dual-spin stabilization is also feasible | <ul style="list-style-type: none"> - Need for accurate attitude reference leads to tracker sensors & possibly gyros - Reaction wheels typical with thrusters for momentum unloading and coarse control - Magnetic torquers feasible on light vehicles (magnetometer also required) |
| $< 0.1^\circ$ | <ul style="list-style-type: none"> - 3-axis stabilization is necessary - May require articulated & vibration-isolated payload platform with separate sensors | <ul style="list-style-type: none"> - Same as above for 0.1° to 1° but needs star sensor and better class of gyros - Control laws and computational needs are more complex - Flexible body performance very important |

Table 2.3: Comparison of Attitude Control Actuators [16]

| Actuator | Typical application | Precision (deg) | ACS control bandwidth (Hz) | Torque/power (Nm/W) |
|-----------------------|---|--------------------------------|----------------------------|---------------------|
| Spin stabilization | Low-precision omnidirectional RF payloads | 0.1 – 1 in 2 axes | N/A | N/A |
| Gravity-gradient boom | Coarse Earth observation | 5 – 20 in 2 axes | N/A | N/A |
| Magnetic torquer | Momentum dumps, nanosatellites in LEO, gravity-gradient augmentation | 1 – 10 in 2 axes | 0.01 – 0.1 | 0.001 – 0.01 |
| Momentum wheels | Astronomy, communication | 0.001 – 1 in 3 axes | 0.01 – 0.1 | 0.001 – 0.01 |
| Reaction wheels | Astronomy, communication, Earth observation | 0.001 – 1 in 3 axes | 0.01 – 1 | 0.001 – 0.1 |
| Control-moment gyros | Earth imaging and radar, satellite servicing, asteroid grappling | 0.001 – 1 in 3 axes, or better | 0.1 – 1 | 1 – 10 |
| Electric thrusters | GEO station keeping | 0.01 – 0.1 in 3 axes | 0.001 – 0.01 | 0.0001 – 0.001 |
| Chemical thrusters | Missile defense, interplanetary transfer, spin-speed adjustment and reorientation, momentum dumps | 1 – 10 in 3 axes | 0.1 – 1 | Very high |

In the on-station or normal mode, where most of the satellite's lifetime would be spent, the nominal operations should comply the payload pointing requirements such as:

- Nadir pointing, in which the satellite is three-axis stabilized and the payload's field of view is pointed to nadir along the ground track. The attitude control system should give spacecraft slew capability to point at a certain object on the cross-track. This mode is primarily utilized for applications such as systematic imaging to deliver complete maps of certain areas.
- Target pointing, in which the attitude control has the capability to keep the spacecraft payloads continuously looking towards a target point by slew compensation maneuver. It is a useful mode for a real-time video surveillance as well as for stereo imaging by the satellite on a single pass that expect the spacecraft could capture the same area from two different view angles so the ground image processing system could combine the images to get height information of the target.
- Interactive pointing, in which the ground operator conducts roll, pitch and yaw maneuvers to obtain images of adjacent scenes. The control algorithm of this mode could be modified and adopted as an automatic control to artificially widen the swath width of payload.
- Inertial pointing, in which the satellite is three-axis stabilized towards a certain inertial reference. It will be the main operation mode for astronomy mission to observe celestial object as well as an important mode for an Earth oriented satellite to conduct Sun pointing in aiming certain illumination or thermal condition.

Most of the missions containing imager or directional instrument require three-axis stabilization and must be stabilized in a high accuracy. Unstable attitude control would make the obtained images are blurred and not crisp. A medium resolution of remote sensing mission might expect the attitude control accuracy of 8×10^{-3} to 5.5×10^{-4} deg/s, while an astrometry satellite that has to accurately estimate the positions of stars should control its angular velocity within accuracy of 2.5×10^{-5} deg/s to satisfy the mission requirements [9].

When the satellite is carrying communication payload, the requirement on allowed pointing error is often 10% of the antenna beamwidth. However, although this is typical of many missions, it is no more than a rule of thumb. In order to have a proper definition of the real requirement, accuracy must be related to the communications link budget by considering the effect of a pointing error on the signal received by the ground stations [17].

There are two additional modes that should be prepared to support the whole satellite missions, slew mode and safe mode. A need for attitude slews maneuvers, and the frequency and speed of those maneuvers must be defined. Table 2.4 show that slewing requirements will affect control actuator selection and oftentimes a spacecraft slew agility can demand larger actuators for intermittent use. Reasons for slews can include:

- acquiring the desired spacecraft attitude initially or after a failure
- repointing the payload's sensing systems to targets of opportunity or for calibration purposes
- tracking stationary or moving targets, including communication stations
- directing the vehicle's strongest motor(s) to the proper direction relative to orbital motion

Table 2.4: Slewing Requirements and Control Actuator Selection [17]

| Slewing | Effect on Spacecraft | Effect on ADCS |
|---|---|--|
| None or Time-Unconstrained | Spacecraft constrained to one attitude (highly improbable), or reorientations can take many hours. | <ul style="list-style-type: none"> - Reaction wheels, if planned, can be smaller - If magnetic torquers can dump momentum, reaction control thrusters may not be needed |
| Low Rates from 0.05 deg/s (orbital rate) to 0.5 deg/s | Minimal | <ul style="list-style-type: none"> - Depending on spacecraft size, reaction wheels may be fully capable for slews - If reaction wheels not capable, thrusters will be necessary - Thrusters may be needed for other reasons; i.e. station keeping |
| High Rates >0.5 deg/s | <ul style="list-style-type: none"> - Structural impact on appendages - Weight and cost increase | Control moment gyros or thrusters needed. If thrusters needed for other reasons, two thrust levels may be needed. |

The contingency or safe mode also has to be well defined. Sometimes it is named hibernation mode, in which all system is running with minimum devices. Even though this mode does not relate directly to the payload operation, choosing the right hibernation method will improve the

efficiency of a small satellite mission significantly. The right attitude control strategy for hibernation will also speed up the process of waking up the satellites to carry out the next mission operation while avoiding the satellite from lack of power.

The attitude control system design and requirements also must be supported by proper satellite design. The mass moments of inertia of a spacecraft are critical to the selection and operation of an attitude control system. Moments of inertia affect the sizing of the actuators and determine the effect of disturbance torques on pointing and stability. Simulations of the equations of motion show the relationship between spacecraft inertias, disturbance torques, and pointing requirements. Inertias may be fixed by design constraints or may be a design option that permits optimization for a given orientation and/or disturbance torque profile.

Other satellite design parameters influence the effects of the expected environmental torques. For example, surface properties of the spacecraft determine the effects of solar radiation pressure. The location of the center of pressure with respect to the center of mass, as well as the area, and the coefficient of drag determine the effects of aerodynamic drag torques associated with low altitude orbits. Environmental torques are not necessarily unfavorable since they can be used for passive stabilization through proper spacecraft design. The configuration of the satellite may impose design constraints on the attitude control system in the form of system budgets for weight, power, and volume. These constraints are often imposed on the satellite by available launch opportunities, especially for small satellites.

The orbit of a satellite, including altitude, inclination, and eccentricity, and the satellite configuration, determines the type of environmental torques to be expected during satellite operation. The environment in which the spacecraft will operate constrains what types of control methods will be effective. For example, the relatively strong magnetic fields that occur in low Earth orbit (LEO) can create disturbance torques that need to be managed, but they also allow the use of magnetic torquers, a means of attitude control not available at much higher altitudes like geosynchronous orbit (GEO). Environmental torques, as mentioned previously, can be modeled to determine both passive stabilization feasibility and disturbance torque characteristics. Environmental torque magnitudes are one of several factors that affect the sizing of ACS components.

Environmental disturbance torques, which are including gravity gradient and aerodynamic, magnetic, and solar pressure, fluctuate in a cyclic manner over the orbital period. The torque disturbance models can be used to determine the types and magnitudes of disturbance torques that can be expected for a given orbit. Momentum requirements vary sinusoidally and have an amplitude corresponding to the maximum amplitude of the expected disturbance. The effects of these torques on the spacecraft can be nulled through momentum exchange with a momentum device. Together with required additional momentum if spacecraft slew maneuvers are desired, the typical of momentum and torque required is shown by Figure 2.3.

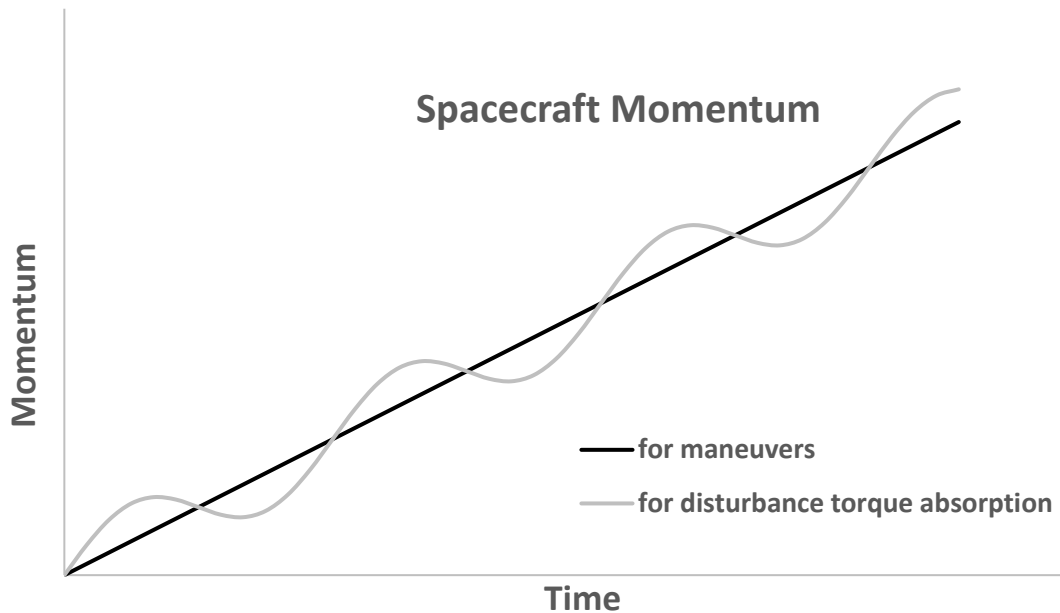


Figure 2.3: Typical Spacecraft Momentum Requirements

2.2 Momentum Bias Attitude Control in GSO

Momentum bias technique has been implemented since first communication satellite program of geosynchronous orbit (GSO) named Syncom. The simplest way to apply momentum directly to attitude control is to allow the whole spacecraft to spin about a single axis. Of course, this severely constraints the design and mission applications, but is inherently stable and essentially passive. In other words, a large spinning body is gyroscopically stiff. Design constraints include the requirement that the spacecraft be configured to permit spin about its major principal axis due to the stability criterion [18]. Such designs have typically been axisymmetric, such as the first successful synchronous communications satellite launched at 1963, Syncom II. Small perturbing torques may precess the momentum vector slowly away from desired orbit-normal direction. Periodic attitude corrections are carried out with small thrusters. Very similar control system was used in the first commercial communications satellite of the International Telecommunications Satellite Organization (INTELSAT), Early Bird or INTELSAT 1, launched in April, 1965. The system is splendidly simple, and its pointing accuracy of about 1 degree is quite suitable for the toroidal antenna beam width 11 degrees.

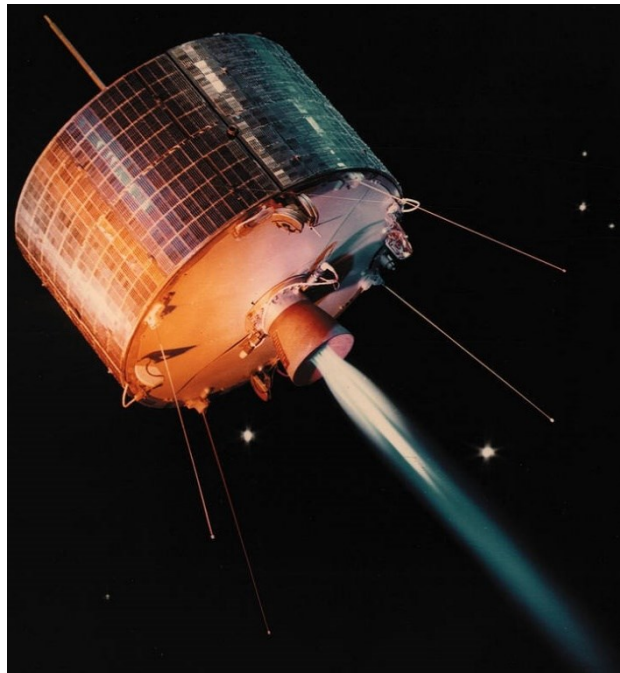


Figure 2.4: Spin-stabilized Communication Satellites [19]

Soon, there was demand for higher antenna gain, and correspondingly narrower antenna beams. Most missions cannot be accomplished with simple/single spinners such as Syncom II, so other momentum exchange techniques have been developed. The primary limitation of single spinner satellites is that no oriented sensors or antennas can be employed, because all parts rotate together about the spin axis. The next logical step in the evolution of such spacecraft was to combine an oriented platform and a rotor. This concept appeared to maintain the advantage of gyroscopic stiffness and permit an oriented platform for directional instruments or antennas. The state of technology was insufficient to allow a change to three-axis stabilization and there was some debate as to whether a pencil beam should be produced by despining the beam electronically or mechanically [20].

The first of the Lincoln Experimental Satellites (LES-1) and the first NASA Applications Technology Satellite (ATS-1) both produced a pencil beam of some 17 degrees by electrical despin in February 1965 and December, 1966, respectively. This proved to be an interim solution to the problem with mechanical despin being used first on ATS-3 in November, 1967. Since then, this configuration of a simple spinner, with its very simple attitude and orbit control system, together with a mechanically despun antenna section, has developed into being the most used configuration. Some examples are INTELSAT III, Skynet, NATO, Anik A, DSCS II, Palapa A and Marisat.

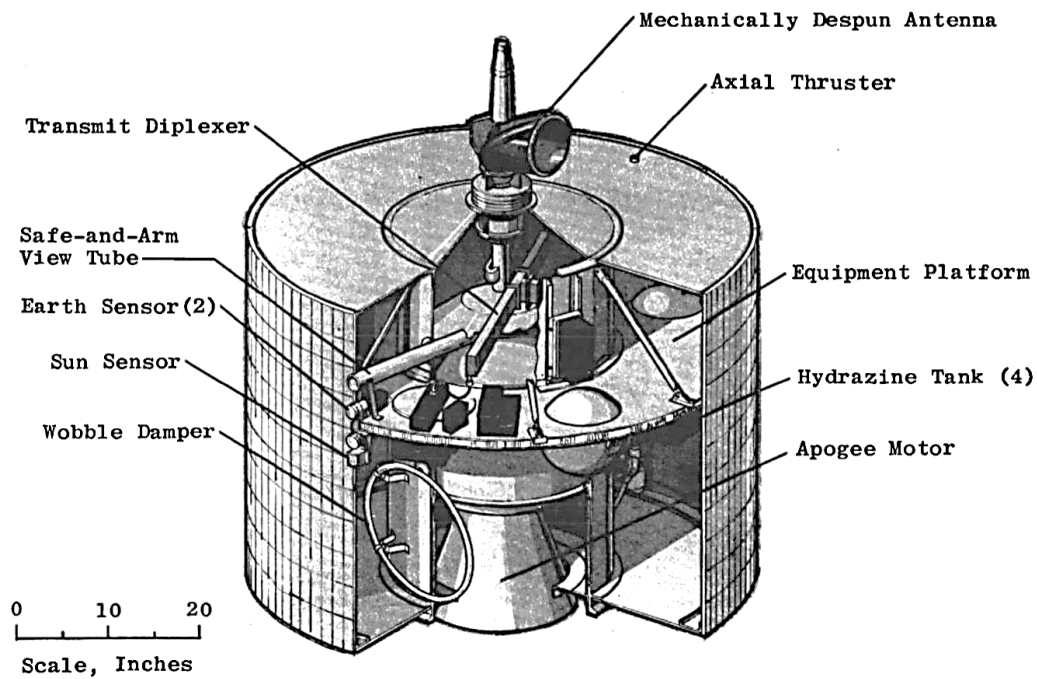


Figure 2.5: Mechanically Despun Antenna on INTELSAT III Spacecraft [21]

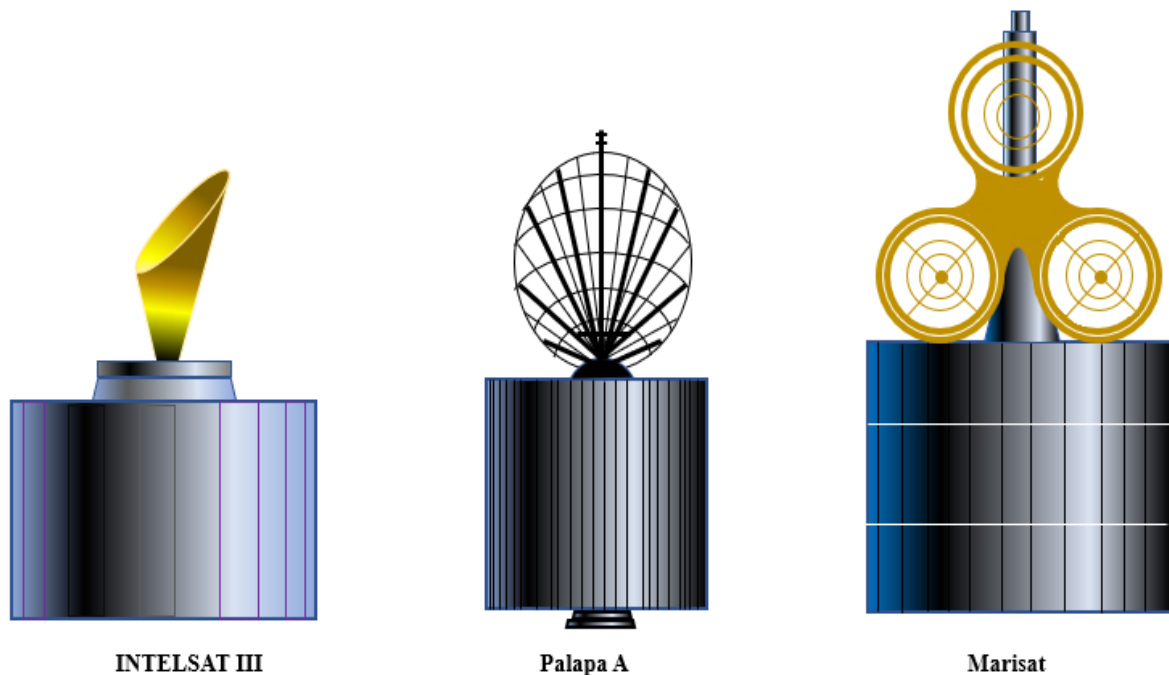


Figure 2.6: Spin-stabilized Satellites with A Mechanically Despun Antenna

Even though the spin-stabilized satellites with a mechanically despun antenna became the most used configuration, the larger communications satellites were in demand in the mid-1960's. Hughes Aircraft Company, under the direction of the U.S. Air Force, designed and built The Tactical Communications Satellite (TACSAT). It was the largest and most powerful communications satellite at the time when it was launched into synchronous orbit in 1969.

Unlike the INTELSAT III which was oblate in its inertia distribution, this satellite was prolate and spins about its minor principal axis of inertia. The platform is despun and Earth-pointing, while the rotor maintains gyroscopic stiffness. The spacecraft with large rotors and despun (oriented) platforms is called dual spinners. Most of the commercial communications satellites launched in the 1970's will have this configuration as shown by Figure 2.7.

When dual spinner satellite was introduced, it prompted the question of stability. The foregoing satellites all spin about the axis of maximum inertia, and it can be shown that, for a given amount of angular momentum, spin about the axis of maximum inertia has a lower kinetic energy than spin about any other axis. Hence, if there is a source of energy dissipation on-board the satellite, then spin about any other axis will be damped out, leaving pure spin about the maximum inertia axis, which is the desired state. When the satellite is made longer, by incorporating a longer solar array drum and a taller antenna farm, the spin axis becomes the axis of minimum inertia and energy dissipation makes this spin an unstable condition. Early designs, such as INTELSAT III, had relatively small platforms or despun antennas and rotors spun about the major spacecraft axis. Stability criteria were assumed identical to those of a single spinner, and flight performance demonstrated that the essentially stable. However, launch vehicle shroud constraints limited rotor diameters. The major axis stability condition effectively limited spinning spacecraft sizes. Nevertheless, larger communications satellites were in demand to provide more power from solar arrays fixed to the rotating drum of the satellite body and to provide multiple spot beams from large parabolic antenna dishes.

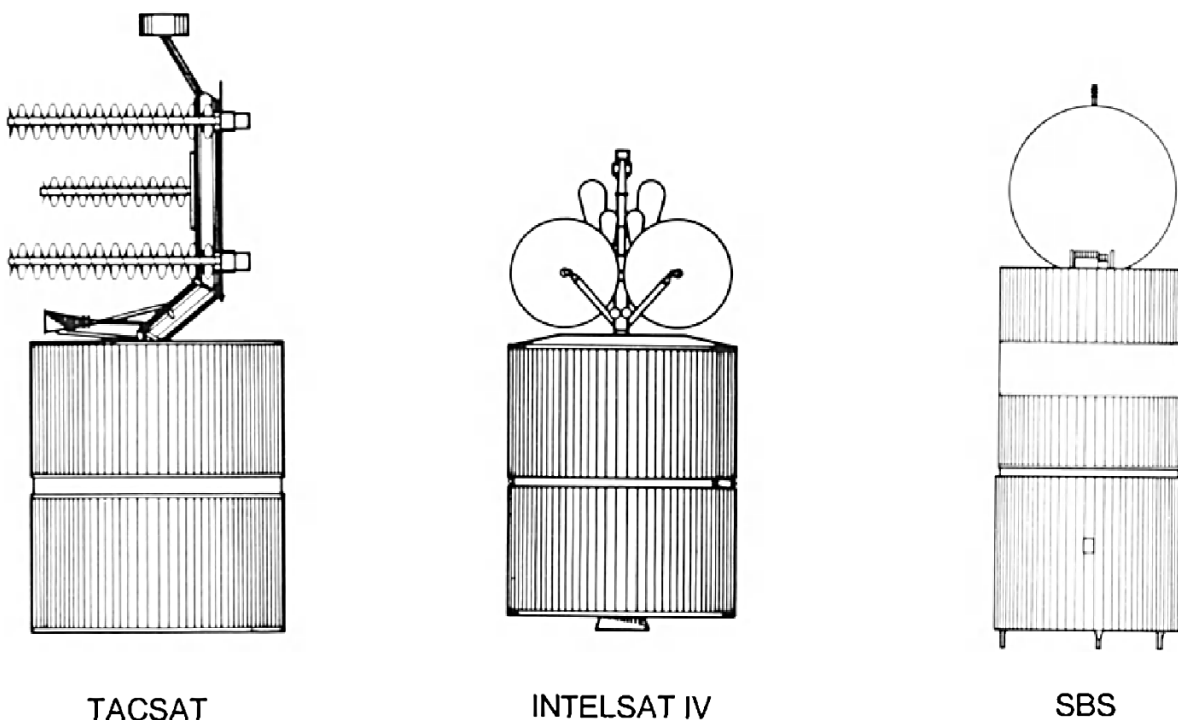


Figure 2.7: Dual Spinner Satellites [20]

The Tactical Communications Satellite (TACSAT) tried to bypass this limitation by implementing experimental dual-spinner whose rotor spun about the spacecraft minor axis. The primary problem was to devise appropriate stability criteria for such a configuration. Hughes Aircraft Company did develop a concept and labeled it *Gyrostat*, a set of conditions which were related to energy dissipation mechanisms in the platform and rotor. Briefly stated, the additional dissipating devices on the despun portion of a dual spinner would offset the destabilizing effect of dissipation in the rotor. Furthermore, a large nutation damper mounted on the platform would provide nutational stability about the minor axis. This development meant that the platform size no longer limited by inertia ratio constraints. The rotor need not be rigid, but it must not dissipate energy at a higher rate than the platform in order to be stable. TACSAT was launched in February 1969. The spacecraft performed successfully and followed by the INTELSAT IV.

In the field of Earth observation, spin-stabilized satellites have been applied in many meteorological missions from geostationary orbit. ATS-1 (Applications Technology Satellite) was the first experimental meteorological satellite systems in the equatorial synchronous satellite. Though intended as a communications satellite rather than as a weather satellite, it carried the spin scan camera. This camera was providing the first high-quality cloud-cover pictures taken from the Western Hemisphere. Today such images are an indispensable part of weather analysis and forecasting. After the successes achieved by ATS-1 which demonstrated the feasibility of using satellites in geosynchronous orbit for meteorology, NASA established the Synchronous Meteorological Satellite (SMS) program that developed two weather satellites, SMS-1 and SMS-2, which were launched in 1974 and 1975. The SMS satellites were spin stabilized spacecraft which preceded the Geostationary Operational Environmental Satellite system (GOES), operated by the United States' National Oceanic and Atmospheric Administration (NOAA) to supports weather forecasting, severe storm tracking, and meteorology research. The latest GOES's first generation (GOES-7) was operated until 2012.

In 1972, ESRO (European Space Research Organization) initiated Meteosat series that used spin-stabilized satellites for European meteorological program. The first generation of Meteosat satellites, Meteosat-1 to Meteosat-7, provided images every half-hour in three spectral channels (visible, infrared) and water vapor, via the Meteosat Visible and Infrared Imager (MVIRI) instrument. In 1990, with Eumetsat endorsement, ESA initiated the development of a spin-stabilized geostationary satellite with a 12-channel imager, called the 'Meteosat Second Generation' satellite. The spin-stabilized satellite should have a capability for air mass analysis as the essential part of the former sounding mission and a high-resolution visible channel (1 km resolution from 36000 km altitude). The provision of high-resolution imagery would enable to monitor significant weather evolution on a local scale [22]. A second-generation series of Meteosat was launched its first satellite (MSG-1) at 2002 and followed by three more satellites, ensuring operational continuity in GSO for at least 16 years.

The first three-axis stabilized communication satellite, ATS-6 launched in May 1974, has also been one of the most complex in configuration and in control. The spacecraft configuration used the 9 m diameter unfurlable antenna, fixed solar arrays 16 m tip-to-tip, and the communications and service module supported on trusses some 5 m from the antenna and solar arrays. The attitude control system comprised 3 reaction wheels, hydrazine thrusters, cesium bombardment ion engines, coarse and fine Sun sensors, IR Earth sensors, a Polaris star-tracker, RF sensing by interferometer and by monopulse, 3-axis rate gyros, yaw rate-integrating gyros, and re-programmable digital control electronics [23], [24]. The second three-axis stabilized communication satellite was the Franco-German satellite, Symphonie, that was also the first European geostationary broadcast satellite launched in December, 1974. This satellite pioneered the use of bi-propellant for the apogee boost motor, and momentum-bias for three-axis attitude control without measurement of yaw attitude. In retrospect it does appear to have some similarity to spin-stabilized configurations (the body-fixed solar arrays and the general disc-shape) but from the control system point-of-view the major step has been made.

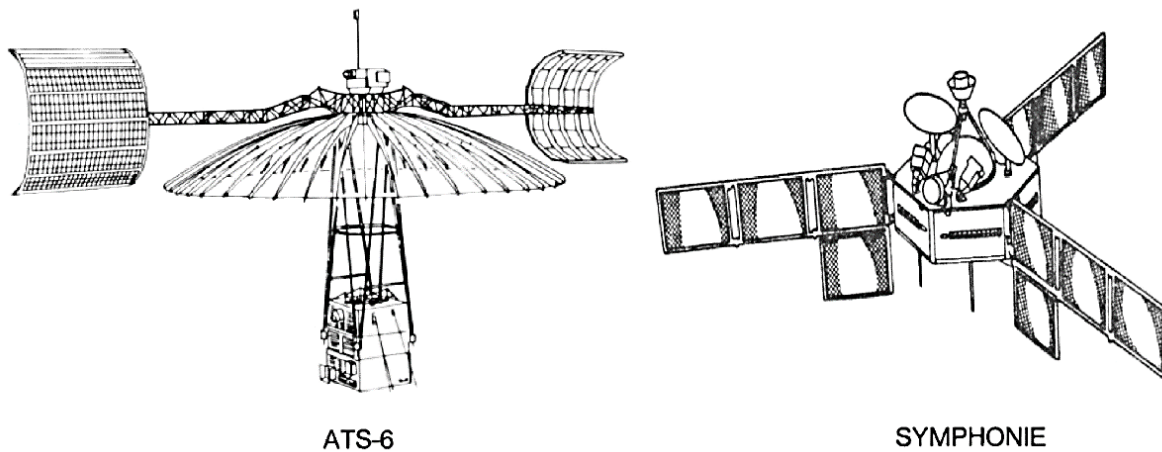


Figure 2.8: The Predecessor of Three-axis Stabilized Communication Satellites [20]

Further spacecraft configuration studies, driven by the need for higher satellite power to mass ratios, have resulted in the trend to three-axis stabilization with Sun-pointing solar arrays and Earth-pointing central body. In contrast to Symphonie, the solar arrays rotate to track the Sun while the body-fixed antennas track the Earth by employing a single, fixed-axis momentum wheel. The term three-axis stabilization means that all three geometric axes of the satellite are controlled to point in a given direction, whereas in spin stabilization only the spin axis is controlled to have a given direction while the other two axes rotate freely. The conventional axis set is shown in Figure 2.9, and the satellite axes are defined with following nominal orientations:

- the yaw axis (z) is in the plane of the orbit and it points to the center of the Earth,
- the roll axis (x) is also in the plane of the orbit pointing along the orbital velocity vector,

- the pitch axis (y) completes the right-hand set by being perpendicular to the orbit plane, and if the orbit inclination is zero then it points southward.

Establishing this new configuration, the two flight RCA Satcom satellites that implemented Sun-oriented solar array were successfully launched on December, 1975 and March, 1976 [25]. There was also a joint effort of Canada's Department of Communications and NASA to launch The Communications Technology Satellite (CTS/Hermes) in January, 1976. Meanwhile, ESA's first satellite in this field was the Orbital Test Satellite (OTS). Two of the experimental spacecrafts were built, but the first of the pair of OTS satellites (OTS-1) was lost at launch in the failure of its US Delta launcher in September 1977. OTS-2 was successfully launched in 1978. Those satellites have momentum bias. RCA Satcom was interesting to extend the use of magnetic torquing into geostationary orbit, while CTS used hydrazine and had very large solar arrays. Since then, this overall configuration of communication satellite has been used on many missions, e.g. Fleetsatcom, BSE, Anik B, and INTELSAT V. This three-axis stabilized configuration has virtually become the 'classical' pattern for all present satellites in the GSO, but with variations on the momentum bias configuration or with zero momentum.

After injection into synchronous orbit, the spacecraft is despun and the solar arrays and antenna reflectors are deployed, the spacecraft roll axis is aligned with the Sun line by firing hydrazine thrusters. Slowly rotating about the roll axis until the Earth is viewed by the geostationary Earth sensors, the spacecraft is then locked onto the Earth by switching the attitude control system to station keeping mode when the pitch axis is parallel to the Earth spin axis. Finally, momentum wheel is spun up.

In the normal on-station mode of INTELSAT V for example, pitch control is maintained by momentum bias. The momentum wheels operate 3500 rpm and provide nominally 35 Nms of stored momentum. Roll and yaw control is provided by firing small hydrazine thrusters. Three geostationary IR sensors provide Earth reference data: two redundant sensors scan the Earth east - west; a third redundant Earth sensor scans the Earth north-south. To allow repointing of the spacecraft for antenna pattern measurement, a pair of E-W and N-S scanning Earth sensors are used to provide a wide field of view [26].

The simplest momentum-bias system uses a single fixed momentum wheel aligned with the pitch axis. Both gas jet and magnetic actuators have been proposed for roll-yaw control. The system used on Fleetsatcom is a low-gain gas jet system, and a similar system is used on OTS and INTELSAT V. In this system, damping of the nutational mode is ensured by commanding two pulses from an offset thruster when a roll threshold is encountered. The first pulse drives the roll angle away from the threshold and into a nutational motion, and the second pulse is given after half the nutation cycle is complete which stops the nutation because it makes the satellite momentum vector coincide with the wheel momentum [20].

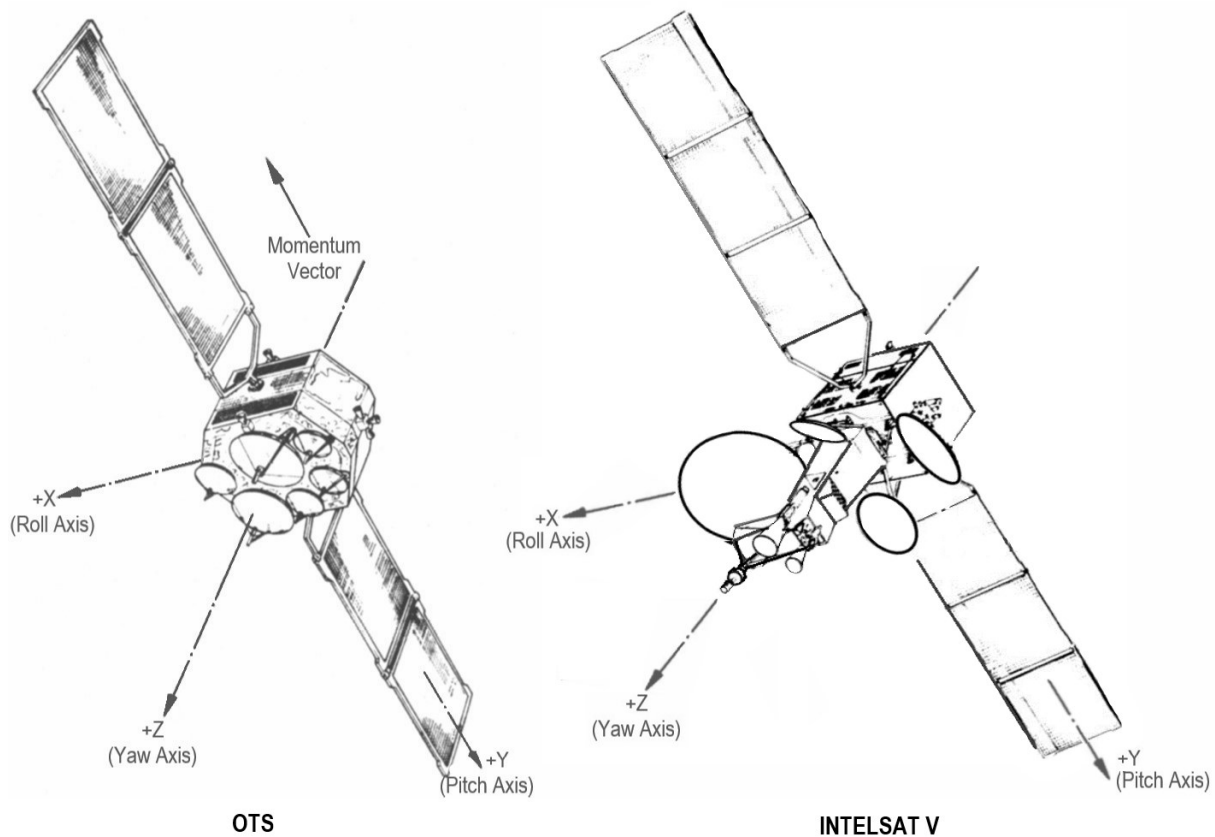


Figure 2.9: Earlier Generation of Three-axis Momentum Bias Stabilized Satellites in GSO [20], [26]

2.3 Momentum Bias Attitude Control in LEO

In the 1966 Harold Perkel presented of a three-axis system utilizing a single reaction wheel and magnetic torquer for controlling transverse momentum components. *Stabilite* is the name to this concept of controlling pitch, roll, and yaw such that pitch is maintained parallel to the orbit normal and yaw parallel to the local vertical (nadir). Thus, roll and yaw axes rotate once per orbit about the orbit normal. Originally, this concept was applied to the Television Infra-Red Observation Satellite (TIROS) weather satellite program, but has been used on the later Improved TIROS Operational System (ITOS) series [18]. This concept was the result of the series of satellite that evolved from a spin-stabilized spacecraft to a three-axis stabilized Earth-oriented platform, in which each of the three orthogonal axes were held to within one-half degree or better throughout the mission [27]. An adaptation of this *Stabilite* three-axis control technique was also applied successfully on geostationary RCA Satcom I and II which launched 1975 and 1976 [28]. These satellites were built by RCA Astro which became the base for many communication satellites that launched until 1996 as a standard configuration of Lockheed Martin AS-3000 spacecraft bus.

The TIROS series of world observation satellite is one of the NASA most successful programs and has pioneered in use of satellites for gathering data on the world's weather. The program was initially conceived as a series of experimental satellites designed to investigate the feasibility of making observations of weather on a worldwide basis from Earth satellites. The first satellite in the series was launch into Low Earth Orbit (LEO) within altitude about 600 km on April 1, 1960 by. The original design of TIROS (TIROS 1 - 8) employed simple spin stabilization. The limitations of this method of stabilization were recognized, but the conservative choice was made since the basic experimental mission could be carried out with this simple approach [29].

The cameras were mounted in the spacecraft with their optical axes along the spin axis of the satellite, which is the axis of maximum moment of inertia. TIROS 1 was injected into orbit with its spin axis lying in the plane of the orbit and tangent to the orbit at the point of injection, spinning at a nominal rate of about 10 rpm. The geometry of launch and injection were chosen so that, for the first few days or weeks in orbit the spin axis would point generally downward when the satellite was in the northern hemisphere. In the first several days following the launch of TIROS 1, the spin axis was precessing at an appreciable rate, e.g., tens of degrees per day. Detailed study led to hypothesizing that the satellite contained a residual magnetic dipole along its spin axis.

The theory showed that it would be possible to steer the spin axis in only a few possible directions, determined by the geometrical relationship between the spin axis at any time and the vector average of the Earth's magnetic field as seen by the satellite in a complete orbit. Nevertheless, it was found that, even with these restrictions, this simple magnetic torqueing scheme would allow sufficient control of the spin-axis direction to achieve useful pictures every day and thus avoid the dead periods caused by the precession of the orbit plane. Such a steering coil was then incorporated into TIROS 2 and all subsequent vehicles through TIROS 8. The current in the coil could be selected to be either zero or any other values, either plus or minus, by ground command.

The new method of stabilization employed in TIROS 9 uses the satellite in the wheel configuration. In this mode of operation, the satellite is still spin-stabilized and is launched into orbit in the normal fashion with the spin axis lying in the orbit plane and tangent to the orbit at the point of injection. However, the satellite is immediately precessed, using a magnetic torqueing scheme, until the spin axis is perpendicular to the orbital plane, at which time the satellite appears to be rolling around the Earth on its orbital track. In TIROS 9 an additional magnetic coil, the plane of which contains the spin axis, is used to generate torques which can be used to control the spin rate of the spacecraft as well. This system has worked very well on TIROS 9. The spin axis is routinely maintained in alignment with the orbit normal to within 0.5 degree. This result lead to the so called *Stabilite* concept of three-axis attitude control for spacecraft.

An examination of the basic ideas behind the TIROS 9 attitude control system shows that it depends upon the provision of stored angular momentum to provide gyroscopic stability in the spacecraft, together with magnetic torquing schemes to provide the means to maintain the vector of stored angular momentum perpendicular to the orbit plane and to make it possible to maintain a constant speed of the spinning spacecraft. The stored angular momentum is fundamentally necessary to the scheme in order to ensure that the existing disturbing torques can cause only very slow changes in desired orientation and spin rate, so that the control loops need not have high response and can be closed through a ground command loop. Detailed analysis of system performance has shown that pointing accuracies about all three axes of 1.0 deg are easily obtainable; performance better than 0.5 deg is altogether feasible. The "jitter" rate (that is the spurious rates of motion of the local-vertical-oriented axes of the spacecraft) can be held to 0.01 deg/s.

Figure 2.10 illustrates a satellite which uses *Stabilite*. The single momentum wheel is the chief active element and is the only moving part in this attitude control system. Yaw and roll axes are controlled by magnetic torquing, which refers to an interaction with the Earth's magnetic field to provide torque in the yaw and roll directions. The pitch axis is controlled by changing the wheel speed. Periodically a net excess or deficit of momentum can also be corrected by magnetic torquing. Reaction jets are incorporated as backup control elements. A simple coil is wound with its plane normal to the spin axis, and a current is passed through this to produce a dipole moment parallel to the spin axis. One coil is sufficient to control both roll and yaw because of gyroscopic coupling between these two axes [30].

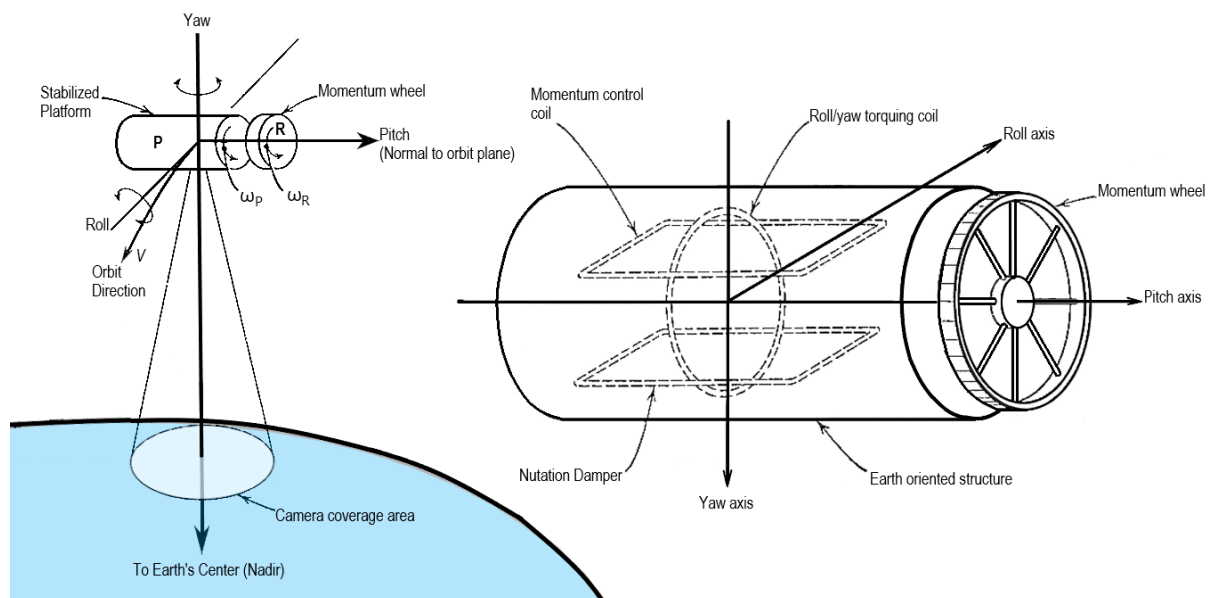


Figure 2.10: Simplified Schematic of *Stabilite* and Its Control Elements [30]

Another famous mission that implement momentum bias in LEO was SEASAT. SEASAT (also referred to as SEASAT-A prior to launch and SEASAT-1 after launch) was flown in 1978 as a

pioneering Earth observation experimental mission using spaceborne imaging radar instrument (SAR) of NASA/JPL. Weighing about 1800 kg, the satellite was three-axis stabilized and operated from near-polar orbit at an altitude of 800 km. The spacecraft control system was a momentum adaptation of the *WHECON* control concept as shown in the Figure 2.11. *WHECON* is an acronym for *WHEEL CONTROL*, the one-wheel control system with thrusters. The significant feature of the roll-yaw control is the placement of the thrusters so that the roll and yaw are purposely cross-coupled. In this system, the horizon sensor is the single attitude reference. It provides pitch and roll attitude signals. Pitch control modulates the reaction wheel around from bias level. The roll error after compensation regulates the cross-coupled roll-yaw valves. A roll-yaw thrust will give a plus roll torque associated with a minus yaw torque. Similarly, negative thrust gives a negative roll torque and positive yaw [31].

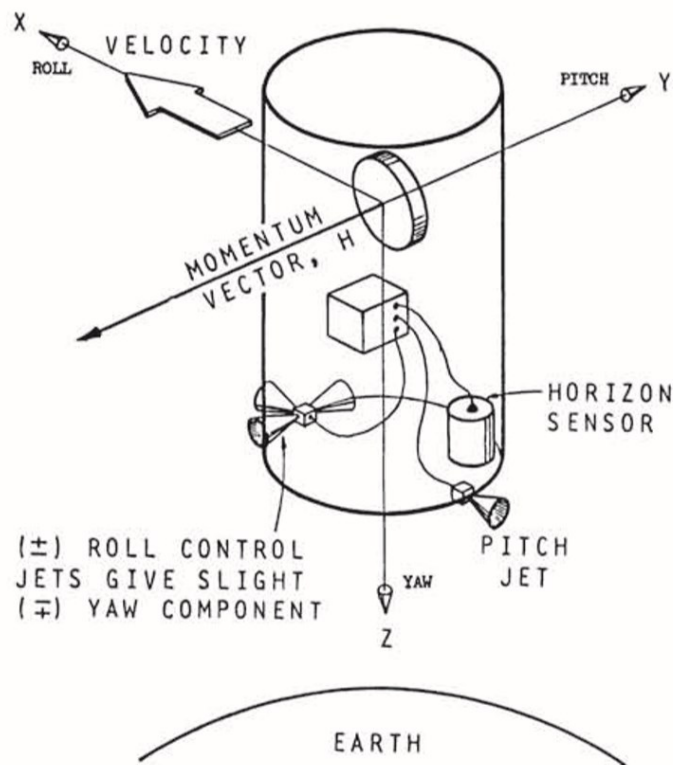


Figure 2.11: The Schematic of WHECON Attitude Control [31]

The SEASAT attitude control subsystem required functions are to:

1. provide three-axis attitude control during powered and coast phases of ascent through injection into final circular orbit,
2. provide attitude control during orbit adjust and trim phases,
3. provide three-axis attitude control to within ± 0.5 deg (3σ) throughout the 3-year mission,
4. provide attitude signals enabling the determination of payload sensor pointing direction to within ± 0.2 deg (3σ).

These functions were met in system design and subsequently verified in the flight operation. Four reaction momentum wheels are used for attitude control. Two of these are the scan wheel to provide not only control momentum but have bolometer detectors attached which are processed to give horizon sensor data. A large pitch wheel provides bias momentum. The roll wheel completes the set and allows coupled control operation with the scan wheels. Wheel speed data combined with the magnetometer produces commands to the magnets to produce torques which desaturate the wheels. The physical arrangement of control hardware on the SEASAT spacecraft is depicted in Figure 2.12.

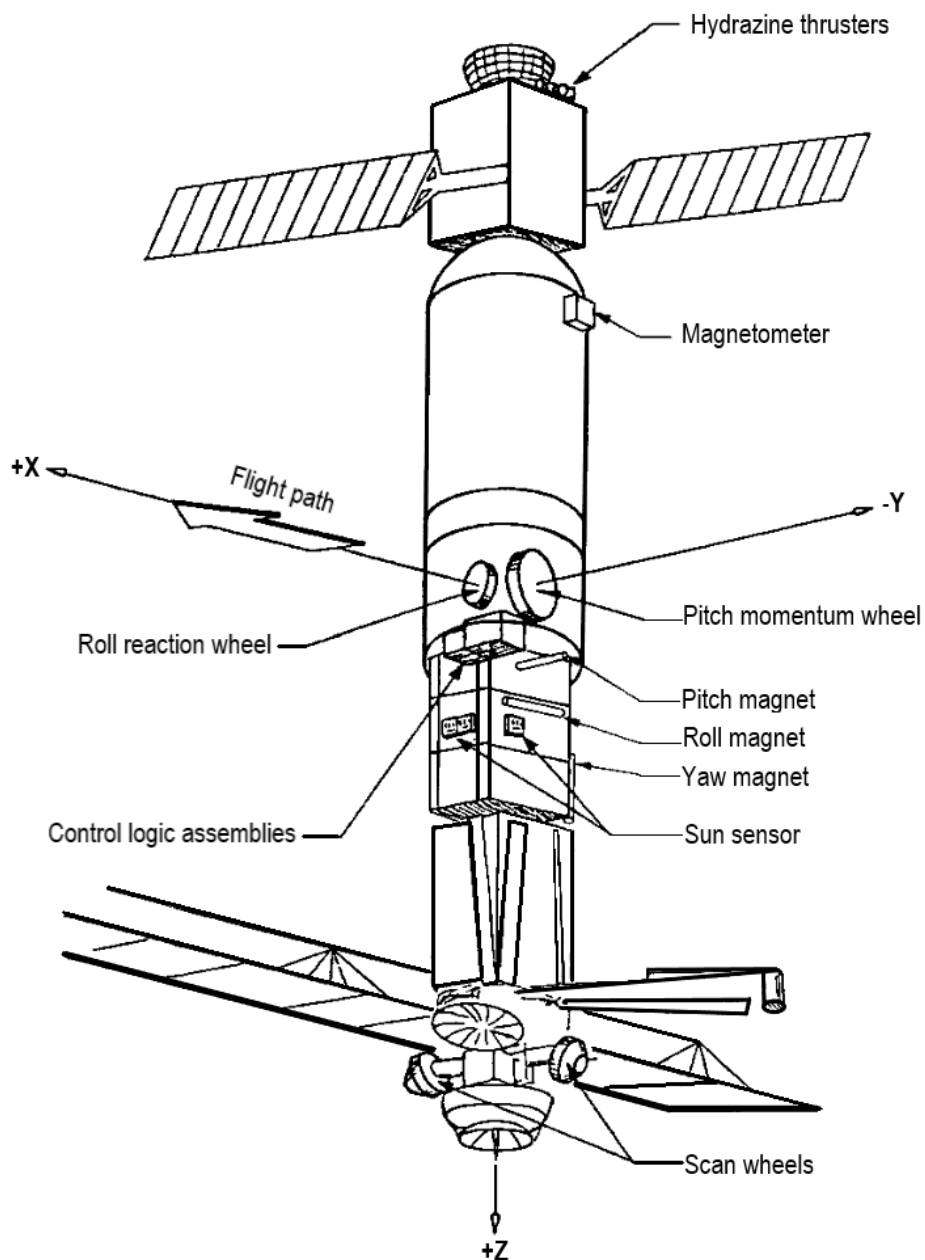


Figure 2.12: SEASAT On-Orbit Control Hardware [32]

The system regulates changes of the momentum components in pitch, roll, and yaw in response to horizon sensor-measured pitch and roll signals to maintain pitch and roll attitudes to within ± 0.2 deg. The yaw axis is restrained by a bias momentum along the negative pitch axis, chosen large enough to keep yaw within limits of ± 0.65 deg. The bias momentum is established by a 20 Nms momentum wheel aligned in pitch together with the net pitch momentum bias established in a pair of 2 Nms scan wheels. Changes in pitch momentum are achieved by a $\pm 10\%$ modulation of pitch wheel speed. Yaw nutation damping is provided by differentially changing the speed of the scan wheels to changes the yaw components of momentum of the canted scan wheels. Roll torques are produced by changing the speed of a roll axis reaction wheel.

The early 1980s ushered in the beginning of the era of the new generation small satellite. Physically small satellites by themselves were nothing new; many of the early U.S. and Soviet satellites and later experimental satellites from other nations would fall into small satellite classification so that, over the last 60 years, some 1500 satellites under ~ 100 kg have been launched worldwide. However, what differentiates the later generation of small satellites was the combination of a different management approach with the use of commercially available microelectronics devices to create reprogrammable, reconfigurable satellites capable of sophisticated functions with high utility in a fraction of the volume, mass, cost, and timescales.

In the earlier emerging of new generation small satellite, within limitation of its mass, weight and space, most of the missions using passive attitude stabilization. However, as small satellite technical capabilities gradually developed throughout the 1990s, interest grew in their use for technology demonstration and verification. A series of microsattellites demonstrated steadily improved EO capabilities so one of small satellite built by Surrey Satellite Technology Ltd. (SSTL), TMSat (ThaiPhutt) launched in 1997, became the first multispectral imaging microsatellite to achieve 300-m GSD (NIR, red, green, blue). It was achieved by using three-axis momentum bias approach in combination with the implementation of 6 m gravity gradient boom. The success of TMSat mission has been the baseline for the next subsequent SSTL's small satellite product such as TiungSat-1, UoSat-12, Alsat-1 and so on [33]–[35].

UoSAT-12 is an SSTL developed proof-of-concept mission in low-cost minisatellite engineering techniques. Started in 1996, the design of a new standard minisatellite platform was aiming to demonstrate and qualify the new platform, up to 400 kg weight, to fly an Earth observation package and to qualify new technology for flight on subsequent missions. Its structure is essentially hexagonal with a height of about 1 m and a diameter of 0.6 m, supporting a payload mass in the range of 50 to 150 kg.

The orbit control and determination system comprise a GPS receiver, and a cold gas thruster system. Both are also an integral part of attitude control and determination system. The attitude control actuators include: two SSTL developed reaction wheels, one Ithaco momentum wheel, cold-gas reaction jets, magnetorquers, and a gravity gradient boom. The sensors include: three

three-axis magnetometers, four two-axis analog Sun sensors, a GPS receiver, and two star-cameras, an Earth sensor and a magnetometer and a solid-state gyro. The three-axis control system maintains Earth pointing to an accuracy of 0.5 deg, with an experimental target of 0.1 deg, for Earth observation payloads and communication antennas. The spacecraft attitude can be operated in momentum-biased mode, zero momentum mode, or in gravity gradient mode. Additionally, UoSAT-12 carries an electric propulsion system, a 90 W resistojet producing 93 mN of thrust, which uses nitrous oxide as its working fluid.

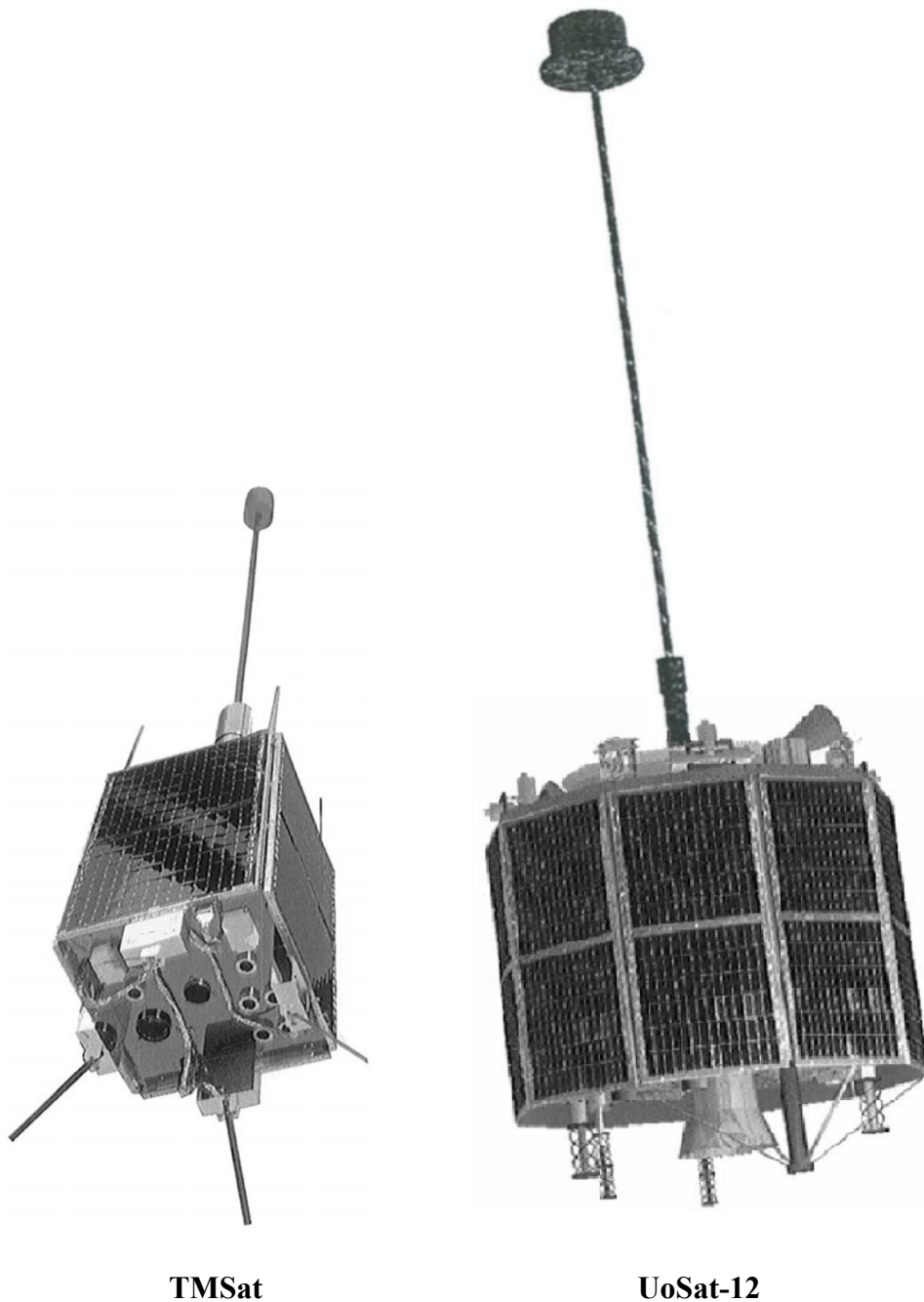


Figure 2.13: Combination of Gravity Gradient and Momentum Bias Stabilization on Small Satellite [36]

Table 2.5: Attitude and Orbit Determination Sensors Onboard UoSAT-12 [37]

| Parameter | Manufacturer | Quantity | Type | Range | Accuracy | Power |
|------------------------------|-----------------------|------------|-------------------------|---|----------------------------|--------|
| Magnetometer | SSTL (2), Ultra (1) | 3 units | Flux gate | $\pm 60 \mu\text{Tesla}$ | 30nT (3σ) | <0.8 W |
| Sun sensors | SSTL | 4 x 2 axis | slit & photo cell | $\pm 50^\circ$ | 0.2° (3σ) | <0.1 W |
| Horizon sensor | Servo-MIDES, SSTL I/F | 1 x 2 axis | IR pyro array & chopper | $\pm 5.5^\circ$ | 0.06° (3σ) | 2.8 W |
| Star sensor | SSTL | 2 units | CCD matrix | $14.4^\circ \times 19.2^\circ$ $+1.0\text{-}6.0 \text{ m}_v$ | 0.02° (3σ) | 4 W |
| Rate gyro | BEI, SSTL I/F | 1 unit | Gyro chip | $\pm 5^\circ/\text{s}$ | $0.02^\circ/\text{s}$ | 1.4 W |
| GPS receiver SGR-20 model | SSTL | 1 unit | MITEL chip set | 24 channels 4 antennas | 50 m (1σ) | 5-7 W |

Table 2.6: Attitude and Orbit Control Actuators Onboard UoSAT-12 [37]

| Parameter | Magnetorquers | Reaction/Momentum Wheels | Propulsion System |
|-----------------|--|--|--|
| Manufacturer | SSTL | SSTL (2), Ithaco (1) | SSTL & Polyflex |
| Quantity | 8 x PCB, 4 x Wire coils | 3 units, (x/y/z) | 10 x N ₂ CG thrusters |
| Type | Air core | Brushless DC motor Dry lubricated bearings | 4 bar cold gas N ₂ O plus 100 W heater |
| Operation range | x/y = $\pm 14.2 \text{ Am}^2$ z = $\pm 13.3 \text{ Am}^2$ | $\pm 4 \text{ Nms @ } \pm 5000 \text{ rpm}$ $\pm 0.02 \text{ Nm max}$ | 0.125 N (R-jet) $\Delta v = 14 \text{ m/s (CG)}$ 9.7 m/s (R-jet) |
| Power | 20 W max (80% duty cycle) | 2.8-14.6 W (zero to max acceleration) | 3 W (CG) 100 W (R-jet) |
| Operation | PWM controlled | Speed controlled | PWM controlled |
| Accuracy | 20 ms min pulse | $\pm 1 \text{ rpm}$ | >10 ms pulse (CG) >600 s pulse (R-jet) |

In the early of new generation small satellite, there was also an educational program including the design, manufacture, testing, launching and operation of microsatellites, named TUBSAT, that was initiated in 1986 for students at the Technical University of Berlin (TUB). TUBSAT is a program to define, design and built the microsatellite series in a low-cost and fast-turnaround. The objective is to explore technical capabilities in microsatellite design, especially in the field of attitude determination and control, and space-related applications. Meanwhile not only students but also engineers from space agencies in Germany (DLR-TUBSAT), Morocco (MAROC-TUBSAT) and Indonesia (LAPAN-TUBSAT) participate in this program.

The first experimental platform, TUBSAT-A, the attitude of spacecraft is not controlled but very precisely reconstituted via a three-axis magnetometer and mainly the star sensor. Figure 2.14 shows a typical sequence of 16 superimposed star pictures at 0.5 sec intervals. This raw star data contains a few single spots (i.e. sensor noise) and missing star pictures. Then star sensor processor eliminates the noise, interpolates the missing stars and identifies several star tracks. The experiment was very valuable for the next mission (TUBSAT-B) because: a) the star sensor could be qualified and calibrated, b) the dynamic behavior of the spacecraft could be analyzed and c) the disturbance torque environment could be established, so that the appropriate size of the reaction wheels for TUBSAT-B could be identified. TUBSAT-B was three-axis controlled and provided with high accuracy (arc sec) attitude control to any desired direction via star sensor plus 3 reaction wheels. Each wheel, within 1 kg mass, can be accelerated and decelerated with a reaction torque of up to 60 mNm and reach their nominal angular momentum of 0.1 Nms within seconds [38].

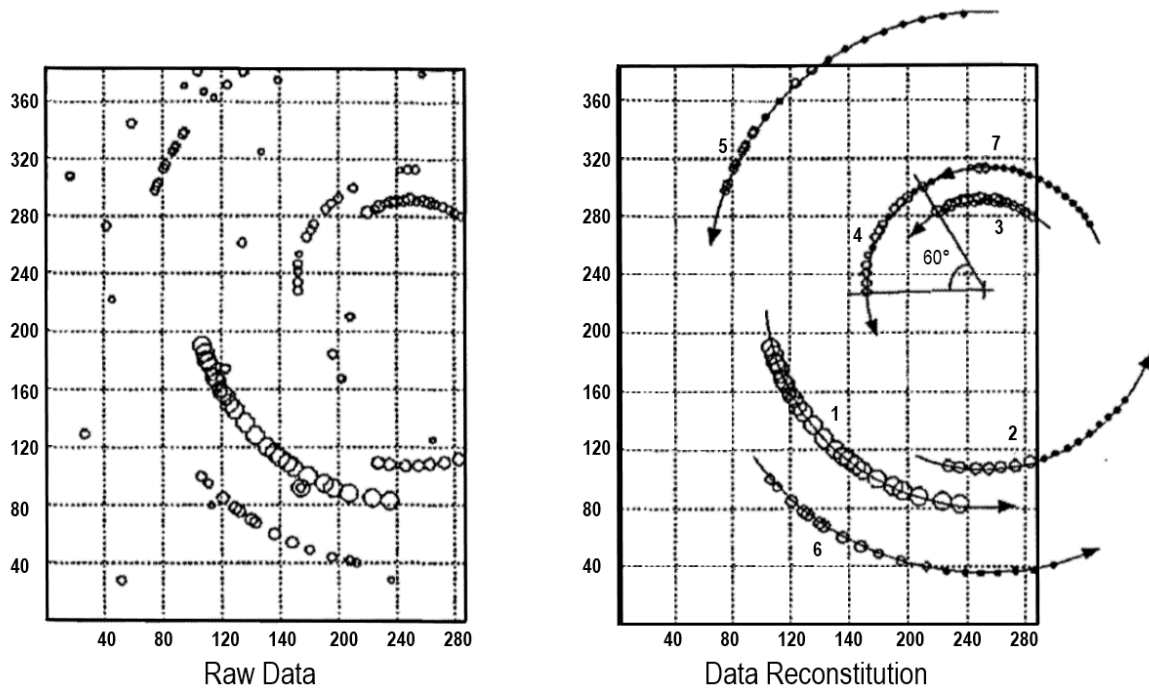


Figure 2.14: Reconstitution of Star Data on TUBSAT-A [38]

Based on the experience gained with TUBSAT-A and TUBSAT-B, an attitude control unit of minimal dimensions has been developed for the DLR-TUBSAT microsatellite. The objective of the DLR-TUBSAT mission is to show the degree of pointing accuracy, in both static and dynamic, that can be achieved. This basic design of the attitude control system composed of three different components: a three-axis star sensor with an integrated star recognition software, 3 fiber optic laser gyros and 3 reaction wheels. The attitude control design of the DLR-TUBSAT microsatellite facilitates inertial stabilization as well as dynamic stabilization to obtain constant and variable angular velocities. Research tasks are inertial pointing on one hand and target pointing on the other hand [39].

Table 2.7: Overview of the TUBSAT Program

| Satellite | Payload Class | S/C Mass | Launch Date |
|------------------|----------------------|-----------------|---------------------------|
| TUBSAT-A | S&F communications | 35 kg | July 17, 1991 by Ariane-4 |
| TUBSAT-B | Earth observation | 45 kg | Jan. 25, 1994 by Tsyklon |
| TUBSAT-N, N1 | S&F communications | 8 kg, 3 kg | July 7, 1998 by SHTIL |
| DLR-TUBSAT | Earth observation | 45 kg | May 26, 1999 by PSLV |
| MAROC-TUBSAT | Earth observation | 47 kg | Dec. 10, 2001 by Zenit |
| LAPAN-TUBSAT | Earth observation | 56 kg | Jan. 10, 2007 by PSLV-C7 |

For inertial pointing, an angular momentum vector is generated by means of the on-board magnetorquer that is perpendicular to the optical axis of the 1 m lens. The angular momentum vector is then taken over by the wheel which is located on this axis. This momentum bias stabilization is advantageous because two axes are passively pre-stabilized. The difficulty is, however, to control the pitch axis and to attenuate the nutation of the satellite. The aim of the in-orbit tests is to show the maximum pointing accuracy of the attitude control system in the range of the possible resolution of the sensor used.

Apart from the inertial pointing accuracy, evidence is to be supplied showing that the field of high-resolution earth observation from different visual angles can be covered autonomously by future microsatellites. In contrast to inertial pointing, it is of advantage here to integrate another sensor as a forefield sensor to facilitate orientation. The DLR-TUBSAT microsatellite is therefore equipped with two optical sensors consisting of a 16 mm and a 50 mm lens. The Earth observation within a target pointing scenario should take the following steps. First the tumbling motion of the satellite, which is sensed via the fiber-optic laser gyros, is buffered by the reaction wheels. Subsequently, inertial attitude determination can be carried out with the help of the star sensor using a star recognition system. This is the basis for a subsequent slew maneuver in the course of which the optical axis is directed towards earth.

The picture from the forefield sensors can be transmitted to the ground station via the analogue S band data link. At the ground station the angular velocity of one axis of the satellite is then interactively changed to prevent the target aimed at from moving during the period of exposure. For fine adjustment the station then switches over to the higher resolution camera (1 m lens) and proceeds in the same way. The control mode was very impressive since the satellite attitude and hence camera pointing was simply controlled via keyboard, joystick, or mouse control commands from a ground station terminal. This interactive control mode differs from all other previous existing Earth observation projects and have been successfully introduced by DLR-TUBSAT.

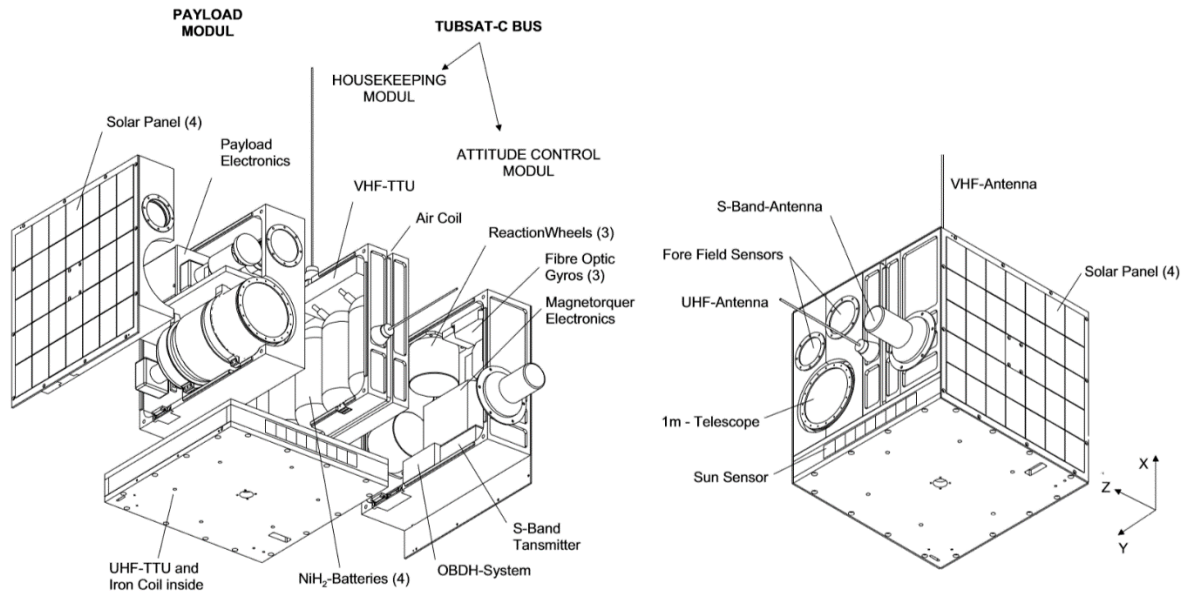


Figure 2.15: DLR-TUBSAT Satellite [40]

The capability of miniaturized momentum-based attitude control unit has been demonstrated by DLR-TUBSAT microsatellite. The small reaction wheels, developed by the Technical University of Berlin (TUB), have an integrated wheel drive electronic (WDE) with a micro controller to provide flexible operation modes such as current control, wheel speed control and torque control. Furthermore, the WDE could also perform close-loop control by connecting the reaction wheel to fiber-optic gyro via a serial communication interface in which both are mounted in one body axis of the satellite. The micro controller of the WDE receives the angular velocity from the gyro four times per second and calculates an accumulated angle. Establishing close-loop control between the reaction wheel and gyro by WDE would provide two high level attitude control modes i.e. angular velocity control and angle control in one axis of the spacecraft. With three of them working independently in each body axis as depicted in the Figure 2.16, the spacecraft could perform three axis stabilized attitude control. The highly integrated wheel-gyro was designed especially for microsatellites with requirements in the field of low power consumption, low mass, small volume, and simple connection through serial interfaces.

The successful operation of DLR-TUBSAT has been strengthen the confident to deploy the small satellite in the space application. MAROC-TUBSAT, the sixth satellite of TUB, is a cooperation project between the TUB and CRERS, Rabat, Morocco. The primary concept is a decentralized system, which is primary used for the automated operation of the satellite. The MAROC-TUBSAT design and operation strategy, especially the easy to understand momentum bias attitude control system. The momentum bias standby mode makes it possible to take a picture of any place in the world and send the picture data down within one day, by using only one ground station [41]. Subsequently the experiences gained by DLR-TUBSAT and MAROC-TUBSAT have been further utilized in the development of LAPAN-TUBSAT microsatellites.

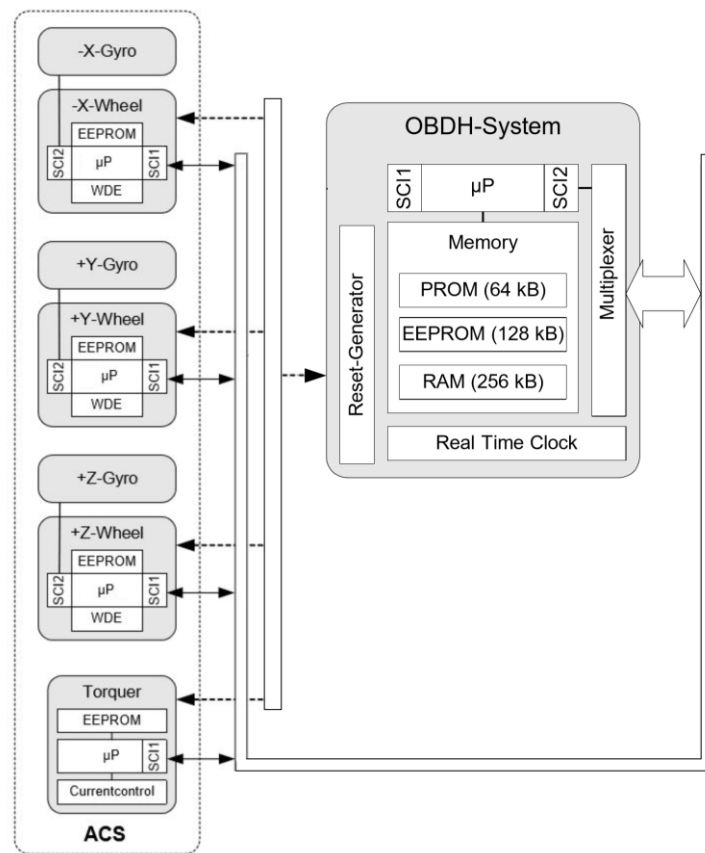


Figure 2.16: System Architecture of DLR-TUBSAT's Attitude Control System [40]

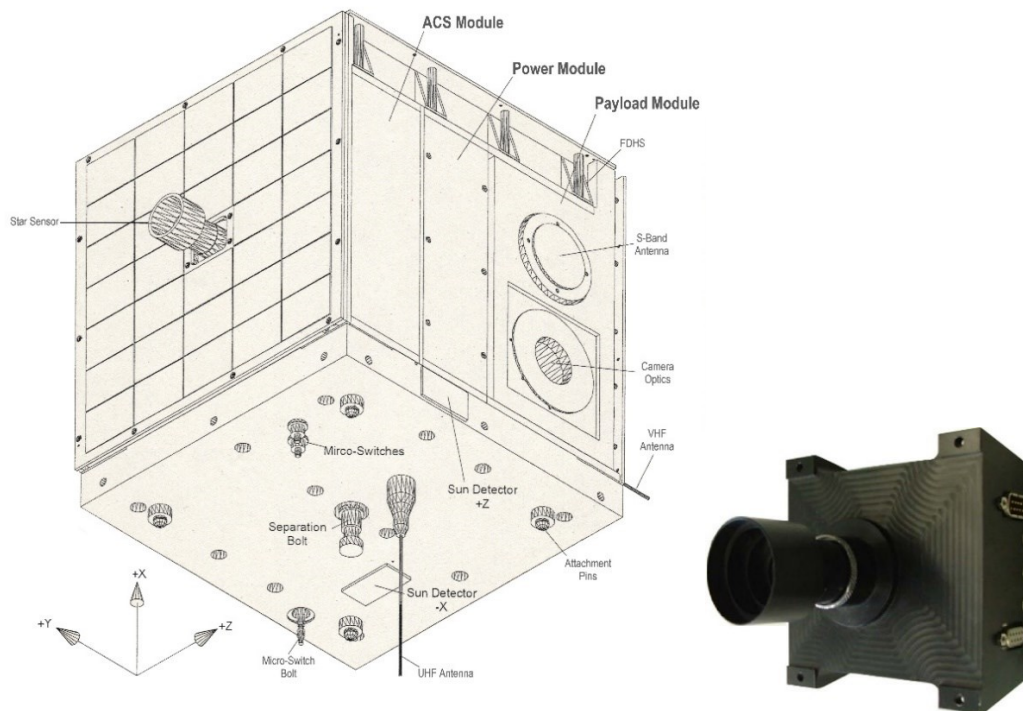


Figure 2.17: MAROC-TUBSAT Satellite and Its Star Sensor [42]

Another model of small satellite that applied momentum exchange technique was Korean satellite, KITSAT-3. The main objective of KITSAT-3 is to test and demonstrate the new satellite bus and its payloads. The pushbroom type remote sensing imager required a pointing accuracy 0.5 degree with 0.014 deg/s stability of the platform for quality images. Attitude of the box-like satellite (495 mm x 604 mm x 852 mm) is sensed by a Sun sensor (two-axis), Earth horizon sensor, star sensor (CCD type), fiber optic gyro, and a three-axis magnetometer; control is provided by a three-axis magnetorquer and a reaction wheel as actuators. Basically, all the proposed operation modes are controllable with the pitch torque as shown by Figure 2.18. However, due to 22.5° tilt along the roll axis for maximum solar power, it cannot take advantage of the simplicity of a single momentum wheel system [43].

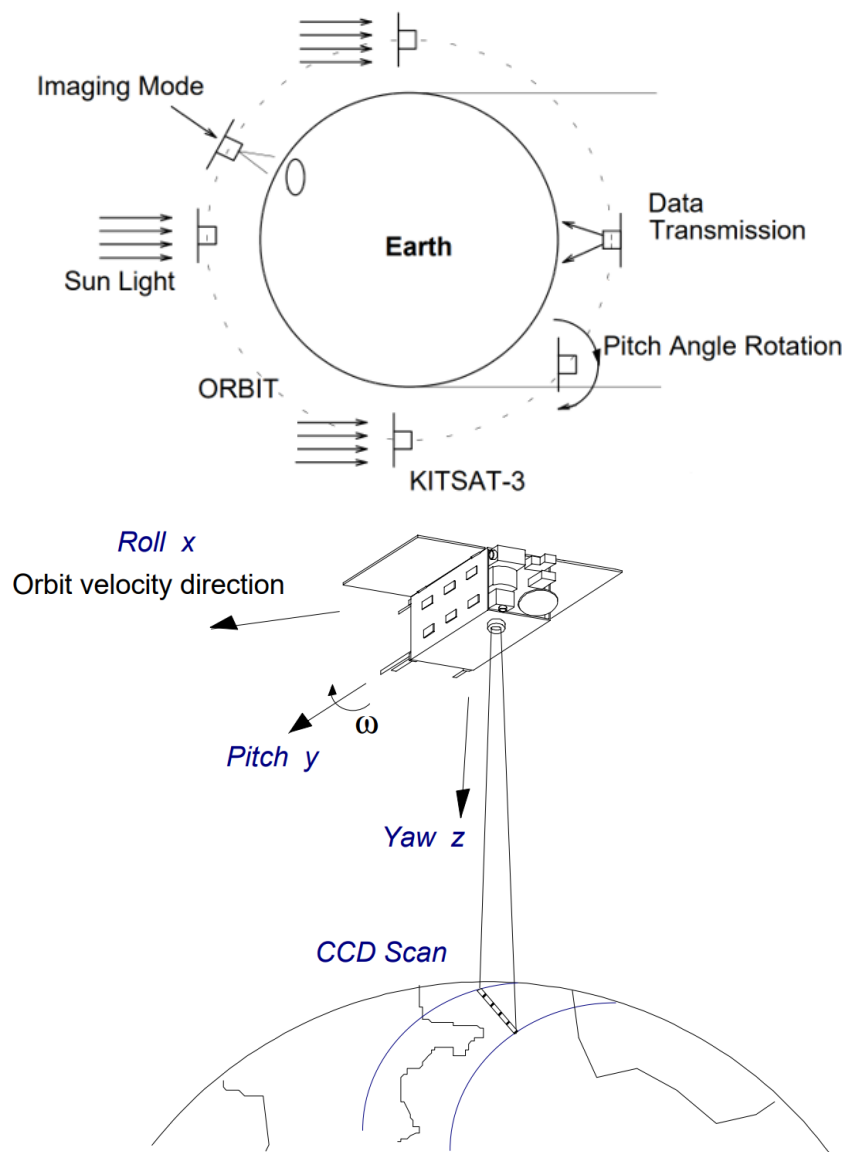


Figure 2.18: KITSAT-3 Operation Mode [43]

3 IMPROVEMENT OF THE STATE OF THE ART BY LAPAN-A SATELLITE SERIES

Small satellites are more greatly affected than standard-sized satellites by attitude disturbances because of their relatively small moment of inertia. The effect of disturbance torques, which may be considered small on standard-sized satellites, become dominant in small satellites [44]. The most effective method for small satellites with small moments of inertia to gain stability is momentum bias. By rotating motion, they will gain gyroscopic stability, so the disturbance torques will only cause a small precession to the spacecraft. However, the spacecraft will also experience small oscillations on its axis of rotation, which is called nutation that occurs when the axis of rotation is not perfectly aligned to the principal axis of inertia.

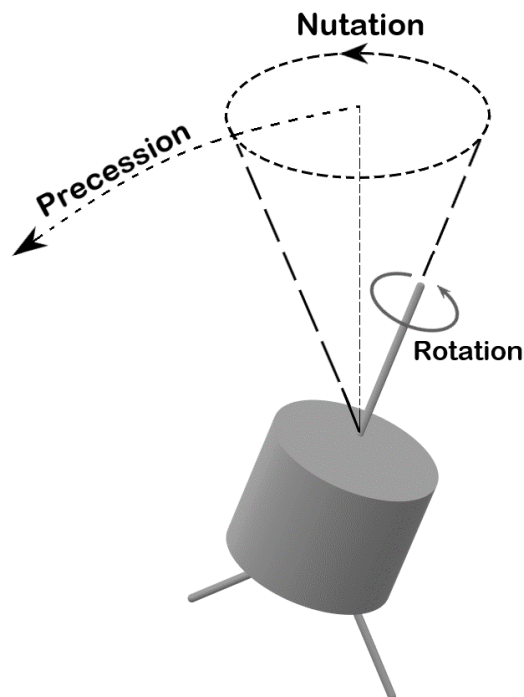


Figure 3.1: Precession and Nutation of Spinning Satellite

The concept of momentum bias is very popular in geosynchronous equatorial orbit (GEO) because the disturbance torque caused by solar pressure is easily understood and compensated

for. However, dealing with disturbance torques in low Earth orbit (LEO) is more challenging. The source of disturbance torque at LEO is more complex, there are gravity gradient, solar pressure, atmospheric drag, and magnetic field. The atmospheric drag is generally negligible above an altitude of 500 km. Meanwhile, gravity gradient and magnetic field that are neglected in GEO, they are very dominant in LEO. An incautious handling of magnetic and gravity gradient disturbances will quickly lead the satellite's attitude control system into uncontrolled momentum precession and saturation conditions, where the wheels can no longer absorb all the momentum. Therefore, not many satellites use momentum bias in LEO. This thesis presents the attitude control of LAPAN-A satellite series which have found an approach for implementing the momentum bias method in LEO, both polar and equatorial, that matches the characteristics required by a small satellite:

- **Efficient**, by using minimum instruments so only required devices are active, hence it needs less power for operation.
- **Full performance**, by overcoming the drawback of the general momentum bias system and performing high accuracy pointing.
- **Reliable**, by decentralizing the attitude control system to reduce complicated in the main computer, very simple testing before launch, and adaptive for new operation method and approach.

3.1 Momentum Bias Attitude Control of LAPAN-A Satellite Series

The first LAPAN satellite series is a polar orbiting satellite, LAPAN-A1. It was designed for 3-axis interactive attitude control to support high-resolution video surveillance mission with the spatial ground resolution about 5 m on a swath width of 3.5 km. Unfortunately, the star sensors didn't work at the equator and failed completely after one year. Once the star sensor was completely gone, the wide-angle video camera acted as a horizon sensor for a new approach to attitude determination. However, this video camera was only available once a day when the satellite was in contact with the ground station. For the continuation of the mission, momentum bias attitude control is applied to utilize gyroscopic stability as a robust attitude control, so that it can bridge longer phases where attitude information was not available. By applying the proper technique for disturbance torque compensation in this mission, momentum precession can be suppressed better than systematic gyro drift [45].

After losing its star sensor, a new effective approach was introduced into LAPAN-A1 satellite operation to control angular momentum using a wheel and magnetic coil as actuators and overcoming the limitations of spacecraft lacking the horizon sensor and the on-board magnetometer commonly used to measure magnetic fields. The determination of angular momentum direction uses a video camera as a horizon sensor even though it is available once

a day of ground station contact. This idea is effective if only the disturbance torque has been characterized and the angular momentum has been established. After the video camera gives attitude information the satellite operator tries to control the direction of angular momentum by over or under-compensate the disturbance torque using magnetic coil. On LAPAN-A1 satellite, the disturbance torque level is in the order of 10^{-5} Nm, i.e. 10% of the maximum coil torque. This approach converts the magnetic and gravity gradients torque into control torque and is described in more detail in section 5.1.3.

The second LAPAN satellite series is an equatorial orbiting satellite, which is designed, integrated and tested in Indonesia, LAPAN-A2. This satellite carries two cameras, the first one is the same model as flown on LAPAN-A1 with a video analog output, the second camera has a digital image output with the spatial ground resolution about 4 m on a swath width of 7 km. It is designed for autonomous operation, there are nadir pointing, interactive pointing, and lunar pointing mode. LAPAN-A2 satellite has two star sensors to support the continuous operation on the equatorial orbit with the variation of Sun illumination as depicted in Figure 3.2 and Figure 3.3. However, one of its star sensors failed in the initial orbital phase, so autonomous operation does not function properly.

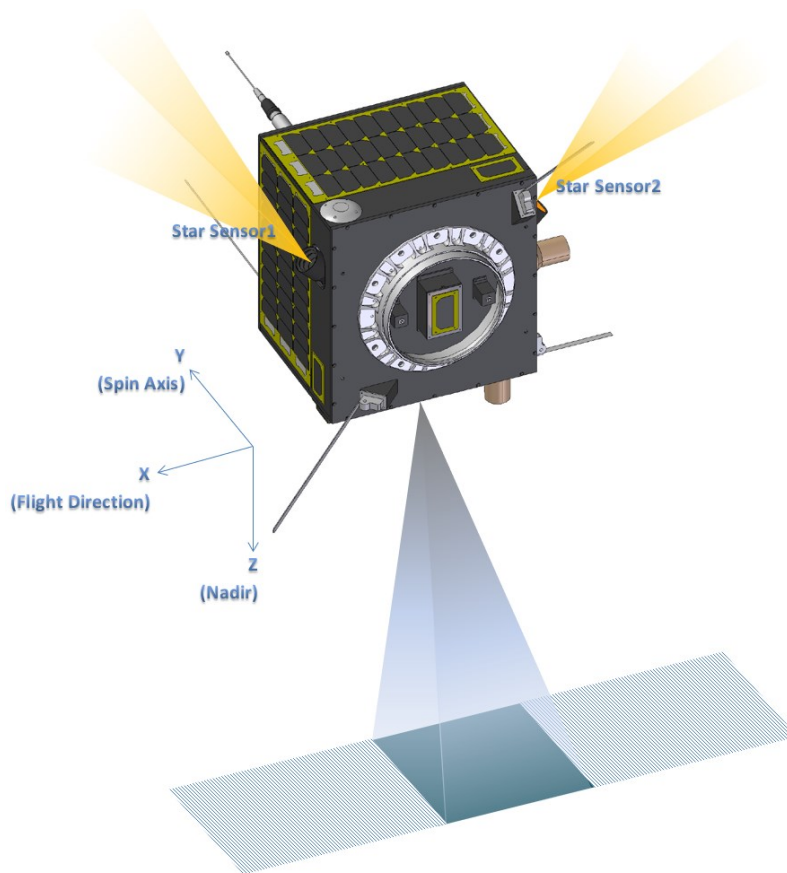


Figure 3.2: Flight Configuration Design of LAPAN-A2 Equatorial Satellite [46]

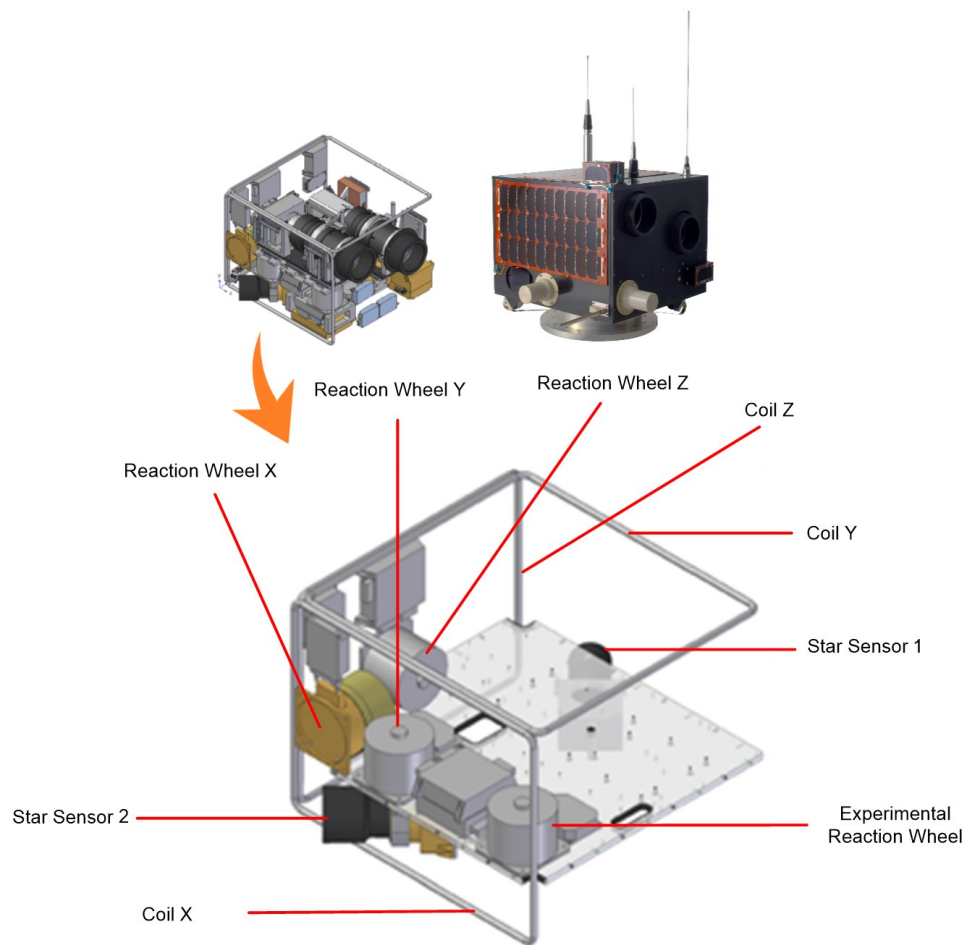


Figure 3.3: Layout Design of LAPAN-A2 Attitude Control System [46]

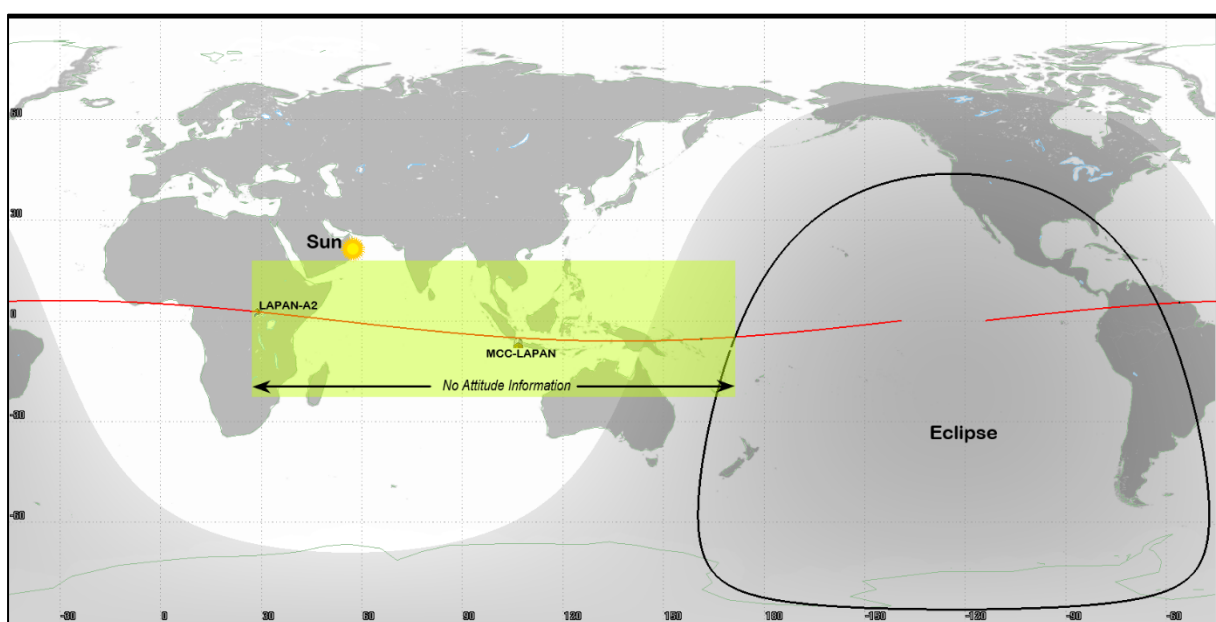


Figure 3.4: Orbital Section of LAPAN-A2 Satellite Where No Attitude Information Available

To solve the problem of losing one of its star sensors, the first thing to do in the LAPAN-A2 satellite is decoupling the loop for automatic attitude control in OBDH. The satellite hereafter operates manually by taking commands from the ground. There are two types of commands given from the ground station, i.e., immediately executed commands and scheduler commands which will be executed at the specified time. In the condition of losing one of its star sensors, LAPAN-A2 satellite then applies momentum bias stabilization to maintain its attitude properly to meet the payload requirements.

For momentum bias operations, a new set of indigenous software in the ground station has been created to assist operator in calculating and maintaining the satellite attitude. Figure 3.5 to Figure 3.8 show there are four consoles in the ground station software that are heavily used by operator to control the satellite attitude, namely the power switch button, magnetic coil controller, wheel-gyro controller, and star sensor controller. The power console is frequently accessed by the operator to turn attitude control devices on or off, since not all devices are required to operate continuously to save power. The magnetic coil controller is used by operators to adapt the coil current setup to the satellite attitude precession requirements. Aiming for real-time awareness of the spacecraft's momentum, the gyro-wheel controller takes telemetry of all the gyro-wheel pairs to estimate the total angular momentum of the spacecraft. The spacecraft's angular momentum is expressed in terms of wheel speed, RPM, to give the operator an awareness of whether the wheels are working within their operating range or over the limit. Meanwhile, the star sensor console estimates the attitude deviation from the target in real time during the star sensor data acquisition.

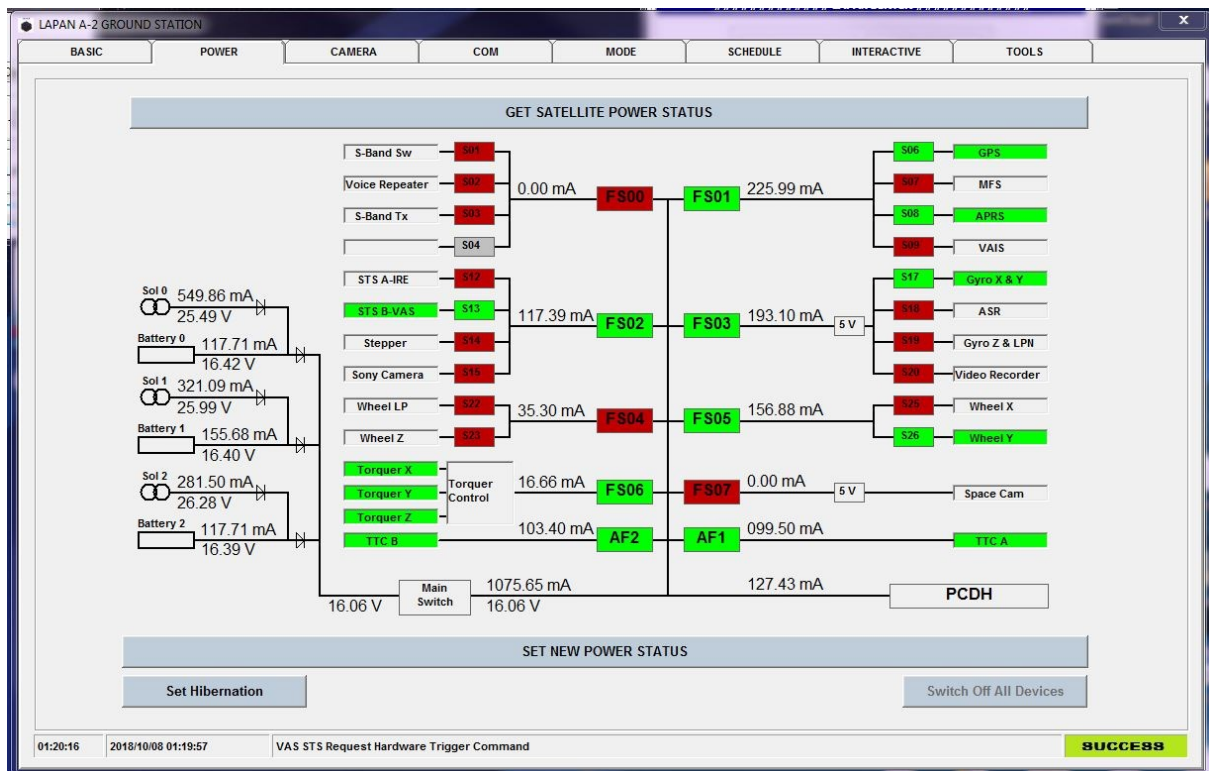


Figure 3.5: Power Switch Button on The Ground Station Software

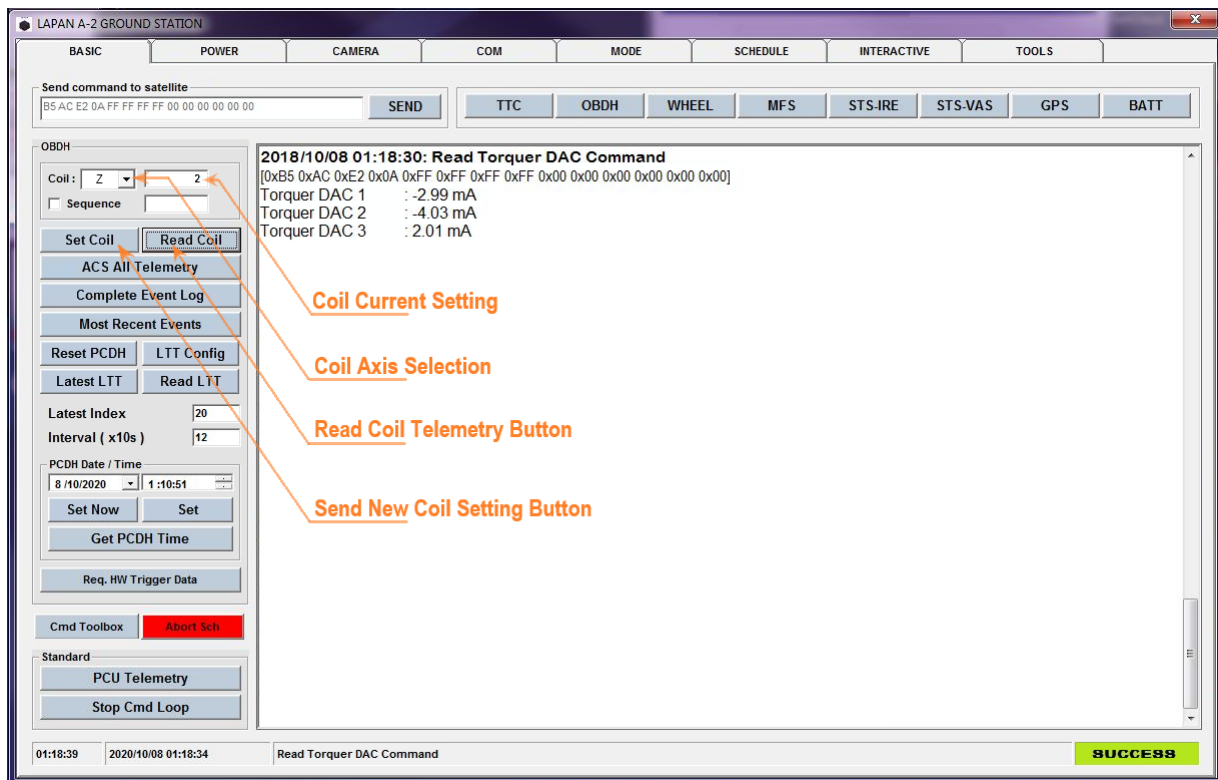


Figure 3.6: Magnetic Coil Controller and Telemetry on The Ground Station Software

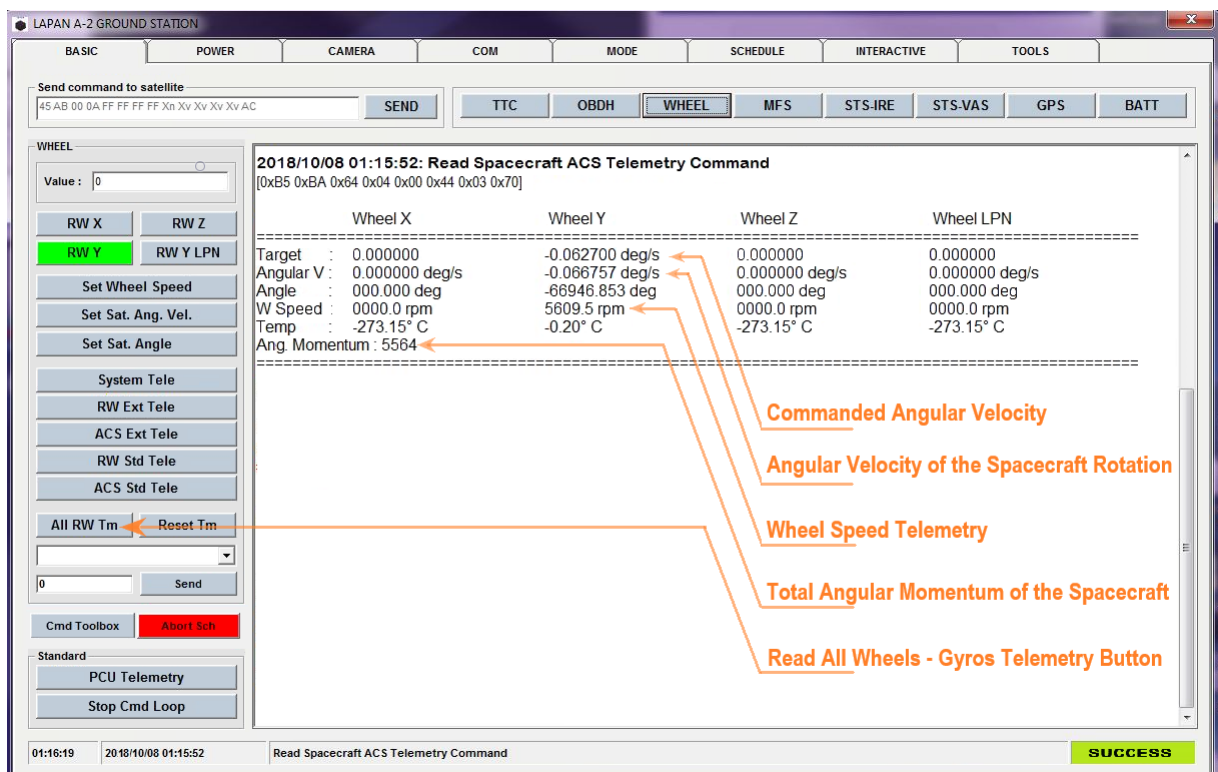


Figure 3.7: Wheel - Gyro Telemetry and Real Time Estimation of Total Angular Momentum

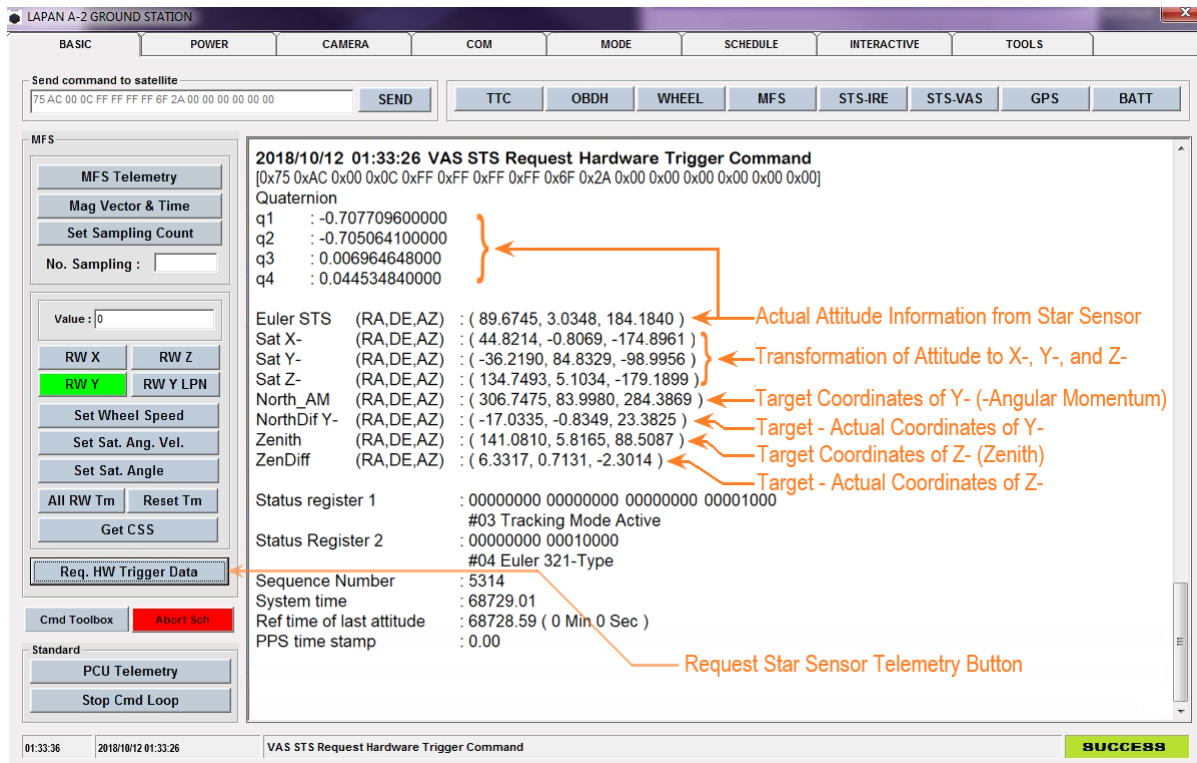


Figure 3.8: Star Sensor Telemetry and Real Time Estimation of Attitude Deviation from Target

Unlike the polar orbit, in the equatorial orbit, the direction of the local Earth's magnetic field is almost the same. The good thing is that the torque generated by each satellite axis will be consistent. However, generating momentum pointing towards the poles is quite challenging because most of the local Earth's magnetic field at the equator is pointing north, resulting in perpendicular torque and momentum. Therefore, the LAPAN-A2 satellite had to find a new approach to using magnetic coils for applying momentum bias in the equatorial LEO. Then after several measurement in nadir pointing mode, it is found an asymmetric variation in the x and z magnetic vectors that could be used for generating the angular momentum in y axis. By utilizing magnetic variation in the z axis, setting a constant current to the x coil would increase the angular momentum in the y axis. However, this procedure will also produce a torque in unwanted axis. Therefore, an attitude correction has to be taken by setting a big current to the x coil when the magnetic vectors of z is zero. The objectives of this procedure are:

- Eliminate the angular momentum on the z axis.
- Remain the angular momentum on the desired y axis.

In equatorial orbit, the daily operation of attitude correction is starting with nutation damping and taking star sensor data. Here the angular momentum coordinates are very close to the pole which is easily misinterpreted by the operator, because a small movement at the poles seems like a long step in the celestial coordinates. Therefore, instead of the angular momentum coordinates, the zenith coordinates are used for attitude evaluation. The ground station software assists operator to calculate the deviation of $-z$ axis from the target of zenith for attitude

correction in the real time. In the zenith coordinates of the equatorial orbiting satellite, right ascension represents pitch, declination represents roll, and azimuth represents yaw. Therefore, pitch correction requires an angle adjustment using the y wheel. Meanwhile, roll correction is performed by activating the x coil, and yaw correction by activating z coil. Calculation of the target coordinates associated with the orbital elements following the control procedures is specifically described in the discussion of momentum bias in equatorial orbits in the section 5.5.

In order to obtain attitude information in a blind area, the stability of the momentum bias system enables attitude interpolation from available data of star sensor. In high-accuracy imaging missions, the star sensor data collection is carried out for two consecutive orbital periods to determine the precession rate. Additional knowledge about the precession rate at known attitude deviations allows precise estimation of attitude maneuvers for high-resolution imaging mission.

The third LAPAN satellite series is LAPAN-A3, a sun synchronous polar orbiting satellite. Initially this satellite was designed as part of a twin satellite development program for disaster mitigation missions called TWINSAT. To support disaster management, the first satellite will carry disaster telecommunications support equipment while the second satellite will carry an imaging system for quickly assessing severity and impact of damage due to disasters. Later, due to risk considerations, especially at launch, the program was divided into two independent satellite development programs, namely LAPAN-A2 and LAPAN-A3.

Since LAPAN-A3 and LAPAN-A2 satellites are twin satellites, all their attitude control devices are similar. Based on the experience and lessons learned from the previous mission, it was decided that the LAPAN-A3 satellite implemented the momentum bias technique from the very beginning of its operation. However, its launch date, which was only 9 months after the launch of the LAPAN-A2, did not give sufficient time for modifications to the attitude control software in the OBDH. The momentum bias system of this satellite, thereby adopts the LAPAN-A2 satellite control operating system that uses human interference and ground control software assistance.

To support momentum bias operation, especially when satellite makes single spinning in hibernation mode, an extra effort has been done in the LAPAN-A3 mechanical design to get desired mass properties. In the hibernation mode, when all attitude devices switched off, the satellite will start spinning. To minimize the nutation or oscillation effects, the spin axis and the major axis of the satellite should coincide. The satellite will be stable if it spins in major axis, i.e. the principal axis that has the biggest moment of inertia [18]. The moment of inertia is one measure of the distribution of the mass of an object relative to a given axis, it is equal to mass times the square of perpendicular distance to the rotation axis. The moment of inertia of a composite system is the sum of the moments of inertia of its components which are all taken about the same axis. To fit the aforementioned requirement, the satellite components have to be

arranged in such a way that the angle (θ) between the spin axis (ω) and the major axis (I_{max}) is very small or equal to zero, as illustrated in Figure 3.9.

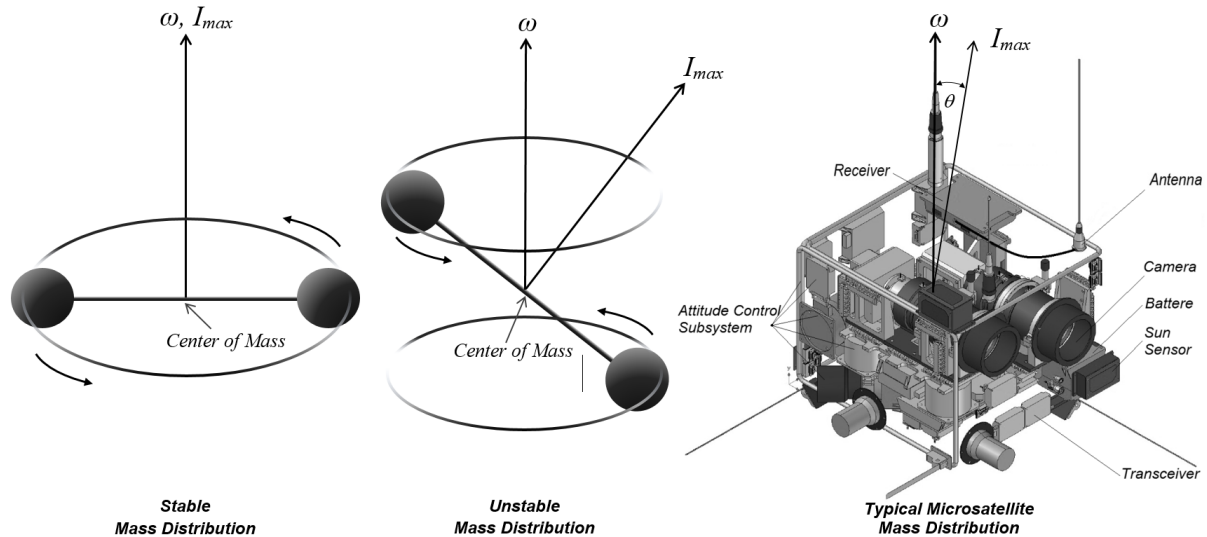


Figure 3.9: Stability of the Spinning Satellite Related to the Mass Distribution and the Spin Axis [47]

To reduce the dependency of the satellite layout from the intuition of its designer which is ordinarily based on trial and error, the genetic algorithm has been used to find the optimal layout of LAPAN-A3's components [47]. In accordance with the position of the resulting layout optimization program, all the satellite components have been placed precisely using a 3D computer aided design, Solid Edge. Figure 3.10 illustrates the optimal layout of satellite components on the middle structure of LAPAN-A3.

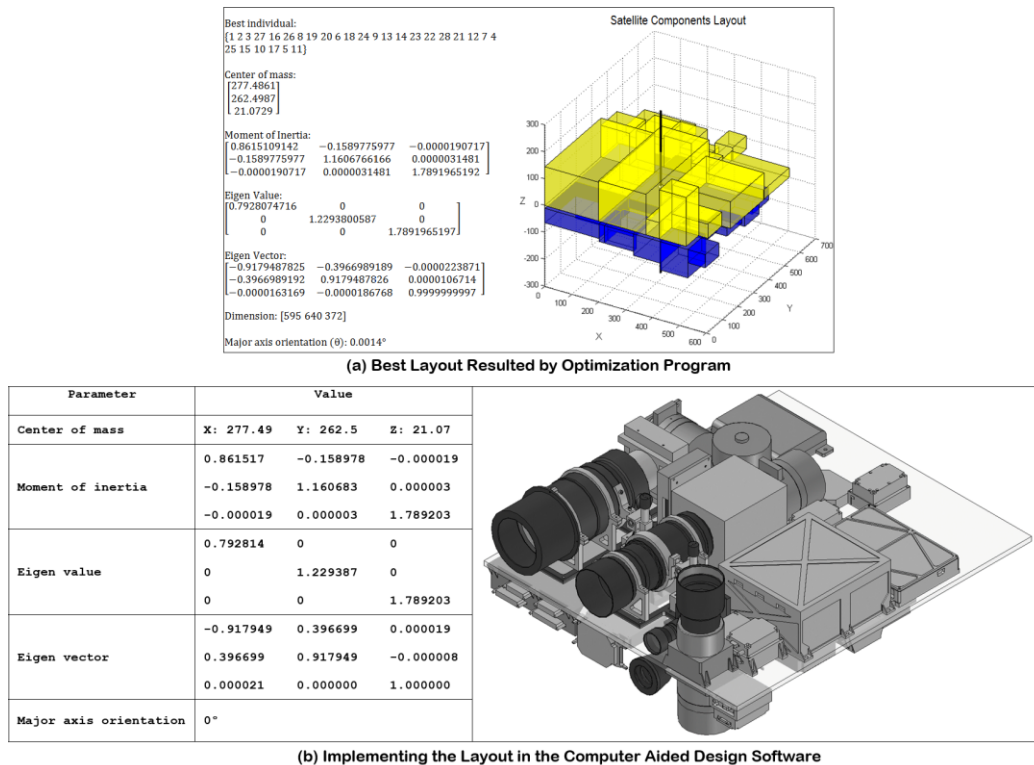


Figure 3.10: Layout Optimization of LAPAN-A3 Satellite [47]

The direct effect of the optimal layout is increased stability of the spinning satellite operation due to balanced mass distribution. Optimal layout would also avoid the use of ballasts to balance the mass distribution of the satellite. It will reduce the entire weight and eventually decrease the launch cost by 10.000 – 100.000 US\$ per kg, depending on the launcher [48]. This study has provided significant contribution to improve the layout design of the satellite. Compared to the previous generation of LAPAN satellite, the model of LAPAN-A3 has better layout concerning to the smaller major axis orientation angle.

3.2 Momentum Bias Establishment and Disturbance Torque Compensation

Just after the launch separation, the angular momentum has to be generated by following procedure:

- Stop the satellite rotation on all axes using reaction wheels.
- Set maximum currents to the coil that produces a big torque.
- Increase the momentum so the wheel is running about 80% max speed.
- Overspeed the wheel on y axis to absorb all the momentum.
- Use one of the transverse wheels to damp the nutation.

The resulting momentum from this procedure can point anywhere in the celestial sphere, then make a precession due to disturbance torques. The most dominant disturbance torque in low Earth orbit comes from magnetic fields. For polar orbiting satellites, the Earth's magnetic field is constantly changing over the orbit. Its strength at the equator is half that of the poles. Thus, in one orbital cycle, the average magnetic field is not zero, but about half of the polar strength to the south. Instead of fighting the disturbance torques continuously with the fraction of seconds control intervals as autonomous control systems do, the LAPAN satellites use this average disturbance torques to estimate attitude precession.

Naturally, due to disturbance torque caused by average of Earth's magnetic field, the angular momentum makes precession along the parallel lines. Actually, a momentum bias system is very stable where the momentum precession can be much lower than the systematic gyro drift. However, it has a precondition, specifically that the disturbance torques must be adequately compensated to stop precession using a magnetic torquer by setting the bias current on y coil. Then controlling the precession in right ascension and in declination to the target that is perpendicular to the orbit plane. A precession in right ascension is simply controlled through overcompensating and undercompensating of the disturbance torques by adjusting the bias current on y coil. Meanwhile, controlling the declination precession requires a larger current in the y coil at a certain position because it utilizes the local magnetic field in an orbital section between the equator and the poles which is called a quarter orbit maneuver. Figure 3.11 illustrates the precession of the spacecraft angular momentum, H , in the celestial sphere.

The momentum bias system provides three-axis stabilization to the spacecraft. While the roll and yaw axes are passively stabilized by preconditioned momentum in right ascension and declination, the pitch rotation is actively controlled through the exchange of momentum between the spacecraft and the integrated wheel-gyro system. Most of the time LAPAN-A1 spins -1 deg/s on the pitch axis and only takes 10 minutes of interactive operation before returning to spin mode again. Meanwhile, LAPAN-A2 & LAPAN-A3 always assigns the angular velocity of nadir pointing to the pitch wheel-gyro system. Due to the systematic drift of the gyro angle measurement, an intermittent acquisition of attitude information from the star sensor is carried out for calibration usually once or twice a day.

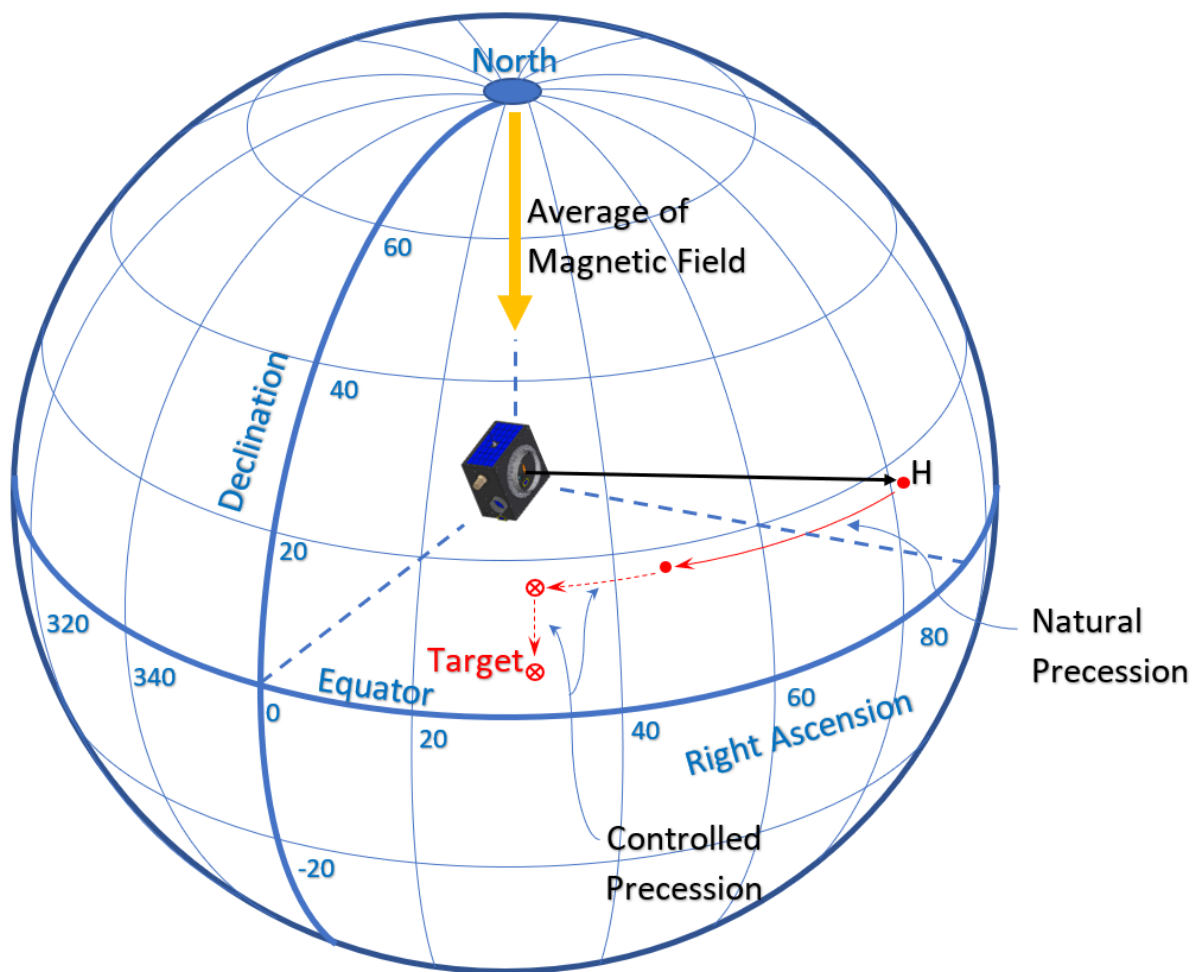


Figure 3.11: Precession of the Angular Momentum

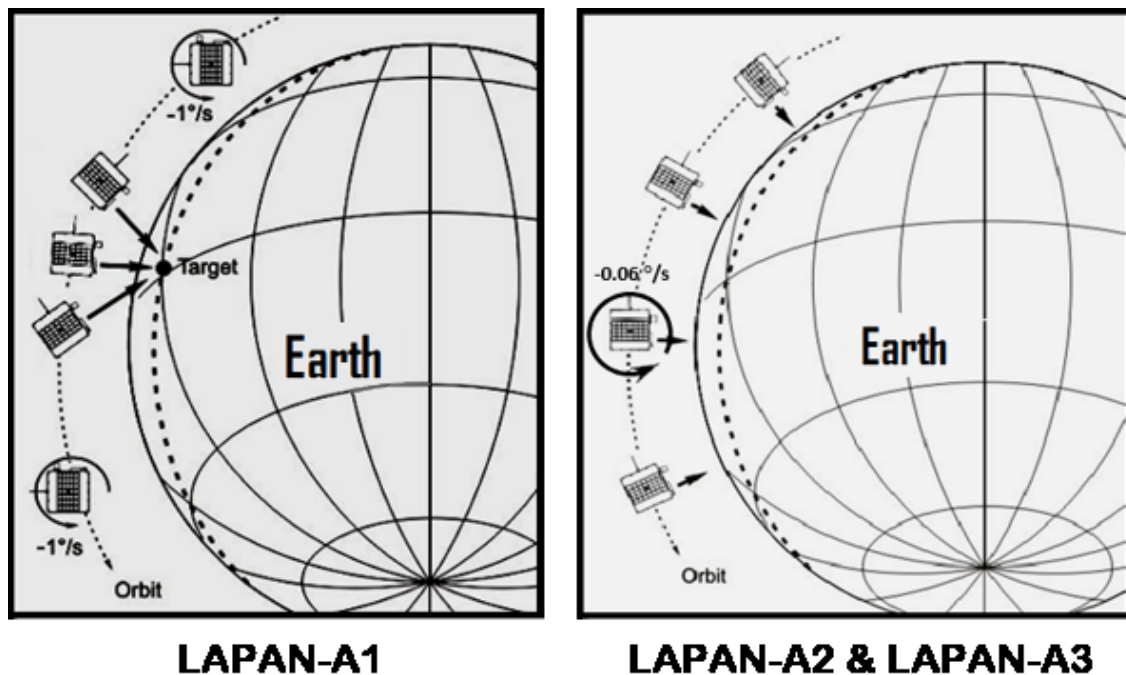


Figure 3.12: Nominal Pitch Rotation of LAPAN-A Satellite Series

3.3 Full Performance and Efficient Attitude Control

One of the major drawbacks of momentum bias stabilization is the difficulty of maneuvering. The second drawback is nutation, so the gyroscopic stiffness effect is insufficient to maintain high pointing accuracies in the axis that perpendicular to the momentum vector. The third drawback is a micro vibration into the payload that is induced by spinning motion of the wheel, especially when its flywheel is not properly balanced. However, since well-balanced wheels for small satellite are quite available in today's technology, micro-vibrations are no longer a problem.

Considering that most satellites operate in nadir pointing, either communication or Earth observation mission, choosing the momentum bias method which is aligning its pitch axis to the orbit normal is appropriate and straightforward. To overcome the maneuverability problem, a major drawback of momentum bias, LAPAN-A series equipped with three orthogonal wheels instead of a single reaction wheel. Doing so, LAPAN-A series still could take the advantages of a three-axis stabilized system using three orthogonal wheels, in particular for large-angle slewing maneuvers. A slew, or attitude reorientation maneuver, can be executed using the set of reaction wheels to rotate the body about a commanded axis, usually one of the wheel axes [49]. As shown in Figure 3.13, the angular momentum vector remains inertially fixed, although the attitude angles change as do the angular momentum components in a body-fixed coordinate

system. In the example shown, the x axis wheel should absorb additional momentum when moving to its location at t_2 . The momentum distribution on wheel x and wheel y will determine the resulting slew angle. Therefore, it is also necessary to maintain the total momentum in certain level so that the slew maneuver can be executed in the right duration.

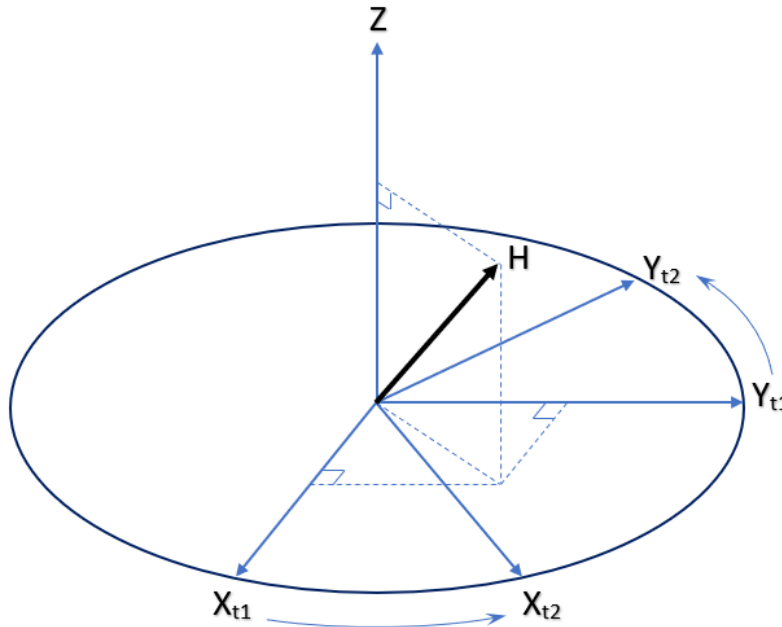


Figure 3.13: A Slew Rotation About Z Axis in Inertial Space

Compared to the whole duty cycle of the satellite, the necessity of slew maneuver in the nominal operation is relatively rare. Therefore, the most of satellite life cycle will be in a momentum bias condition where only a single wheel operates on the spacecraft's pitch axis. Although LAPAN-A satellite series could use three orthogonal wheels to perform a three-axis stabilization, employing all wheels together with gyros and star sensor in continuous operation is very power consuming. Table 3.1 will provide an overview of the power allocation for carrying out small satellite missions in its orbital cycle. In the case of LAPAN-A1, it takes around 50% of the spacecraft's total power consumption to run three pairs of wheel-gyro, star sensor, and magnetic coils simultaneously all the time.

Implementing the momentum bias strategy would drastically reduce the power consumption of attitude control system. Momentum bias does not require star sensor all the time since the angular momentum will not change fast during nominal operation. Spacecraft operators can occasionally switch on the star sensor to get an attitude reference for pointing corrections that performed once per orbital cycle up to once per day, depending on the expected pointing accuracy. If the spacecraft only uses single wheel and gyro in the standby mode and in the nominal mission, it would consume only 15% of the total power that allocated in one orbital cycle. Thus, satellite power can be allocated for maximizing the payload operations and increasing services rate of the satellite.

Table 3.1: Power Consumption of LAPAN-A1 Satellite

| Device | No | Voltage (V) | Current (mA) | Duty-Cycle (%) | Mean Power (W) |
|---|----|-------------|--------------|----------------|----------------|
| Power Control & Data Handling Unit | 1 | 14 | 60 | 100 | 0.84 |
| TTC Receiver | 2 | 14 | 60 | 95 | 0.80 |
| TTC Transmitter | 1 | 14 | 2000 | 5 | 1.40 |
| Total of Communication & Data Handling | | | | | 3.04 |
| Wheel drive electronics | 3 | 14 | 60 | 100 | 0.84 |
| Wheel's motor | 3 | 14 | 100 | 100 | 1.40 |
| Gyro | 3 | 5 | 340 | 100 | 1.70 |
| Star Sensor | 1 | 14 | 160 | 100 | 2.24 |
| Coil | 3 | 14 | 250 | 15 | 0.53 |
| Total of Attitude Control System | | | | | 6.71 |
| S-Band Payload Transmitter | 1 | 12 | 1055 | 15 | 1.90 |
| Kappa Camera | 1 | 12 | 250 | 15 | 0.45 |
| Sony Camera | 1 | 12 | 660 | 15 | 1.19 |
| Focusing Motor | 1 | 12 | 70 | 15 | 0.13 |
| Total of Payload System | | | | | 3.66 |
| Total Power Consumption | | | | | 13.41 |

Even in the cases where the spacecraft suffers from a lack of power, the operator could totally shut down the attitude control system to the hibernation mode so that the satellite will rotate on one axis, i.e. the pitch axis, such as a single spinner satellite. To reactivate the satellite, the acquisition process only requires a simple spinning maneuver in the pitch axis for scanning an attitude to the desired target. Another attitude control strategy to restore the satellite power is to stop spacecraft rotation at a point so that the Sunlight falls in the corner of boxlike spacecraft where more body mounted solar panels are illuminated. This Sun pointing maneuver would be simply handling by a single reaction wheel, thereby the power recovery could be achieved immediately.

To overcome the nutation effect, which is the second drawback of the momentum bias system, LAPAN satellites utilize one of the remaining wheels that is perpendicular to the pitch axis. Activation of the second wheel as a nutation damper could be carried out in an intermittent period. The other alternative device for nutation damping is a magnetic coil. This second alternative of nutation damping has an advantage over the utilization of reaction wheel since it has no stiction or static friction that occurs in the wheel motor when it crosses zero speed. Once nutation has been damped in 1 – 2 minutes of nutation damping, a stable condition would generally remain in a long period. Thus, performing a nutation damping once or twice a day will be sufficient to fulfill high pointing accuracy missions of LAPAN satellites. This effective nutation damping performance will directly affect the pointing accuracy of the satellite payloads. The high accuracy of stabilization in the LAPAN-A satellite series is expected to satisfy a reasonable pointing error, i.e. about 10% - 20% of the field of view of their high-resolution payloads. Implementation of nutation damping on the LAPAN satellites and the flight result are described in section 6.1.2.

3.4 High Precision and Accuracy

In order to realize high-precision attitude control through the momentum bias method, in addition to a good compensation of disturbance torques and an effective nutation damping method, LAPAN-A satellite series must be supported by a good pointing calibration. Nevertheless, performing pointing calibration by using objects on the Earth's surface is difficult since the satellite projection is moving fast over the ground track with the speed about 7 km/s in low Earth orbit with 500 - 650 km height. Furthermore, the spacecraft should rotate around 0.06 deg/s to maintain the pointing toward Earth's center or nadir. Therefore, inaccuracy in a few seconds will make pointing of the camera away from the target. Alternatively, pointing calibration can be executed by exposing satellite's camera towards celestial objects using inertial pointing.

One of the interesting targets for celestial bodies is the Moon. In addition of giving absolute accuracy for pointing calibration, Moon also a good target for focusing calibration of the camera optical system. However, in the case of the LAPAN satellites, the diameter of the Moon is only slightly smaller than the swath width of the camera, leaving only a small margin of the camera frame. Thus, the Moon image will only completely visible in the frame if the camera pointing is exactly toward the center of the Moon [50].

Since the Moon is not too far from the Earth, it is not really an inertial object. Hence, the Moon position in celestial coordinates depends on the observer position. It means the pointing angle to capture the Moon image would slightly changes related to the movement of the spacecraft. Thus, contrary with geocentric coordinate system that puts the reference point at the center of the Earth, Moon observation uses the observer's local horizon as the fundamental plane called topocentric coordinates. The closer a celestial object to the Earth, the larger its angular offset when moving an observer along the Earth's surface. For a celestial object nearest the Earth, this offset from a geocentric position is called parallax. Figure 3.14 illustrates the difference between system coordinates or parallax.

Since topocentric coordinates use observer location as reference for defining the celestial object so the positions of the Moon on the celestial sphere depend on the observer's location. Figure 3.15 illustrated three observers at different position. For a simple example, the maximum of Moon parallax viewed by an orbiting spacecraft on 650 km above the Earth's surface can be calculated by following equation.

$$\alpha = \tan^{-1}\left(\frac{R_E + h_o}{h_M}\right) \quad (3.1)$$

where: $R_E = 6378.14$ km;

$h_o = 650$ km;

$h_M = 384000$ km

According to the aforementioned orbit, the maximum parallax is about 1.049 deg from the geocentric position. Since the parallax might be larger than the field of view of the camera, ignoring parallax will lead to failure of the Moon imaging. Measuring the misalignment between the star sensor as an attitude determination sensor, the spacecraft axis, and the camera by lunar pointing calibration have improved the pointing accuracy of LAPAN satellites in high-resolution imaging better than 0.1 deg. The pointing calibration procedure in more detail and the flight results are described in section 6.2.1.

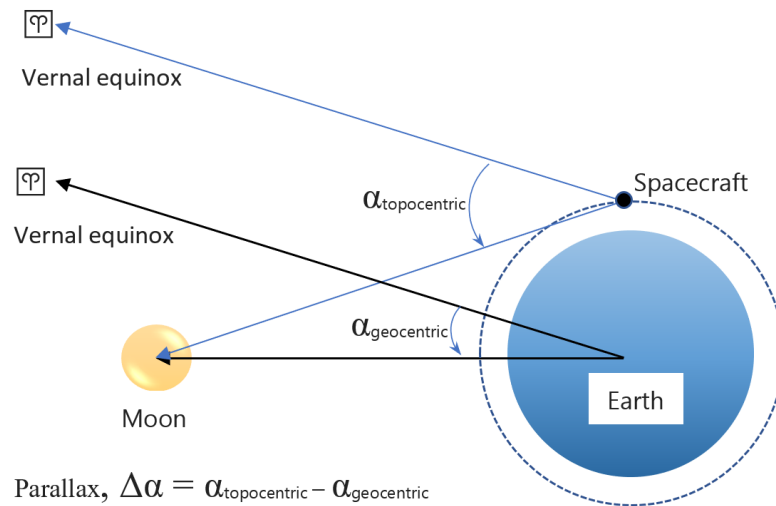


Figure 3.14: Illustration of Moon Parallax [50]

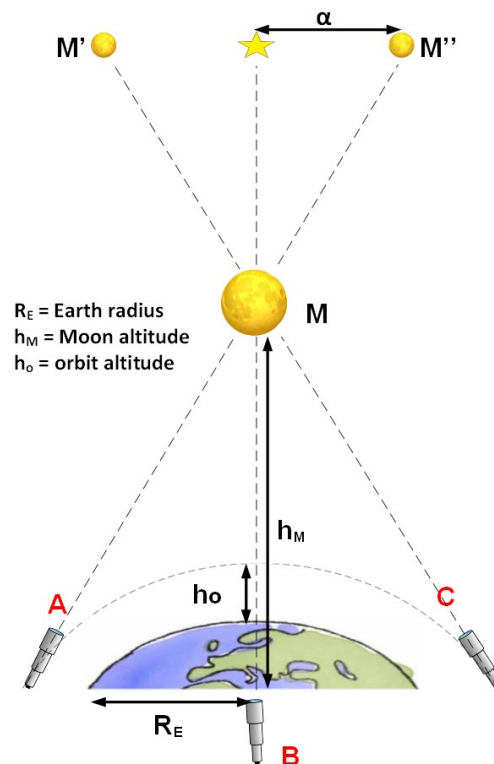


Figure 3.15: Difference of Moon Position Based on Observer Location [50]

3.5 Higher Reliability

The attitude control system can be classified as either open-loop or closed-loop. Open-loop control utilizes ground-based computation or software and analysis to determine the attitude and sending commands to an onboard torqueing system on the spacecraft. Open-loop control may either maintain the spacecraft at a given orientation, which is defined as stabilization, or maneuver the spacecraft to a new attitude. In contrast, closed-loop control uses attitude errors measured by sensors to automatically activate torqueing devices via onboard computer or analog electronics and thereby maintain the attitude errors within specified limits.

Closed-loop control primarily aims to provide an improvement in both cost and accuracy over open-loop systems, which require frequent, complex, and expensive ground-based operational support to maintain a high pointing accuracy. Autonomy, however, is not a solution for all problems because of the added hardware cost, complexity, weight and the reduced flexibility. Autonomous systems are less fault tolerant of data or environmental anomalies than being ground-based systems. They do not have available either the sophisticated ground processing software or the "common sense" judgment of the operator or analyst. Modifications to attitude control systems are impossible after launch and expensive before launch, and changes to onboard software, while possible, are more difficult than comparable changes to ground-based software.

The attitude control system of LAPAN-A satellite series consists of open-loop and closed-loop control system. In the initial phase, the open-loop control system plays a role in establishing of momentum bias and compensating the disturbance torques using magnetic coils which requires human interference with the assistance of ground control software. This open loop control system continues its role in day-to-day operations to maintain momentum and control the precession which directly affects the roll and yaw. Meanwhile, the closed loop control system is responsible for pitch rotation using a highly integrated wheel-gyro system as an autonomous system. Nevertheless, since there is a systematic error in the angle measurement of fiber-optic gyro that used for the closed-loop feedback sensor, a man-in-the-loop calibration using the star sensor is required once or twice a day. As a decentralized attitude control system, an integrated wheel-gyro by *wheel drive electronic* (WDE) takes advantage of reducing complication and minimizing the task of the main computer. It also needs a simple computation and fast response; therefore, it gives better transparency and easy to test on the ground before the launch by using a simple single-axis air bearing platform. This integrated wheel-gyro is also adaptable for new operating methods and approaches, such as replacing feedback sensor, to accommodate future innovations and technologies.

The combination of open loop and closed loop control of LAPAN satellites frees from depends on the continuous availability of data from star sensors. Although star sensors are powerful and accurate in attitude determination, they are also vulnerable to failure. Either require very slow

motion of the spacecraft, a star sensor should avoid the blind area caused by the Sun, Moon and Earth (albedo). Therefore, a star sensor should orient away from those light sources and must be equipped with a good baffle to avoid stray light to the sensor. The other serious problem in the star sensor lifetime is the occurrence of hotspots due to the high radiation levels in LEO, mainly high energy protons, that hit the sensors. Hotspots are pixels that suffered radiation damage resulting in a significant higher dark current and are permanent. Bright hotspots can shadow the pixels and therefore block up the stars to be detected by the sensor. Over time the pixel number that is shadowed by these hotspots would grow that cause the algorithm of extracting the star positions from the image would fail.

Several missions have a problem to acquire attitude information from the star sensors due to underestimate the light source in the orbit, while the others were not survived from radiation in the space environment. The problem is still happening in the LAPAN-A satellite series while they are experiencing partial or total loss of the star sensor. While LAPAN-A1 totally lost its single star sensor after one year in orbit, LAPAN-A2 lost one of its double star sensors in early orbit phase, and sometimes LAPAN-A3 could not get the star sensor data while it was closing to the Sun position along its orbit. The loss of the star sensor, if not anticipated, could potentially mess with attitude control leading to a complete loss of mission, particularly for high-resolution imaging or narrow beam communications. A satellite cannot carry out any mission operations without proper attitude reference.

Since previous missions and projects have evinced that the star sensor could not work all the time, instead of using the star sensor in the closed-loop system, LAPAN-A satellite series propose it remain in the open-loop. Applying a star sensor in the closed-loop control should be anticipated with an option to disable the loop. By doing so together with implementing momentum bias strategy, partial or even total loss of the star sensor would still give an opportunity to the satellites to continue their missions. For partial working star sensors that are happening to LAPAN-A2 and LAPAN-A3 satellites, an interpolation of previous data together with an estimation of the attitude precession due to disturbance torque are used to predict the succeeding attitude for upcoming imaging operations. If the satellite has a device that can also be used as a fine attitude sensor, even the loss of the star sensor will not stop mission operations such as the case of LAPAN-A1 which uses the camera payload as a horizon sensor to replace the missing star sensor.

4 ATTITUDE GEOMETRY AND DYNAMICS

Many space flight analyses require information of the apparent position and motion of objects seen by the spacecraft. This type of analysis is mostly related to geometry of direction. This analysis is needed to know how to direct a spacecraft or instrument, or how to interpret a camera's view or spacecraft's antenna pattern. Two formal mechanisms for dealing with directional geometry are unit vectors and celestial spheres. Unit vectors are more common in most fields of analysis. However, celestial spheres provide much better physical insight that can be very important for space mission designers [51].

This chapter introduces the idea of attitude and control as a geometric problem, describes the most common attitude coordinate system, and summarizes the geometry of celestial spheres. Most spacecraft sensors measure only angles. Considering that the attitude of the spacecraft is its orientation relative to the Sun, the Earth, or the stars regardless of the distance to these various objects. Just as unit vectors, which are also used to represent direction, have a length of one, the celestial sphere is assumed to have a radius of one so that only the angular coordinates on the sphere are relevant. Therefore, after introducing the basic concept of using a celestial sphere for directional geometry, the concept was then applied to space mission geometry as seen from Earth or a spacecraft to develop a methodology for constructing the spacecraft pointing and mapping budgets.

4.1 Coordinate Systems

To start any formal problem in the space mission's geometry, the first action is choosing a coordinate system. In principle, any coordinate system will be carried out. In practice, choosing the right one can increase insight into the problem and substantially reduce the possibility of errors. The most common source of error in space geometry analysis is defining the coordinate systems involved. To define a coordinate system for space applications, the initial step is determining two characteristics: the central location and what coordinate system is fixed with respect to. Usually, choosing the Earth's center as the center of the coordinate system is helpful for problems in orbit analyses or geometry on the Earth's surface; and choosing the spacecraft's

position is useful for problems involving the apparent position and motion of objects seen from the spacecraft. Sometimes, coordinates are centered on certain spacecraft instruments when attentions are not only in seeing the outside world but also in obstructions to the field of view by other spacecraft components. Typical ways to fix a coordinate system are with respect to inertial space, towards the Earth direction or other objects, to the spacecraft, or to an instrument on the spacecraft. Table 4.1 lists the basic coordinate systems in the analysis of space missions and their applications that used in this study.

Table 4.1: Common Coordinate Systems Used in Space Application [51]

| Name | Fixed with Respect to | Origin | Pole (Z-axis) | Reference Point (X-axis) | Applications |
|------------------------------------|-----------------------|---------------------------------|------------------------------|---|--|
| Spacecraft-fixed | Spacecraft | Defined by engineering drawings | Spacecraft axis toward nadir | Spacecraft axis in direction of velocity vector | Position and orientation of spacecraft instruments |
| Celestial/Inertial | Inertial space | Earth or spacecraft | Celestial pole | Vernal equinox | Orbit analysis, inertial motion, astronomy |
| Earth-fixed | Earth | Earth | Earth pole = celestial pole | Greenwich meridian | Geolocation, satellite trajectory |
| RPY (Roll, Pitch, Yaw) Coordinate* | Orbit | Spacecraft | Nadir | Perpendicular to nadir toward velocity vector | Earth observations, attitude maneuvers |

* Also called Local Horizontal or Local Tangent Coordinate

4.1.1 Spacecraft-Centered Coordinates

The spherical coordinate systems normally used for spacecraft have a few properties in common. The spacecraft-centered celestial sphere is illustrated in Figure 4.1. Each spherical coordinate system has two *poles* diametrically opposite each other on the celestial sphere and an *equator*, or great circle, halfway between the poles. The great circles through the poles and perpendicular to the equator are called *meridians* and the small circles a fixed distance above or below the equator are called *parallels*.

The position of any point on the sphere is given in terms of two components equivalent to latitude and longitude on the surface of the Earth. The arc length distance above or below the equator is called the *latitude* or *elevation* component. The angular distance around the equator between the meridian passing through a particular point and an arbitrary *reference meridian*, or *prime meridian*, is known as the *longitude* or *azimuth* component.

Coordinate systems fixed in the spacecraft are used to define the orientation of attitude determination and control hardware and are the systems in which attitude measurements are made. Refer to previous description, spacecraft-centered spherical coordinates will use ϕ for the azimuth component and λ for the elevation. Alternatively, θ will be used for the co-

elevation; that is, $\theta = 90^\circ - \lambda$. For spinning spacecraft, the positive pole of the coordinate system will be the positive spin vector, unless otherwise specified. The reference meridian is taken as passing through an arbitrary reference point on the spin plane which is the equator of the coordinate system. For three-axis stabilized (non-spinning) spacecraft, no standard orientation is defined. For attitude-sensing hardware, it is the orientation of the field of view of the hardware in the spacecraft system that is important, not the location of the hardware within the spacecraft.

The following equations transform the azimuth, ϕ , and elevation, λ , to the corresponding unit vector coordinates (x, y, z):

$$x = \cos(\phi)\cos(\lambda) \quad (4.1a)$$

$$y = \sin(\phi)\cos(\lambda) \quad (4.1b)$$

$$z = \sin(\lambda) \quad (4.1c)$$

Similarly, to transform unit vector into the corresponding spherical coordinates, use

$$\tan(\phi) = \frac{y}{x} \quad (4.2a)$$

$$\sin(\lambda) = z \quad (4.2b)$$

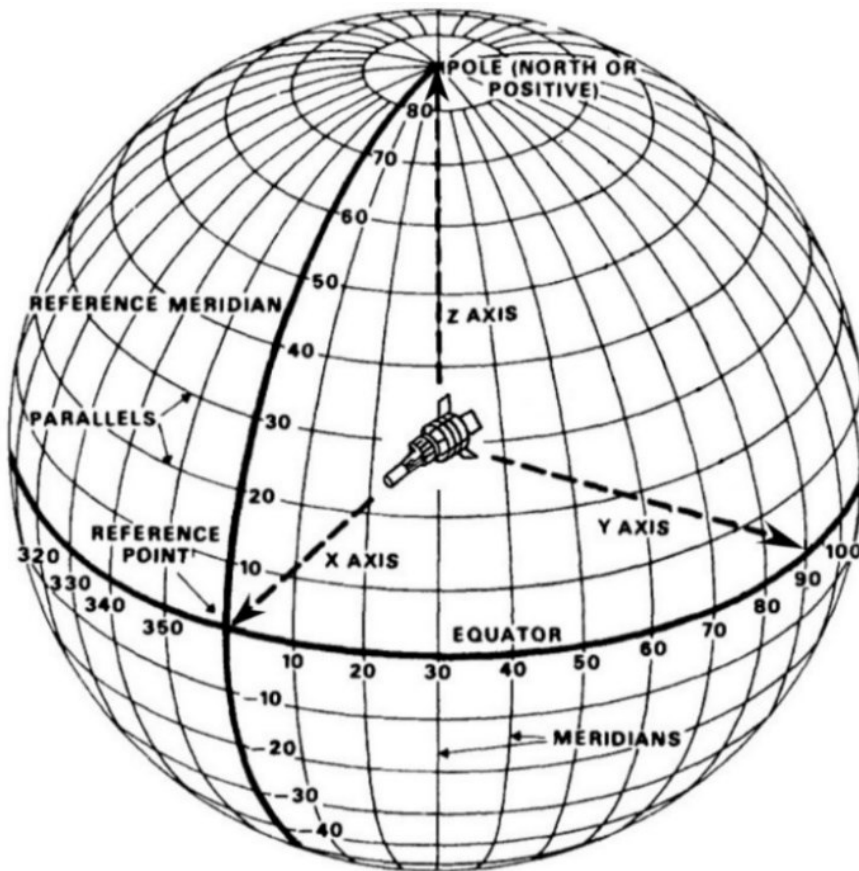


Figure 4.1: Spacecraft-Fixed Coordinate System [51]

Several spherical coordinate systems in common use have special names for the azimuth and elevation coordinates as shown in Table 4.2.

Table 4.2: Azimuth and Elevation Coordinates in Several Spherical Coordinate System [51]

| Coordinate System | Azimuth Coordinate | Elevation Coordinate | Applications |
|------------------------|---------------------|----------------------|--|
| Local horizontal | Azimuth | Elevation | Directions relatives to central observer |
| Geocentric coordinates | Longitude | Latitude | Earth application |
| Celestial coordinates | Right ascension | Declination | Inertial measurements and astronomy |
| Ecliptic coordinates | Celestial longitude | Celestial latitude | Planetary motion |

Recall that the spacecraft is at the center of the sphere in Figure 4.1, the axis of the *spacecraft-centered inertial* coordinate system joining the north and south celestial poles is defined as parallel to the rotation axis of the Earth. Thus, the north celestial pole is approximately 1 deg from the bright star Polaris, the Pole Star. To fully define the coordinate system, the reference meridian or reference point must be defined. The point on the celestial equator chosen as the reference is the point where the *ecliptic*, or plane of the Earth's orbit about the Sun, crosses the equator going from south to north, known as the *vernal equinox* as shown in Figure 4.2. This is the direction parallel to the line from the center of the Earth to the Sun on the first day of spring.

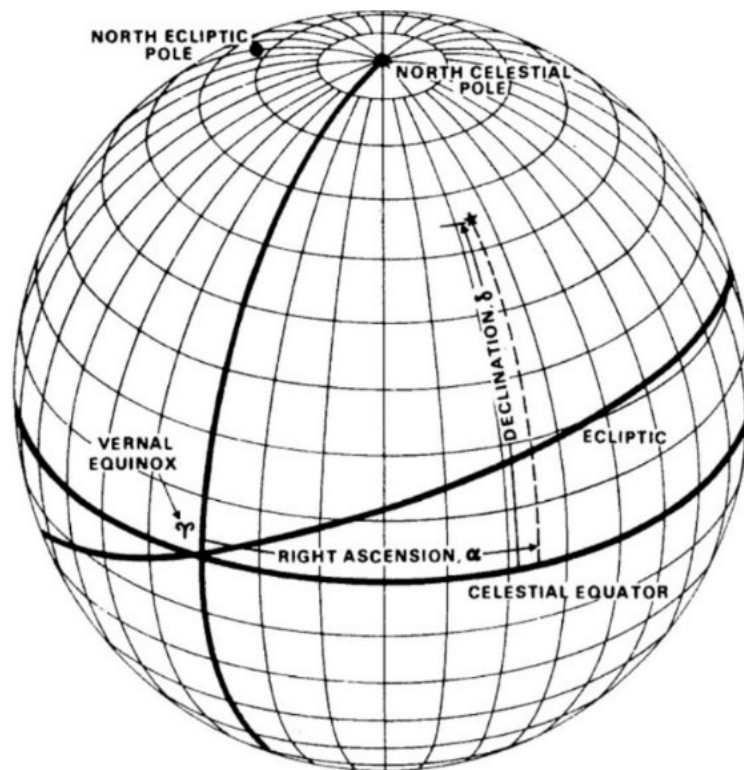


Figure 4.2: Celestial Coordinates [52]

Unfortunately, the celestial coordinate system is not truly inertial in that it is not fixed relative to the mean positions of the stars close to the Sun. The gravitational force of the Moon and the Sun on the Earth's equatorial bulge causes a torque which results in the slow rotation of the Earth's spin axis about the ecliptic pole, taking 26,000 years for one complete period for the motion of the axis. This phenomenon is known as the *precession of the equinoxes*, since it results in the vernal equinox sliding along the ecliptic relative to the fixed stars at the rate of approximately 50 sec of arc per year. When the zodiacal constellations were given their present names several thousand years ago, the vernal equinox was in the constellation of Aries, the Ram. Thus, the zodiacal symbol for the Ram, ♈ is used astronomically for the vernal equinox, which is also called the *First Point of Aries*. Since that time, the vernal equinox has moved through the constellation of Pisces and is now entering Aquarius, bringing the dawn of the zodiacal "Age of Aquarius." The other intersection of the ecliptic and the equator is called the *autumnal equinox* and is represented by the zodiacal symbol for Libra.

The importance of the precession of the equinoxes is that it causes a slow change in the celestial coordinates of "fixed" objects, such as stars, which must be considered for accurate determination of orientation. Thus, celestial coordinates require that a date be attached to accurately define the position of the vernal equinox. The most commonly used systems are *1950 coordinates*, *2000 coordinates*, and *true of date* (TOD). The latter coordinates are defined at the epoch time of the orbit and are commonly used in spacecraft work.

The elevation or latitude component of celestial coordinates is universally known as the *declination*, δ . Similarly, the azimuth component is known as *right ascension*, α . Although right ascension is measured in degrees in all spacecraft work, in most astronomical tables it is measured in *hours*, *minutes*, and *seconds* where 1 hour = 15 deg, 1 min = 1/ 60th hour = 1/4 deg, and 1 sec = 1/ 60th min = 0.0041666... deg. Each of these measurements corresponds to the amount of rotation of the Earth in that period of time. Note that minutes and seconds of right ascension are not equivalent to minutes and seconds of arc, even along the equator.

4.1.2 Nonspacecraft-Centered Coordinates

For attitude work, the most important coordinate systems are all centered on the spacecraft. However, occasionally the use of nonspacecraft-centered coordinates is convenient, primarily as a means of obtaining reference vectors such as the position vectors to objects being viewed by the spacecraft or magnetic field vector. Thus, orbit work is ordinarily done in geocentric inertial coordinates, equivalent to the celestial coordinates defined above, except that the center of the coordinate system is at the center of the Earth. The position vector of the Earth in spacecraft-centered celestial coordinates is just the negative of the position vector of the spacecraft in geocentric inertial coordinates.

To describe the motion of the satellites, an inertial coordinate system has to be defined. Since the satellites revolve around the center of the Earth, it seems natural to have the center (origin)

of the coordinate system at the center of the Earth, hence it is named the Earth-Centered Inertial (ECI) coordinate system. Inertial, in this context, simply means that the coordinate system is not moving. In other words, it is 'fixed' in space relative to the stars. This is an ideal definition of the ECI coordinate system [53].

The ECI coordinate system as seen in Figure 4.3 is typically defined as a Cartesian coordinate system, where the coordinates (position) are defined as the distance from the origin along the three orthogonal axes. The z axis runs along the Earth's rotational axis pointing north, the x axis points in the direction of the vernal equinox, and the y axis completes the right-handed orthogonal system. These three axes defining the Earth-Centered Inertial coordinate system are 'fixed' in space and do not rotate with the Earth.

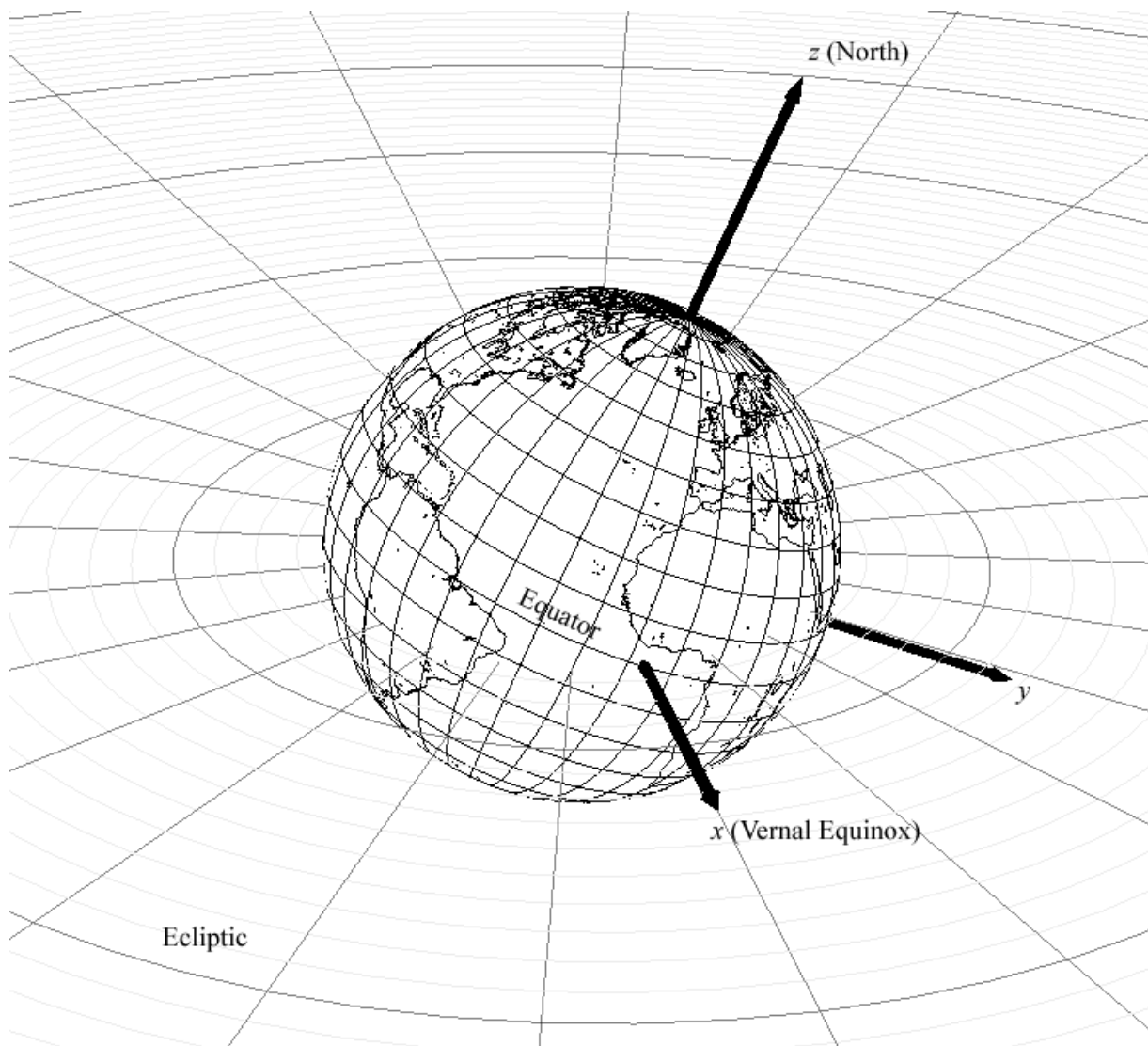


Figure 4.3: Celestial Coordinates [53]

Another coordinate frames that have the same origins as ECI are the Earth-centered, Earth-fixed (ECEF) coordinates. In contrast to the ECI frames that are inertial, the ECEF frames

remain fixed with respect to Earth's surface in its rotation. The ECEF coordinate system is also known as the "conventional terrestrial" coordinate system. It is a simple Cartesian coordinate system with the center of the Earth as its origin. The $+z$ axis passes through the North Pole. The x - y plane will be the equatorial plane. The $+x$ axis passes through the Equator and Prime Meridian intersection. The $+y$ axis is orthogonal to $+x$ and $+z$. As a result, this coordinate system rotates with the Earth. The distances used along each axis are meters. These ECEF coordinates are the ones used by most satellites systems to designate an Earth position.

At the highest accuracy, geodesy is done in an ECEF coordinate system that is called World Geodetic System 84 (WGS84). This World Geodetic System has several components. One of these is the reference frame. WGS84 is used as the basis of the GPS solutions. This was done by finding the WGS84 ECEF locations of the stations that supply data for the Broad Cast Ephemeris (BCE) computation. The Geodetic system uses polar coordinates defined as follows:

- **Latitude:** Angle north and south of the equator. Positive angles are in the northern hemisphere, and negative angles are in the southern hemisphere. The range of angles is -90 degrees ($-\pi/2$ radian) to $+90$ degrees ($+\pi/2$ radians). Points on the equator have a latitude of zero.
- **Longitude:** Angle east and west of the Prime Meridian. The Prime Meridian is a north-south line that passes through Greenwich, United Kingdom. Positive longitudes are to the east of the Prime Meridian, and negative angles are to the west. The range of angles is -180 degrees ($-\pi$ radians) to $+180$ degrees ($+\pi$ radians).
- **Height:** Also called altitude or elevation, this represents the height above the Earth ellipsoid, measured in meters. The Earth ellipsoid is a mathematical surface defined by a semi-major axis and a semi-minor axis. The WGS-84 ellipsoid is intended to correspond to mean sea level, although in practice the actual mean sea level varies around the world due to ocean currents, Coriolis effects, and local variations in Earth's gravitational field. A Geodetic height of zero therefore roughly corresponds to sea level, with positive values increasing away from the Earth's center. The theoretical range of height values is from the center of the Earth (about $-6,371\text{km}$) to positive infinity. In practice, however, height values deeper than a few kilometers, or higher than geosynchronous orbit (about $36,000\text{km}$) are seldom used.

Some cases, such as imaging vectors on the Earth's surface, analysis of the Earth's magnetic or gravitational field, may wish to associate a vector with each point in a spherical coordinate system. To do this it is convenient to define at each point in space an orthogonal coordinate system whose three axes are each parallel to the change in one of the three spherical coordinates, as illustrated in Figure 4.4. Such systems are called local horizontal coordinates or local tangent coordinates, since the reference plane at any point is always tangent to the sphere centered on the origin of the system and passing through the point in question. If the components of the global spherical coordinate system are r , λ , and ϕ (the radius, elevation, and azimuth, respectively), then at any point in space, the three reference axes of the local horizontal system are: north axis (N) in the direction of increasing λ , east axis (E) in the direction of increasing ϕ ,

and zenith axis (Z) in the direction of increasing r . South (S), west (W), and nadir (n) are used for the negatives of the three axes. Thus, the names for the axes would correspond to the usual definitions of the four directions, the zenith, and nadir on the surface of a spherical Earth. Within the local horizontal coordinate system, the reference plane is the N-S-E-W plane and the reference direction of 0 azimuth is north. Elevation is used for the angular height above the reference plane (i.e., toward the zenith), and azimuth is used for the rotation angle in the reference plane measured from north toward east.

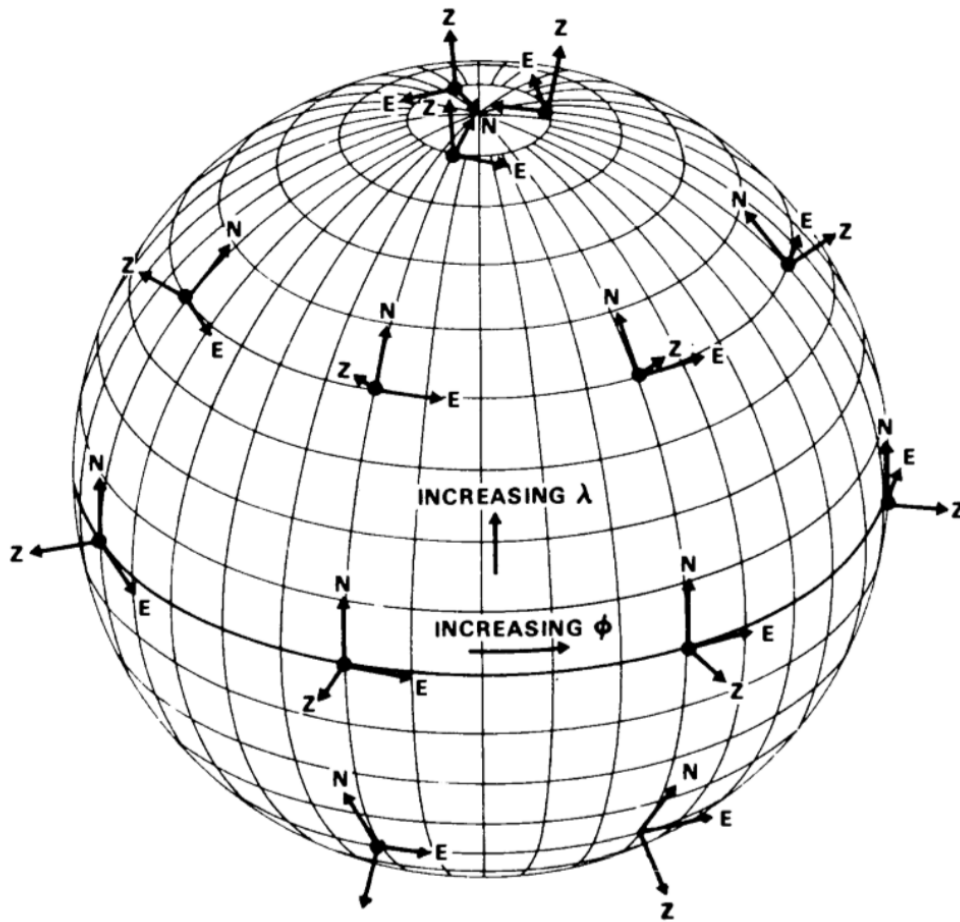


Figure 4.4: Local Horizontal Coordinates [52]

4.1.3 RPY (Roll, Pitch, Yaw) Coordinates

Lastly, defining a system of coordinates that maintain their orientation relative to the Earth as the spacecraft moves in its orbit. These coordinates are known as *roll*, *pitch*, and *yaw* or *RPY*, and are illustrated in Figure 4.5. In this system, the *yaw axis* is directed toward the nadir (i.e., toward the center of the Earth), the *pitch axis* is directed toward the negative orbit normal, and the *roll axis* is perpendicular to the other two such that unit vectors along the three axes have the relation $\mathbf{R} = \mathbf{P} \times \mathbf{Y}$. Thus, in a circular orbit, the roll axis will be along the velocity vector.

The *roll*, *pitch*, and *yaw* angles (ϕ , θ , and ψ) are defined as right-handed rotations about their

respective axes. Therefore, for a spacecraft in a circular orbit and an observer on the spacecraft facing in the direction of motion with the Earth below, a positive pitch rotation brings the nose of the spacecraft upward, positive yaw moves it to the right, and positive roll rotates the spacecraft clockwise. The RPY system is most commonly used for Earth-oriented spacecraft.

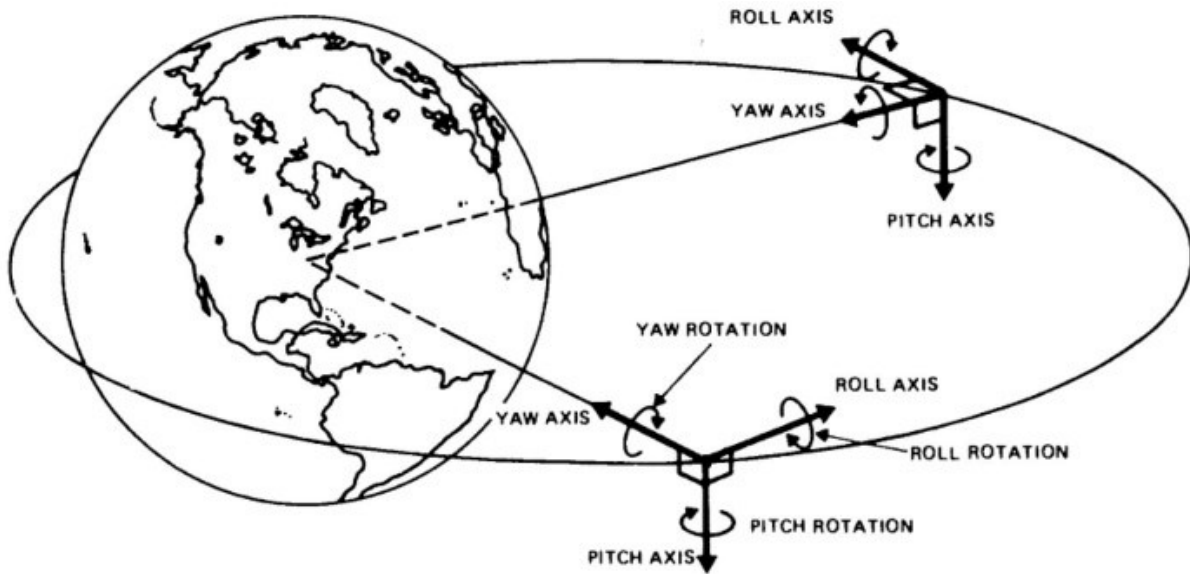


Figure 4.5: Roll, Pitch, and Yaw (RPY) Coordinate System [51]

4.2 Coordinate Transformation

Any orientation can be achieved by composing three elemental rotations, i.e. rotations about the axes of a coordinate system. Those associated rotations are introduced by Leonhard Euler to describe the orientation of a rigid body with respect to a fixed coordinate system, that is why they are called Euler's angles. Euler angles can be defined by three of these rotations. They can also be defined by elemental geometry and the geometrical definition demonstrates that three rotations are always sufficient to reach any frame. Start by assuming both the reference X, Y, Z and body-fixed x, y, z frame coincides. The rotation of body about x, y, z axes with respect to reference are typically denoted as ϕ, θ, ψ .

One convenient sequence on the use of three Euler angles was introduced by Bryan, who used a set of Euler angles to parameterize the yaw (rotation about z), pitch (rotation about y), and roll (rotation about x) of an airplane in the early 1900s [54]. Figure 4.6 illustrates rotations by ψ about z axis followed by θ about y axis and then ϕ about x axis. This set of Euler angles is often referred to as the yaw-pitch-roll sequence or 3-2-1 sequence.

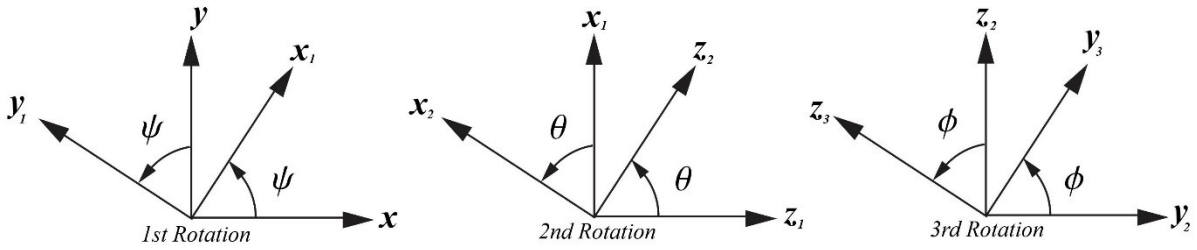


Figure 4.6: Sequence of 3-2-1 Euler Angles

It is not difficult to express the various basis vectors as linear combinations of each other:

$$\begin{bmatrix} x_1 \\ y_1 \\ z_1 \end{bmatrix} = \begin{bmatrix} \cos(\psi) & \sin(\psi) & 0 \\ -\sin(\psi) & \cos(\psi) & 0 \\ 0 & 0 & 1 \end{bmatrix} \begin{bmatrix} x \\ y \\ z \end{bmatrix} \quad (4.3a)$$

$$\begin{bmatrix} x_2 \\ y_2 \\ z_2 \end{bmatrix} = \begin{bmatrix} \cos(\theta) & 0 & -\sin(\theta) \\ 0 & 1 & 0 \\ \sin(\theta) & 0 & \cos(\theta) \end{bmatrix} \begin{bmatrix} x_1 \\ y_1 \\ z_1 \end{bmatrix} \quad (4.3b)$$

$$\begin{bmatrix} x_3 \\ y_3 \\ z_3 \end{bmatrix} = \begin{bmatrix} 1 & 0 & 0 \\ 0 & \cos(\phi) & \sin(\phi) \\ 0 & -\sin(\phi) & \cos(\phi) \end{bmatrix} \begin{bmatrix} x_2 \\ y_2 \\ z_2 \end{bmatrix} \quad (4.3c)$$

The inverses of these relationships are easy to obtain because each of the three matrices in (4.3a, 4.3b, 4.3c) is orthogonal. As the inverse of an orthogonal matrix is its transpose, we quickly arrive at the sought-after results:

$$\begin{bmatrix} x \\ y \\ z \end{bmatrix} = \begin{bmatrix} \cos(\psi) & -\sin(\psi) & 0 \\ \sin(\psi) & \cos(\psi) & 0 \\ 0 & 0 & 1 \end{bmatrix} \begin{bmatrix} x_1 \\ y_1 \\ z_1 \end{bmatrix} \quad (4.4a)$$

$$\begin{bmatrix} x_1 \\ y_1 \\ z_1 \end{bmatrix} = \begin{bmatrix} \cos(\theta) & 0 & \sin(\theta) \\ 0 & 1 & 0 \\ -\sin(\theta) & 0 & \cos(\theta) \end{bmatrix} \begin{bmatrix} x_2 \\ y_2 \\ z_2 \end{bmatrix} \quad (4.4b)$$

$$\begin{bmatrix} x_2 \\ y_2 \\ z_2 \end{bmatrix} = \begin{bmatrix} 1 & 0 & 0 \\ 0 & \cos(\phi) & -\sin(\phi) \\ 0 & \sin(\phi) & \cos(\phi) \end{bmatrix} \begin{bmatrix} x_3 \\ y_3 \\ z_3 \end{bmatrix} \quad (4.4c)$$

The directional cosine matrix for the overall rotation sequence is the matrix product of the three matrices for the individual rotations, with the first rotation matrix on the right and the last on the left:

$$\begin{aligned}
R_{321}(\psi, \theta, \phi) &= R_1(\phi)R_2(\theta)R_3(\psi) \\
&= \begin{bmatrix} 1 & 0 & 0 \\ 0 & \cos(\phi) & \sin(\phi) \\ 0 & -\sin(\phi) & \cos(\phi) \end{bmatrix} \begin{bmatrix} \cos(\theta) & 0 & -\sin(\theta) \\ 0 & 1 & 0 \\ \sin(\theta) & 0 & \cos(\theta) \end{bmatrix} \begin{bmatrix} \cos(\psi) & \sin(\psi) & 0 \\ -\sin(\psi) & \cos(\psi) & 0 \\ 0 & 0 & 1 \end{bmatrix} \\
&= \begin{bmatrix} \cos(\theta)\cos(\psi) & \cos(\theta)\sin(\psi) & -\sin(\theta) \\ -\cos(\phi)\sin(\psi) + \sin(\phi)\sin(\theta)\cos(\psi) & \cos(\phi)\cos(\psi) + \sin(\phi)\sin(\theta)\sin(\psi) & \sin(\phi)\cos(\theta) \\ \sin(\phi)\sin(\psi) + \cos(\phi)\sin(\theta)\cos(\psi) & -\sin(\phi)\cos(\psi) + \cos(\phi)\sin(\theta)\sin(\psi) & \cos(\phi)\cos(\theta) \end{bmatrix} \quad (4.5)
\end{aligned}$$

Representation (4.5) is the transpose of what one might naively expect. Indeed, it is useful to note that

$$\begin{bmatrix} x_3 \\ y_3 \\ z_3 \end{bmatrix} = \begin{bmatrix} R_{11} & R_{12} & R_{13} \\ R_{21} & R_{22} & R_{23} \\ R_{31} & R_{32} & R_{33} \end{bmatrix} \begin{bmatrix} x \\ y \\ z \end{bmatrix} \quad (4.6)$$

$$\begin{bmatrix} x \\ y \\ z \end{bmatrix} = \begin{bmatrix} R_{11} & R_{21} & R_{31} \\ R_{12} & R_{22} & R_{32} \\ R_{13} & R_{23} & R_{33} \end{bmatrix} \begin{bmatrix} x_3 \\ y_3 \\ z_3 \end{bmatrix} \quad (4.7)$$

Implementing Euler angles to get spacecraft orientation toward inertia frame through star sensor measurement could be described in the following steps.

Step 1: Transform inertia to star sensor frame. Rotations by ψ about z axis of star sensor defined as *right ascension* (RA), followed by θ about y axis of star sensor defined as the negative of declination (-DE), and then ϕ about x axis of star sensor defined as azimuth (AZ). This transformation will obtain direction cosine matrix of rotation from inertia to star sensor frame ($\mathbf{R}_{\text{in} \rightarrow \text{sts}}$).

Step 2: Transform star sensor frame to spacecraft frame by performing rotations by ψ about z axis of spacecraft, followed by θ about y axis of the spacecraft, and then ϕ about x axis of the spacecraft. This transformation will result direction cosine matrix of rotation from star sensor frame to spacecraft frame ($\mathbf{R}_{\text{sts} \rightarrow \text{sat}}$).

Step 3: Calculate the orientation of the spacecraft frame from inertia coordinate

$$\mathbf{R}_{\text{in} \rightarrow \text{sc}} = \mathbf{R}_{\text{sts} \rightarrow \text{sc}} \mathbf{R}_{\text{in} \rightarrow \text{sts}} \quad (4.8)$$

The Euler angles ψ_{sc} , θ_{sc} , ϕ_{sc} which respectively represent right ascension, declination and azimuth of the spacecraft (RA_{sc} , DE_{sc} , AZ_{sc}) is obtained from the element matrix $\mathbf{R}_{\text{in} \rightarrow \text{sc}}$.

$$\text{RA}_{sc} = \psi_{sc} = \text{atan2}(R_{12}, R_{11}) \quad (4.9a)$$

$$\text{DE}_{sc} = \theta_{sc} = \arcsin(-R_{13}) \quad (4.9b)$$

$$\text{AZ}_{sc} = \phi_{sc} = \text{atan2}(R_{23}, R_{33}) \quad (4.9c)$$

4.3 Mapping and Pointing Budget

All spacecrafts need to know and control their orientation. The problem of orientation may conveniently be divided into two areas of pointing and mapping. Pointing means orienting the spacecraft, camera sensor, or antenna to a target having a specific geographic position or inertial direction, for example point the antenna to the certain region. Mapping is determining the geographic position of the look point of a camera sensor, or antenna, e.g. determine the geographic location of the new building captured by satellite's camera.

Satellites used only for communications will generally require only pointing. Satellites having some type of viewing instrument, such as weather, ground surveillance, or Earth resources satellites, will ordinarily require both pointing and mapping. If components in the budget are left out or incorrectly assessed, the satellite may not be able to meet its performance objectives. More commonly, people who define the system requirements make the budgets for pointing and mapping too stringent and, therefore, unnecessarily drive up the cost of the mission.

Basic pointing and mapping errors are associated with spacecraft navigation, that is knowledge of its position and attitude in space. But even if the position and attitude are known precisely, a number of other errors will be present. An error in the observation time will result in an error in the computed location of the target, because the target frame of reference moves relative to the spacecraft. A spacecraft that is orbiting in the 500 - 650 km altitude will have ground track velocity about 7 km/s. An error in the observation time for one second would produce an error of 7 km in the computed geographic location of the target. The instrument-mounting error represents the misalignment between the pointed antenna, the payload sensors, or any sensors used to determine the attitude. This error is extremely difficult to remove because it cannot be determined from the attitude data alone, hence it must be viewed as a critical parameter and keep it small while integrating the spacecraft.

The errors associated with mapping depend strongly on how close to the horizon we choose to work. Working in a very small region directly under the spacecraft provides very poor coverage but excellent mapping accuracy and resolution. The uncertainty in target altitude typically contributes most to determining a geographic location on the Earth. The oblateness of the Earth has the largest effect on target altitude. It causes a variation in distance from the center of the Earth of approximately 25 km between the poles and the equator. Nevertheless, for features on the Earth's surface, the uncertainty in target altitude reduces to approximately 1 km. The second principal contributor to mapping error is the uncertainty in attitude determination.

The pointing error must include the entire control error for the spacecraft. Specifically, pointing errors should include inaccuracies in attitude control and angular motion. The angular motion during the exposure or observation time such as short-term jitter results in a blurring of the look point of the instrument. Pointing requirements normally arise from the spacecraft's housekeeping functions such as Sun pointing for power/heat cultivating or from the need to

point a particular instrument or antenna toward a ground target. For most missions, the need to point the mission sensor or antenna is more important. If the sensor is wished to point at a single target, then the spacecraft will generally try to point the center of the sensor at the target. By doing so, a pointing requirement should be established to place the target within the field of view. It is common to have a pointing accuracy of 10% to 20% of the field of view diameter. Driving the pointing under 10% of the field of view diameter will only slightly improve overall coverage. On the other hand, a pointing error worse than 20% of the field of view size can require substantial overlap, thus greatly diminishing the overall system's coverage and resource utilization. Table 4.3 presents the mapping and pointing budget for LAPAN-A satellite series with an accuracy of 20%.

Table 4.3: Mapping and Pointing Budget of LAPAN-A Satellite Series

| Mission | Main Payload | Mapping Budget | Pointing Budget |
|-----------------|---|--|-----------------|
| LAPAN-A1 | High-resolution SONY analog video camera: CCD with 752×582 picture elements; 1000 mm Cassegrain lens; 3.5 km swath and 5 m ground resolution from 630 km altitude. | <i>interactive (man in the loop) control</i> | |
| LAPAN-A2 | Digital space camera (SPACECAM): CCD with 2048×2048 picture elements; 1000 mm Cassegrain lens; 7.2 km swath and 3.5 m ground resolution from 650 km altitude. | 1.44 km | 0.13 deg |
| LAPAN-A3 | Four band pushbroom Line Imager Space Application (LISA): CCD with 8002×4 pixels array; 300 mm lens; 120 km swath and 15 m ground resolution from 508 km altitude | 24 km | 2.7 deg |

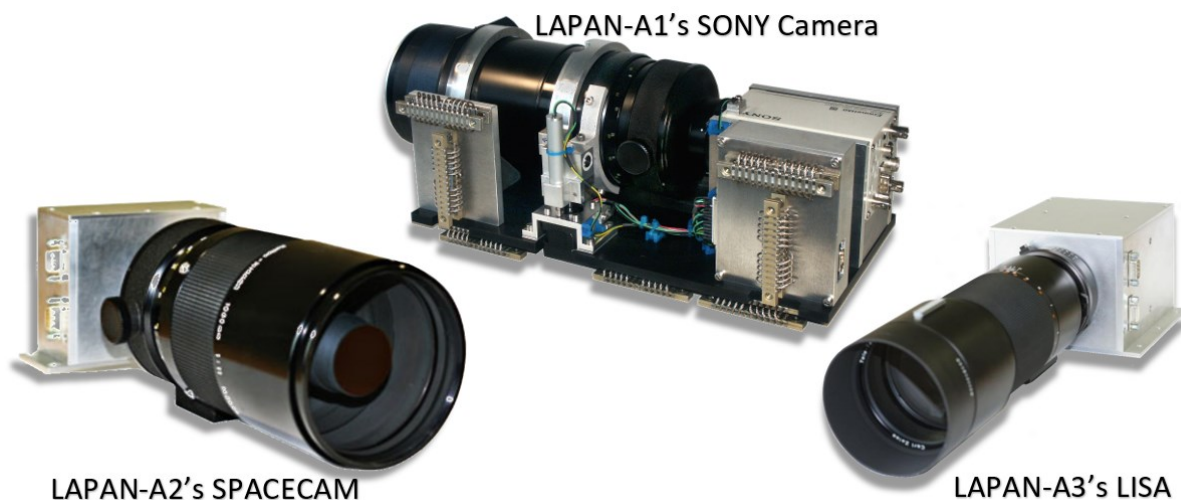


Figure 4.7: Main Payload of LAPAN-A Satellite Series

4.4 Mission Planning Software

Development of mission planning software is necessary for the preparation of mission operations, which can simulate the entire overflight including acquisitions and rotational maneuvers. In addition to the classical plot of the trajectory where the ground track is drawn in a 2D map as shown in Figure 4.8, simulation of high-resolution imaging with a narrow coverage requires a more detailed map. Fortunately, there is a Google Earth application nowadays that allows simulations that plot the spacecraft's ground track on high-resolution Earth imagery via Keyhole Markup Language (KML). KML is a file format used to display geographic data and visualization within internet-based, two-dimensional maps and three-dimensional Earth browsers. KML was developed for application with Google Earth to pinpoint locations, add image overlays, and expose rich data in new ways. KML is an international standard maintained by the Open Geospatial Consortium, Inc. (OGC).

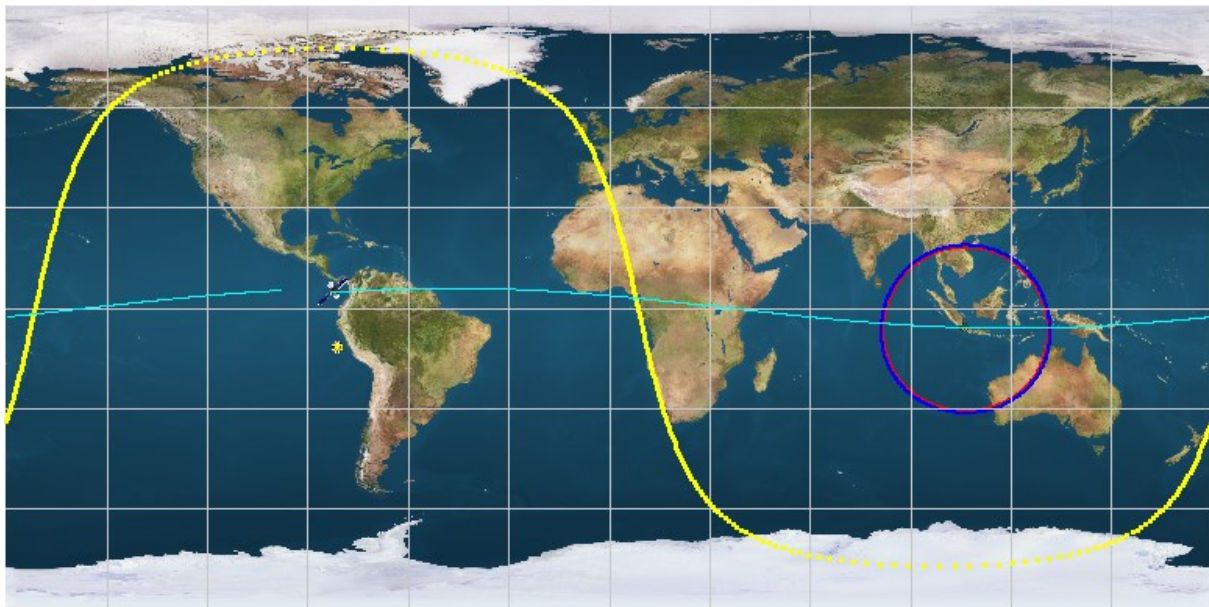


Figure 4.8: Classical Plot of the Satellite Ground Track

By using the KML format, operators could utilize all the tools and features in the Google Earth application, specifically to assist in selecting the target on a high-resolution imaging mission. Google Earth is very helpful in mission planning for high-resolution imaging, especially in showing the last 24 hours of the cloud movement around the world. Data is updated hourly, or as new data become available. If new data is not available, Google Earth will display the most recent complete data instead of showing no cloud. Without global weather awareness, a narrow view camera often produces useless images covered in clouds as shown in Figure 4.9. Google Earth has also equipped with tools to measure the distance between objects on the Earth's surface. Therefore, the operator could easily estimate the maneuver required for imaging, by

measuring the distance between the subsatellite point on the ground to the target, and also evaluates whereby the current weather conditions are permitting for imaging mission.

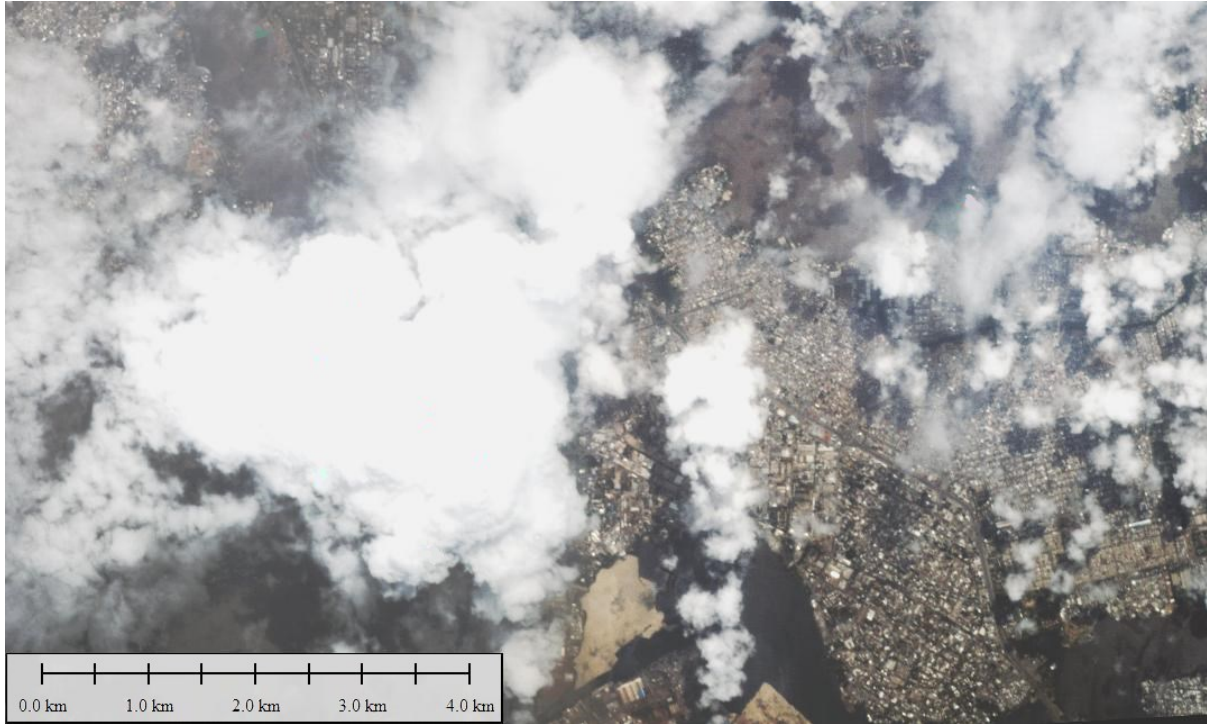


Figure 4.9: Hi-Res Image of Cloudy Abidjan Port, Ivory Coast by SPACECAM of LAPAN-A2 Satellite

The mission planning software uses NORAD – Two Line Elements (TLE) format as the basis of orbit calculation. A set of TLE is a data format encoding a list of parameters of an Earth-orbiting object for a given point in time, the epoch (t_0). Table 4.4 presents the orbital elements contained in TLE related to the observation time or epoch and is provided with an index 0. For ease of calculation, the units in this table are converted into seconds, radians and radians/second.

Table 4.4: The Orbital Elements in the NORAD -TLE

| <i>Element</i> | <i>Notation</i> | <i>Unit</i> |
|--|-----------------|-----------------------|
| <i>Observation time or epoch</i> | t_0 | day |
| <i>Inclination</i> | i_0 | deg |
| <i>Right Ascension of the Ascending Node</i> | Ω_0 | deg |
| <i>Eccentricity</i> | ϵ_0 | decimal point assumed |
| <i>Argument of Perigee</i> | ω_0 | deg |
| <i>Mean Anomaly</i> | M_0 | deg |
| <i>Mean Motion</i> | n_0 | revolutions/day |

To solve the problem of relating position in the orbit to the elapsed time, $t - t_0$, Kepler used the mean anomaly M , that is calculated by using time of flight and the mean motion. In celestial mechanics, the mean anomaly is the fraction of an elliptical orbit's period that has elapsed since

the orbiting body passed periapsis, expressed as an angle which can be used in calculating the position of that body in the classical two-body problem. It is the angular distance from the pericenter which a fictitious body would have if it moved in a circular orbit, with constant speed, in the same orbital period as the actual body in its elliptical orbit.

$$M = M_0 + 2\pi n_0(t - t_0) \quad (4.10)$$

Mean anomaly does not measure an angle between any physical objects. It is simply a convenient uniform measure of how far around its orbit a body has progressed since pericenter. The mean anomaly is one of three angular parameters (known historically as "anomalies") that define a position along an orbit, the other two being the eccentric anomaly and the true anomaly. The eccentric anomaly is an angular parameter that defines the position of a body that is moving along an elliptic orbit. The mean anomaly M can be computed from the eccentric anomaly E and the eccentricity ε_0 with Kepler's Equation.

$$M = E - \varepsilon_0 \sin E \quad (4.11)$$

This equation does not have a closed-form solution for E given M , therefore it is usually solved by numerical methods. The Newton–Raphson method of equation 4.12 is used to calculate the eccentric anomaly from equation 4.11.

$$x_{i+1} = x_i - \frac{f(x_i)}{f'(x_i)} \quad (4.12)$$

To do this, equation 4.11 is resolved to zero and the first derivative is formed.

$$f(E) = E - M - \varepsilon_0 \sin E = 0 \quad (4.13)$$

$$f'(E) = 1 - \varepsilon_0 \cos E \quad (4.14)$$

Substituting equations 4.13 and 4.14 into 4.12 gives equation 4.15.

$$E_{i+1} = E_i - \frac{E_i - M - \varepsilon_0 \sin E_i}{1 - \varepsilon_0 \cos E_i} \quad (4.15)$$

After the iterative calculation of the eccentric anomaly with the Newton–Raphson method, the true anomaly ϕ is calculated with equation 4.16 and the radius r with 4.17.

$$\phi = 2 \arctan \left[\sqrt{\frac{1 + \varepsilon_0}{1 - \varepsilon_0}} \tan \frac{E}{2} \right] \quad (4.16)$$

$$r = \frac{a(1 - \varepsilon_0^2)}{1 + \varepsilon_0 \cos \phi} \quad (4.17)$$

where a is semi-major axis to be calculated considering the orbit perturbation.

When developing the two-body equations of motion, it assumed the Earth has radius R_E with a spherically symmetric mass distribution. In fact, the Earth has a bulge at the equator, a slight pear shape, and flattening at the poles. The orbit perturbation due to a non-spherical Earth,

represented by the J_2 term in the geopotential expansion, gives dominant effects to the secular variations in right ascension of the ascending node Ω and argument of perigee ω [55].

$$\Omega = \Omega_0 + \frac{d\Omega}{dt}(t - t_0) \quad (4.18)$$

$$\Omega = \Omega_0 - \frac{3}{2}J_2n\left(\frac{R_E}{a}\right)^2(1 - \varepsilon^2)^{-2}(\cos i)(t - t_0) \quad (4.19)$$

$$\omega = \omega_0 + \frac{d\omega}{dt}(t - t_0) \quad (4.20)$$

$$\omega = \omega_0 + \frac{3}{2}J_2n\left(\frac{R_E}{a}\right)^2(1 - \varepsilon^2)^{-2}\left(2 - \frac{5}{2}\sin^2 i\right)(t - t_0) \quad (4.21)$$

The semi-major axis a is calculated from the mean motion n by using equations 4.22 and 4.23 [56].

$$n = \frac{dM}{dt} = n_0 \left[1 + \frac{3}{2}J_2\left(\frac{R_E}{a}\right)^2(1 - \varepsilon^2)^{-\frac{3}{2}}\left(1 - \frac{3}{2}\sin^2 i\right) \right] \quad (4.22)$$

$$n_0 = \sqrt{\frac{\mu}{a^3}} \quad (4.23)$$

where μ is the Earth gravitation constant $= 3.986 \times 10^{14} \text{ m}^3\text{s}^{-2}$. Substituting equation 4.23 into 4.22 yields 4.24.

$$n = \frac{dM}{dt} = \sqrt{\frac{\mu}{a^3}} \left[1 + \frac{3}{2}J_2\left(\frac{R_E}{a}\right)^2(1 - \varepsilon^2)^{-\frac{3}{2}}\left(1 - \frac{3}{2}\sin^2 i\right) \right] \quad (4.24)$$

To calculate the semi-major axis a using the Newton–Raphson method, equation 4.24 is solved for zero and the function $f(a)$ and its derivative $f'(a)$ are formed.

$$f(a) = \sqrt{\mu}a^{-\frac{3}{2}} + \frac{3}{2}J_2R_E^2(1 - \varepsilon^2)^{-\frac{3}{2}}\left(1 - \frac{3}{2}\sin^2 i\right)\sqrt{\mu}a^{-\frac{7}{2}} - n = 0 \quad (4.25)$$

$$f'(a) = -\frac{3}{2}\sqrt{\mu}a^{-\frac{5}{2}} - \frac{21}{4}J_2R_E^2(1 - \varepsilon^2)^{-\frac{3}{2}}\left(1 - \frac{3}{2}\sin^2 i\right)\sqrt{\mu}a^{-\frac{9}{2}} \quad (4.26)$$

The function $f(a)$ and $f'(a)$ are inserted into equation 4.12, so the semi-major axis, like the eccentric anomaly, is then calculated iteratively according to equation 4.27.

$$a_{i+1} = a_i - \frac{f(a_i)}{f'(a_i)} \quad (4.27)$$

By calculating the orbit perturbation, the right ascension of the ascending node and the argument of perigee at time t which related to the certain Greenwich sidereal time or Greenwich hour angle of the Vernal Equinox, θ_G , the satellite footprint can be traced via its subsatellite point on the Earth's surface. The subsatellite point (S) is defined as a point where a straight line drawn from a satellite to the center of the Earth intersects the Earth's surface, that is expressed in latitude (φ) and longitude (λ), S (φ , λ). This point can be found by formulas derived from Napier's Rules for right spherical triangles.

$$\sin \varphi = \sin(\omega + \phi) \sin i \quad (4.28)$$

$$\lambda = \lambda_0 + \Omega - \theta_G \quad (4.29)$$

where:

$$\sin \lambda_0 = \frac{\tan \varphi}{\tan i} \quad (4.30)$$

$$\cos \lambda_0 = \frac{\cos(\omega + \phi)}{\cos \varphi} \quad (4.31)$$

$$\lambda_0 = \arctan2(\sin \lambda_0, \cos \lambda_0) \quad (4.32)$$

Assuming the satellite always points its z axis to nadir and the y axis is perpendicular to the orbital plane, then the coordinates of the attitude target associated with the orbit are defined as follows.

- For direction of $-z$ (zenith coordinates):

$$RA_{-z} = \lambda + \theta_G \quad (4.33a)$$

$$DE_{-z} = \varphi \quad (4.33b)$$

$$\begin{aligned} \text{if } |i| < \frac{\pi}{2}; \quad AZ_{-z} &= \frac{\pi}{2} + i \cos(\omega + M) \\ \text{if } |i| > \frac{\pi}{2}; \quad AZ_{-z} &= \frac{3}{2}\pi + (\pi - i) \cos(\omega + M) \\ \text{if } |i| = \frac{\pi}{2}; \quad AZ_{-z} &= \frac{\pi}{2} + i \frac{\cos(\omega + M)}{|\cos(\omega + M)|} \end{aligned} \quad (4.33c)$$

- For direction of $+z$ (nadir coordinates):

$$RA_{+z} = RA_{-z} + \pi \quad (4.34a)$$

$$DE_{+z} = -DE_{-z} \quad (4.34b)$$

$$AZ_{+z} = AZ_{-z} + \pi \quad (4.34c)$$

- For direction of $+y$:

$$RA_{+y} = \Omega + \frac{\pi}{2} \quad (4.35a)$$

$$DE_{+y} = i - \frac{\pi}{2} \quad (4.35b)$$

$$AZ_{+y} = -(\omega + M) \quad (4.35c)$$

- For direction of $-y$:

$$RA_{-y} = RA_{+y} + \pi \quad (4.36a)$$

$$DE_{-y} = -DE_{+y} \quad (4.36b)$$

$$AZ_{-y} = AZ_{+y} + \pi \quad (4.36c)$$

To simulate the rotation angle for any given attitude information to the target coordinate, the coordinate transformation from section 4.2 is used. Therefore, the required maneuver of the spacecraft in roll, pitch and yaw can be determined to meet the target.

Another feature of the mission planning software is calculating the contact schedule of the satellite from any specific locations on the Earth's surface that may refer to the ground stations or the imaging targets. Tracking the satellite by an observer on the Earth's surface use the

horizontal coordinate system, which is also known as topocentric coordinate system, is a celestial coordinate system that uses the observer's local horizon as the fundamental plane. Coordinates of a spacecraft in the sky are expressed in terms of azimuth and elevation angle. For any location of the ground station expressed in latitude (φ_G), longitude (λ_G) and altitude (h_G), the radius of ground station from Earth's center, R_G , is defined.

$$R_G = R_E + h_G \quad (4.37)$$

Given the coordinates of the satellite and the ground station, the angular distance (β) from the subsatellite point to the station will meet the following equation [51].

$$\cos \beta = \sin \varphi_G \sin \varphi + \cos \varphi_G \cos \varphi \cos(\lambda - \lambda_G) \quad (4.38)$$

Applying cosines law for triangle at Figure 4.10 yields equation for a slant range (L) between a satellite and the ground station. This range changes over time since the satellite flies fast above the ground station.

$$L^2 = R_G^2 + r^2 - 2rR_G \cos \beta \quad (4.39)$$

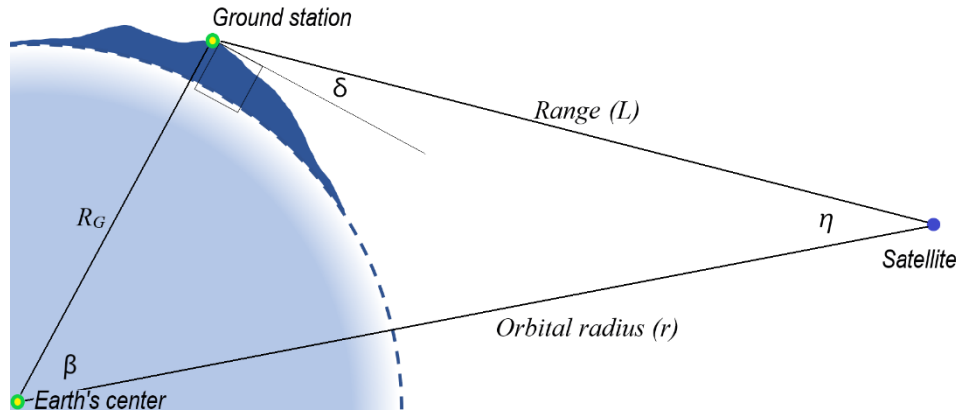


Figure 4.10: Ground Station Geometry

The tracking angle in azimuth (α) and elevation (δ) then be solved by the following relation.

$$\sin \alpha = \frac{\sin(\lambda - \lambda_G) \cos \varphi}{\sin \beta} \quad (4.40)$$

$$\cos \alpha = \frac{\sin \varphi - \sin \varphi_G \cos \beta}{\cos \varphi_G \sin \beta} \quad (4.41)$$

$$\alpha = \arctan2(\sin \alpha, \cos \alpha) \quad (4.42)$$

$$\sin \delta = \frac{r^2 - R_G^2 - L^2}{2R_GL} \quad (4.43)$$

By using those aforementioned equations of orbital dynamics and mission geometry, the mission planning software was developed through the flowchart presented in Figure 4.11.

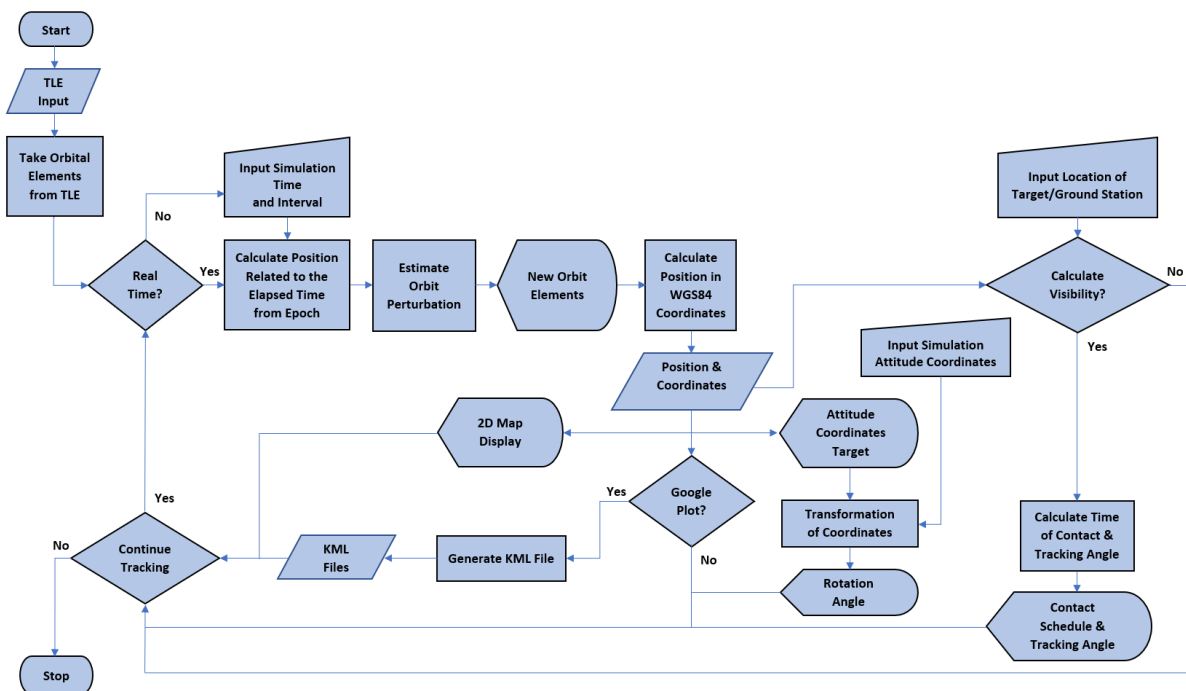


Figure 4.11: Flowchart of the Mission Planning Software

There are three user interfaces in the mission planning software shown in Figure 4.12, i.e., the main interface, the 2D Earth map and the Google Earth plotter. The main interface has three menus named Satellite, Orbit, and Schedule. In the Satellite menu, users could select the satellite and the ground station showing calculated range, tracking angle, the next schedule of AOS (Acquisition of Satellite), maximum elevation in TCA (Time of Closest Approach), and LOS (Loss of Satellite).

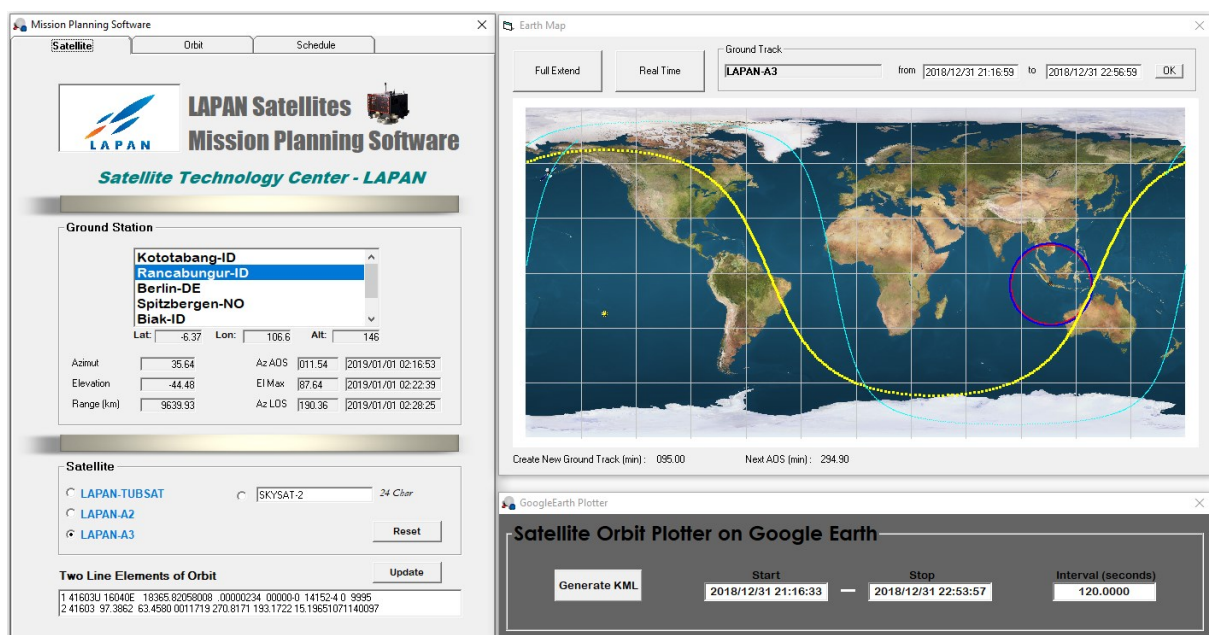


Figure 4.12: User Interfaces of the Mission Planning Software

Figure 4.13 shows Orbit and Schedule menus in the main interface of the software. Orbit menu displays the orbital element, celestial coordinates of the attitude target, and the attitude maneuver simulation. In the orbital element frame, the software displays the elements that are taken from TLE as well as the updated elements due to orbit perturbation. Celestial coordinates frame presents the attitude target associated with the orbit which is assuming the satellite always points toward nadir. Coordinates of z and y in both positive and negative direction are continuously calculated by software since they are generally used in the estimation of attitude correction or maneuver. The third frame in the Orbit menu is attitude maneuver. Two coordinates can be manually input by user, spacecraft zenith (S/C Zenith) as an initial attitude before maneuver and the star coordinates, to simulate the required maneuver in roll, pitch, and yaw to achieve the target. In this frame, users have 5 options of maneuver estimation from initial attitude to the target coordinates of star, zenith, nadir, $+y$ direction, or $-y$ direction.

Meanwhile, the Schedule menu allows users to create the schedule of satellite visibility from the specific location or ground station as well as calculation of its tracking angle. Users only need to enter the number of passes they will make from the time specified in the text box. This Schedule menu can also create the tracking angle represented by azimuth – elevation and range from the specified AOS time.

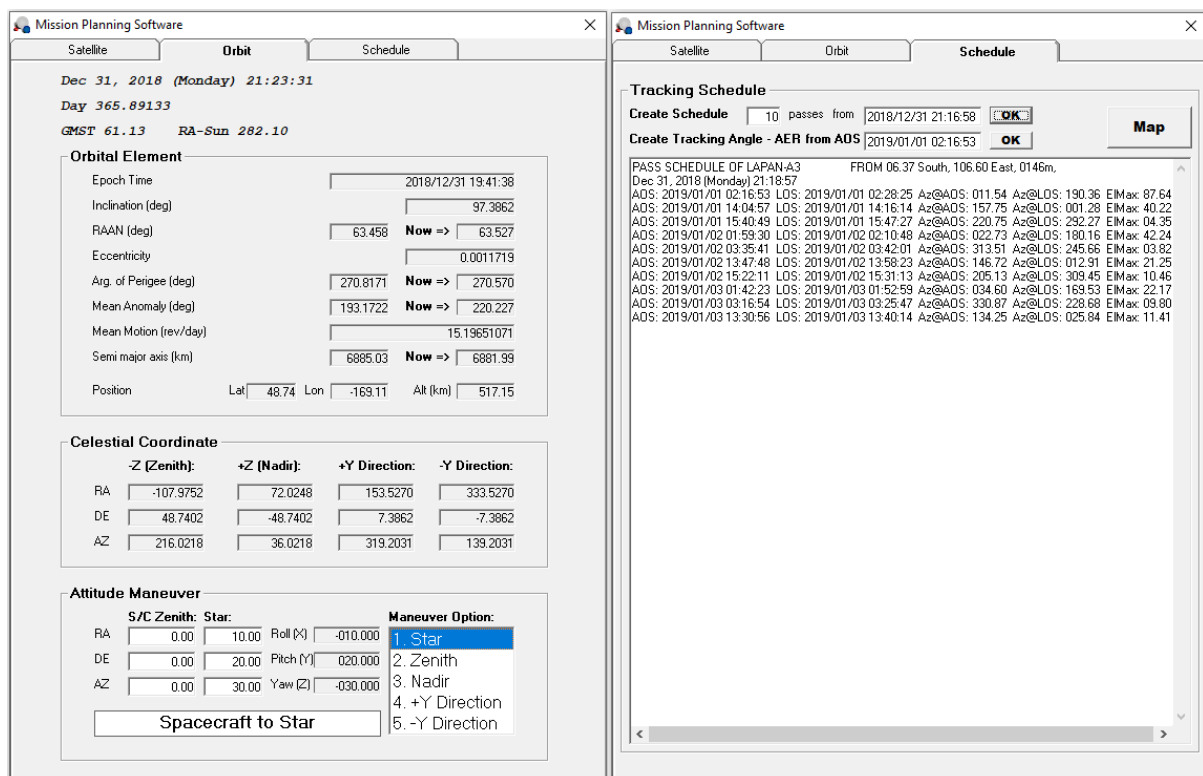


Figure 4.13: Orbit and Schedule Menus in the Main Interface

Figure 4.14 displays the interface of 2D Earth map that simulates the satellite ground track. By default, the software would present real time tracking and plot a single orbital period of ground track onto 2D map. Nevertheless, users are possible to plot multiple cycles of ground track

depends on the designated start and end time in the input text box. The user could also zoom the map to get better visualization as shown in the figure, but it is limited by the resolution of the map image.

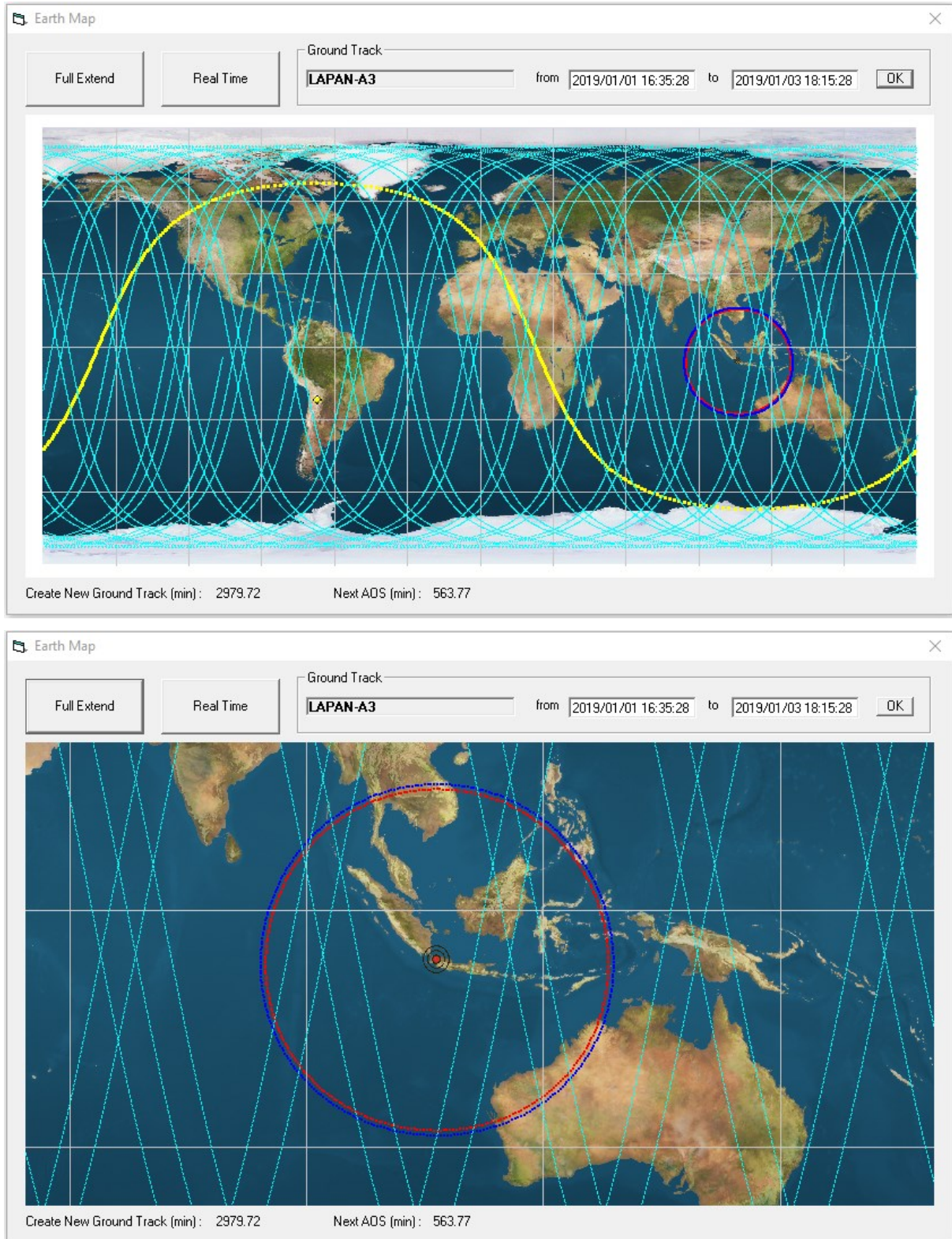


Figure 4.14: 2D Earth Map Interface

For better visualization, Google Earth plotter interface generates a KML file containing a satellite ground tracks in a specified time duration an interval inputted by users. Figure 4.15 shows a KML file code containing ground track coordinates that is placed in a text file. Meanwhile, Figure 4.16 and Figure 4.17 display the satellite ground track in the Google Earth application.

```

1  <?xml version="1.0" encoding="UTF-8"?>
2  <kml xmlns="http://www.opengis.net/kml/2.2" xmlns:gx="http://www.google.com/kml/ext/2.2"
   xmlns:kml="http://www.opengis.net/kml/2.2" xmlns:atom="http://www.w3.org/2005/Atom">
3  <Document>
4    <name>LAPAN-A2_GroundTrack.kml</name>
5    <StyleMap id="m_ylw-pushpin">
6      <Pair>
7        <key>normal</key>
8        <styleUrl>#s_ylw-pushpin</styleUrl>
9      </Pair>
10     <Pair>
11       <key>highlight</key>
12       <styleUrl>#s_ylw-pushpin_hl</styleUrl>
13     </Pair>
14   </StyleMap>
15   <Style id="s_ylw-pushpin_hl">
16     <IconStyle>
17       <scale>1.3</scale>
18       <Icon>
19         <href>http://maps.google.com/mapfiles/kml/pushpin/ylw-pushpin.png</href>
20       </Icon>
21       <hotSpot x="20" y="2" xunits="pixels" yunits="pixels"/>
22     </IconStyle>
23   </Style>
24   <Style id="s_ylw-pushpin">
25     <IconStyle>
26       <scale>1.1</scale>
27       <Icon>
28         <href>http://maps.google.com/mapfiles/kml/pushpin/ylw-pushpin.png</href>
29       </Icon>
30       <hotSpot x="20" y="2" xunits="pixels" yunits="pixels"/>
31     </IconStyle>
32   </Style>
33   <Placemark>
34     <name>PATH1</name>
35     <styleUrl>#m_ylw-pushpin</styleUrl>
36     <LineString>
37       <tessellate>1</tessellate>
38       <coordinates>
39         -150.149040,35.663849,0
40         -156.763484,5.562165,0
41         -162.879204,-24.535211,0
42         -171.922091,-54.408200,0
43         138.601838,-81.300753,0
44         29.471466,-63.333230,0
45         17.465983,-33.664564,0
46         10.980807,-3.604235,0
47         4.805073,26.512972,0
48         -4.756847,56.442668,0
49         -67.521332,82.239696,0
50         -163.925606,61.065041,0
51         -174.979468,31.227799,0
52       </coordinates>
53     </LineString>
54   </Placemark>
55 </Document>
56 </kml>

```

Figure 4.15: Placing KML File Code in A Text File

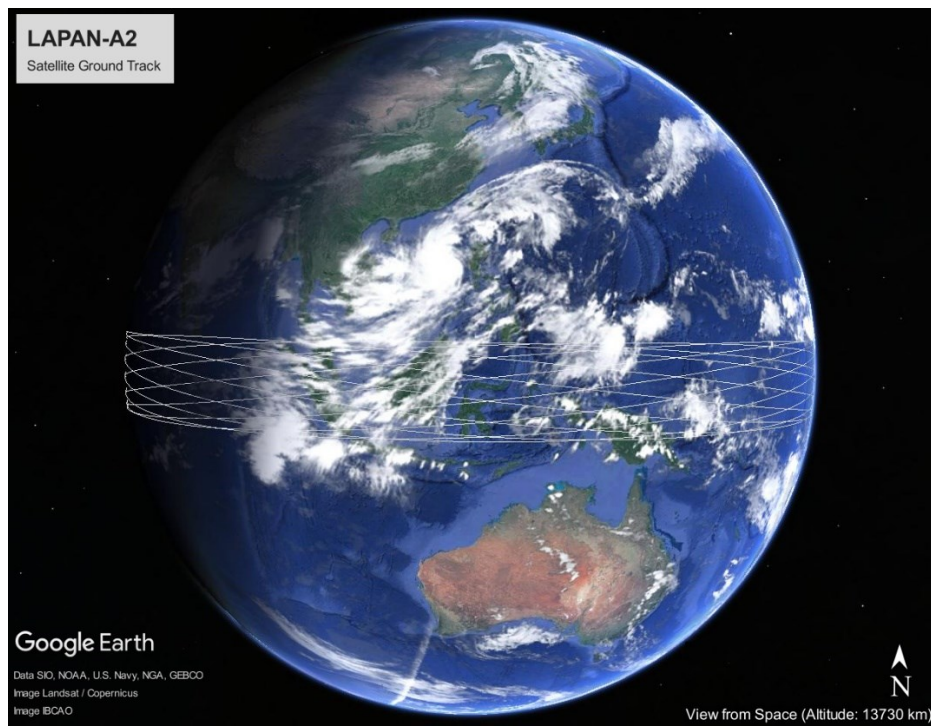


Figure 4.16: Plotting the Ground Track of LAPAN-A2 Satellite in the Google Earth

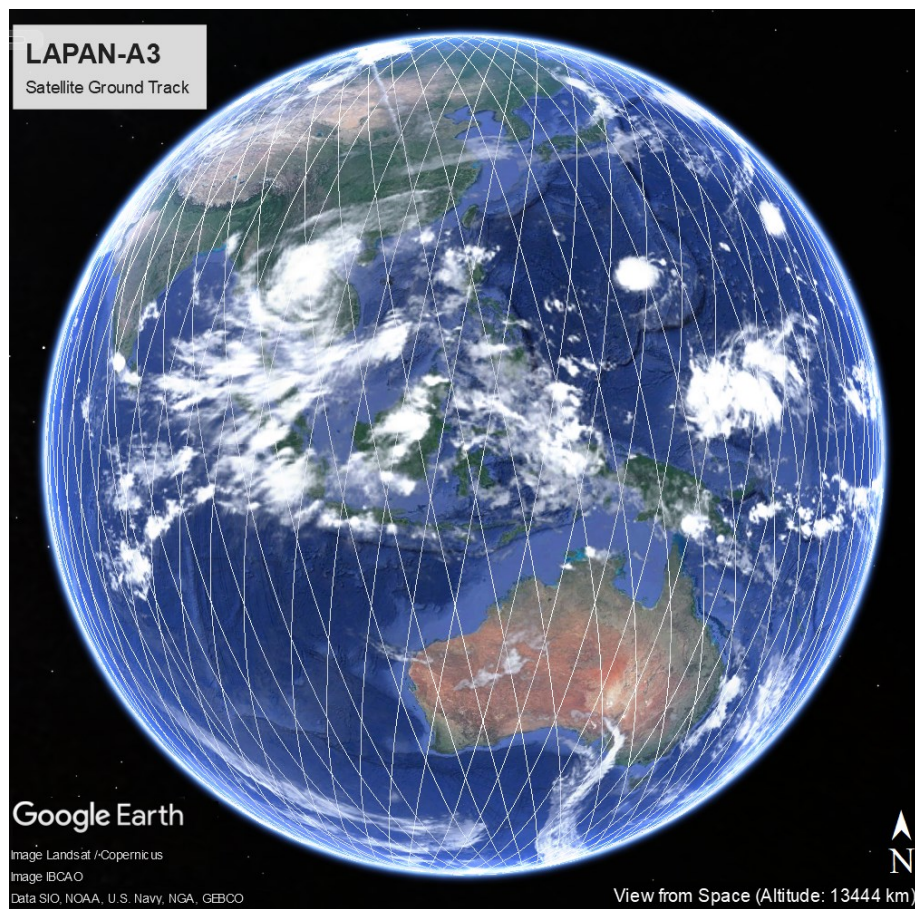


Figure 4.17: Plotting the Ground Track of LAPAN-A3 Satellite in the Google Earth

In addition to the advantages of high-resolution image of Google Earth and near real time cloud images, there are many tools in the Google Earth that are useful for mission planning of high-resolution imaging when the satellite ground track is plotted on the Google Earth application. For example, Google Earth provides a *ruler* tool to measure the distance between two objects on the Earth's surface. By accurately measuring the target's distance from the ground track, the attitude maneuver could be properly estimated. Figure 4.18 shows measuring the target distance from the satellite ground track during an imaging mission of Krakatau Volcano Eruption at April 11th, 2020. Since the angular distance β has been known, then, the nadir angle (η) will be found from the following equation.

$$\tan \eta = \frac{\sin \beta \left[\frac{R_E}{r} \right]}{1 - \cos \beta \left[\frac{R_E}{r} \right]} \quad (4.44)$$

In the example case of Krakatau imaging, the angular distance is 0.31 deg, which equals to 3.04 deg of nadir angle from the orbit of LAPAN-A2 satellite. This nadir angle corresponds to the roll maneuver required for imaging. Once the imaging process is complete, the images produced by the satellite can also be converted into a KML file so that it can be overlaid on Google Earth images. Nowadays, the process of converting images to KML files can be done using GIS (Geographic Information Systems) software such as Global Mapper and so on. Thus, in addition to mission planning, satellite ground track plots in the Google Earth application can also be used for post-imaging pointing evaluation.

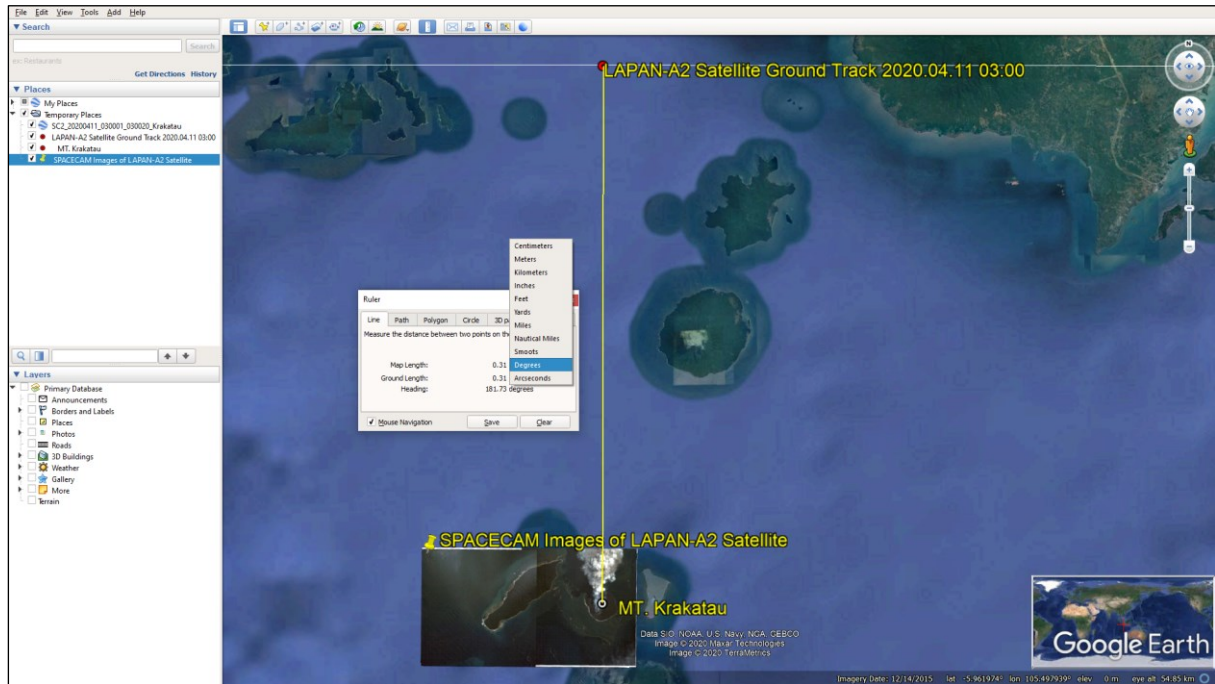


Figure 4.18: Measuring Distance of the Target from Satellite Ground Track in the Google Earth

4.5 Attitude Dynamic

The fundamental quantity in rotational mechanics is the angular momentum, H . For a rigid body that rotate at an angular velocity of ω about its center of mass, the total angular momentum of rigid body is expressed in the simple form

$$H = I \cdot \omega \quad (4.45)$$

where I identify moments and products of inertia which is known as the inertia tensor. It may be written in matrix form as

$$H = \begin{bmatrix} H_x \\ H_y \\ H_z \end{bmatrix} = \begin{bmatrix} I_x & -I_{xy} & -I_{xz} \\ -I_{xy} & I_y & -I_{yz} \\ -I_{xz} & -I_{yz} & I_z \end{bmatrix} \begin{bmatrix} \omega_x \\ \omega_y \\ \omega_z \end{bmatrix} \quad (4.46)$$

The rotational kinetic energy of a rigid body about its center of mass, T_{rot} , is related to angular momentum that takes the simple form

$$2T_{rot} = \omega \cdot H = \omega \cdot I \cdot \omega \quad (4.47)$$

Furthermore, H is fixed in space, if ω is parallel to H then this condition corresponds to simple spin about the axis. But in general, ω and H are not colinear and two cones may be used to describe the motion, i.e. body cone and space cone. The body cone is attached to the principal axis coordinate system of the body, while the space cone is attached to H and is fixed in inertial space. The path of ω creates a body cone and a space cone, so that motion is simply described as the body cone rolling on the space cone with corresponding to the line of tangency.

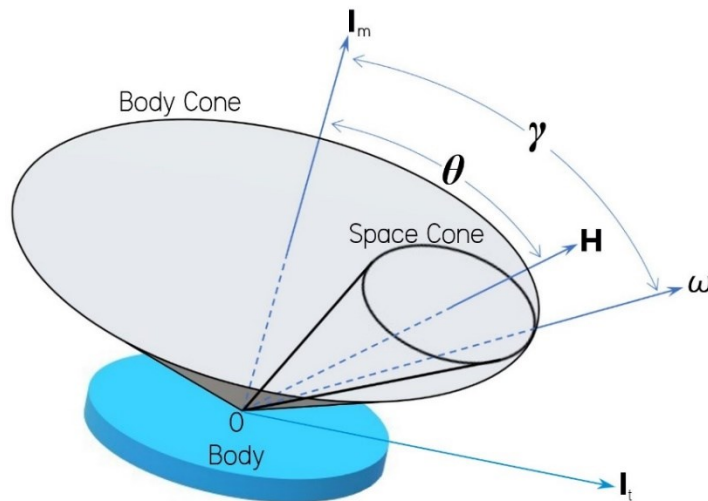


Figure 4.19: Cones Motion of Axisymmetric Body

For an axisymmetric body whose symmetry axis coincides with its mayor axis which contain moment of inertia I_m , as depicted in Figure 4.19, and has transverse of moment of inertia I_t , would apply

$$\tan \theta = \frac{H_t}{H_m} = \frac{I_t \omega_t}{I_m \omega_m} \quad (4.48)$$

$$\tan \gamma = \frac{\omega_t}{\omega_m} \quad (4.49)$$

Both θ and γ are constant, and they are related by

$$\tan \theta = \frac{I_t}{I_m} \tan \gamma \quad (4.50)$$

Angle θ provides the body axis orientation with respect to an inertial direction and is usually called the nutation angle.

The rate of change of momentum can be related to an applied torque about the center of mass. It can be represented by three differential equation that are relating applied torque components to angular momentum changes.

$$\tau_x = \dot{H}_x + \omega_y H_z - \omega_z H_y \quad (4.51)$$

$$\tau_y = \dot{H}_y + \omega_z H_x - \omega_x H_z \quad (4.52)$$

$$\tau_z = \dot{H}_z + \omega_x H_y - \omega_y H_x \quad (4.53)$$

These three simply written equations modeled the general attitude motion of a rigid body, which are known also as Euler's moment equation.

At a low Earth orbit the sources of external disturbance torque can be gravity gradient, solar pressure, atmospheric drag, and magnetic field. The relatively strong magnetic fields that occur in low Earth orbit can create disturbance torques that need to be managed, but they also allow the use of magnetic torquers, a means of attitude control not available at much higher altitudes like geosynchronous orbit. As well as gravity gradient, it has been used to passively stabilize satellites in a fixed orientation using only the orbited body's mass distribution and gravitational field, in particular for low eccentricity orbiting missions.

Gravity gradient. The Earth's gravitational field varies inversely with distance from the Earth, so that the gravitational field varies slightly across a spacecraft's length. This difference in acceleration causes a torque on the spacecraft. The gravity gradient torque increases with the angle between the local vertical and the spacecraft's principal axes, always trying to align the minimum principal axis with the local vertical. A simplified expression for the gravity gradient torque for a spacecraft with the minimum principal axis in its z direction is

$$\tau_{gg} = \frac{3\mu}{2R^3} |I_z - I_x| \sin(2\theta_z) \quad (4.54)$$

where μ is the Earth gravitation constant $= 3.986 \times 10^{14} \text{ m}^3\text{s}^{-2}$, R is orbit radius in m, θ_z is maximum deviation of spacecraft vertical axis (z) from local vertical, I_x is moment inertia on x or y axis, depends on the axis being analyzed, and I_z is moment inertia on vertical axis (z)

Solar pressure. Sunlight has momentum, and therefore it exerts pressure on those objects it strikes. The amount of momentum transferred depends on the type of surface being illuminated. It will be lowest for transparent surfaces, higher for absorbent surfaces and highest for reflective surfaces. In general, it can be said that solar arrays are absorbers and a spacecraft's body is a reflector. The torque exerted on a spacecraft by solar radiation is as follows.

$$\tau_{sp} = C_{sp} A_{sp} l \quad (4.55)$$

where C_{sp} is solar pressure constant $= 0.5 \times 10^{-5} \text{ N/m}^2$, A_{sp} is solar panel area in m^2 , and l is lever arm of solar panel in m.

Atmospheric drag. The atmospheric density is roughly an exponentially decaying function of altitude, so that generally only spacecraft in low Earth orbit encounter enough particles to cause noticeable disturbances. Those that do experience a pressure force known as atmospheric or aerodynamic drag. For spacecraft above an altitude of 500 km this can generally be neglected. The torque experienced on a spacecraft by aerodynamic drag is as follows.

$$\tau_a = 0.5[\rho C_d A V^2](c_{pa} - c_m) \quad (4.56)$$

where ρ is the atmospheric density in kg/m^3 , C_d is the drag coefficient (usually between 2.0 and 2.5 for spacecraft), A is the ram area in m^2 , V is the spacecraft's orbital velocity in m/s , and c_{pa} and c_m are the centers of aerodynamic pressure and mass in m.

Magnetic field. Most spacecraft have some level of a residual dipole moment, meaning they have a weak magnetic field of their own. When a spacecraft's residual dipole moment is not aligned with a local magnetic field, it experiences a magnetic torque that attempts to align the magnet to the local field, much like a compass needle. The magnetic field of the Earth causes a cyclic torque across the spacecraft no matter its orientation due to interactions with the spacecraft's magnetic dipole. The maximum torque can be approximated using the following formula

$$\tau_m = DB = D \left[\lambda \frac{M}{R^3} \right] \quad (4.57)$$

where D is the spacecraft's residual dipole moment in $\text{A}\cdot\text{m}^2$, and B is the magnetic field strength in tesla. The magnetic field strength in turn is calculated from M , the magnetic moment of the Earth multiplied by the magnetic constant ($M = 7.8 \times 10^{15} \text{ tesla}\cdot\text{m}^3$); R , the distance between the spacecraft and the Earth's center in m; and λ , which is a unitless function of the magnetic latitude that ranges from 1 at the magnetic equator to 2 at the magnetic poles. Similar to the gravity gradient, the magnetic field is inversely proportional to the Earth radius to the power of 3, that is why they are neglected in GEO but are very dominant in LEO.

Figure 4.20 illustrates the local Earth's magnetic field direction of the polar orbiting satellite

that is constantly changing over the orbit. The situation is more complex as not only the direction is varied, but its strength also changes such that at the equator is about half of that of the poles. So rather than zero, the average sum of the magnetic field in an orbital cycle is about half the polar strength to the south. This magnetic field interacts with the residual dipole from the spacecraft to produce a disturbance torque. This residual dipole moment can originate from electrical currents and magnetic materials inside the spacecraft. In the design of satellite, it is important to minimize this value, for instance by including twist in the cables and avoiding large loops on the electronic boards because due to different currents over time, it is hard to estimate.

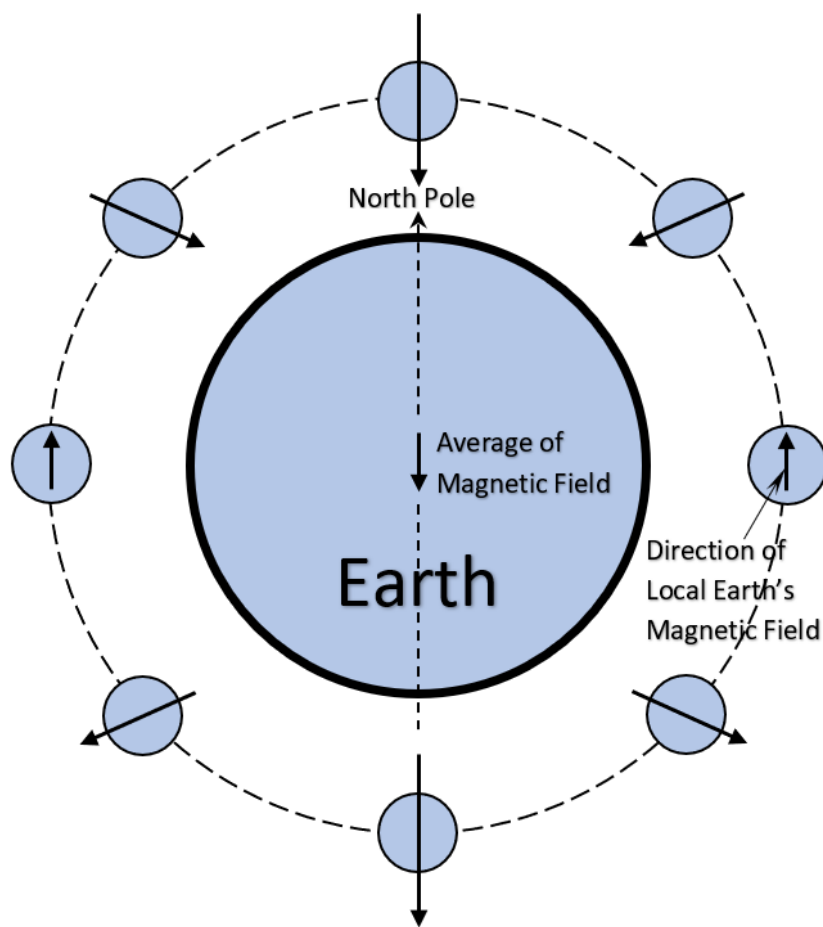


Figure 4.20: Local Earth's Magnetic Field Direction of Polar Orbiting Satellite

5 ATTITUDE CONTROL SYSTEM OF LAPAN-A SATELLITE SERIES

5.1 Momentum Bias Strategy

As a small satellite, LAPAN-A satellite series have very limited power generation due to the constraint of not using a deployable solar panel system. Therefore, the satellite requires a power saving operation mode, so that only a minimal number of components are operated and therefore minimized the power consumption. Hence, the momentum bias technique that uses a minimum device is the most appropriate choice for the attitude control system. Even in idle mode or what is sometimes referred to as hibernation mode, all of attitude control devices could be switched off, remains only the data handling, telemetry and command unit are activated in order to keep the readiness of command receptions from the ground station.

Performing momentum bias operation, the satellite angular momentum is maintained to be perpendicular to the orbit plane. The maximum moment of inertia or mayor axis is designed to be aligned or very close to the pitch axis, so that the rotation along the pitch axis is stable. The cross product of inertia would be minimized to keep the nutation very small when the system for nutation damping is switched off. The reaction wheel on the pitch axis is set as the main controller of angular momentum exchange so that the satellite will rotate according to operating requirements, whether directing the satellite towards the earth or stopping the spacecraft rotation. With the aim of gyroscopic stability, the pitch wheel will rotate about 80% of its maximum speed or angular momentum storage capacity, while one of the wheels on the transverse axis has to damp the oscillation motion called nutation. Once the oscillation motion has been damped in a few minutes' operation, the pitch wheel will be the only device that works continuously to control attitude for more than 90% of the satellite work cycle. Thus, the momentum bias strategy is very efficient and more power saving.

In the flight configuration, as illustrated by Figure 5.1, LAPAN-A satellite series define x as roll axis which point to the flight direction, y as pitch axis that is perpendicular to the orbit plane, and z as yaw axis which point toward nadir. The attitude control system uses 3 pairs of highly integrated reaction wheel-gyro and 3 magnetic torquers as actuators that are placed in

three orthogonal axes. For attitude acquisition, 6 solar cells/panels which attaches to each side of the spacecraft are applied as Sun sensor. In the later series, the spacecraft also equips its attitude control system with a magnetometer. These two types of coarse attitude sensor would provide an attitude reference in the acquisition phase while the spacecraft was rotating in the faster speed e.g. after launch separation or in the hibernation mode. Once the reaction wheel could handle the spacecraft rotation below 0.5 deg/s, the star tracker/sensor will establish a more accurate attitude determination, in particular to find the direction of momentum vector.

However, operating momentum bias stabilization for small satellites in low Earth orbit requires special provision. Unlike in geostationary orbit, in which the strategy is quite popular, the angular momentum in low Earth orbit is dominantly disturbed by Earth's magnetic field and the aerodynamic drag. But in the case of LAPAN-A satellite series that orbiting above 500 km, the aerodynamic effect is negligible. Magnetic disturbance could be minimized by compensating the residual magnetic dipole on the spacecraft, which could be done by the 3 air coils after the internal magnetism can be measured. While geostationary frequently use thrusters to maintain the angular momentum and horizon sensor to monitor the direction of the vector, LAPAN-A satellite series use magnetic torquers to generate external torque together with three reaction wheels and utilize star sensor to keep track of the angular momentum vector [46] [57].

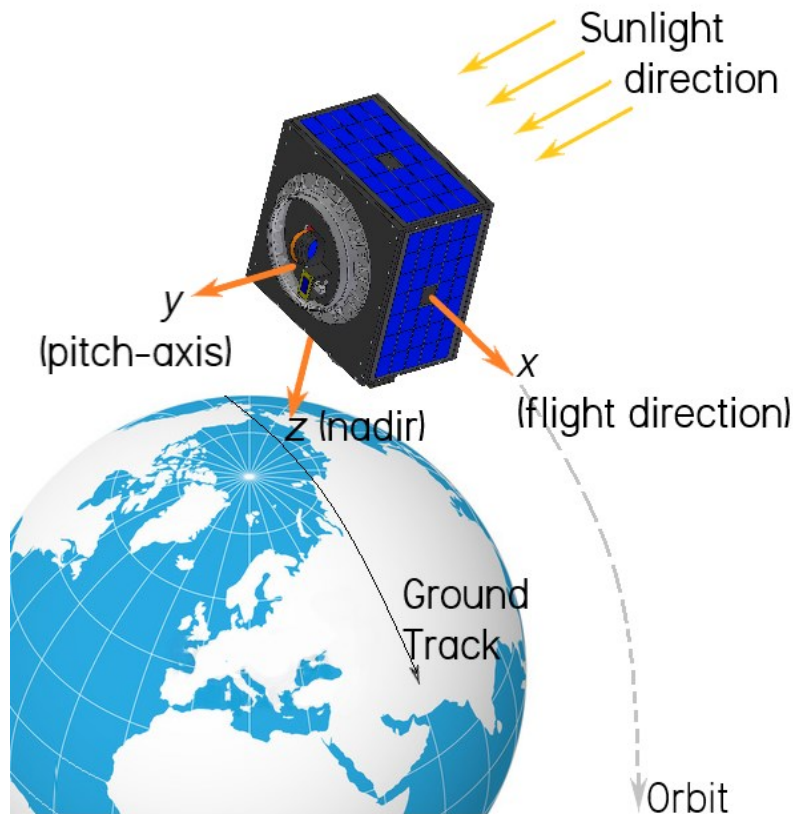


Figure 5.1: Satellite's Flight Configuration

The nominal operation of momentum bias attitude control for LAPAN-A satellite series can be divided into 3 main modes:

1. **Nadir Pointing Mode**, that take more than 90% of the spacecraft duty cycle, in which the angular momentum is maintained in pitch axis which is perpendicular to the orbital plane. Here the reaction wheel on the y axis is set to handle the angular momentum, so that the spacecraft is three-axis stabilized with the camera or directional antennas on the z axis point toward nadir.
2. **Slew Mode**, in which the satellite performs three-axis control to achieve certain targets by utilizing its slew capability through three pairs wheel-gyro operation. This mode is often referred to as *off-nadir pointing mode* while scanning the Earth's surface with a certain offset angle from the spacecraft ground track. This mode could be any modes that operate three wheels-gyros simultaneously, such as a *target pointing mode* or an *inertial pointing mode*.
3. **Hibernation Mode**, in which all systems are switched off except the OBDH and TTC. In this mode, the spacecraft rotates as a single spinner.

5.1.1 Nadir Pointing Mode

While the spacecraft in the nadir pointing mode, the y wheel-gyro loop which is on the y axis, is commanded to angular velocity integrating mode with a constant rate that maintains the z axis nadir orienting. The y wheel runs at a nominal high speed and contains the momentum bias. With a certain bias setting of angular velocity this loop can control the y wheel speed due to disturbance torques. Nevertheless, the gyro signal has systematic error that drifts the attitude away from the target and needs regular attitude correction using the star sensor. For nutation damping, the x wheel-gyro loop which is on the x axis, is commanded to the angular velocity of zero. It will damp nutation in both x and z axis and transfers automatically any wheel speed to the y wheel. Thus, the y wheel and spacecraft angular velocity in y axis will absorb all of angular momentum that leads y axis to be aligned with the angular momentum direction of the spacecraft.

Since the angular momentum is aligned with y axis, the drift of angular momentum is observed directly through y axis. As a target point on the celestial sphere that is illustrated in the Figure 5.2, the angular momentum coordinates are expressed as right ascension (RA) and declination (DE). The right ascension measures the angular distance eastward along the celestial equator from the vernal equinox to the target. The declination measures the angular distance of the target perpendicular to the celestial equator, positive to the north, and negative to the south. Nevertheless, knowing angular momentum coordinates is not sufficient to determine the spacecraft attitude, thereby the third coordinate have to be introduced by defining azimuth (AZ) as rotation along pitch axis.

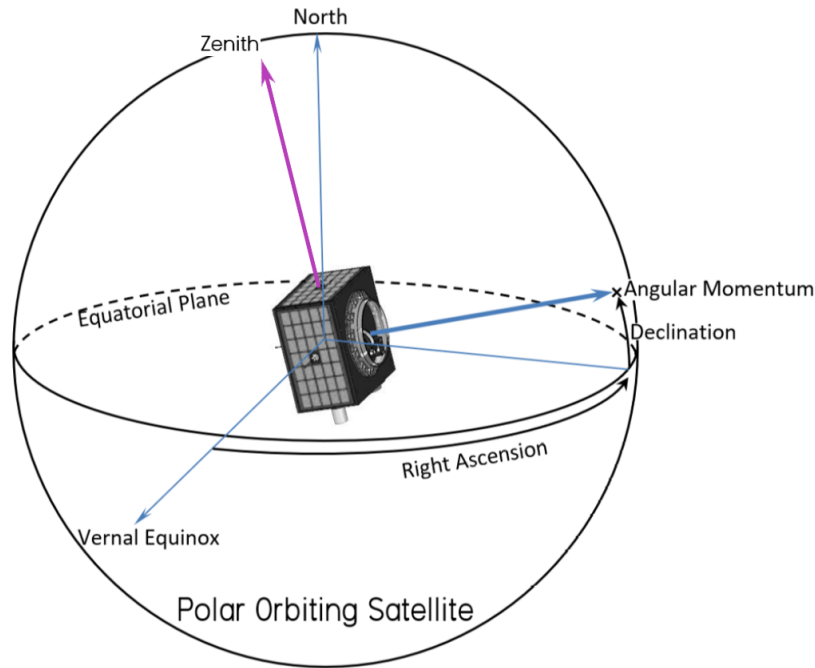


Figure 5.2: Angular Momentum Direction [45]

The attitude angles RA , DE and AZ are quasi stable, i.e. they will slowly drift away due to disturbance torques and need to be adjusted at certain intervals, typically once or twice a day which is convenient for the operator. Meanwhile the changing of AZ can directly manage by y wheel that control pitch rotation, the drift of RA and DE are to some extent compensated by a bias current setting of the y magnetic torquer or air coil. The current of the coil will induce magnetic dipole that interact with a local Earth's magnetic field to produce external torque. The y coil of Figure 5.3 produces a magnetic dipole when current I_y flows around the loop. An interaction between the y coil and local Earth's magnetic field B would produce different direction of torque τ_y , which depends on the satellite orientation and position above the Earth. Above the pole, applying positive current on the y coil in nadir pointing would deviate right ascension of angular momentum H in a positive direction, but above the equator, it drifts in a negative direction.

Even though the geomagnetic field is continuously changing over the orbit, the average field over 24 hours is constant. For this reason, there is not necessary to read RA and DE continuously, but in intervals of 24 hours would enough. Based on the actual data and the data from the previous day the new y coil command is calculated that maintains the RA angle at a constant bias value. The bias is responsible for the control of DE through gravity gradient torque utilization. In this way a single constant y coil current is able to (1) compensate the disturbance torque, (2) control RA , and (3) control DE .

A constant bias value on the y coil for a long time would slowly precess RA . The drift of angular momentum in RA will tilt the z axis from local vertical, in particular when the spacecraft in the

equator region. Hence, it will generate the gravity gradient torque where the maximum deviation of the spacecraft vertical axis from local vertical is equal to the right ascension drift. The gravity gradient torque due to right ascension drift will create drifting also on declination of angular momentum. On average the net effect of the inclined momentum vector is only a half of the orbital period, thus, the angular momentum that generated by the gravity gradient torque is multiplied by the factor of $\frac{1}{2}$.

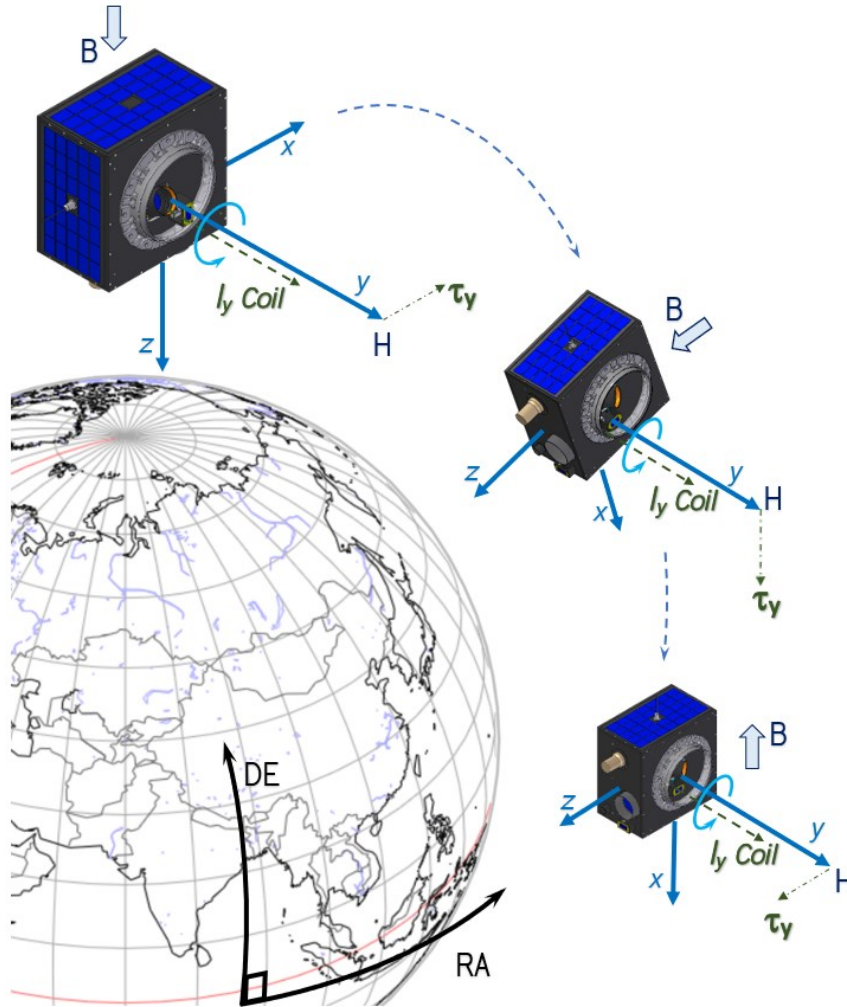


Figure 5.3: Magnetic Torque and Angular Momentum of Polar Orbiting Satellite

The angular momentum direction which coincides with the y axis or pitch axis has to be perpendicular to the orbital plane. Therefore, the target coordinates of right ascension and declination of the angular momentum, RA_{AM} and DE_{AM} in degree respectively, in the celestial sphere are related to the orbital elements and can be obtained by the following equation.

$$RA_{AM} = \Omega + 90^\circ \quad (5.1)$$

$$DE_{AM} = i - 90^\circ \quad (5.2)$$

where Ω is orbital right ascension of ascending node and i is orbital inclination. Meanwhile, azimuth or rotation along the pitch axis will follow

$$AZ_{AM} = \theta_o - (\omega + M) \quad (5.3)$$

where θ_o is initial angle or offset angle, ω is orbital argument of perigee, and M is orbital mean anomaly.

To conduct a real time evaluation toward an angular momentum direction, the target coordinates of angular momentum has been calculated by a program that are embedded in the operating software for acquisition of satellite telemetry. While the target coordinates are derived from orbital elements of the satellites, the actual coordinates are obtained and transformed directly from the star sensors during telemetry acquisition. The required maneuver for attitude correction, as hereinafter calculated, is provided in real time by operating software as the difference between actual and target coordinates.

As an example, Figure 5.4 displays a real time calculation of attitude deviation from the target of LAPAN-A3 satellites that is obtained from transformed star sensor coordinates, SolarPanels (Y-), and the target, Target (Y-). Based on those calculated deviation or difference, [diff], the satellite operator could perform “man in the loop” maneuver of angular momentum correction. This maneuver is started by choosing and activating the right torquer and simultaneously request the telemetry to get the feedback. Once the angular momentum reaches the target, that is indicated by difference of zero, the maneuver is stopped. In doing so, the operators could freely adjust the maneuver by their preference whether working with large torque in a short duration or using a smaller torque in a longer duration.

| | | | | | | |
|---|---|-------------------------------------|-----------------|------------|---------|-------------|
| ----- | | | | | | |
| 2019/09/01 13:49:19 STS VAS Request Hardware Trigger Command | | | | | | |
| [0x75 0xAC 0x00 0x0C 0xFF 0xFF 0xFF 0xFF 0x6F 0x2A 0x00 0x00 0x00 0x00 0x00 0x00] | | | | | | |
| Quaternion | | | | | | |
| q1 | : | -0.790366500000 | | | | |
| q2 | : | -0.254123800000 | | | | |
| q3 | : | -0.542423200000 | | | | |
| q4 | : | 0.128526100000 | | | | |
| | | | | | | |
| RA | : | 42.884 | | | | |
| DE | : | 67.331 | | | | |
| AZ | : | 169.154 | | | | |
| | | PitchSensor(Y+) | SolarPanels(Y-) | Target(Y-) | [diff] | Zenith (Z-) |
| RA | : | 33.346 | 213.346 | 211.42 | [-1.93] | 181.16 |
| DE | : | 6.679 | -6.679 | -7.36 | [-0.68] | 82.12 |
| AZ | : | 175.813 | 355.813 | 356.04 | [0.23] | 31.95 |
| Status register 1 | : | 00000000 00000000 00000000 00001000 | | | | |
| | | #03 Tracking Mode Active | | | | |
| Status Register 2 | : | 00000000 00000000 | | | | |
| Sequence Number | : | 52164 | | | | |
| System time | : | 19927.75 | | | | |
| Ref time of last valid attitude | : | 19927.55 (0 Min 0 Sec) | | | | |
| PPS time stamp | : | 0.00 | | | | |
| Predicted AZ Y-/Diff | : | 355.80 / 0.00 | | | | |

Figure 5.4: Angular Momentum Monitoring on the LAPAN-A3 Satellite Telemetry

5.1.2 Slew and Hibernation Mode

Each LAPAN-A satellite series carries three integrated wheels-gyros in orthogonal axis. By distributing the angular momentum to each wheel, the satellite could perform slew maneuver in certain orientation. Operating three wheels-gyros simultaneously will enable satellites perform off-nadir pointing or target pointing as well as inertial pointing without any limitation. Figure 5.5 shows the slew capability that could be performed by LAPAN-A satellite series. In the off-nadir pointing, a satellite is rolling to a certain angle to make the camera point to the designated region that usually across the ground track. Such advantage makes the revisit time, the interval of time the satellites can make the same picture of a certain area, become shorter than around 16 days of conventional nadir-pointing by polar orbiting satellites. The off-nadir pointing would enable the polar orbiting satellite to make imaging of the equatorial region in two consecutive days. Generally, it requires a short maneuver within the transient time of less than 60 seconds as shown in the Figure 5.6. Even for a small roll maneuver (≤ 10 deg), the transient time is less than 30 seconds.

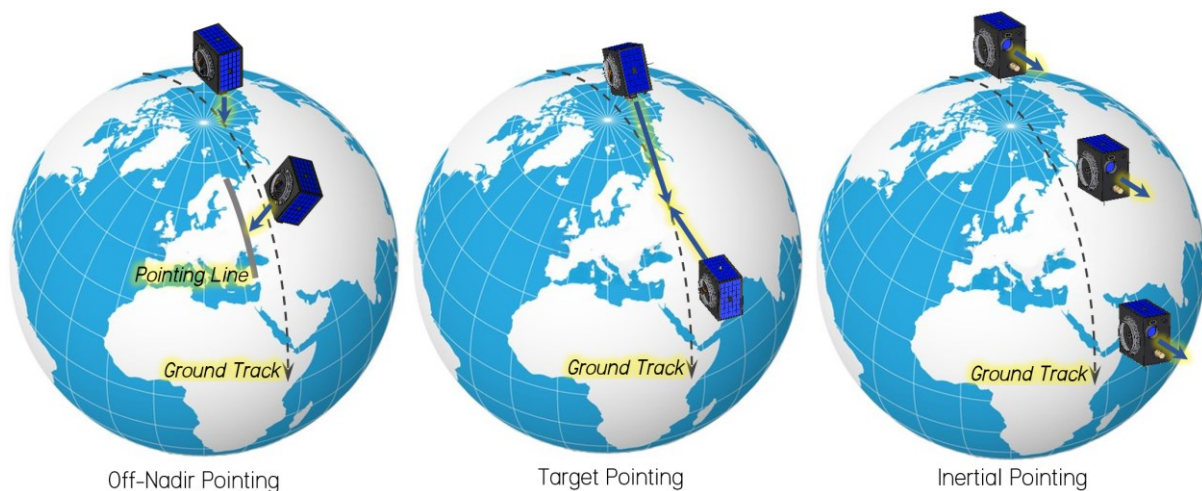


Figure 5.5: Slew Capability of LAPAN-A1 Satellite

The other form of slew mode is target pointing, in which the satellite keeps its camera pointing to a certain region in its ground track. Here the satellite pitch rate compensation is controlled continuously so that z axis would be pointed to the designated point. Application of such imaging mode is for example recording moving objects in an area of interest or for producing stereographic images. The combination of pitch and roll maneuver can also be done to record moving object in or acquire a stereographic image of region at some lateral distance from the ground track. The target pointing maneuver can be controlled interactively by “man in the loop” technique or by scheduler command in the satellite’s onboard and data handling.

Nevertheless, the slew mode may be used not only for Earth observations, but could also be applied for observing celestial bodies. To make observations of celestial objects, satellites should perform inertial pointing, which may useful for scientific observations such as space

exploration or astronomical research. In the satellite operating cycle, it could be utilized for Sun pointing for power or thermal acquisition as well as for camera pointing calibration. Inertial pointing gives an alternative calibration method for satellite's camera pointing by exposing it towards celestial objects such as Moon, planets, or stars. This alternative is motivated by that performing a pointing calibration on the Earth's surface is difficult since the satellite projection is moving fast over the ground track. Moreover, inaccuracy of a few seconds in the satellite system time will make the pointing of the camera away from the target.

The important capability of using momentum bias operation is ability to implement hibernation mode so the spacecraft will passively be stabilized in a single spinner without any active attitude control system, therefore all attitude control devices could be switched off. This such mode is implemented when the spacecraft requires operation reset or in lack of power condition. With very minimal power requirement, the satellite still could conduct operations of omnidirectional communication. The nutation in this mode would be minimal since the satellites rotate on its mayor axis (maximum inertia axis) and it is designed to have very small cross product of inertia.

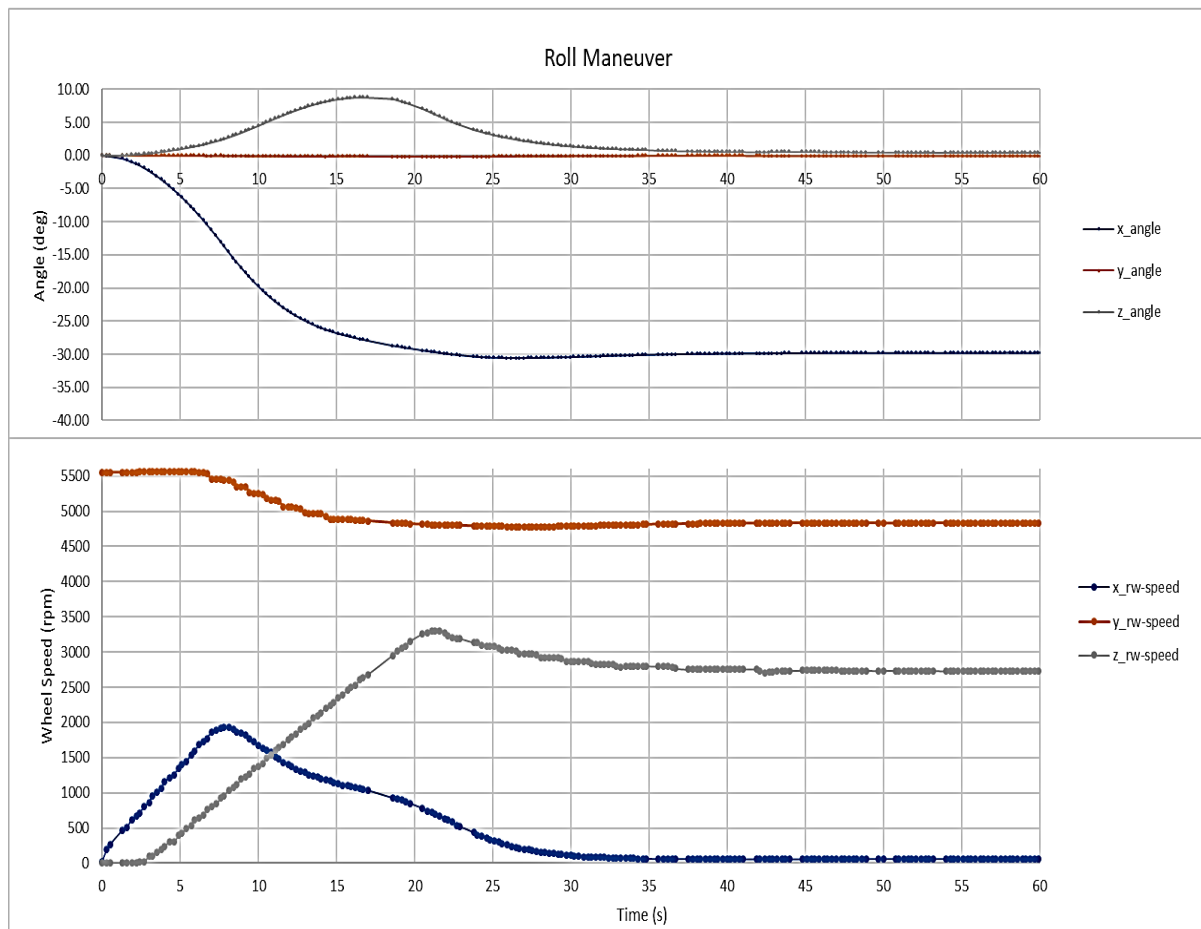


Figure 5.6: Roll Maneuver for Off-Nadir Pointing Mode

5.1.3 Contingency Operations

As opposed to normal or nominal operations, contingency operations contain the procedures and specifies the actions for the control of unforeseen situations. In attitude control operations, contingency operations are often triggered by the failure of one (or more) subsystems that cause attitude control operations cannot be run nominally. Since the momentum bias method deals with angular momentum which is very stable and inertially fixed for relatively long periods, the contingency operations in attitude control generally easier to handle until new approach of nominal operations have been established. There are two cases presented in this section when the attitude control devices are not working nominally, both are related to star sensor malfunction. Star sensor is a relatively new emerging technology in small satellites so that in its maturation phase sometimes it gets fail. There are many factors that cause star sensor failure, ranging from underestimating the design of the lens baffle for avoiding straylight to failure of recognizing star patterns due to hotspots on the sensor/ detector.

Case 1: Partially Working Star Sensor

The partially malfunctioning star sensor was happened in MAROC-TUBSAT when its lens baffle could not handle a straylight in the brighter region or pointing too close to the Sun that leads to Sun blinding. This similar case also happens in the operations of equatorial orbiting satellites, LAPAN-A2. Actually, LAPAN-A2 brings two star sensors to anticipate varying illumination in the equatorial orbit, but one of them got a system failure in the early orbit operation phase. The failure of one star sensor is enough to make the automatic control algorithm installed on the OBDH system does not work. It happens because the automatic control algorithm requires the availability of attitude data continuously.

To overcome the partial malfunction problem on star sensors, the first thing to do is obviously decouple the loop for automatic attitude control in the OBDH. To get an attitude information in the blank spot area, an interpolation of previous data is applied to predict the succeeding attitude for upcoming imaging or other mission operations. Data interpolation is needed to predict the coordinates before and after obtaining information to provide awareness about the deviation of attitude towards the target or reference. Generally, in the Earth observation mission that scan Earth's surface along the ground track, the deviation in the roll axis becomes critical information to make sure that the target is covered by camera's field of view.

Case 2: Totally Lost Star Sensor

Originally, LAPAN-A1 satellite carried star sensor for fine attitude determination, but it got failure in the second year of its operation. Aiming to continue the momentum bias operation, then a simple technique was composed to modify the nominal operation in controlling the angular momentum. The idea of this new introduced mode was how to use video cameras and solar panels to replace star sensors for attitude determination. Furthermore, the video camera was available only once per 24 hours when the spacecraft was in contact with the ground station.



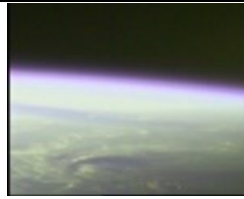
Nevertheless, it could determine the drift of angular momentum since the residual drift rate of the angular momentum could be compensated for a level of better than 1 deg/day.

The angular momentum drift in right ascension would be shown by the slope of the horizon in the capturing images. If the angular momentum was perpendicular to the orbit, the horizon will be perfectly level. But if its right ascension drifts off from the desired position, the video camera would cut the horizon on the left or right side of the ground track so that the horizon captured by the camera looks inclined. Since the angular radius of the horizon from 630 km altitude is about 65 deg, the relation between the right ascension drift, $Drift_{RA}$, and the horizon slope, θ_h , in degrees will approximately follow the equation below.

$$Drift_{RA} = 65 \sin \theta_h \quad (5.4)$$

The right ascension drift of angular momentum resulted from viewed horizon is presented in the Table 5.1.

Table 5.1: Right Ascension (RA) Drift of Angular Momentum Viewed from Video Camera [45]

| | | | |
|--------------------------------------|--|---|--|
| Horizon Images |  |  |  |
| Horizon Slope (deg) | 4.97 | 0.41 | -5.37 |
| $Drift_{RA}$ (deg) | 5.63 | 0.47 | -6.08 |

A constant bias value on the y coil for a few orbital periods would control the right ascension precession. Figure 5.7 show that by setting 15 mA bias current to the y coil of LAPAN-A1, the drift is about zero from one to another day. However, it will drift to the left when undercompensated, and drift to the right if overcompensated

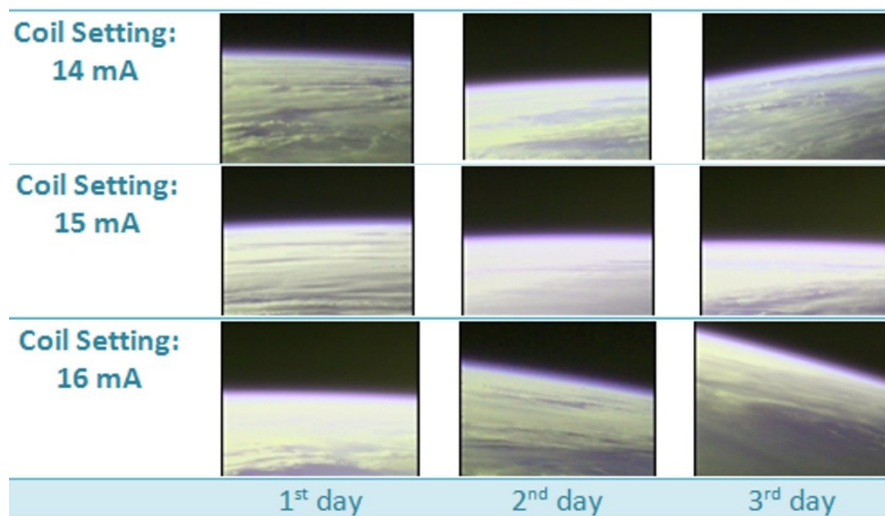


Figure 5.7: Right Ascension Precession of LAPAN-A1 due to Bias Current Setting of Y Coil

As described in the section 5.1.1, the drift of right ascension will tilt the angular momentum from local horizon, therefore, it induces the gravity gradient torque. This gravity gradient torque hereupon will cause a declination drift of angular momentum. The declination of the momentum vector was evaluated directly using the Sun angle on the $-y$ (minus y) side solar panel. The other alternative to measure the declination drift is by tracking the object movement on the video during nadir pointing imaging.

For polar orbiting satellite, the declination drift can be known through nadir pointing imaging in the equatorial area. If nutation is well damped, the inclination created by movement of the object in the video is proportional to the deviation of declination from the target as displayed in the Figure 5.8. If the declination matches the target, the object captured by the video camera will move straight forward. Conversely, if the declination deviates from the target, the object captured in the video will create sideways movement.

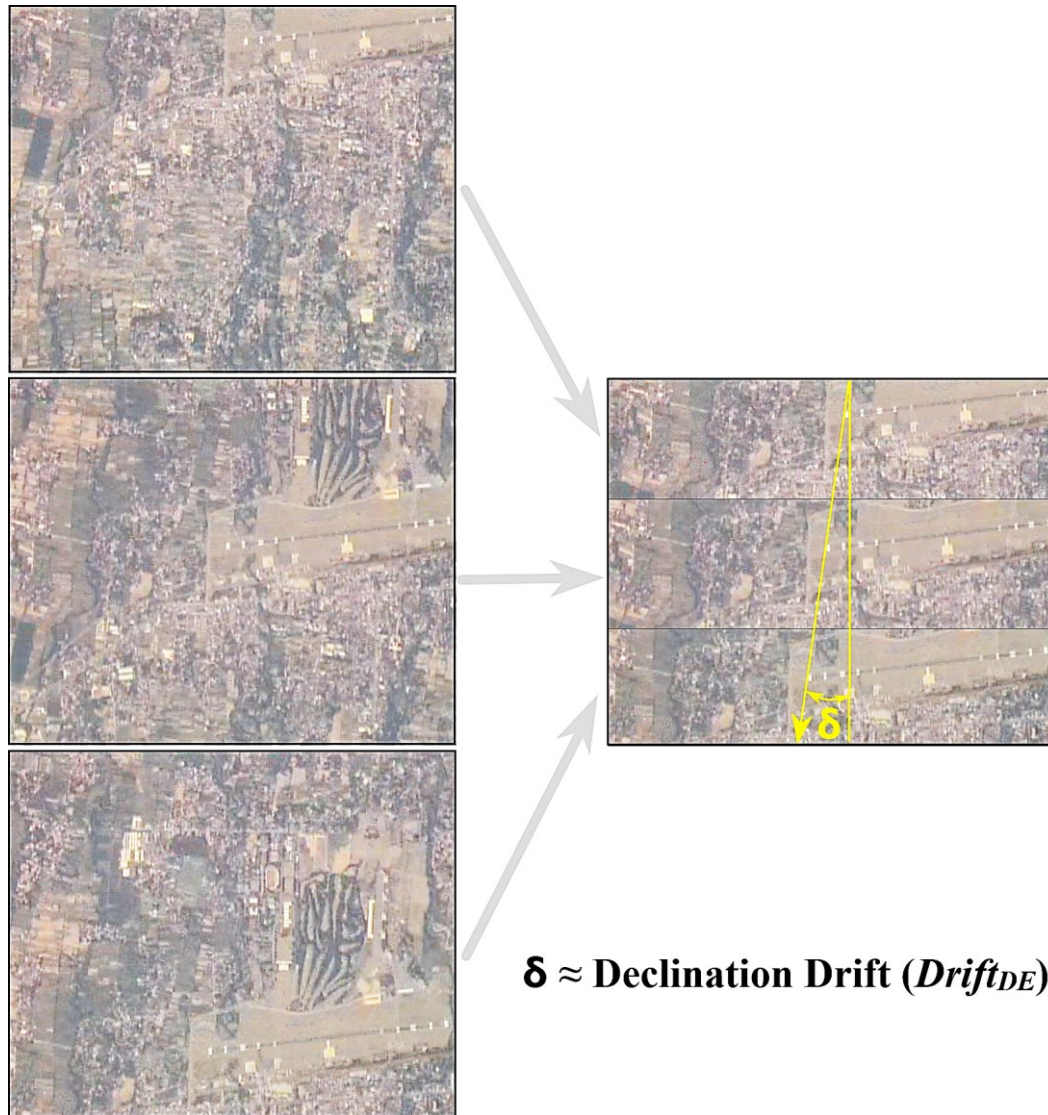


Figure 5.8: Declination (DE) Drift of Angular Momentum Viewed from Video Camera

5.2 Advantages and Disadvantages of Momentum Bias

The main advantage of momentum bias is its gyroscopic stability, which could remain for a long time. This stability is proportional to the amount of momentum stored by the spacecraft, so the higher the momentum stored, the more stable the spacecraft will be. Thus, the external disturbance torques only cause a small precession to the spacecraft attitude, so that it could be easily predicted. Even this precession is better than a systematic drift property by attitude sensors. In the case of partial lack of attitude information, momentum bias can bridge the phase of unavailability, e.g. due to sun blinding or obstruction of the star sensor, where no attitude information is available. In principle, a gyro could also store the attitude for a while, but the momentum bias system has a much lower drift rate about several degrees per day instead of several degrees per hour (a typical drift of gyro reading). As discussed in the previous section, a typical application was MAROC-TUBSAT where due to sun blinding, the star sensor was working only during eclipse. Another example is LAPAN-A1 where the attitude information from video of the horizon was available only at the daylight passes when the satellite is in contact with the ground station.

Applying momentum bias means the basic system that runs continuously is only a pitch wheel-gyro loop. Since the single wheel-gyro attitude control operation is decentralized into a subsystem and the fact that the loop is decoupled from OBDH, the momentum bias operation would realize the robustness of the attitude control loop. Decoupling the attitude loop from OBDH will reduce satellite dependency on the continuous availability of attitude data. By involving minimum devices, momentum bias control still provides a reasonable pointing accuracy that is sufficient for normal tasks like line scanner pushbroom imaging as well as transferring data using directional and high data rates downlink such as S to X band frequencies. However, few activities that need a higher pointing accuracy such for high-resolution Moon imaging could always use the star sensor information and activate the angle control loops for the wheels on three axes that would also damp the nutation. Hence star sensors and other devices would be activated intermittently when high pointing accuracy or attitude correction is required at the convenient intervals.

This elegance of momentum bias techniques comes into play, especially when wheels have been used since one wheel yields three axis control versus three wheels for a zero-momentum spacecraft. The economies of momentum bias techniques are obvious [58]. This simplicity of design, i.e. the significantly lower number of equipment, become main advantage of the momentum bias attitude control. In terms of power usage, applying a single wheel-gyro to the most of satellite operating cycles clearly proves the efficiency of this technique. This attitude control system is also easy to test on the ground by a simple air bearing platform as shown in the Figure 5.9. A single axis air bearing is sufficient to test the closed-loop system of wheel-

gyro to perform an angle or an angular velocity control against the disturbance torque. This air bearing platform could also accommodate a magnetic coil/torquer, either to be used as a magnetic disturbance torque simulator for testing the wheel-gyro system, the magnetic coil could also generate or dump the angular momentum. The integrated system of the wheel-gyro would immediately respond any activation of the magnetic coil by increasing or decreasing the wheel speed to maintain the angle or the angular velocity that has been commanded to the system. By this testing setup, the observers/operators could directly evaluate the transient time as well as the accuracy of the control system, so they could adjust the control parameter of the system for the best result. While the autonomous control in each axis is easy to test before launch, this configuration would also give a better education for ground personnel to analyze the spacecraft attitude later in the orbit.

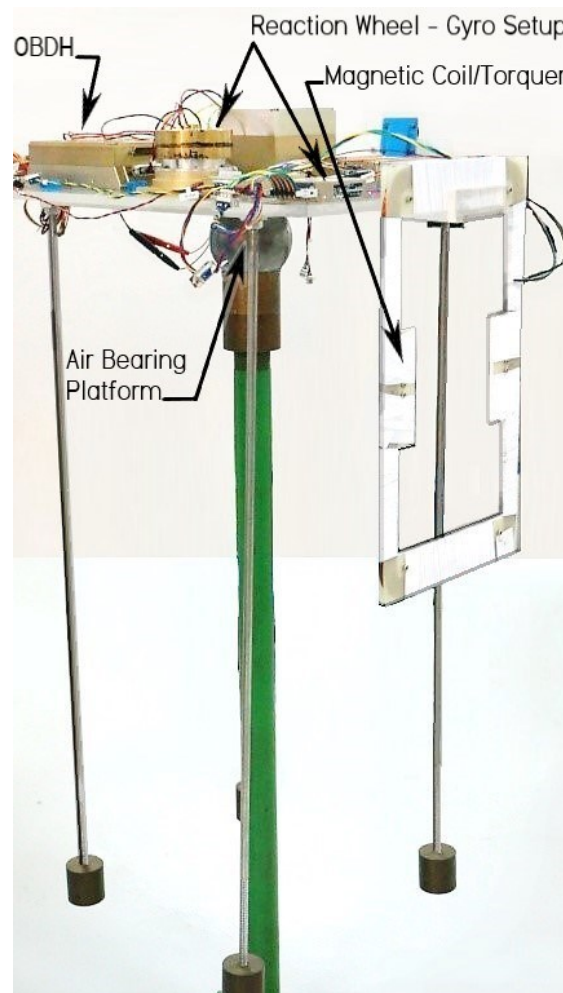


Figure 5.9: Attitude Control System Testing on Single Axis Air Bearing Platform

Although momentum bias offers various advantages, operating the spacecraft in this technique might face a challenge since it requires high awareness about the disturbance torques which drift the angular momentum from the desired direction. Especially for the satellites whose attitude control loop is decoupled from OBDH, they need for human interference. However, the angular momentum drift is only a few degrees per day. Knowing the source of disturbance

torque would give understanding how to compensate it, so the disturbance torque could be eliminated or even use it for attitude control by overcompensating and undercompensating. Since then, the knowledge of disturbance torque has become an advantage. The problem might raise by human interference could be managed by designing an operating software of satellite telemetry that could assist the operators in performing a maneuver of angular momentum correction.

The real disadvantage in the momentum bias attitude control is the steady state error of the nutation damping. The nutation of a spinning spacecraft reveals itself as small oscillation and shivering of the precessing axis. Nutation is a rotational motion for which the instantaneous rotation axis is not aligned with a principal axis. In this case, the angular momentum vector, which remains fixed in space, will not be aligned with either principal axis or instantaneous rotation axis. The deviation angle between principal axis and angular momentum is a magnitude of the nutation, called also as nutation angle. This nutation is absent only for carefully chosen specific initial conditions. Hence, in practice, it is hard to avoid a nutation, but there is possible to damp it.

There are two techniques applied in the LAPAN-A satellite series to damp the nutation. The first technique is using one of transverse wheels as nutation damper, and the other is using magnetic coil. Choosing the right nutation damping technique will realize a high accuracy of stabilization that is needful to meet an error pointing requirement of high-resolution payload. A stable condition would generally remain in a long period for up to a day, especially while the disturbance torques have been handled properly.

In the hibernation mode, the spacecraft deactivates the wheel so its body would start spinning. A good balancing of the spacecraft and aligning its principal axis to the pitch wheel axis would reduce the potential of nutation when the spacecraft switched from dual spinner to single spinner motion. Since the principal axis is defined by the spacecraft mass distribution, it is fixed in the spacecraft. Meaning the design of spacecrafts that intended to work in both dual and single spinner modes such as LAPAN-A satellite series should minimize the products of inertia and align their main of principal axis to the pitch wheel axis [47]. The mass properties of the LAPAN-A satellite series are shown in the Table 5.2.

Table 5.2: Inertia Tensor of LAPAN-A Satellite Series

| | | LAPAN-A1 | LAPAN-A2 | LAPAN-A3 |
|--|----------|----------|----------|----------|
| Moment of Inertia (kg.m²) | I_x | 1.386 | 2.932 | 5.794 |
| | I_y | 2.062 | 3.624 | 6.695 |
| | I_z | 1.441 | 2.814 | 5.098 |
| Product of Inertia (kg.m²) | I_{xy} | 0.035 | -0.088 | -0.018 |
| | I_{xz} | 0.063 | -0.018 | 0.050 |
| | I_{yz} | -0.003 | -0.028 | 0.009 |

Another effort in designing a momentum bias system is estimating the disturbance torques. The knowledge and compensation of the precession torque are mainly for the sizing of the

momentum wheel and magnetic coil. There are devices that potentially produce the magnetic torque: batteries, antenna, wheels, and loops in the wiring. Magnetic dipoles of magnetized materials in the batteries and antenna are constant in most cases, therefore they are not so critical and can be easily compensated in orbit by magnetic coils. However, non-constant torques mainly from the wheels & from wiring loops should be eliminated on the ground before the launch. For example, a magnetic shielding from mu-metal shown in Figure 5.10, that is applied in later mission could effectively absorb the magnetic dipole of the wheel's motor. While this dipole moment has not been anticipated yet in LAPAN-A1 and LAPAN-A2 missions, LAPAN-A3 implements magnetic shielding, in particular to shield the wheels which have uncertain start and stop operation. In the solar panels, positive and negative cable routing should be brought closer together as shown in Figure 5.11 to avoid wide loops.

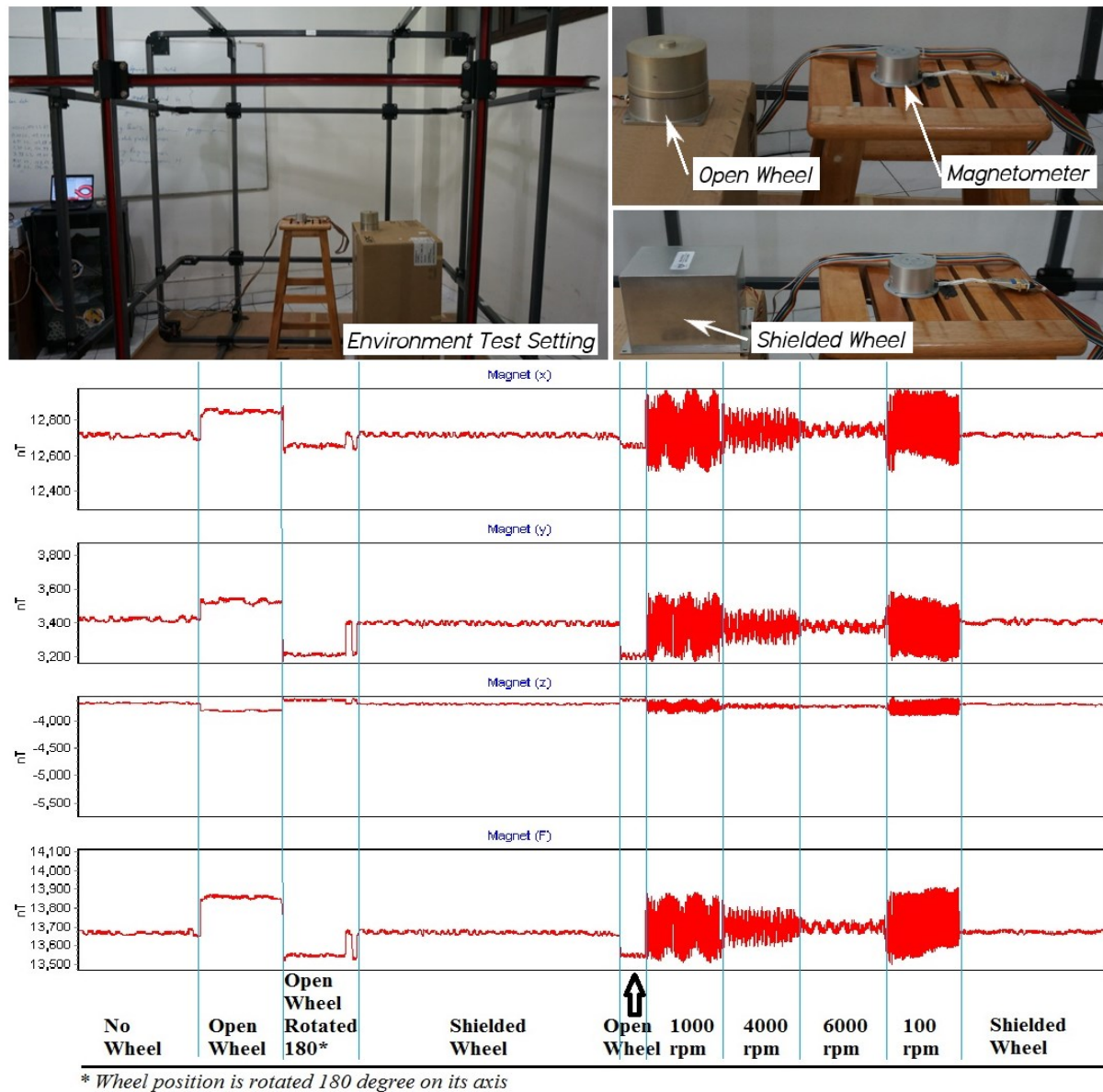


Figure 5.10: Measurement of Magnetic Dipole of Reaction Wheel

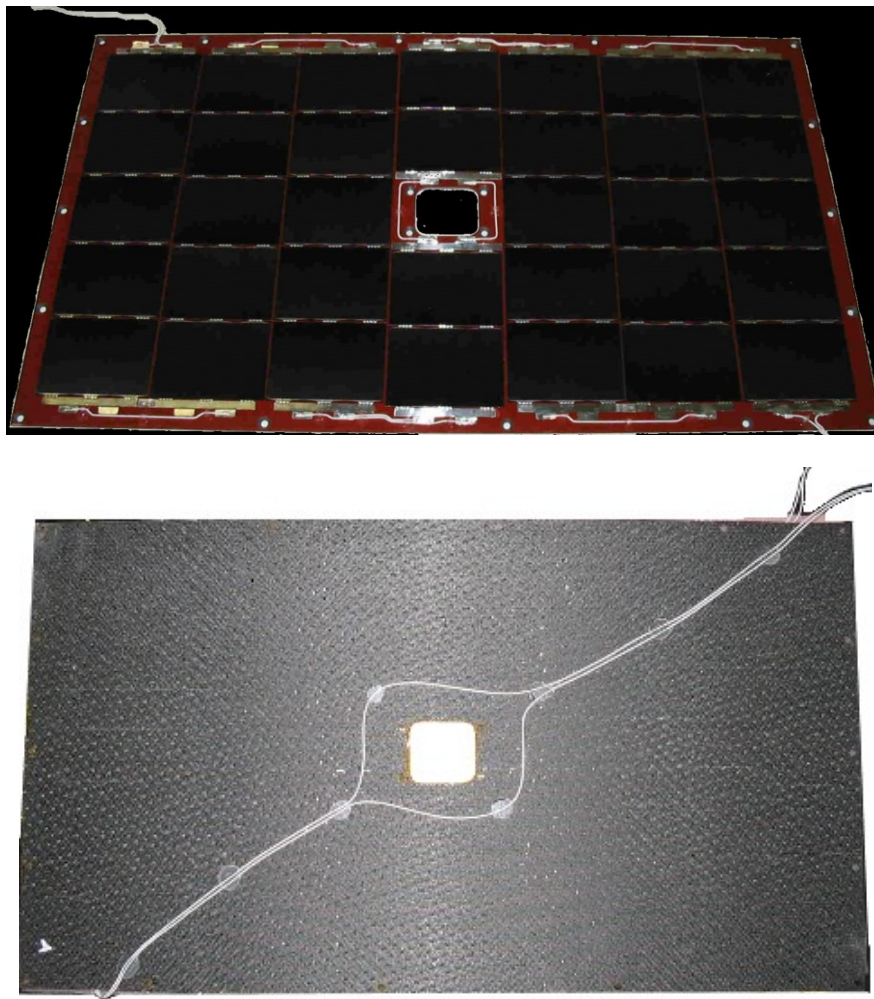


Figure 5.11: Cable Routing of Solar Panel

Magnetic shielding could be applied also in batteries for many of them have Nickel (Ni) content which is easy to be magnetized. However, since the mu-metal material is quite heavy, the added weight to the satellite design due to its application must be carefully considered. A small and constant magnetic dipole moment in the batteries could be simply compensated by bias current setting on the magnetic coil such as performed in the LAPAN-A1 satellite which carried 5 NiH_2 battery cells for its energy storage system.

However, there are other alternatives to minimize a bigger magnetic dipole moment in the batteries, i.e. by arranging the placement of batteries so in each module is rotated 180 deg with respect to each other. Therefore, the magnetic moment from the one module will cancel the magnetic moment produced in the other one. The design, thereby could eliminate the magnetic moments. This configuration has been demonstrated on the Li-ion type batteries by SAR (Synthetic Aperture Radar) mission satellites, COSMO-SkyMed [59]. To know the magnetic dipole and the effect of battery placement, a test setup and measurement, as seen in Figure 5.13, have been conducted using Li-ion batteries that are similar as carried on LAPAN-A2 satellite.

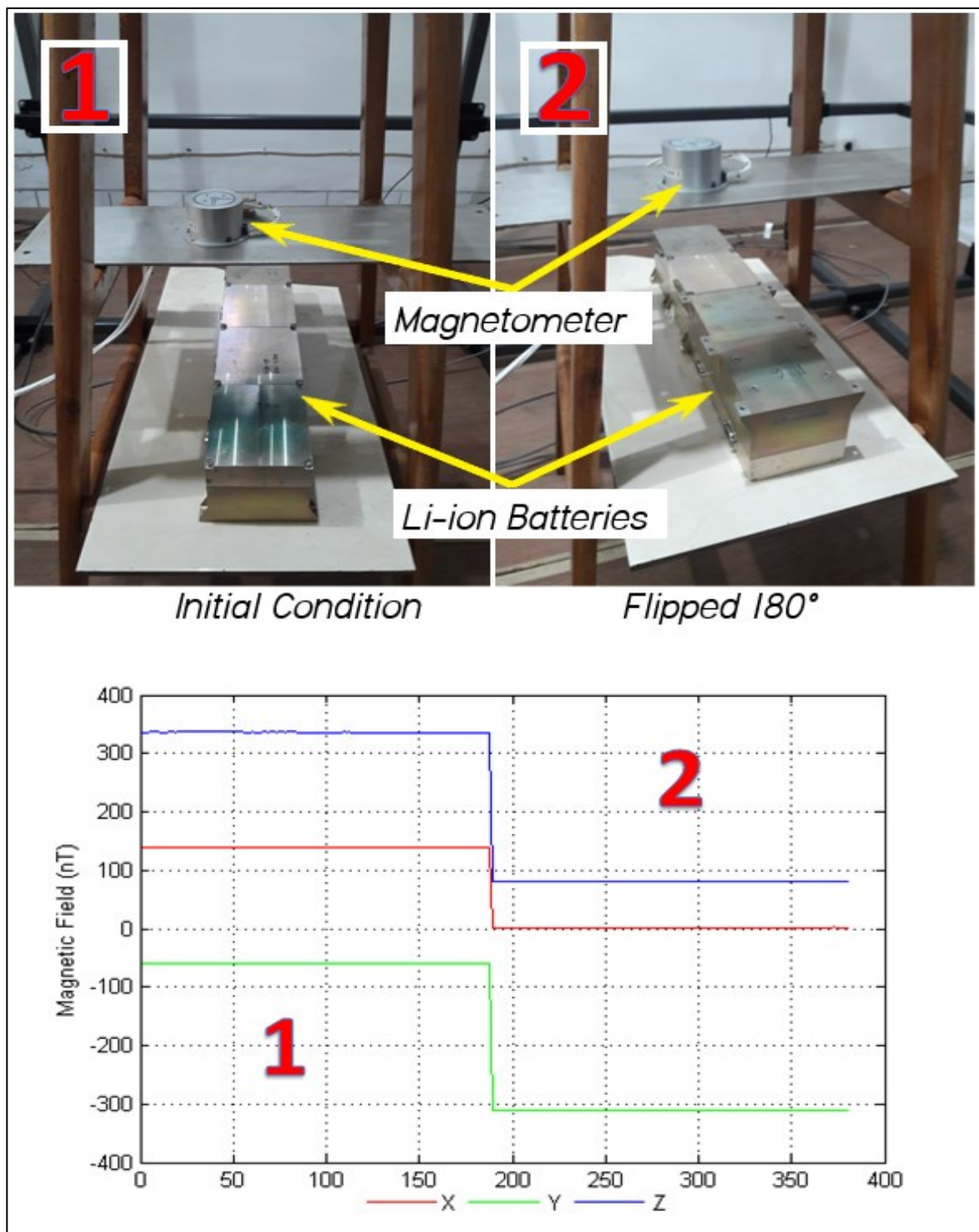


Figure 5.12: The Measurement of the Magnetic Field on the Li-ion Batteries

5.3 Attitude Hardware

LAPAN-A satellite series involves several sensors and actuators to perform the attitude control. Establishing LAPAN-A1 (LAPAN-TUBSAT) as the baseline of attitude control system, that is shown in the Figure 5.13, the hardware should meet the requirements for micro satellite that enumerate below [60].

1. Small mass, small dimensions
2. Low power consumption
3. Low complexity
4. Modular hardware and software
5. High agility of the system.

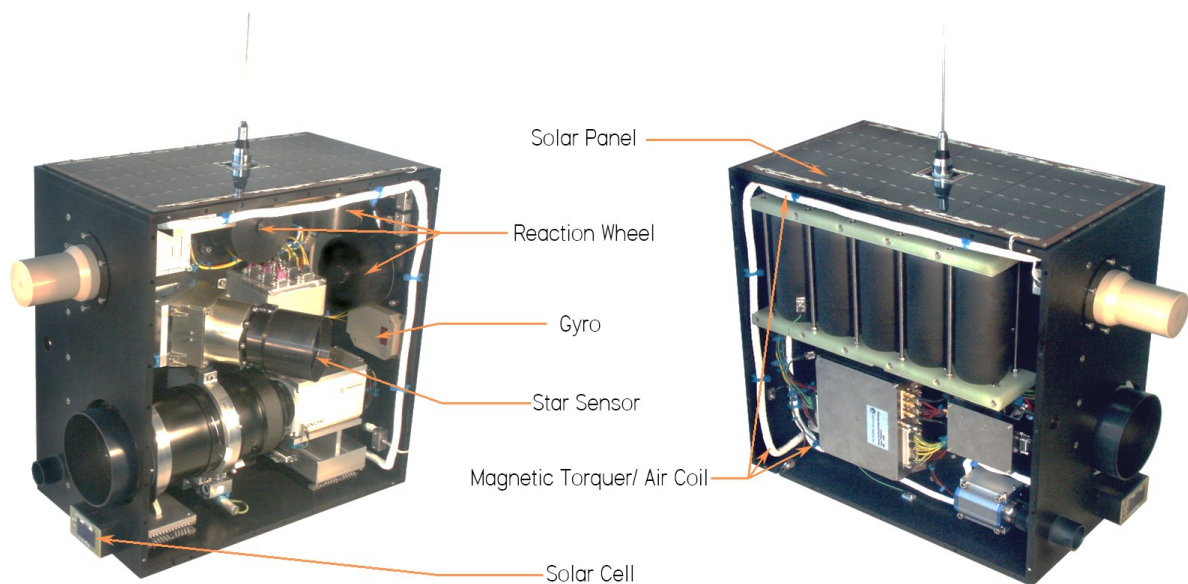


Figure 5.13: Attitude Control System Assembly of LAPAN-A1 Satellite

The mass and dimension limitation of a small satellite is also applied to the attitude control system. The smaller dimension of the satellite does not only limit the primary power available, but also the bus voltage which is generally has 12 V – 28 V due to lower number of solar cells per string. In order to avoid the applying potential transformers which is made the bus voltage worst, the actuators and sensors are required not only have low power absorption, but should be have electrical interface in the bus voltage.

The low complexity is achieved by the use as few as possible of a microprocessor with a clear architecture which is connected by serial interfaces. By this way, the microprocessors particulars can be assigned task packages. Whereby, the use of only one processor, the

complexity would be shifted into the software. These microprocessors generally not over parallel interfaces, so the gyroscope should have serial data interface.

The modularity of the hardware gives the optimal utilization of the small volume of a micro satellite, whereby the components of attitude control system can be individually integrated. That modularity of the software allows reaction wheels as an actuator in connection with an additional sensor to perform a maneuver. The reaction wheels should have several operating modes, such as spacecraft angle control, spacecraft angular velocity control, wheel current control, and wheel speed control.

High agility of the attitude control system is reached by use of a combination of three gyroscopes and three reaction wheels. They are attached in pairs in the three body-fixed axes of the satellite, so that they could make the unrestricted rotation possible for the spacecraft around three axes. Figure 5.144 shows the structure of highly integrated wheel-gyro as the main attitude control system of LAPAN-A satellite series. Following the previous of TUBSAT satellite series, the motion control is decentralized since its first step. Meaning control of the angular motion between the axes is independent, thereby the control loops are shifted to the individual body-fixed axes. By designing wheel-gyro units in each axis, a reaction wheel forms a single axis attitude control system with a gyro to control the spacecraft angular velocity and angle. The integration between wheel and gyro is performed by Wheel Drive Electronic (WDE) that contains a microprocessor and the serial interfaces to connect wheel and gyro. The other serial interface is required to connect the OBDH system.

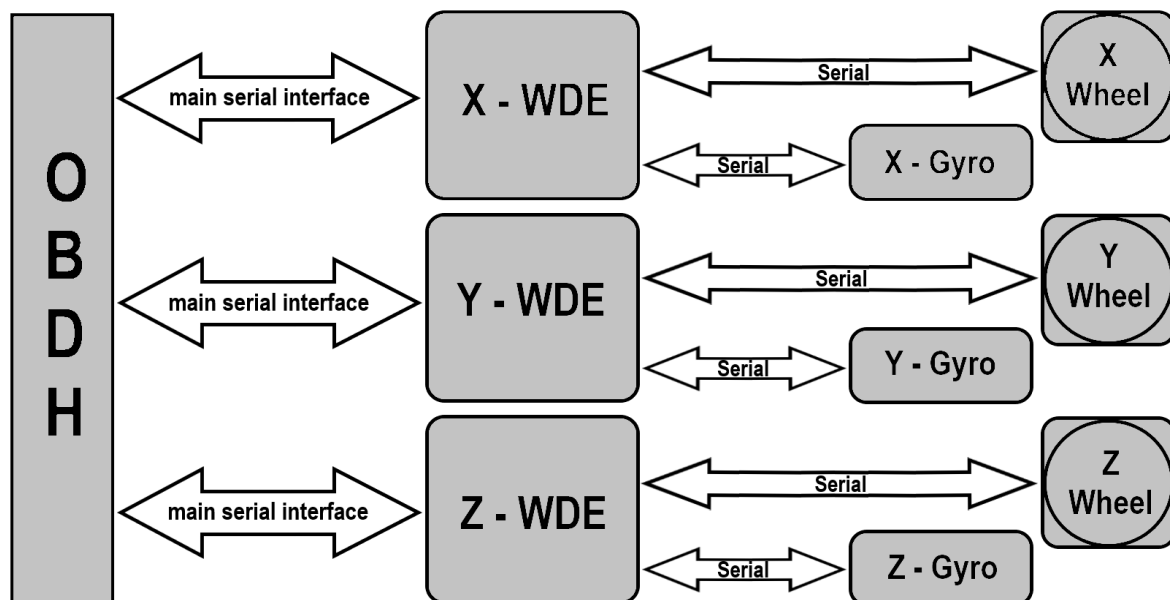


Figure 5.14: Decentralized Attitude Control System

The gyroscopes could also do independent angular measurement from one of the references (stars, Sun, Earth). The other sensor such as a star sensor can be dazzled by albedo of the Earth,

while a Sun sensor would not work in the eclipse. The very important maneuver for an inertial stabilization of the spacecraft at the beginning of the flight is reliable and fast, thereby it is done in less than 10 seconds. Therefore, for maneuvers that is commanding by operator in the ground station, they are reduced to just an adjustment of the pointing of the antenna or camera.

5.3.1 Fiber Optic Gyro

LAPAN-A satellite series use fiber optic gyroscopes made by LITEF company as a sensor for the attitude control system. It works on the Sagnac effect, using a beam of coherent light that is split and propagated both clockwise and anticlockwise through a coil of optic fiber. When the gyro experiences a movement around its axis, one half of the split beam travels further than the other half relative to an observer outside the coil. A photo-detector measures the phase-difference patterns between the two beams, which are directly related to the rotation. As the gyro uses closed loop techniques, the output is linear and high angular rates can be measured. The gyro measures angular movements about its sensitive axis, as shown in Figure 5.155.

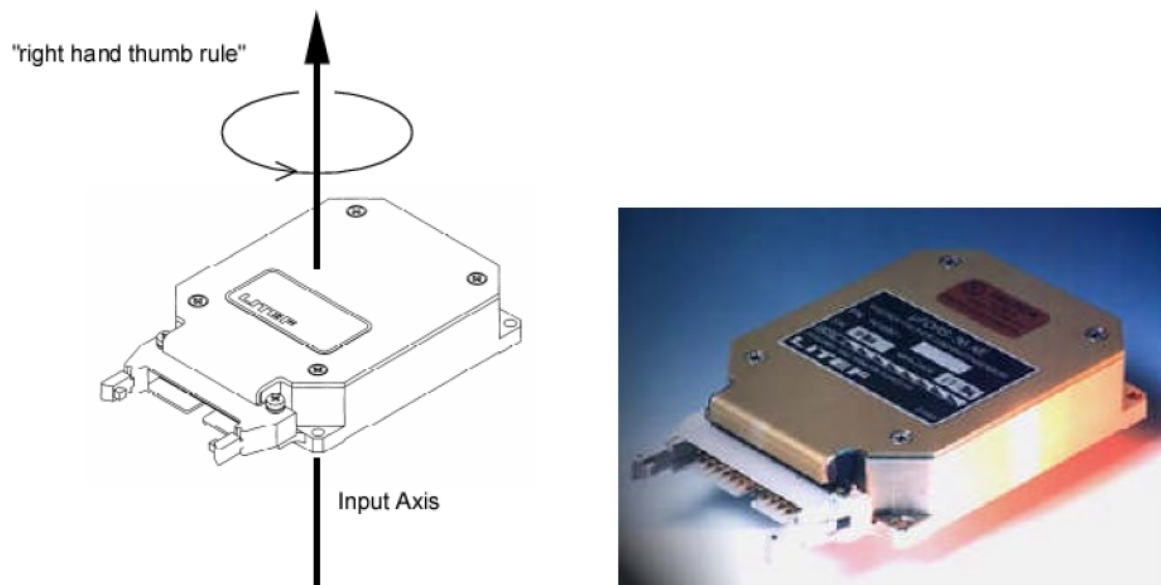


Figure 5.15: LITEF μ FORS Fiber Optic Gyroscopes and its Rotation Axis

Three gyros are placed on the orthogonal axis, where each of them is integrated into the reaction wheel on the same axis. These fiber optic gyroscopes can be configured to one of three measurement modes:

- Angle increment: returns the angle that the gyro has moved through since the last data output
- Angle accumulated: returns the total angle moved through since the last reset
- Rate: In this mode, the gyro returns the current angular rate in degree-per-second

Even though the gyro is designed for aviation purposed, the gyros have been flown and perform well on DLR-TUBSAT and MAROC-TUBSAT satellites. The gyro is relatively compact, lightweight and also consuming low power. The specification of gyro that is utilized by LAPAN-A satellite series is displayed in the Table 5.3. Since the fiber optic gyroscopes have a very sensitive measurement for the angular rate movement, in this case 16-bit resolution, which can measure the minimum angular rate change 2.44×10^{-4} deg. Hence, it can be used to measure the Earth rotation on the ground for testing.

Table 5.3: Technical Specification of Fiber Optic Gyroscopes

| | <i>LAPAN-A1</i> | <i>LAPAN-A2/LAPAN-A3</i> |
|--|--|--|
| <i>Gyro type</i> | μFORS-6 | μFORS-4 |
| <i>Performance:</i> | | |
| - Bias drift at full temperature range (1σ) | ≤ 6.0 deg/h | ≤ 4 deg/h |
| - Bias drift at stabilized temperature (1σ) | ≤ 3.0 deg/h (1σ) | ≤ 2 deg/h (1σ) |
| - Noise (1σ) | ≤ 0.6 deg/ \sqrt{h} | ≤ 0.6 deg/ \sqrt{h} |
| - Bias drift at ground testing in the room temperature | 0.355 deg/h | 0.852 deg/h |
| <i>Initialisation time</i> | ≤ 120 ms | |
| <i>Measurement mode</i> | angle increment, maximum ± 8 deg, 16-bit resolution | |
| <i>Update rate</i> | asynchronous 5 – 1000 Hz | |
| <i>Supply voltage</i> | 5 VDC | |
| <i>Maximum power</i> | ≤ 2.3 W | |
| <i>Weight</i> | ≤ 150 g | |
| <i>Dimensions</i> | $100 \times 65 \times 20$ mm ³ | $90 \times 65 \times 21$ mm ³ |

5.3.2 Solar Cells as Sun Sensor

LAPAN-A1 has 4 solar panels for power generation which are placed at $+x$, $-x$, $-y$, and $-z$ side. These solar panels also can be used to determine orientation of the spacecraft. Additional solar cells have to be placed on $+z$ and $+y$ side for monitoring the illumination on all sides of the spacecraft. Solar panels and solar cells configuration are illustrated in Figure 5.166. However, this configuration still has ambiguity because it is rather difficult to determine between Sun and albedo. Accordingly, the direction of the Sun could be estimated by knowing the side which has maximum current. Since the Sun sensors only give two axis information, additional information from the camera or star tracker are needed to assist Sun sensor in determining the third axis of spacecraft orientation.

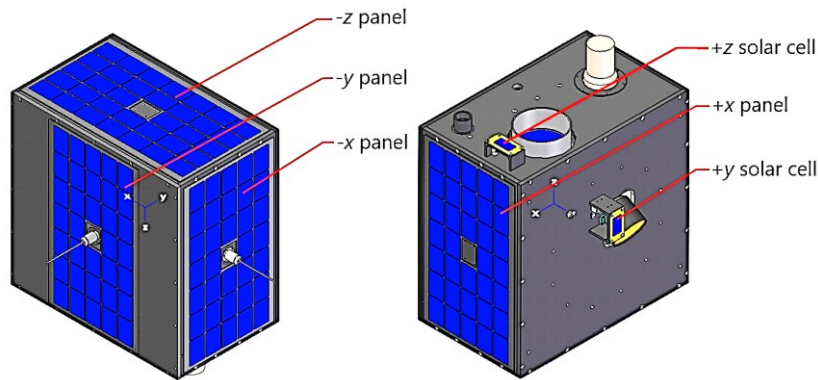


Figure 5.16: Placement of Solar Cells/ Panels on the LAPAN-A1 Satellite

The solar cell/ panel can be functioned as an attitude sensor since the intensity of solar radiation is proportional to the electric current that is obtained from a cell/panel. The smaller of incidence angle between the sunlight direction and the normal direction of the solar cell, the greater of radiation intensity as well as the electric current that is obtained by the solar cell. Since each side of the satellite has body mounted solar cell/panel, it is easy to find out which side is closest to the direction of sunlight.

In the normal operation of nadir pointing, the $-z$ side usually faces closer to the Sun so that the camera or the transmission antenna placed on the $+z$ side is directed towards the Earth. To determine the direction of the sunlight, a two-dimensional analysis should be conducted by performing x or y as the rotation axis of the atan2 trigonometric equation. $\text{Atan2}(y, x)$ is the angle formed by the x axis, the center point $(0,0)$ and a point (x, y) in two-dimensional Cartesian coordinates. A positive sign indicates a counter-clockwise direction while a negative result indicates a clockwise direction. The two sides that obtain the highest electric current are chosen for the calculation of the Sun's angle. Figure 5.17 explains the geometrical relationship between the direction of sunlight and the rotation that should be performed by the certain axis so that the $-z$ side will face the Sun.

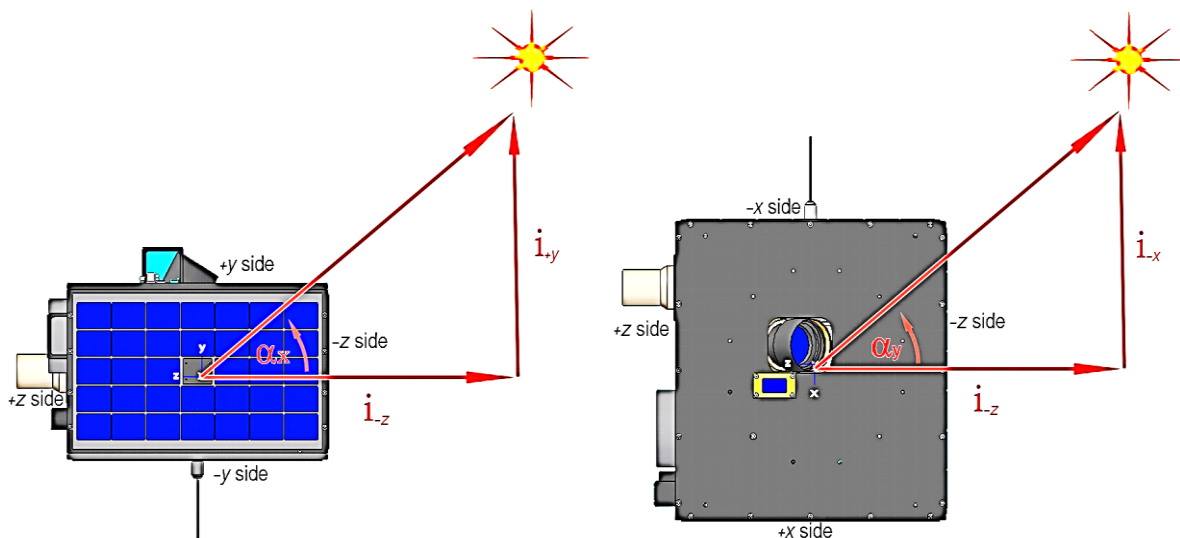


Figure 5.17: Geometry of Sun Illumination on the Solar Cell

Following the geometric relationship, the rotation angle of the spacecraft's x axis, α_x , is obtained from

$$\alpha_x = \text{atan2}(i_{+y}, i_{-z}) \quad (5.5)$$

where i_n is electric current on the side n . In the same way, the rotation angle of the spacecraft's y axis, α_y , is following

$$\alpha_y = \text{atan2}(i_{-x}, i_{-z}) \quad (5.6)$$

These calculations should be integrated in the ground station software as shown in Figure 5.188, to assist the satellite operators to give attitude maneuver commands to satellites. It will be very useful in the acquisition phase after tumbling condition. Moreover, it is also an efficient step to direct the wider solar panel to face the Sun, in particular when the satellites require a lot of power.

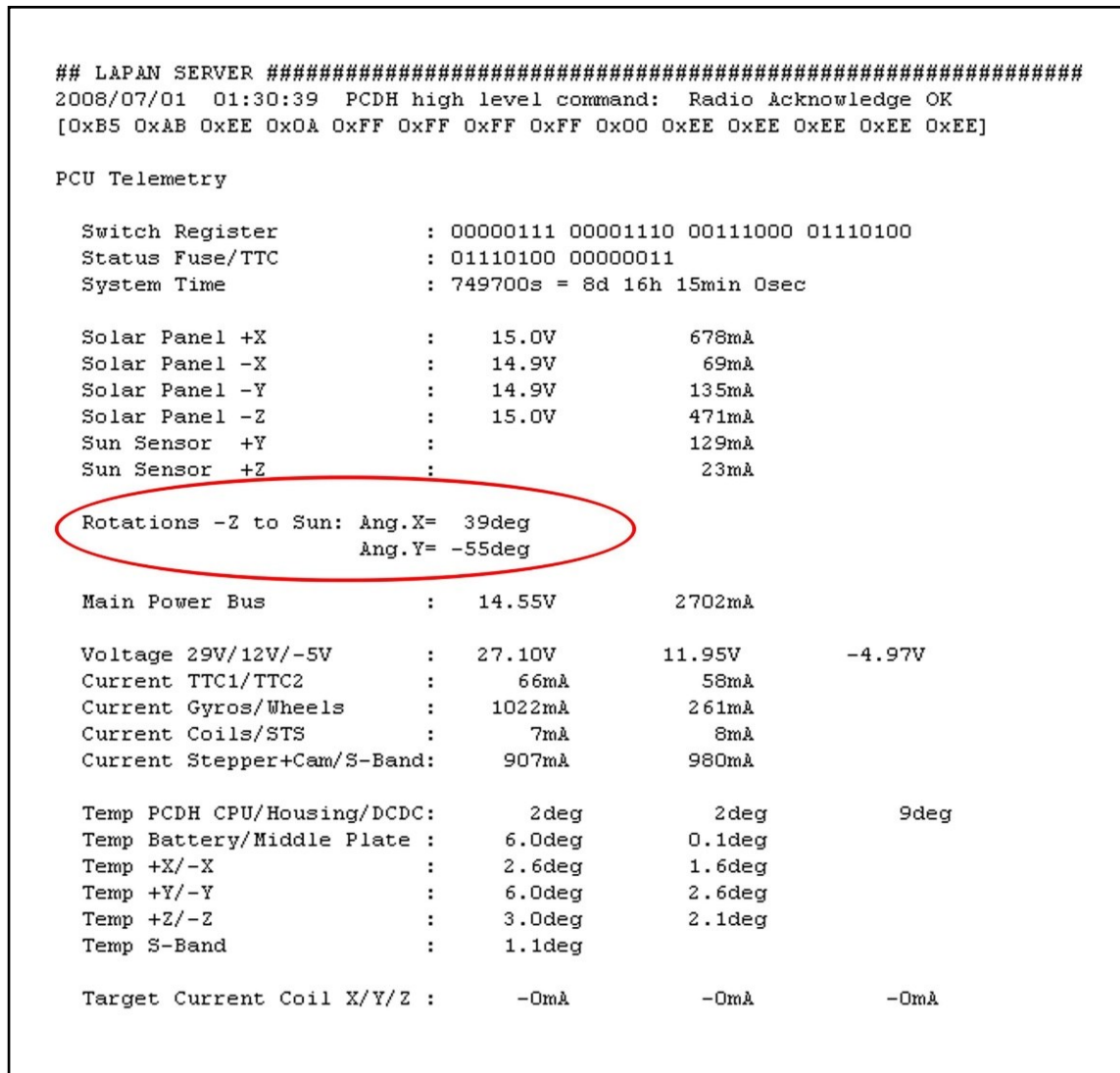


Figure 5.18: Sun Angle Calculation on the Ground Station Software of LAPAN-A1 Telemetry

5.3.3 Star Sensor

Star sensors are very reliable to provide reference for attitude determination; however, they have limitations on their working conditions. Since the star sensors technology is based on the imaging system, they will not work when the spacecraft rotated at high rates of angular velocity. Further limitation of the star sensors, they could not operate in the regions that are too close to the light sources such as the Sun, Moon, and Earth (Albedo). Therefore, especially for equatorial orbits, spacecraft may require more than one star sensor due to variations of solar illumination as illustrated in Figure 5.199.

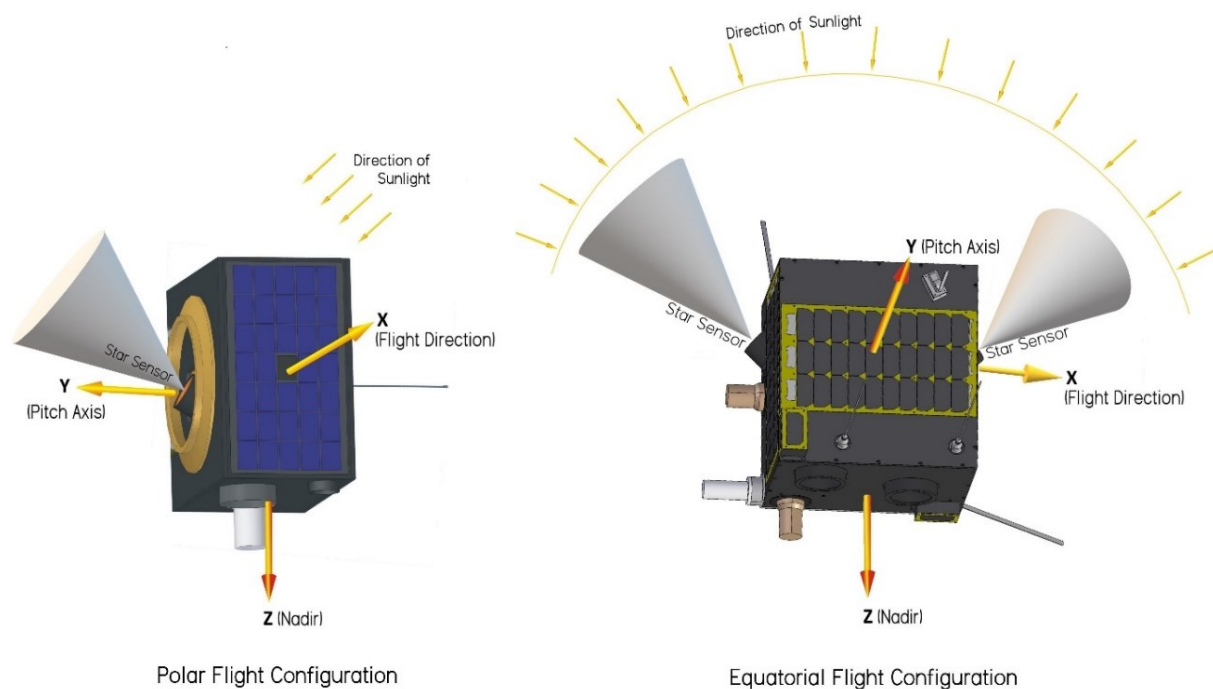
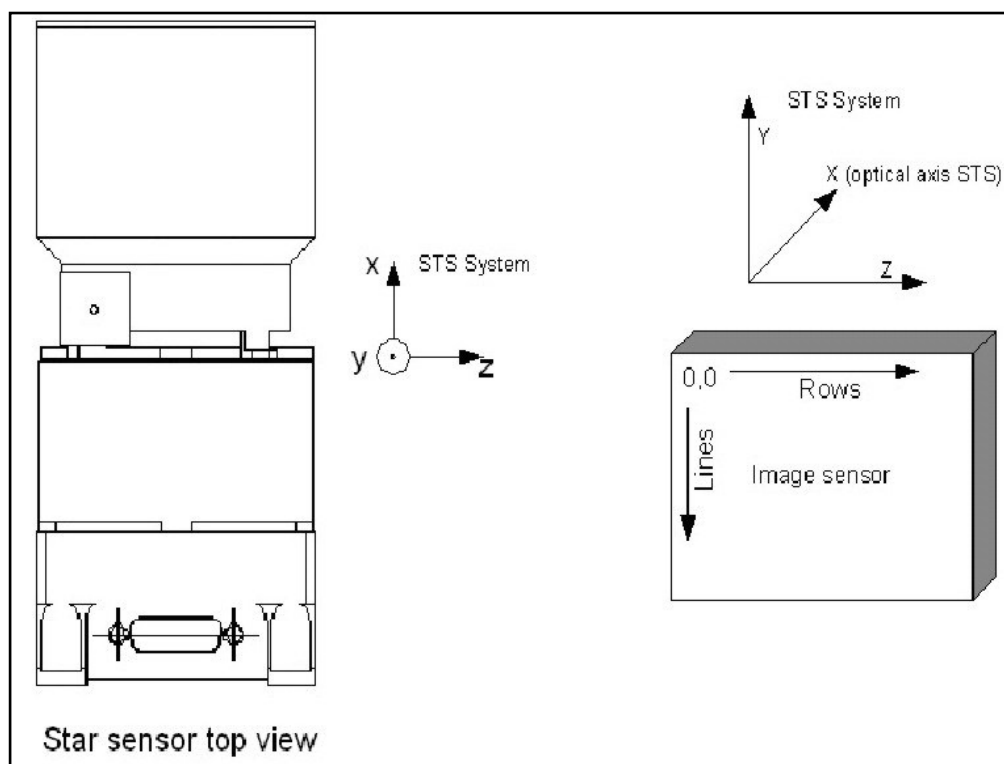


Figure 5.19: Flight Configuration and Star Sensor Placement on LAPAN-A Series

Star sensor or star tracker provides a fully autonomous attitude determination. In order to achieve this purpose, it integrates generally an image sensor to take pictures from the sky and micro controller to processes and analyses this stellar information. LAPAN-A satellite series employ a star tracker that uses 512×512 pixels radiation tolerant CMOS active pixels as image sensor which is shown in the Figure 5.20. Its optical system has 50 mm focal length, so it gives a field of view about $14^\circ \times 14^\circ$.

The image sensor transforms star images through the lens into analogue electrical information. The output of the image sensor is converted to a digital signal and deliver $512 \times 512 \times 14$ bits data for internal image processing by the microcontroller. The result of the processing is attitude parameter of the satellite in different format such as Euler Angle or Quaternion. This format has an accuracy of 18 arc sec in x axis and 122 arc sec y/z (imager axis). The star sensor had placed its focal axis corresponds to the x axis and its base plane is parallel to the z axis and the connector is upturned as shown in Figure 5.211.

**Figure 5.20: CMOS Star Tracker****Figure 5.21: Reference Frame Definition of Star Sensor**

In order to process the new acquired pattern data efficiently, a reference image already stored in memory to eliminate fixed pattern noise. As experience with the micro satellites TUBSAT-A and MAROC-TUBSAT, it is advantageous to compare the actual image with an up to date dark image to correct pixel-blemish and transients caused by radiation effects. This procedure, however presumes that there is little coincidence between the actual image and the reference image.

Bright stars provide a clear advantage in the determination accuracy for the calculation of the center of intensity distribution. The coordinates of the brightest stars calculated by the microcontroller are based on the average value of all adjacent pixels, which belong to the same star. The star recognition is done by the microcontroller per comparison between the star database and the actual acquired star image.

After power on reset, the camera and all control variables are initialized and the star sensor turns automatically in a mode called *First Acquisition Mode*. In this mode the sensor performs one image of the sky and the whole data in the field of view of the star sensor is processed. At angular rates lower than 0.6 deg/s, it has an acquisition probability >99.7%. This First Acquisition Mode is activated only for the first attitude calculation and takes generally 900 ms. After First Acquisition Mode is successfully passed over and the attitude of the satellite is known, the sensor turns automatically into a second mode, *Tracking Mode*. In this mode the image sensor is continuously and completely read out (approximately every 250 ms). The star sensor has an unregulated power input interface of 9 V to 18 V within maximal power consumption during operation is 2.5 W.

5.3.4 Magnetic Field Sensor

LAPAN-A satellite series employ *magnetic field sensor* (MFS) since LAPAN-A2 satellite mission. It is used for attitude determination, especially in the initial operation mode after launch separation or after the spacecraft tumbling condition. Even though it is not primary attitude sensor, MFS is useful when the main attitude sensor such as star sensor could not determine the attitude reference, e.g. while the spacecraft is rotating at the relatively fast speed. MFS is three-axis attitude sensor which is designed for low earth orbit satellite that affected by Earth's magnetic field.

The tree-axis magnetic field sensor is designed especially for navigation purposes of small satellites. The intensity of the Earth's magnetic field is measured in three dimensions and the result is a description of the magnetic field in the form of a value and a unit vector relative to the body fixed reference system of spacecraft. The magnetic field specification of LAPAN-A2 satellite is displayed in the Table 5.4.

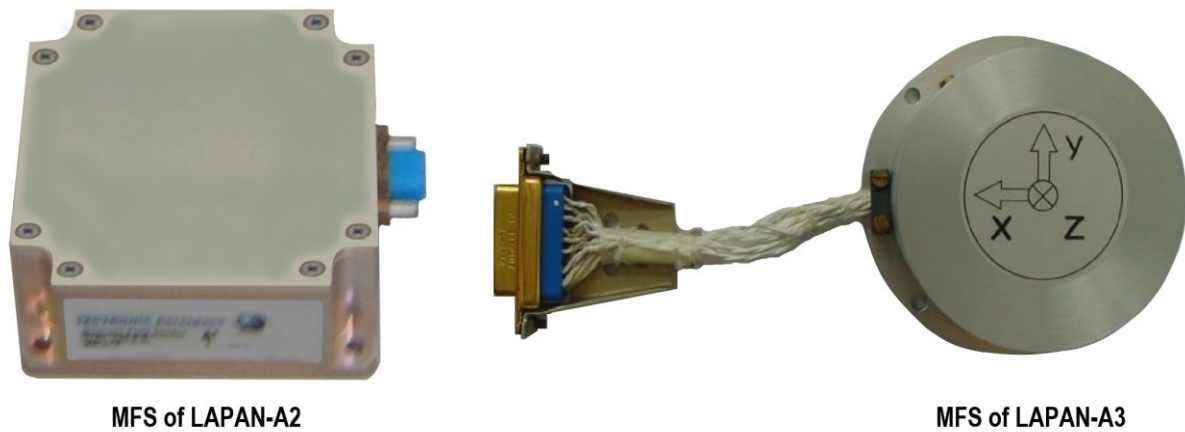


Figure 5.22: Magnetic Field Sensor (MFS)

Table 5.4: Technical Specification of Magnetic Field Sensor

| Items | Description |
|-------------------|---|
| Measurement range | ± 0.6 gauss ($\pm \mu\text{Tesla}$) |
| Accuracy | better than 2 miligauss ($0.2 \mu\text{Tesla}$) |
| Housing material | AlZnMgCu 1.5 |
| Length | $65 \times 65 \times 28 \text{ mm}^3$ |
| Weight | Max 220 g |

5.3.5 Reaction Wheel and Wheel Drive Electronics

As an actuator of the attitude control system, the reaction wheel essentially consists of a brushless direct current motor with a flywheel, electronics to control the actuator called *wheel drive electronics* (WDE) and housing for installing those components. LAPAN-A satellite series employ small and compact reaction wheels that have moment inertia around 880 kg.mm^2 of LAPAN-A1, 912.6 kg.mm^2 of LAPAN-A2 and LAPAN-A3, and can spin more than 6000 rpm depends on the supply voltage to the motor. The WDE regulates power to the reaction wheel's motor as well as managing the telemetry data of the attitude control system. The unit consists of DC/DC converter and Hitachi H8 processor. The general specification of reaction wheel that is used by LAPAN-A satellite series is presented in the Table 5.5.

Table 5.5: Technical Specification of Reaction Wheel

| Parameter | Value |
|--|--|
| Performance | |
| - Max. torque, at zero speed | 0.024 Nm |
| - Max. angular momentum storage | 0.46 Nms @ 5000 rpm (LAPAN-A1) 0.60 Nms @ 6250 rpm (LAPAN-A2/ LAPAN-A3) |
| - Speed control accuracy (≥ 100 rpm) | ± 0.2 rpm |
| Mechanical Interface | |
| - Weight | 1350 g |
| - Dimensions | $100 \times 100 \times 74$ mm ³ |
| - Housing | Aluminum, mounting 4 \times M5 bolts |
| Electrical Interface | |
| - Motor voltage | 12-16 V |
| - WDE, hall sensors, gyro voltage | 5 VDC |
| - Power consumption | 1 W (steady state), 15 W (max.) |

The complete wheel is protected by an aluminum housing, which is hermetically sealed. The housing consists of two major parts, an upper cover and bottom cover with baseplate, which defines the mechanical interface. The motor that is integrated with the rotating mass (flywheel) is mounted with springs in the housing, to protect the bearing of the motor against vibration load.

The WDE commutes the motor by evaluating the status of the three hall sensors from the motor. It can run the motor in both directions. The current control through the motor is realized as a digital programmable current source based on an operational amplifier and a field effect transistor. There are three basic independent control loops implemented on the WDE:

- direct current control
- precise wheel speed control and
- torque control

The block diagram of the WDE with motor consists of a current regulator and an actuator (see Figure 5.233). The current regulator corresponds to the current control circuit of the WDE, while the actuator correlates with the characteristic of the motor. The input signal of the current regulator corresponds to 13-bit DAC in the interval 0 - 8191. At the reference voltage U_{Ref} , it generates an output voltage U_{DAC} which gives the current I with the reciprocal of the measuring resistor R_M . This current is the output signal of the current regulator and the input signal of the actuator. Considering the friction moments M_f , the moment M_w by which the flywheel is accelerated can be calculated via the motor constant K_M . The frictional moments are made up of bearing friction, air friction and magnetic losses. At a rotation speed of N_{Actual} , the generator voltage U_G is induced, which limits the potential available through the motor operating voltage U_{Mot} and the reciprocal of the phase resistance R_P limits the flowing current to I_{max} .

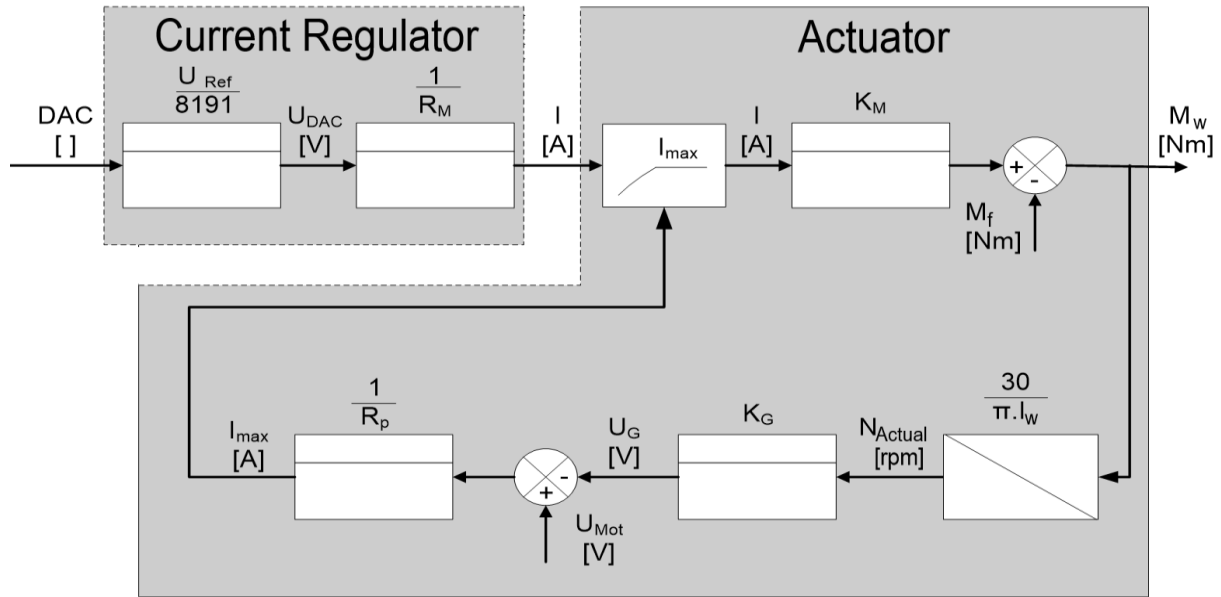


Figure 5.23: Block diagram of the Wheel Drive Electronic with Motor [60]

WDE could also integrate the reaction wheel with the gyro sensors in the loop to perform an angular velocity and an angle control of the spacecraft. All control parameters can be set by telecommand. The control system is based on a PID scheme with default control interval of 256 ms. The current command for angular velocity control loop will follow

$$Current = - \left[K_p \cdot (\omega_{Trg} - \omega_{Act}) + K_i \cdot \int (\omega_{Trg} - \omega_{Act}) dt \right] \quad (5.7)$$

with default factor of proportional K_p is 10000 and integrator K_i is 0. On the other hand, the current command for angle control loop is obtained by following relationship

$$Current = -K_p \cdot (\alpha_{Trg} - \alpha_{Act}) + K_D \cdot \omega_{Act} \quad (5.8)$$

with default factor of proportional K_p is 2000 and derivative K_D is 10000.

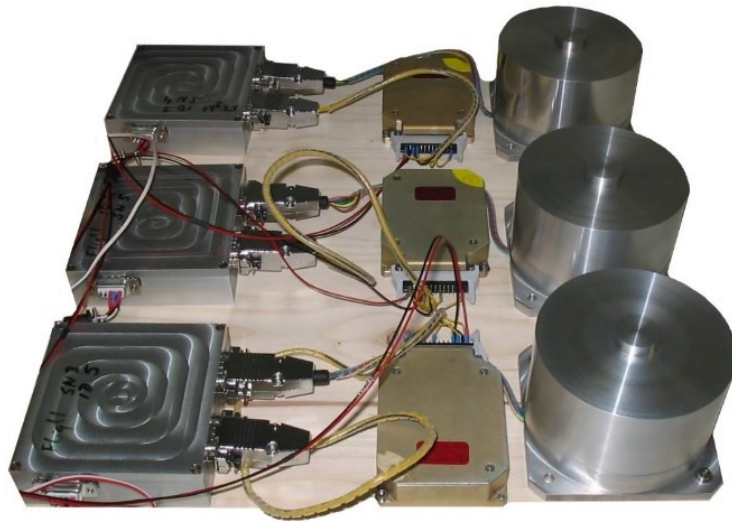


Figure 5.24: Reaction Wheel, Gyro, and WDE

5.3.6 Air Coil

Each LAPAN-A satellite series has three air coil type of magnetic torquers that are made of enameled cooper wire and wrapped with Teflon. These devices are integrated in three axes of the spacecraft as depicted in the Figure 5.255. These air coils could generate magnetic dipole moments to compensate the spacecraft residual magnetic fields or attitude drift from disturbance torques. The other primary task of these air coils is generating the angular momentum. When the satellite separated from the launcher, it may have negligible angular momentum. The angular momentum desired is about 80% of the maximum angular momentum controllable by the wheels. The accumulation of angular momentum is resulted by providing current to the magnetic torquer perpendicular to Earth's magnetic field.

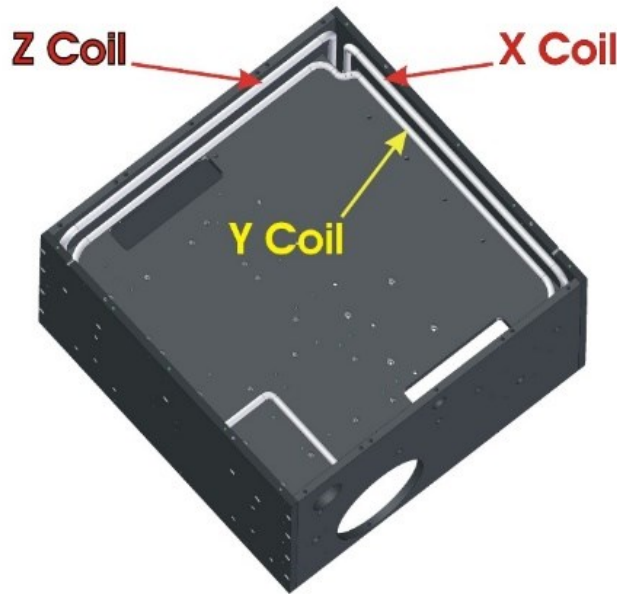


Figure 5.25: Air Coil Assembly on LAPAN-A1 Satellite's Main Structure

The magnetic dipole D generated by the coil is expressed by the formula

$$D = n I A \quad (5.9)$$

where n is the number of winding, I is the current provided, and A is the vector area of the coil. The dipole interacts with the magnetic field generating a torque τ_m whose expression is

$$\tau_m = D \times B \quad (5.10)$$

The Power Control and Data Handling (PCDH) sets the current in the coils using a 12-bit digital-analog-converter. The current is controlled by a transistor with a comparator, while the comparator gets its target value from a DAC. The PCDH of LAPAN-A1 satellite allocated the current for each air coils are no more than 560 mA, while LAPAN-A2 and LAPAN-A3 set the maximum of current around 250 mA. The amount of torque that could be produced by LAPAN-A satellite series is presented in the Table 5.6.

Table 5.6: The Technical Specification of Air Coil

| | | LAPAN-A1 | LAPAN-A2 | LAPAN-A3 |
|---|----------|-----------------------|-----------------------|-----------------------|
| Number of winding (N) | <i>x</i> | 280 | 265 | 375 |
| | <i>y</i> | 150 | 243 | 263 |
| | <i>z</i> | 265 | 279 | 385 |
| Resistance (ohm) | <i>x</i> | 48.0 | 60.0 | 63.6 |
| | <i>y</i> | 53.7 | 60.0 | 64.0 |
| | <i>z</i> | 53.0 | 60.0 | 64.2 |
| Maximum current, I_{max} (A) | <i>x</i> | 0.271 | 0.233 | 0.220 |
| | <i>y</i> | 0.242 | 0.233 | 0.219 |
| | <i>z</i> | 0.245 | 0.233 | 0.218 |
| Area (m ²) | <i>x</i> | 0.092 | 0.156 | 0.106 |
| | <i>y</i> | 0.174 | 0.189 | 0.230 |
| | <i>z</i> | 0.096 | 0.143 | 0.108 |
| Max. torque (Nm) @pole: 0.6 Gauss | <i>x</i> | 4.19×10^{-4} | 5.80×10^{-4} | 5.23×10^{-4} |
| | <i>y</i> | 3.79×10^{-4} | 6.43×10^{-4} | 7.95×10^{-4} |
| | <i>z</i> | 3.73×10^{-4} | 5.58×10^{-4} | 5.42×10^{-4} |
| Max. torque (Nm) @equator: 0.3 Gauss | <i>x</i> | 2.09×10^{-4} | 2.90×10^{-4} | 2.62×10^{-4} |
| | <i>y</i> | 1.89×10^{-4} | 3.21×10^{-4} | 3.98×10^{-4} |
| | <i>z</i> | 1.86×10^{-4} | 2.79×10^{-4} | 2.71×10^{-4} |

5.4 Acquisition Phase of Momentum Bias

Operating LEO satellite stabilization using momentum bias requires special provision. Unlike in GEO satellite, in which the strategy is quite popular, the dominant disturbance that could drift the angular momentum vector in LEO is the Earth's magnetic field. In the case of LAPAN-A satellite series that orbiting above 500 km, the aerodynamic effect is negligible. Minimizing magnetic disturbance could be done providing magnetic cleanliness on the satellite, which could be done by the 3 air coils after the internal magnetism can be measured. While GEO satellite frequently uses thrusters to maintain the angular momentum and horizon sensor to monitor the direction of the vector, LAPAN-A satellite series use magnetic torquers to generate external torque together with three reaction wheels and utilize star sensor to keep track of the angular momentum vector.

Establishing momentum bias attitude control requires preparation phase before the operation. Initialization or acquisition phase is generally conducted in the *Launch and Early Orbit Phase* (LEOP) to characterize the system in the real environment, generate the angular momentum and maintain its magnitude and direction. This phase involves setting an initial value for actuators, adjusting the control parameter and identify the problem before setting the operation procedure. Once the angular momentum is set up and all of the systems are well determined, the operation phase can be conducted.

5.4.1 Disturbance Torque Characterization

The first step to control the satellite attitude is determining the characteristics of the external disturbance torque. The sources of external disturbance torque can be gravity gradient, solar pressure, and magnetic field. Nevertheless, the dominant disturbance torque in low Earth orbit is the magnetic torque. Generally, the devices that potentially generate magnetic torque disturbance are batteries, high permeability materials, and actuators or motors that employ permanent magnet.

To control the drift of angular momentum, the external disturbance torque of the spacecraft should be well determined. Once the disturbance torque is characterized, the magnetic coil torque will compensate it so the drift of angular momentum direction is controlled in the low-level. To control the direction of angular momentum, LAPAN-A satellite series use magnetic torque or gravity gradient torque to obtain the precession on right ascension and declination. The precession of the angular momentum vector is then evaluated by star sensor.

At an altitude above 500 km the sources of external disturbance torque can be gravity gradient, solar pressure, and magnetic field. According to the body fixed coordinate that showed in Figure 5.1, the torque caused by the gravity gradient and solar pressure of LAPAN-A satellite

series are presented in the Table 5.7. Meanwhile, the disturbance torque that caused by magnetic field depends on activity of devices that emit a magnetic dipole, therefore it varies over time. For LAPAN-A satellite series, there are two devices that potentially produce the magnetic torque, the batteries and the permanent magnet of wheel motor that can emit a constant radial dipole when they are not rotating.

Table 5.7: Gravity Gradient Torque and Solar Pressure Torque

| | | LAPAN-A1 | LAPAN-A2 | LAPAN-A3 |
|--|-------------|--|----------------------|----------------------|
| Orbital radius (m) | r | 7.0×10^6 | 7.0×10^6 | 6.9×10^6 |
| Max. gravity gradient torque (Nm) | x axis | 1.1×10^{-6} | 1.4×10^{-6} | 2.9×10^{-6} |
| | y axis | 9.5×10^{-8} | 2.0×10^{-7} | 1.3×10^{-6} |
| Max. solar pressure torque (Nm) | A_{sp} | 0.20 | 0.24 | 0.29 |
| | l | 0.05 | 0.01 | 0.01 |
| | τ_{sp} | 5.1×10^{-8} | 8.2×10^{-9} | 1.1×10^{-8} |
| Magnetic Torque | | <i>Difficult to quantify, depends on the devices that emit a magnetic dipole</i> | | |

LAPAN-A1 satellite establishes three steps to conduct in orbit measurement of the magnetic torque. The first step is measuring the external torque when the satellite in zero momentum and switch off all the wheels, the disturbance torque is quantified by calculating the change of angular momentum through three satellite gyros. The second step is measuring the torque when all the wheels are active. The third step is measuring the torque when all the wheels are switched off and one of the magnetic coils is set with maximum current.

When the spacecraft's momentum was almost zero, the external torque will be equivalent to the changing of angular momentum that is evaluated by gyro reading in each orthogonal axis. The gyros reading for free tumbling condition are shown on Figure 5.266.

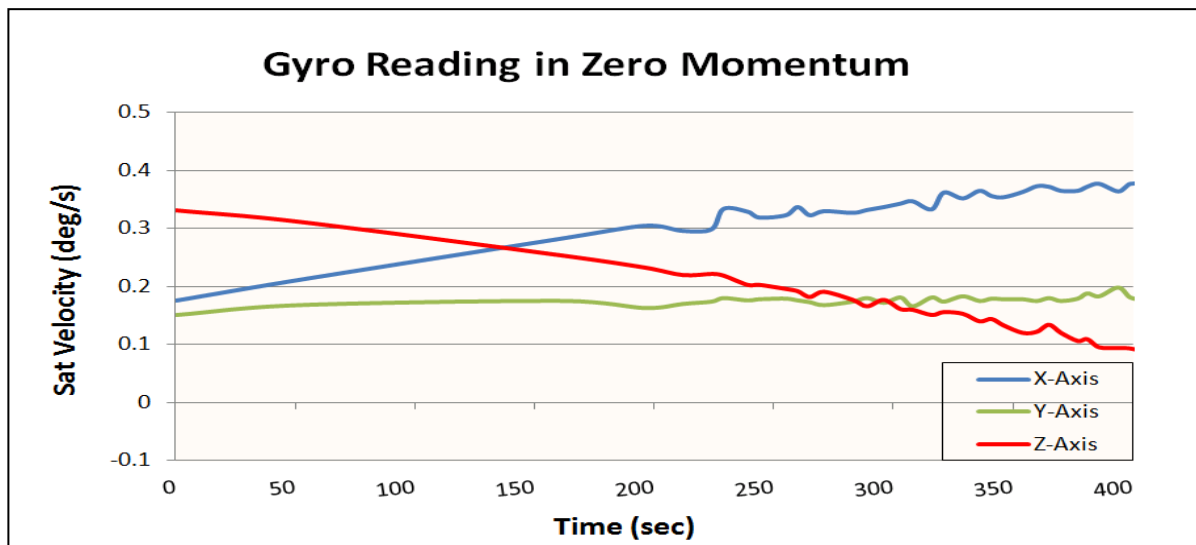


Figure 5.26: Gyro Reading during Free Tumbling Condition [45]

According the first measurement, it shows the angular velocity of the satellite in the x , y , and z axis has been changed 0.201 deg/s, 0.03 deg/s, and 0.239 deg/s respectively in the 400 seconds. These rates of change are equivalent to an external torque 1.956×10^{-5} Nm. Meanwhile, based on the calculation, the maximum theoretical value of gravity gradient torque and solar pressure are 1.1×10^{-6} Nm and 5.1×10^{-8} Nm respectively. This value is very small compared to the total external torque on the satellite. This fact confirms that the most likely sources of the torque are the devices that generate a magnetic field. Figure 5.27 also shows the angular velocity on y axis almost stable. It indicates that the source of the external torque is on the y axis. The external torque can be easily compensated by using a magnetic coil torque on the y axis so that the resultant of the torque become zero.

The second measurement is taken when all the wheels are rotating. As previous explanations, there are two suspected sources of magnetic dipole on the spacecraft i.e. wheels and batteries. The objective of this measurement is to know the magnetic torque that produced by batteries only. The wheels can produce a radial dipole when they are not rotating. The direction of the wheel dipoles is random on a plane perpendicular to the axis of rotation. So far it is not clear which of the dipoles are stronger, the wheels or the batteries. To know the influence of the devices clearly, then this measurement was conducted. This test command zero rate in all 3 satellite axes and collects as many wheel speed data as possible. The main difference from the previous test is that the wheels are now continuously rotating so that all the wheel dipoles are averaged and the torque should be influence of the battery dipole only. The measurement results can be seen in Figure 5.27.

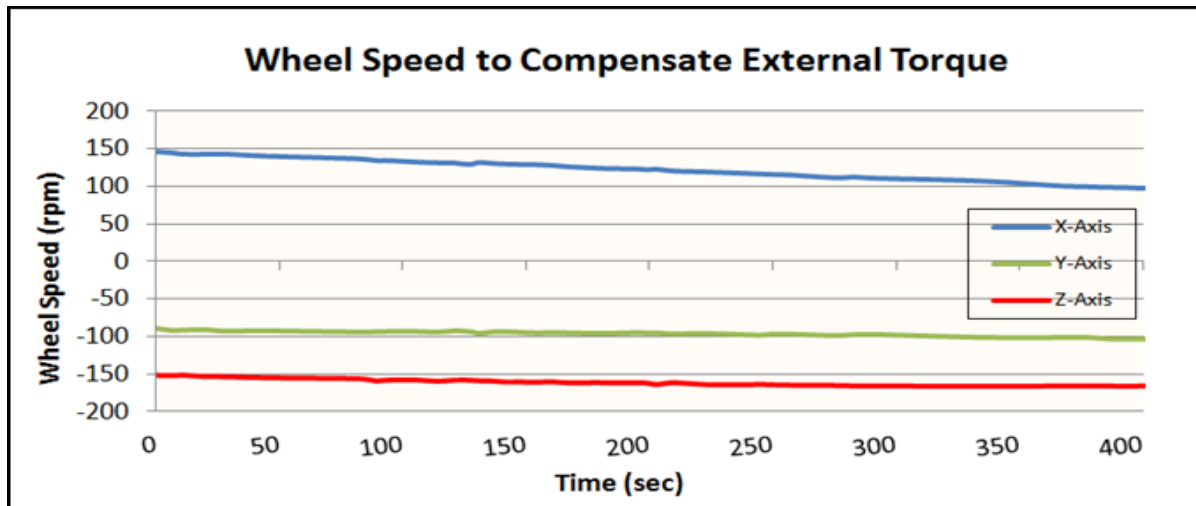


Figure 5.27: Wheel Speed for External Torque Compensation [45]

According the second measurement as shown in Figure 5.27, the changes of wheel speed on the x , y , and z axis are 46.8 rpm, 14.6 rpm and 13.9 rpm respectively in the 394 seconds. The changes of wheel speed are equivalent to a torque of 1.193×10^{-5} Nm due to the effect of the battery only. The maximum torque is a bit lower compared to 1.956×10^{-5} Nm which is caused by wheels and batteries.

To compare the entire test with the knowing source of magnetic dipole, the third measurement should be conducted. At the third test, the spacecraft would be measured in free tumbling mode, but at this time it was provoked by the influence of a known magnetic dipole by switching on the y coil to its maximum current (242 mA) without time limitation. The satellite angular rate was read by gyro as in the first test as shown in the Figure 5.288.

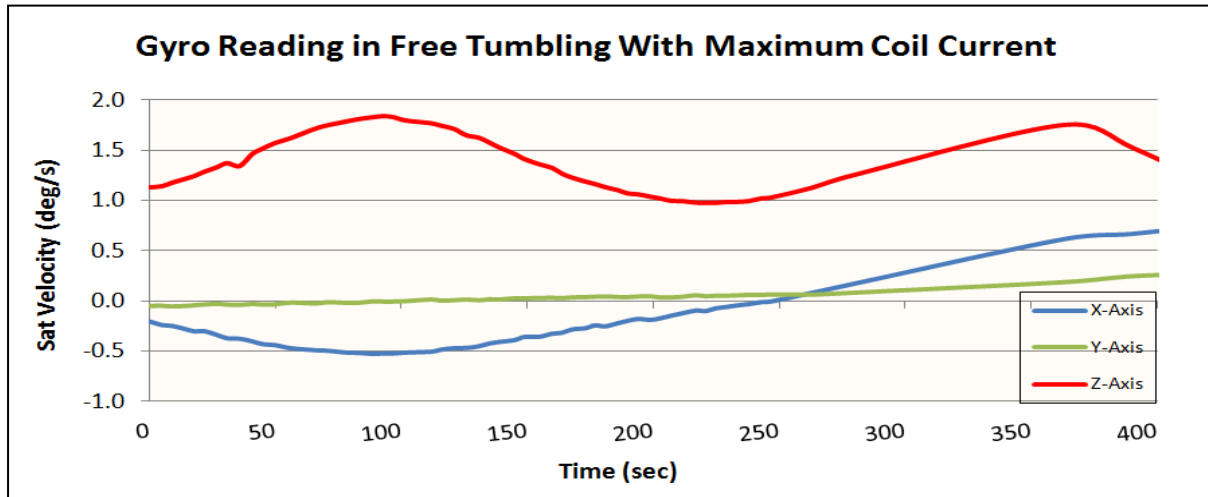


Figure 5.28: Free Tumbling Condition with the Maximum Current Setting on Y Coil [45]

The third measurement result showed that the angular velocity on the y axis is almost stable, while the angular velocity in the x and z axis are always changing. Figure 5.28 shows the changes of angular velocity in the x, y, and z are 0.423 °/s, 0.052 °/s, and 0.861 °/s respectively in the 128 seconds which is equivalent to the torque of 1.88×10^{-4} Nm. If the result is compared to the first measurement, the external torque on the first measurement was about 6.3% of the maximum torque generated by y coil. Therefore, by setting the current of 15 mA (6.3% of 242 mA) to the y coil, it would able to compensate the disturbance torque. Nevertheless, the exact value of the coil current depends whether the wheel rotors are rotating or not. If the wheel rotors are stopping, the influence torque also depends on the actual end position of the wheel rotors. Thus, it will need adjustment after changing the operating status of the wheel from active to idle or vice versa. By using the same approach, the amount of coil current for residual magnetic dipole compensation of LAPAN-A satellite series are presented in the Table 5.8.

Table 5.8: Compensation Current of Residual Magnetic Dipole by Air Coil

| Satellite | Compensation Current (mA) | | |
|-----------|---------------------------|--------|--------|
| | x coil | y coil | z coil |
| LAPAN-A1 | 0 | 15 | 0 |
| LAPAN-A2 | -2 | -4 | 2 |
| LAPAN-A3 | -3 | -22 | 2 |

5.4.2 Raising Angular Momentum

Once the external disturbance torque has been identified, the next step of momentum bias establishment is raising the angular momentum up to 80% of the maximum angular momentum that can be stored by the wheel to get the desired gyroscopic stiffness. Actually, there are many methods for generating angular momentum. Keeping a pitch orientation that deviates the z axis of the spacecraft from the nadir, as illustrated in the Figure 5.29, would induce a constant gravity gradient that could accumulate the angular momentum. However, since the gravity gradients only produce a small torque, generating an angular momentum using the gravity gradient torque is time consuming, therefore, less effective. Moreover, generating angular momentum in the pitch axis (y axis) using gravity gradients is very dependent on the difference of the moment inertia between the x axis and z axis.

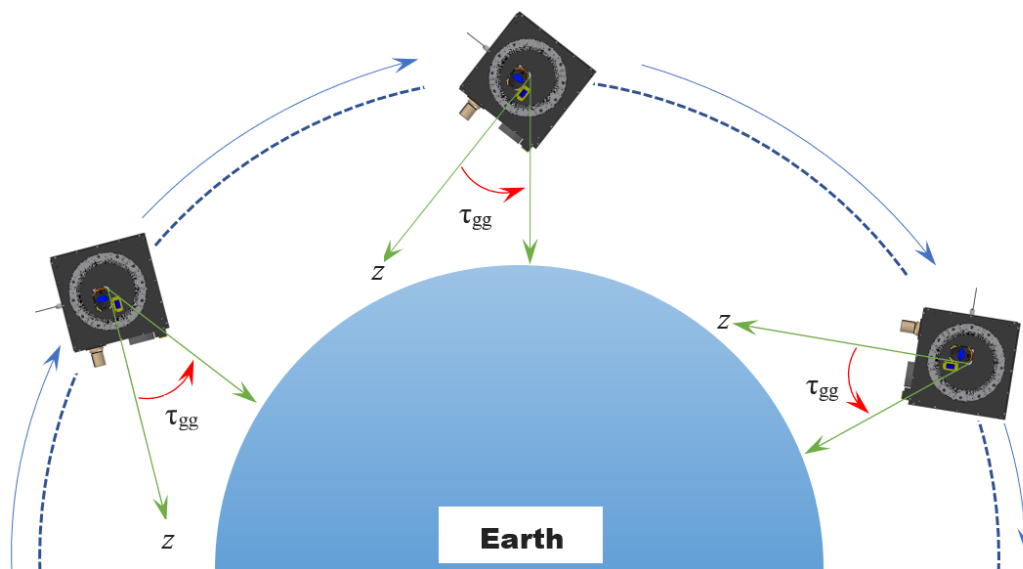


Figure 5.29: The Gravity Gradient Torque of a Constant Pitch Orientation

Generally, raising angular momentum in the normal of orbit direction using magnetic torquer is easy to do since the magnetic torquer of polar orbiting satellite produces the torque that is mostly perpendicular to the direction of the Earth's magnetic field. LAPAN-A satellite series use air coils and reaction wheels, which are fixed on the orthogonal axis x , y , and z , to generate the angular momentum through the following steps:

- Stopping the satellite rotation of all axes using reaction wheels, so that the satellite is in a stationary condition.
- Enables ones of the coil that produces the biggest torque in the pitch axis with maximum currents.

The maneuver to increase the angular momentum could be performed every time the satellite passes through the relay ground station in every 1.5 hours. Figure 5.3030 shows at least three passes are required by polar orbiting satellite of LAPAN-A1 to accumulate the angular

momentum up to 80% of the wheel maximum storage capacity which is equivalent with 0.37 Nms at 4000 rpm of wheel speed. The wheel on the y axis is used to absorb all the momentum, while the other wheel is used for nutation damping.

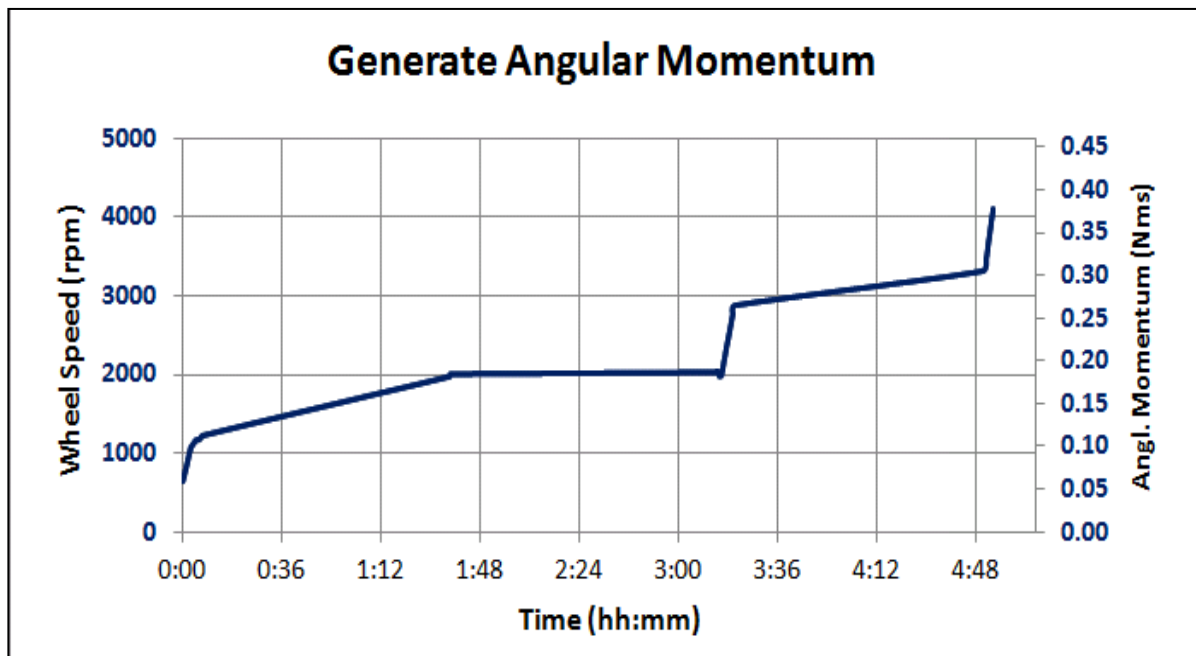


Figure 5.30: Increasing of Angular Momentum [45]

5.5 Momentum Bias in Equatorial Orbit

Generating angular momentum for equatorial orbiting satellite is a little bit challenging. Since the pitch axis of the equatorial orbiting satellite is facing to the pole, there is no such procedure to produce high torque in the pitch axis by setting maximum current on the magnetic coil as a polar orbiting satellite. Nevertheless, the vector of the Earth's magnetic field in the equatorial orbit is not uniform. Based on measurements by the LAPAN-A2 satellite, magnetic vectors in equatorial orbit vary along the Earth's longitude. Figure 5.31 shows the plots of magnetic vectors with respect to the spacecraft axis in the several orbital periods or passes during nadir pointing operation. Since the spacecraft orient its y axis to the south, the magnetic vectors on the y axis will always in negative value. Meanwhile, the magnetic vectors on the x and z axis asymmetrically varied from positive to the negative value. Applying bias current to the coil in these asymmetrical variations of the magnetic vectors for an orbital cycle will result an angular momentum precession as well as changing of its magnitude.

Figure 5.31 also shows that the magnetic vectors have high variation in z axis that could be utilized for generating angular momentum. Setting a constant current to the x coil would

produce the angular momentum in the desired axis, i.e. y axis, while interacting with z vector of magnetic field. However, it would produce also the angular momentum in the z axis while interacting with y vector of magnetic field which lead to angular momentum precession. The growth of angular momentum in the z axis then be annihilated by the short maneuver of setting high current with opposite direction to the x coil in the region that the z vector of magnetic field is zero. This short maneuver procedure will reduce or eliminate the angular momentum on the z axis, but still remain that is on the desired y axis.

However, observing the angular momentum of an equatorial orbiting satellite in the celestial sphere is hard since its coordinates are very close to the pole, so that a small movement in the spacecraft axis will be expressed such as big jump. Therefore, evaluation of the angular momentum in the equatorial orbit then be taken from spacecraft's zenith that is perpendicular to the angular momentum. The right ascension and declination of zenith, RA_{zenith} and DE_{zenith} in degree respectively, are located close to the equator, and derived from a spacecraft's position and the local horizon along the Earth using following relation.

$$RA_{zenith} = \theta_G + \lambda \quad (5.11)$$

$$DE_{zenith} = \varphi \quad (5.12)$$

where θ_G is Greenwich hour angle of the Vernal Equinox, λ is spacecraft's longitude, and φ is spacecraft's latitude. Since knowing zenith coordinates is not sufficient to determine the spacecraft attitude, thereby the third coordinate have to be introduced by defining a rotation along zenith axis as the azimuth of zenith, AZ_{zenith} .

$$AZ_{zenith} = \theta_o + i \cdot \cos(\omega + M) \quad (5.13)$$

where θ_o is initial angle or offset angle, i is orbital inclination, ω is orbital argument of perigee, and M is orbital mean anomaly.

In the case of equatorial orbiting satellite, as illustrated by Figure 5.32, activating the x coil will create torque τ_x that is parallel to the z axis, so the angular momentum H would experience a precession that changes the declination of zenith, DE_{zenith} . In the same way, the z coil will produce torque τ_z parallel to the x axis that drift the angular momentum and rotate the spacecraft in the zenith axis, so AZ_{zenith} is changing. Meanwhile, the changing of RA_{zenith} can directly manage by y wheel that control pitch rotation.

For real time evaluation of angular momentum direction, the target coordinates of zenith are calculated by a program that are embedded in the satellite operating software and then compared with the actual coordinates, $-z$ of satellite (Sat Z -) coordinates, which are obtained and transformed directly from the star sensors. Figure 5.33 displays the deviation of zenith coordinates ($ZenDiff$) of LAPAN-A2 satellite from its target.

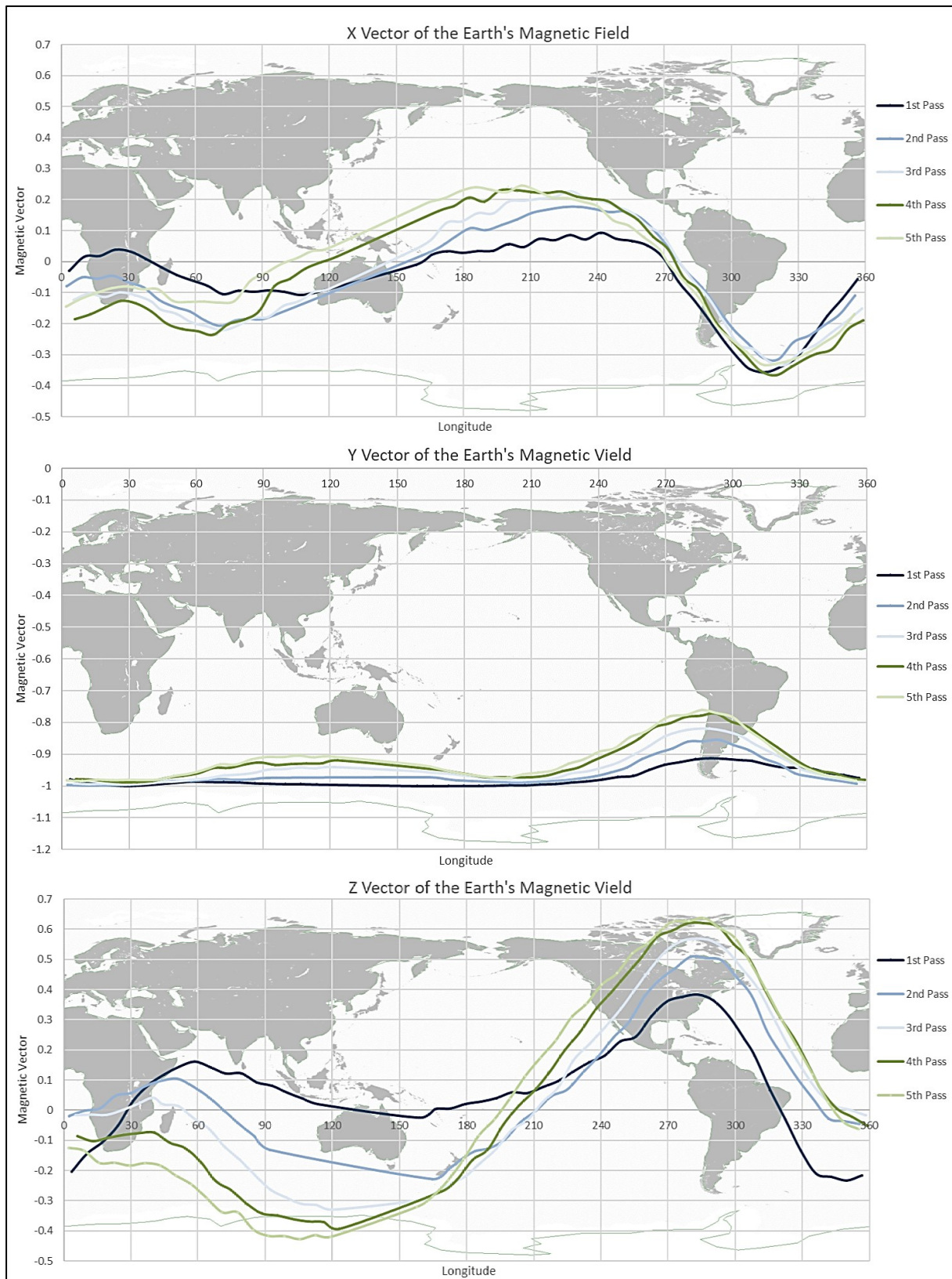


Figure 5.31: The Earth's Magnetic Vector with Respect to the Spacecraft Axis of LAPAN-A2 Satellite

6 FLIGHT RESULT

This chapter discusses the performance of momentum bias in the nominal operation of LAPAN-A satellite series. As described in the previous chapter, the nominal operation of momentum bias attitude control for LAPAN-A satellite series consist of three main modes, i.e. nadir pointing mode, slew mode, and hibernation mode. While LAPAN-A3 satellite represents a momentum bias operation in the polar orbit, LAPAN-A2 satellite has demonstrated momentum bias in the equatorial orbit.

6.1 Nadir Pointing Mode

There are three subjects of activities in the operation of momentum bias attitude control, i.e. maintaining the magnitude of angular momentum, damping the nutation, and controlling the direction of the momentum. On the subject of maintaining angular momentum and controlling its direction, there is a different procedure between polar and equatorial orbiting satellite due to the difference of orientation between spacecraft body's axis towards Earth's magnetic field. In regard to nutation damping, LAPAN-A satellite series applied active nutation damping. There are two alternative devices used to damp the nutation, reaction wheel or magnetic coil. While implementing nutation damping by reaction wheel, there is no difference between polar and equatorial orbiting satellite. However, using a magnetic coil to damp the nutation should consider the local Earth's magnetic field and the direction of resulting torque. The magnetic coil must produce a torque that has an opposite direction toward the angular acceleration of oscillating motion due to nutation.

6.1.1 Maintaining Angular Momentum

To satisfy the gyroscopic stiffness, both LAPAN-A2 and LAPAN-A3 satellites have to maintain the angular momentum $> 80\%$ of wheel momentum storage capacity. It means the pitch wheel should run more than 5000 rpm but still has enough margin from saturation when it reaches the maximum speed of 6250 rpm, so the operation speed of pitch wheel is targeted around 5500

rpm. The speed margin is needed since the maximum speed achieved by wheel could be up and down along the variation of supply voltage due to *counter electromotive force* or also known as *back electromotive force (back EMF)*. The back EMF is the electromotive force or "voltage" that opposes the change in current which induced it. It is represented as a variable EMF that opposes the one driving the motor. Since back EMF is the generator output of a motor, it will be zero when the motor is not turning, and increases proportionally to the motor's angular velocity.

The angular momentum on the pitch axis is directly handled by the reaction wheel y . It could absorb all the momentum so the spacecraft would stop spinning. If the wheel spins beyond its angular momentum, the spacecraft would rotate in the opposite direction. Conversely, if the wheel spins less than its angular momentum, both the wheel and spacecraft would rotate in the same direction. Since the wheels on the LAPAN-A satellite series are highly integrated to the gyro, the spacecraft rotation could be controlled so that the wheel would adjust its speed following a built-in control algorithm in the wheel drive electronic (WDE), which is based on PID

The integrated y wheel-gyro forms a single axis attitude control system to control the spacecraft angular velocity and angle in the pitch axis. At the time of implementation, the gyro must be connected to the WDE through the gyro serial interface and to the supply voltage via the necessary cables. The microprocessor WDE would check whether a gyro is connected and ready for operation. In the active case, the gyro is read continuously in the defined time interval, otherwise the gyro interface of the WDE is deactivated by hardware and software, so that only the basic independent modes of wheel are available, i.e. current control, speed control and torque control. When the reaction wheel is connected to the gyro, it provides the operating modes for controlling the angular velocity and the angle of the spacecraft. The operating mode is automatically switched by the respective telecommand that contain a setting parameter and target value. Commanding a current, a wheel speed or a torque leads to the deactivation of the gyro interface and trigger the deletion of the integrated angle.

The operating mode for controlling the angular velocity in an axis of the spacecraft is fundamental since the camera system is aligned by means of angular velocity set by telecommand. Furthermore, the operating mode is used for inertial stabilization by absorbing the angular momentum. When the telecommand switches the operating mode, it activates the control loop shown in Figure 6.1 and specifies the new angular velocity ω_{Target} as the target for the controller. The controller consists of a parallel connection of proportional controllers with the factor of K_P and an integrator of K_I .

In the LAPAN-A1 satellite that implement interactive control, the control interval corresponds to the readout interval Δt of 256 ms and the default value of K_P is 10000 s/deg. The gain factor of integrator K_I is zeroed to avoid difficulty due to its oscillating properties during interactive control which requires a short transient time. The missing integrator would create a permanent

deviation due to the external disturbance torques M_e , which leads to a wandering of the sensor or payload pointing and could be immediately compensated by the operator in the ground station through interactive control strategy. Conversely, the missing integrator becomes disadvantageous for nadir pointing mission that set a constant angular velocity for a long time. Therefore, after a several in orbit test, the pitch wheel of LAPAN-A2 and LAPAN-A3 satellites have been optimized their K_I into 15 deg^{-1} and 7 deg^{-1} respectively. Meanwhile, the K_P of LAPAN-A2 and LAPAN-A3 pitch wheels have been adjusted to 30000 s/deg and 25000 s/deg respectively, due to their different moment of inertia compare to LAPAN-A1 satellite.

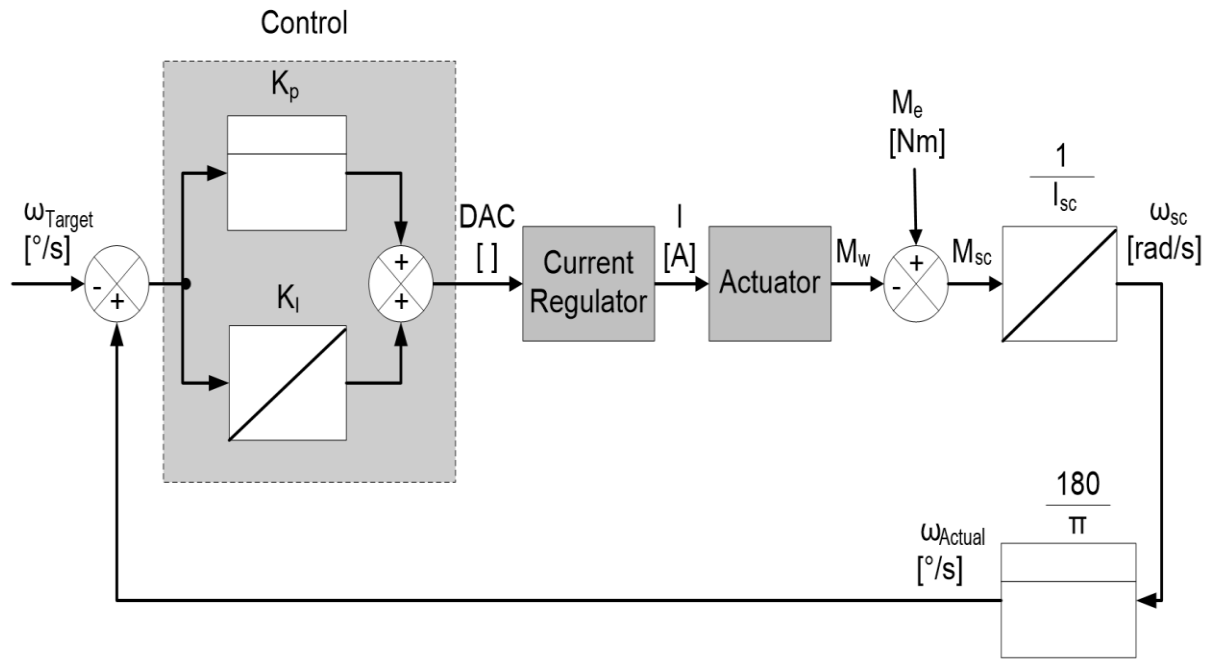


Figure 6.1: Block Diagram of the Spacecraft Angular Velocity Control [60]

The operating mode for controlling the angle in an axis of the spacecraft is used for the acquisition maneuver in order to get star reference as well as attitude correction to align the sensor or payload to the target. When the telecommand switches the operating mode, it deletes the current angle, activates the control loop and specifies the new angle α_{Target} as the target for the controller shown in Figure 6.2. The standard value of the gain factor K_P is 2000 deg^{-1} and that of K_D is equal to 10000 s/deg . Due to the missing integrator, there is a control deviation that is proportional to the external disturbance torques M_e .

Besides angular velocity and angle modes, angular pitch motion can also be controlled by wheel speed mode. In the wheel speed control mode, telecommand switches the operating mode, activates the control loop shown in Figure 6.3 and gives the controller the new wheel speed n_{Target} as the target. The speed controller consists of a parallel connection of proportional controllers with the gain factor K_P and an integrator with the factors K_M and K_I . The speed control takes place in the same time interval of 200 ms as the speed measurement. At speeds

less than 300 rpm, the measuring and control interval becomes longer and the properties of the control loop become worse. Nevertheless, in this momentum bias strategy, the pitch wheel is spinning at high speed. Thus, the lower control accuracy in the low speed is not the issue. But controlling angular motion using the wheel speed mode on the small satellites which have small inertia is very susceptible to the external disturbance torque since it is an open loop control over spacecraft movements.

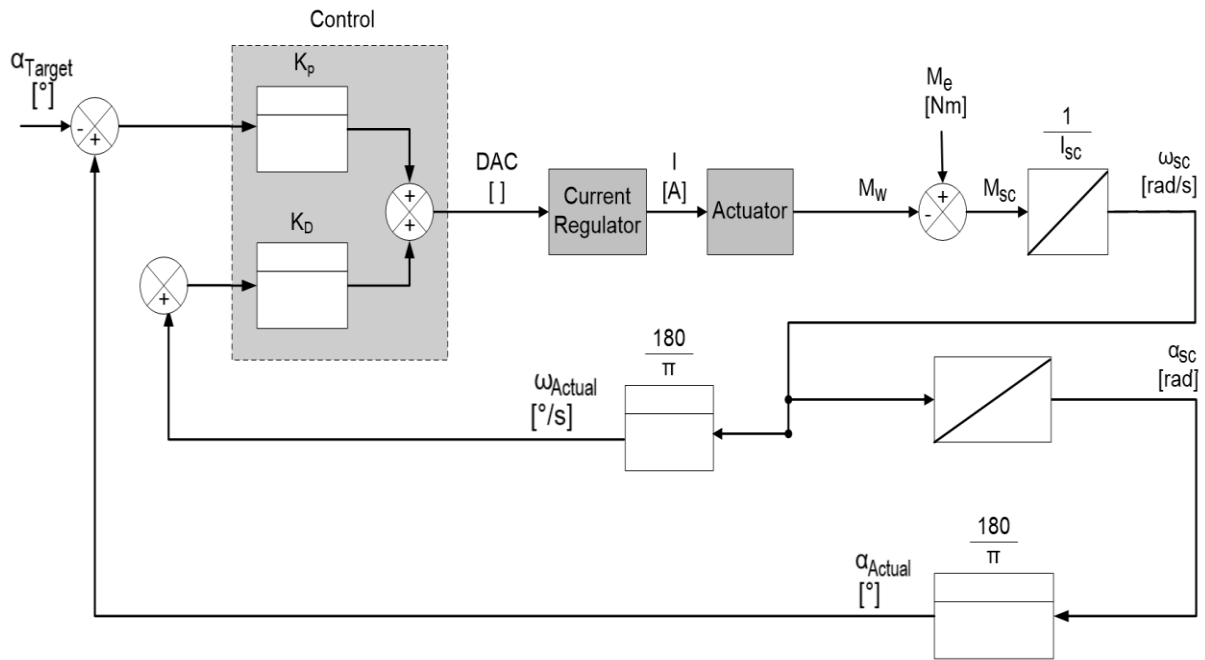


Figure 6.2: Block Diagram of the Spacecraft Angle Control [60]

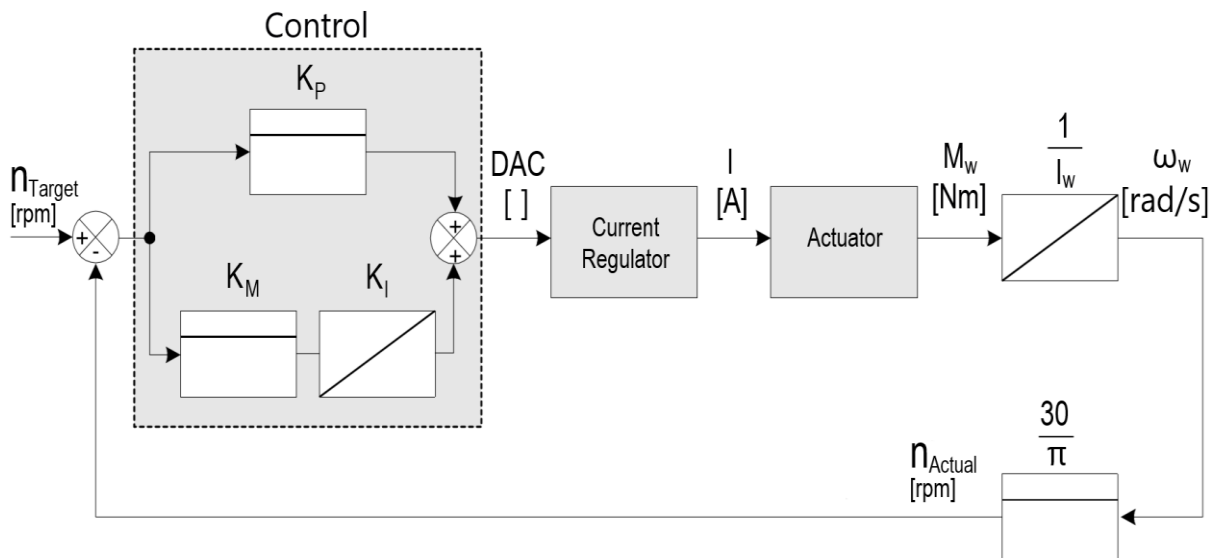


Figure 6.3: Block diagram of the Wheel Speed Control [60]

In the nadir pointing operations, the spacecraft mostly manages its pitch motion using angular

velocity control involving the gyro in the closed loop and letting the wheel spin up and down to react against disturbance torque. In this closed loop, the gyro signal has drift rate about several degrees per hour, hence it needs regular updating from the star sensor. Sometimes the open loop control is needed, especially in the early acquisition phase, to characterize the disturbance torque. When the spacecraft operates in constant wheel speed, its angular velocity would accelerate and decelerate due to external disturbance torque.

Figure 6.4 would give a better view about the attitude control mode in the pitch axis. It plots the two hours of observation result on the angular velocity in the pitch axis of LAPAN-A3 satellite that conducted on January 29th, 2020. This plot consists three flight sequence of nadir pointing operation when the spacecraft implemented angular velocity control (09:00-10:22), switched to wheel speed control (10:22-11:33), and then back to angular velocity control (11:33-12:00). In the wheel speed control mode, it appears that the angular velocity of the spacecraft was swinging from -0.08 deg/s to -0.04 deg/s for 40 minutes. The deviation of spacecraft angular velocity from its nadir pointing rate is proportional to the external disturbance torque, in particular magnetic torque which characterized by its cyclic profiles. Since the maximum acceleration occurred over the pole when the spacecraft was in nadir pointing mode, in which the z axis is pointing to Earth, the source of the disturbance should be in the x axis. Based on the plot, Table 6.1 estimates the amount of disturbance torque and current setting on the x coil to produce equivalent torque as well as maximum fluctuation of the wheel speed if the spacecraft runs angular velocity control.

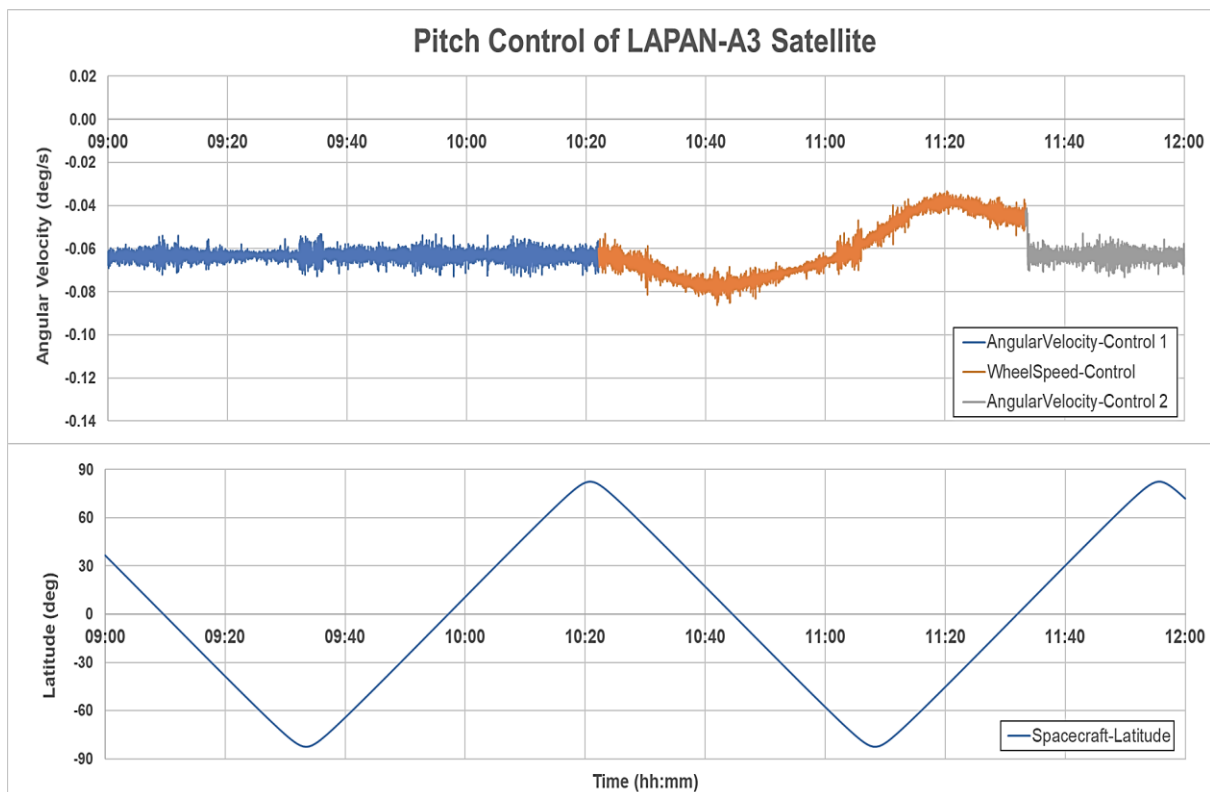


Figure 6.4: Motion in Pitch Axis in the Angular Velocity Control and Wheel Speed Control

Table 6.1: Wheel Speed Fluctuation Due to Disturbance Torque

| Parameter | Value | Unit |
|---|-----------------------|--------------------|
| Change of spacecraft angular velocity | 6.98×10^{-4} | rad/s |
| Delta time | 2400 | s |
| Acceleration of rotation | 2.91×10^{-7} | rad/s ² |
| Spacecraft moment of inertia in pitch axis (I_y) | 6.695 | kg.m ² |
| Estimated disturbance torque | 1.95×10^{-6} | Nm |
| Current setting on x coil to produce equivalent torque (max. torque 5.23×10^{-4} Nm @ 220 mA) | 0.819 | mA |
| Maximum momentum that potentially generated | 4.67×10^{-3} | Nms |
| Maximum wheel speed fluctuation (max. angular momentum 0.60 Nms @ 6250 rpm) | 49 | rpm |

Case 1: Polar Orbiting Satellite

To maintain the angular momentum in the pitch axis, the magnetic coil would be actuated for certain duration to keep the angular momentum in its operational level which indicates by wheel speed in the pitch axis. While the angular momentum is above the operation level, the magnetic coil would create a negative torque to decrease it. Conversely, the magnetic coil might create a positive torque if the angular momentum is below the operating level. The changing between a negative to a positive torque can be done just by simply switching of its current sign.

The magnetic coil will produce highest torque while it is perpendicular to the local Earth's magnetic field. In the nadir pointing mode of polar orbiting satellite, producing a torque that aligns to the pitch axis generally uses x coil above polar region and z coil over the equatorial region. At the north pole and descending node, the coil should apply negative current, while in the south pole and ascending node it should have positive current. The torque resulted in the polar region is one and a half to double of that resulted in the equatorial region. For angular momentum maintenance that need only few hundred rpm, activating coil current of plus or minus 200 mA for a few minutes is sufficient. Table 6.2 shows the typical operation for conserving angular momentum of polar orbiting satellite, LAPAN-A3.

Table 6.2: Conserving Angular Momentum of LAPAN-A3 Satellite

| Start | RPM | Stop | RPM | Coil Setting | Region | Δ RPM/ Minutes |
|---------------------|------|---------------------|------|--------------|-----------------|--------------------------|
| 2019/09/02 02:52:30 | 5085 | 2019/09/02 02:54:13 | 5313 | Z: -200 mA | Descending Node | 132.82 |
| 2019/09/05 03:31:55 | 5170 | 2019/09/05 03:33:00 | 5353 | Z: -200 mA | Descending Node | 168.92 |
| 2019/09/07 02:58:31 | 5181 | 2019/09/07 03:00:09 | 5421 | Z: -200 mA | Descending Node | 146.94 |
| 2019/09/11 14:00:46 | 5161 | 2019/09/11 14:02:00 | 5445 | X: -200 mA | North Pole | 230.27 |
| 2019/09/16 03:26:20 | 5117 | 2019/09/16 03:27:30 | 5308 | Z: -200 mA | Descending Node | 163.71 |
| 2019/09/17 13:46:47 | 5210 | 2019/09/17 13:47:57 | 5484 | X: -200 mA | North Pole | 234.86 |
| 2019/09/20 08:11:14 | 5181 | 2019/09/20 08:12:18 | 5424 | X: -200 mA | North Pole | 227.81 |
| 2019/09/23 10:26:56 | 5101 | 2019/09/23 10:28:20 | 5422 | X: -200 mA | North Pole | 229.29 |
| 2019/09/30 06:49:55 | 5070 | 2019/09/30 06:50:39 | 5238 | X: -200 mA | North Pole | 229.09 |

Case 2: Equatorial Orbiting Satellite

The pitch axis of the equatorial orbiting satellite, where angular momentum is laid, is in the north – south direction and almost coincide with the direction of the local geomagnetic. Therefore, it makes difficulties of generating a desired torque. It leaves only slight variations on the local vertical and east-west elements that could produce a torque in the pitch axis. Meanwhile, in the nadir pointing mode, the vertical axis is parallel with z axis of the spacecraft and east-west axis is parallel to x axis of the spacecraft. Since the variations of local magnetic field on the local vertical element is higher than east-west element, setting a constant current to the x coil continuously would potentially produce higher angular momentum in the pitch axis. This averaging technique, which set the coil with a small and constant current for a long time, will let the spacecraft accumulate the angular momentum cycle by cycle of its orbit as shown in the Table 6.3.

Table 6.3: Conserving Angular Momentum of LAPAN-A2 Satellite

| Start | RPM | Stop | RPM | X-Coil Current (mA) | Δ RPM/Orbit |
|---------------------|------|---------------------|------|---------------------|--------------------|
| 2019/09/01 02:24:48 | 5265 | 2019/09/01 12:36:56 | 5502 | 0 | 38 |
| 2019/09/01 14:29:46 | 5512 | 2019/09/02 00:48:15 | 5536 | -3 | 4 |
| 2019/09/02 06:13:03 | 5491 | 2019/09/02 13:00:27 | 5579 | -1 | 21 |
| 2019/09/02 14:53:57 | 5582 | 2019/09/03 01:10:50 | 5669 | -2 | 14 |
| 2019/09/03 01:25:35 | 5608 | 2019/09/03 15:07:11 | 5698 | -2 | 11 |
| 2019/09/04 03:34:33 | 5675 | 2019/09/04 13:44:14 | 5531 | -5 | -23 |
| 2019/09/05 03:52:57 | 5334 | 2019/09/05 09:05:04 | 5296 | -4 | -12 |
| 2019/09/06 06:01:24 | 5527 | 2019/09/06 12:46:13 | 5497 | -2 | -7 |
| 2019/09/06 14:35:22 | 5474 | 2019/09/07 00:59:18 | 5489 | -1 | 2 |
| 2019/09/07 02:46:21 | 5448 | 2019/09/07 07:56:01 | 5500 | 0 | 16 |
| 2019/09/07 15:05:05 | 5472 | 2019/09/07 23:38:59 | 5442 | -2 | -6 |
| 2019/09/08 03:16:43 | 5407 | 2019/09/08 15:17:24 | 5531 | 0 | 17 |
| 2019/09/08 15:24:07 | 5496 | 2019/09/09 00:04:43 | 5454 | -2 | -8 |
| 2019/09/09 03:27:12 | 5389 | 2019/09/09 08:47:59 | 5385 | -2 | -1 |
| 2019/09/09 14:12:47 | 5378 | 2019/09/10 00:21:20 | 5333 | -2 | -7 |
| 2019/09/10 02:06:12 | 5316 | 2019/09/10 14:16:57 | 5493 | 0 | 24 |
| 2019/09/11 00:54:13 | 5410 | 2019/09/11 04:24:09 | 5413 | -1 | 1 |
| 2019/09/11 04:24:09 | 5413 | 2019/09/11 11:10:28 | 5501 | 0 | 21 |
| 2019/09/12 02:54:28 | 5370 | 2019/09/12 13:17:43 | 5451 | 0 | 13 |
| 2019/09/12 15:15:58 | 5485 | 2019/09/13 01:29:05 | 5628 | 0 | 23 |
| 2019/09/13 03:29:06 | 5617 | 2019/09/13 15:24:04 | 5539 | -3 | -11 |
| 2019/09/13 15:29:10 | 5513 | 2019/09/14 01:51:44 | 5388 | -3 | -20 |
| 2019/09/14 03:46:36 | 5365 | 2019/09/14 12:18:08 | 5321 | -3 | -8 |
| 2019/09/14 14:19:18 | 5277 | 2019/09/15 03:59:51 | 5120 | -3 | -19 |
| 2019/09/15 09:20:14 | 5084 | 2019/09/15 12:50:47 | 5281 | 10 | 91 |
| 2019/09/15 14:34:56 | 5180 | 2019/09/16 00:54:50 | 5312 | 0 | 21 |
| 2019/09/16 14:55:06 | 5347 | 2019/09/17 01:15:48 | 5489 | 0 | 22 |
| 2019/09/17 06:28:12 | 5517 | 2019/09/17 13:26:43 | 5501 | -2 | -4 |
| 2019/09/17 15:10:57 | 5451 | 2019/09/18 01:38:17 | 5391 | -2 | -9 |
| 2019/09/18 03:36:10 | 5391 | 2019/09/18 13:49:32 | 5429 | -2 | 6 |
| 2019/09/18 13:59:09 | 5347 | 2019/09/19 00:19:24 | 5328 | -3 | -3 |
| 2019/09/19 02:19:02 | 5369 | 2019/09/19 14:20:29 | 5375 | -3 | 1 |
| 2019/09/19 14:19:05 | 5372 | 2019/09/20 00:39:27 | 5310 | -3 | -10 |
| 2019/09/20 05:52:32 | 5392 | 2019/09/20 14:35:00 | 5411 | 0 | 4 |

The average of wheel speed increments on the Table 6.3 is plotted by Figure 6.5. According to the plot, the angular momentum increments in an orbital period related to the bias current of magnetic coil will follow the trend below

$$\Delta\omega_{wheel} = 7.5593i_x + 16 \quad (6.1)$$

where $\Delta\omega_{wheel}$ is increment of wheel speed per orbit in rpm and i_x is bias current setting of x coil in mA. When the spacecraft is in contact with the ground station, the operators could adjust the bias current of the magnetic coil and use the equation (6.1) to predict the angular momentum level on the following satellite pass.

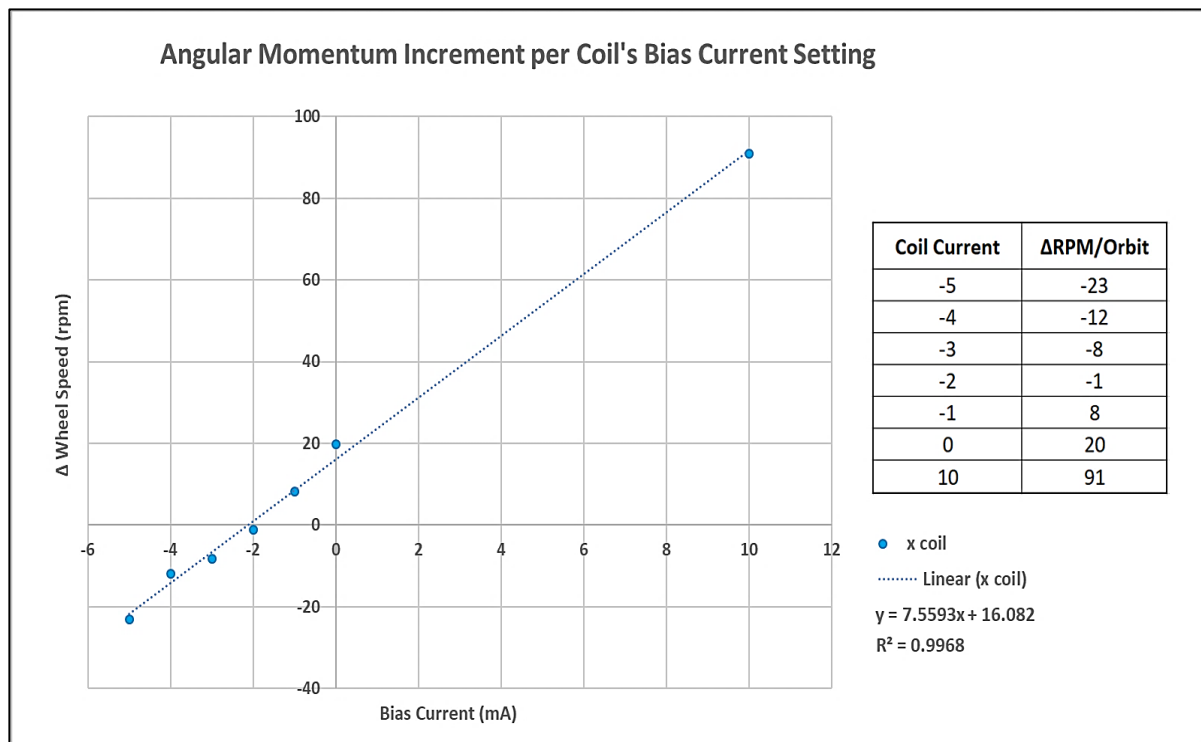


Figure 6.5: Angular Momentum Increment of LAPAN-A2 Satellite due to Bias Coil Current

6.1.2 Nutation Damping

There are two techniques for nutation damping which are applied on the LAPAN-A satellite series, by a reaction wheel and by a magnetic coil. To damp the nutation by a reaction wheel, the spacecraft will use a reaction wheel that perpendicular to the angular momentum. In case of LAPAN-A satellite series, a reaction wheel in the x axis (roll axis) has been utilized to damp the nutation using two different control algorithm, i.e. angular velocity mode and angle mode. For magnetic coil nutation damping, a torque has to be generated in the opposite direction of the angular acceleration to minimize the oscillation motion. Figure 6.6 shows the nutation angle resulted by various techniques of nutation damping.

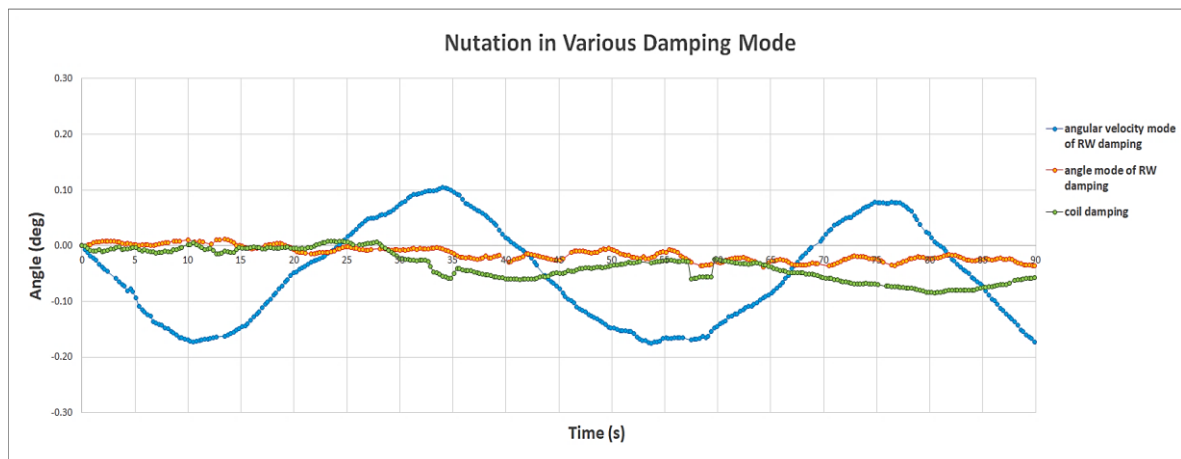


Figure 6.6: Various Nutation Damping Applied on LAPAN-A Satellite Series

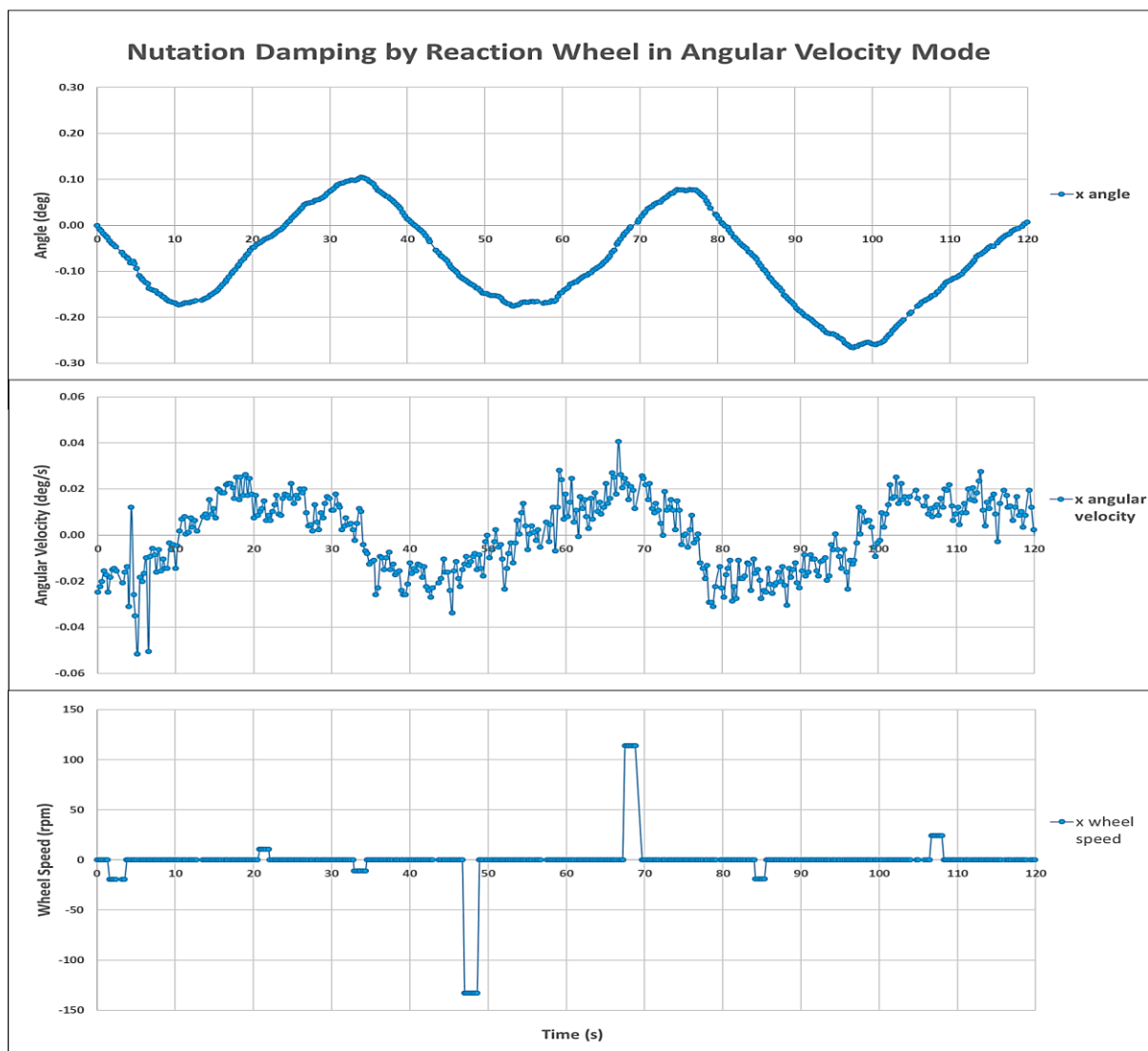


Figure 6.7: Nutation Damping by Reaction Wheel in Angular Velocity Mode

The typical of nutation damping by reaction wheel in angular velocity mode is displayed in the Figure 6.7. The control algorithm of angular velocity mode will follow equation (5.7) which is implemented in the wheel drive electronic. By setting the angular velocity 0 deg/s, the x wheel would give reaction by spinning up its rotor while the spacecraft angular velocity has exceeded a certain threshold of the target. This angular velocity mode uses the instantaneous angular velocity of the spacecraft, which is not affected by drift of gyro angle reading, therefore it can be run all the time within the performance of pointing stability better than 0.4 deg.

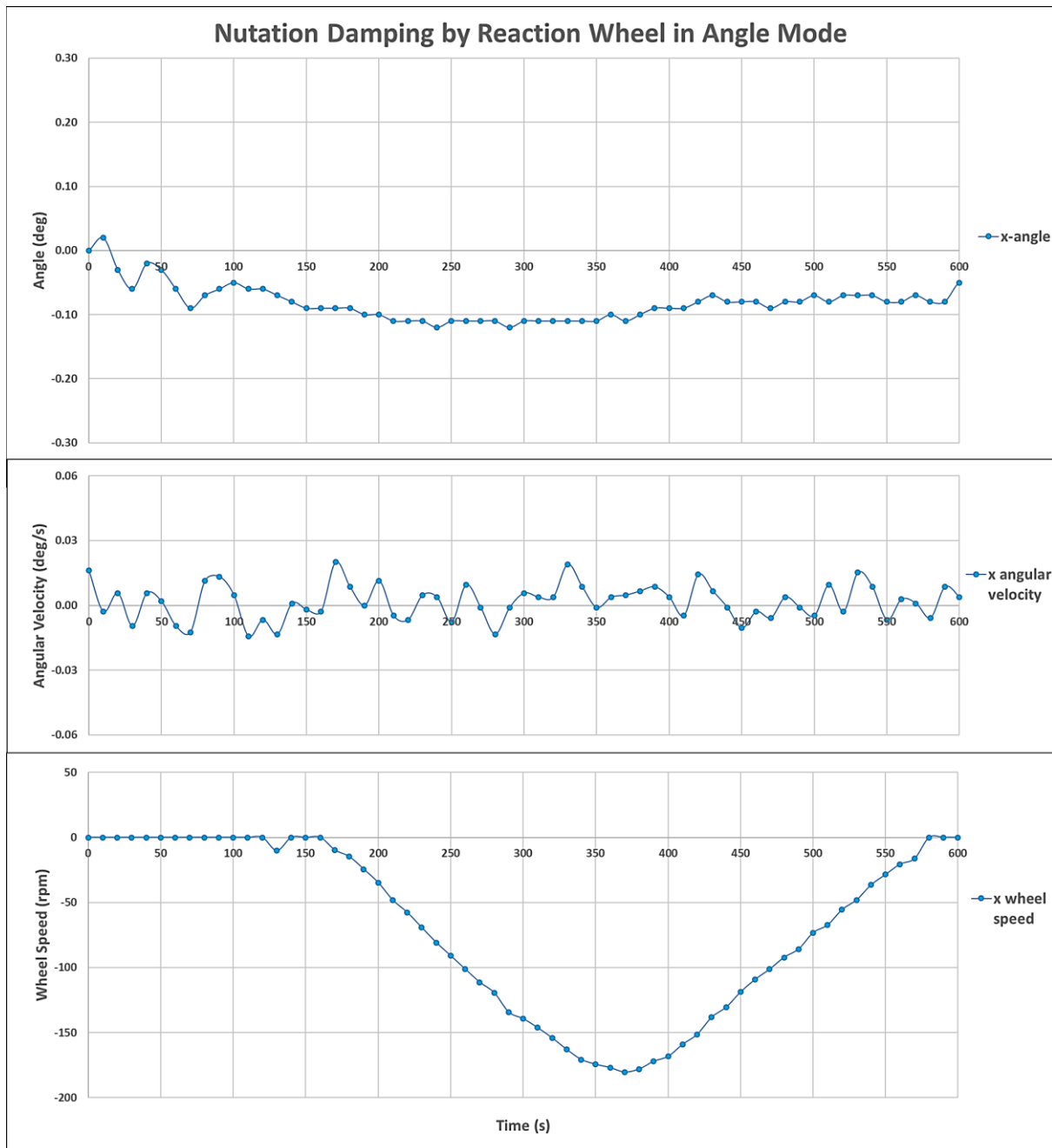


Figure 6.8: Nutation Damping by Reaction Wheel in Angle Mode

Figure 6.8 presents the typical of nutation damping by reaction wheel in angle mode. The control algorithm of angle mode is managed by wheel drive electronic that follow equation (5.8). To damp the nutation, and angle command 0 deg should be sent to the x wheel. In doing so, the reaction of the rotor would depend on actual angular velocity of the spacecraft and the difference between an actual angle and target. Since this algorithm is more responsive against disturbance, the angle mode could achieve high pointing stability of 0.1 deg. However, running the angle mode in the long period would drift the attitude proportional to the systematic error or bias drift of the gyro angle reading.

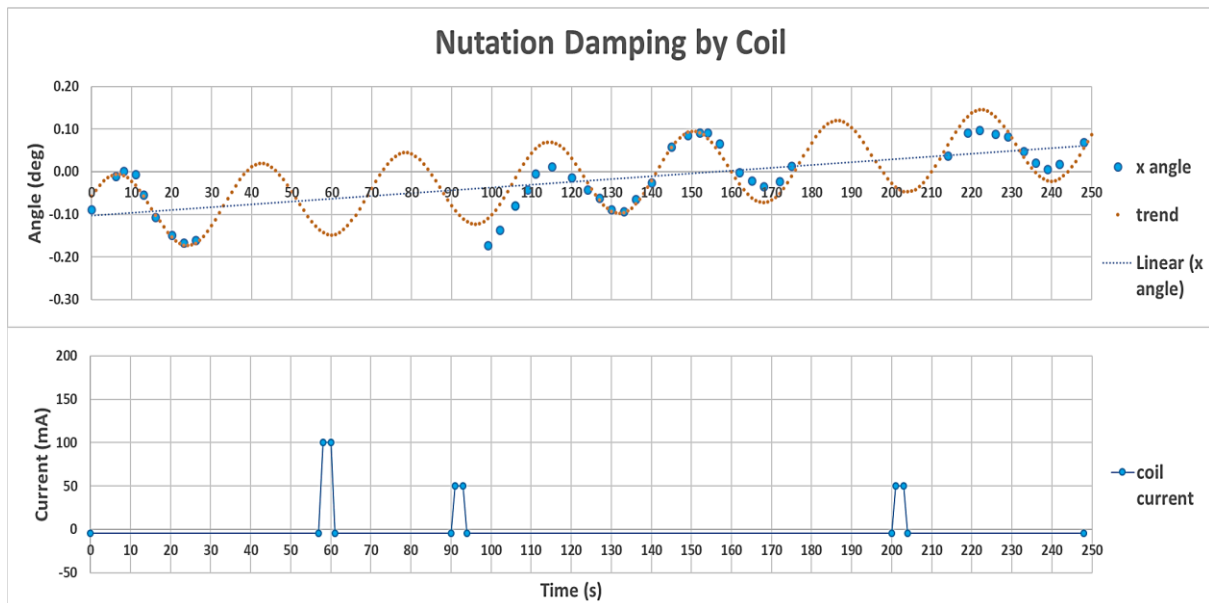


Figure 6.9: Nutation Damping by Magnetic Coil

Procedure of nutation damping using a magnetic coil in the experiment of LAPAN-A satellite series is conducted manually by operator. In a simple oscillatory or harmonic motion, the torque is proportional to the angular displacement. When the displacement is zero the acceleration is also zero, therefore the torque is zero. But when the displacement is maximum, the acceleration becomes maximum, so does the torque. The torque applied in the oscillatory motion is in the opposite direction as the displacement.

To damp the nutation, an external torque produced by magnetic coil can be used to counter the torque applied in the oscillatory motion. Therefore, the torque of magnetic coil should equal to the torque of the oscillatory motion. If the torque of magnetic coil is bigger than needed, it will even induce a bigger nutation. Applying a small torque for a few seconds several times could avoid this mistake in the procedure of nutation damping. Prior to the magnetic coil activation, the spacecraft should deactivate the x wheel which is usually used for nutation damping. It will avoid the conflict between two nutation damping systems. Figure 6.9 shows the typical procedure of nutation damping by a magnetic coil which could achieve 0.1 deg of pointing stability.

Once the nutation angle could be reduced better than 0.1 deg, further procedure conducted on the operation of LAPAN-A satellite series was observing the growth of nutation. Figure 6.10 displays the measurement of nutation growth for almost one day observation. In this observation period, the spacecraft performed a momentum bias attitude control through single pitch wheel operation. This observation result confirms that once the nutation has been damped, the nutation angle will remain low for a long period with the growth around 0.17 deg/day. Thus, the procedure of nutation damping can then be done once per day or another convenient interval.

Even though a nutation damping using an angle mode of reaction wheel or a magnetic coil gives better result, they could not be well applied when the nutation angle is still high. When the spacecraft just wakes up from hibernation or in the post of attitude maneuver, the angular momentum is distributed on all three axes. The effective way to establish momentum bias attitude control is run up the pitch wheel (y wheel) to absorb the most of the momentum and activate the x wheel to damp the nutation in the angular velocity mode by setting a command of 0 deg/s. Generally, this procedure takes 5 to 20 minutes until steady condition has been reached. Once the spacecraft is in a steady condition within a nutation angle lower than 0.5 deg, the operator could switch the nutation damping to the other method to achieve pointing stability better than 0.1 deg. The nutation damping technique using an angle mode of wheel or a magnetic coil normally runs in a short time to get desired pointing stability and can then let the spacecraft to continue the most of its cycle in a single pitch wheel operation.

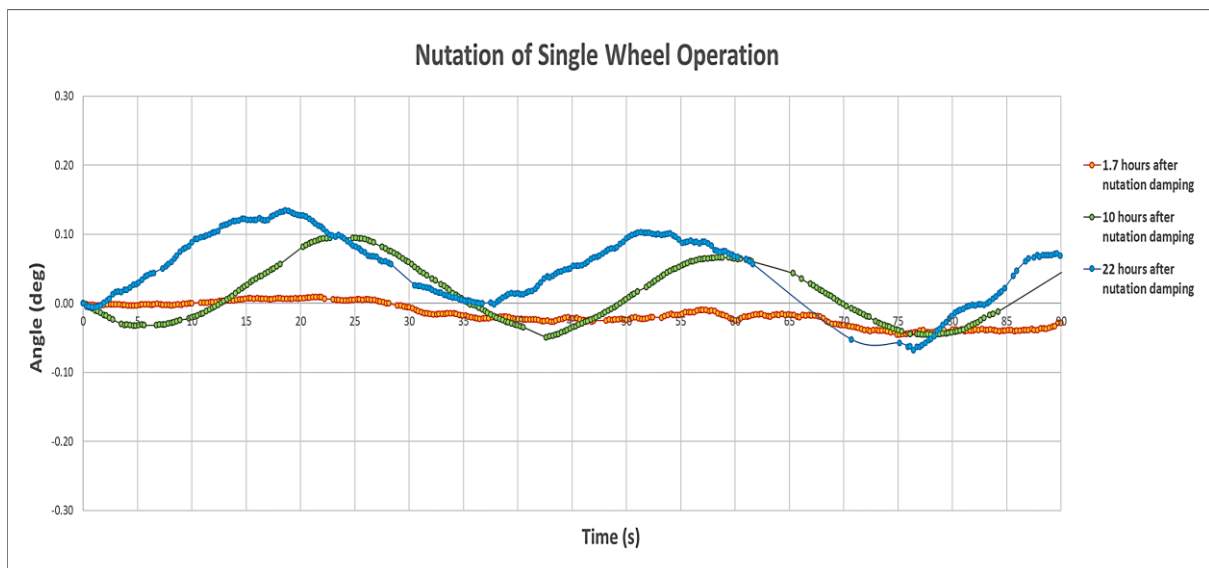


Figure 6.10: Nutation Growth in the Single Wheel Operation Mode

6.1.3 Controlling the Direction of Angular Momentum

The movement of the angular momentum vector will directly influence the satellite attitude and affect the mission payload performance. During the mission operation, two parameters of attitude should be observed, attitude accuracy and attitude stability. While attitude accuracy is defined as how far the attitude different from the target, attitude stability means how fast the attitude change. For imaging mission, attitude accuracy will affect the accuracy of the image, while attitude stability will affect quality of image.

Case 1: Polar Orbiting Satellite

Figure 6.11 displays the typical of attitude motion in an orbital cycle of the momentum bias operation of the polar orbiting satellite, LAPAN-A3, which consists of short period and long period oscillation. While the short period oscillation indicates the nutation, the long period oscillation represents the controlled precession of angular momentum. This controlled precession was performed by compensating the residual dipole of the spacecraft using a magnetic coil and would be described later in this section. Figure 6.11 plots the attitude movement of LAPAN-A3 satellite observed by the star sensor for an orbital period when it was in nadir pointing mode and implemented a nutation damping by setting the angular velocity target of 0 deg/s to x wheel.

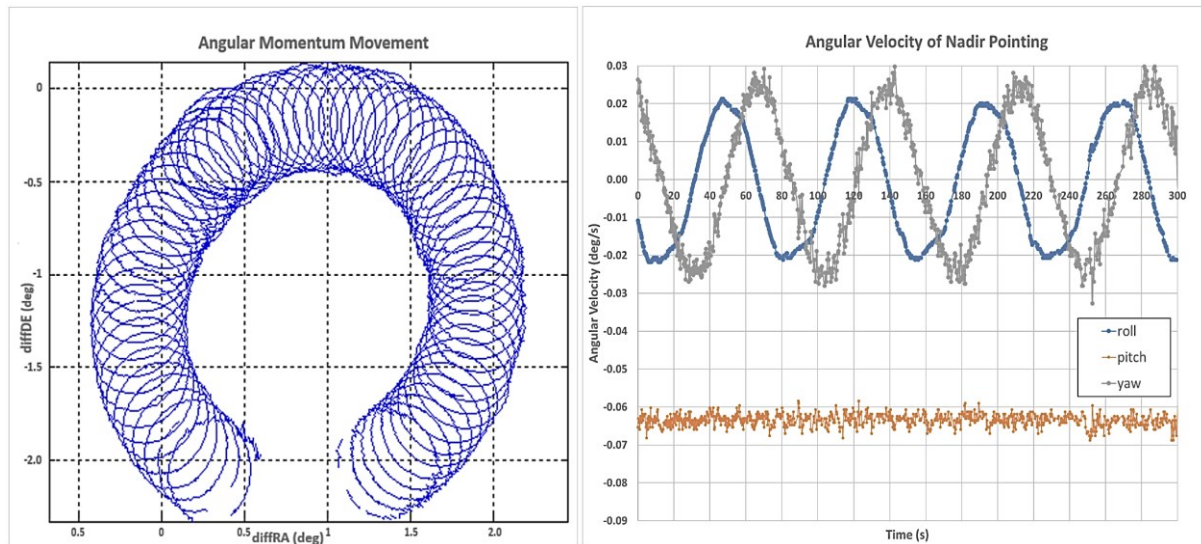


Figure 6.11: Attitude Movement of LAPAN-A3 Satellite Observed by Star Sensor

The measurement of oscillation amplitudes and their periods have been conducted and presented in the Table 6.4 and Table 6.5. These measurement results indicate the average of nutation amplitude around 0.28 deg for 74 second period. Meanwhile, the precession amplitude is 1 deg within 5543 second period. This nutation and precession lead to 2.6 deg of *peak to peak* attitude accuracy, so that the target would still in imager's FOV within a maximum deviation of 11.53 km from its center (10% of swath width).

Table 6.4: Amplitude and Period of Nutation Measured by Star Sensor [61]

| Time | RA | | DE | | Angular Momentum |
|---|-----------------|------------|-----------------|------------|------------------|
| | Amplitude (deg) | Period (s) | Amplitude (deg) | Period (s) | Nms (rpm) |
| 2017/10/31 03:21:38 - 2017/10/31 04:58:45 | 0.2807 | 74.33 | 0.2642 | 67.20 | 0.523 (5474) |
| 2017/11/01 03:04:52 - 2017/11/01 04:41:57 | 0.2812 | 75.20 | 0.2762 | 76.20 | 0.526 (5508) |
| 2017/11/05 05:33:10 - 2017/11/05 07:10:18 | 0.2781 | 72.07 | 0.2725 | 73.40 | 0.533 (5577) |
| 2017/11/06 03:46:11 - 2017/11/06 05:23:18 | 0.2767 | 74.45 | 0.2715 | 75.07 | 0.534 (5591) |
| 2017/11/11 03:51:26 - 2017/11/11 05:28:50 | 0.2749 | 74.33 | 0.2740 | 73.73 | 0.534 (5586) |
| 2017/11/12 03:33:43 - 2017/11/12 05:10:53 | 0.2785 | 75.87 | 0.2700 | 75.40 | 0.533 (5575) |
| Mean | 0.2783 | 74.38 | 0.2714 | 73.50 | |

Table 6.5: Amplitude and Period of Precession Measured by Star Sensor [61]

| Time | RA | | DE | | Center | Angular Momentum |
|---|-----------------|------------|-----------------|------------|----------------|------------------|
| | Amplitude (deg) | Period (s) | Amplitude (deg) | Period (s) | RA, DE (deg) | Nms (rpm) |
| 2017/10/31 03:21:38 - 2017/10/31 04:58:45 | 1.0776 | 6395.00 | 0.9964 | 6390.60 | (0.29, 0.44) | 0.523 (5474) |
| 2017/11/01 03:04:52 - 2017/11/01 04:41:57 | 1.0297 | 6177.80 | 0.9856 | 4840.00 | (-0.53, -1.02) | 0.526 (5508) |
| 2017/11/05 05:33:10 - 2017/11/05 07:10:18 | 1.0106 | 5409.40 | 0.9720 | 6132.40 | (1.12, -0.85) | 0.533 (5577) |
| 2017/11/06 03:46:11 - 2017/11/06 05:23:18 | 1.0251 | 5083.60 | 0.9351 | 6534.20 | (0.88, -1.07) | 0.534 (5591) |
| 2017/11/11 03:51:26 - 2017/11/11 05:28:50 | 1.0046 | 5254.80 | 1.0185 | 6562.20 | (2.59, 0.27) | 0.534 (5586) |
| 2017/11/12 03:33:43 - 2017/11/12 05:10:53 | 0.9848 | 4936.60 | 1.0106 | 6400.00 | (1.66, 1.12) | 0.533 (5575) |
| Mean | 1.0221 | 5542.87 | 0.9864 | 6143.23 | | |

When the star sensor information (RA , DE , AZ) was transformed into flight direction axis in the nadir pointing mode, the movement in the roll (x axis), pitch (y axis), and yaw (z axis) could be well determined. In imaging mission of LAPAN-A3 satellite, the yaw movement is not critical, whereas the angular velocity in roll and pitch are very influential on the performance of the imager. These movement should comply with the pushbroom imager requirements shown in the Table 6.6, which takes 5% image overlap per pixel.

Table 6.6: Imaging Requirements of LAPAN-A3's Multispectral Pushbroom Imager for 5% Overlap

| Orbit Altitude | GSD | Repetition Time | Maximum Movement |
|----------------|-----|-----------------|------------------|
| (km) | (m) | (ms) | (km/s) |
| 600 | 18 | 1.90 | 9.0 |
| 508 | 15 | 1.90 | 7.5 |

Due to oscillatory motion, the angular velocity in roll has an amplitude of 0.02 deg/s. Meanwhile, due to control accuracy of the wheel, the angular velocity in pitch fluctuated from -0.070 deg/s to -0.058 deg/s when it was set to be nadir by -0.063 deg/s. While the ground speed from 508 km altitude of LAPAN-A3 satellite is 7.05 km/s, the fluctuation on the pitch axis ranged from 6.99 km/s to 7.09 km/s. According to the requirement on the Table 6.6, this oscillatory motion can still be tolerated by the multispectral pushbroom imager. However, the angular velocity of the pitch axis can be set higher than the nadir rate to compensate the orbital speed to get a better image in less blur.

Later, when the nutation damping technique has been improved using angle mode of the wheel, and the spacecraft was operated in the single pitch wheel, the attitude accuracy and the attitude stability have also been improved as shown by Figure 6.12. The nutation and precession lead to 1.7 deg of *peak to peak* attitude accuracy.

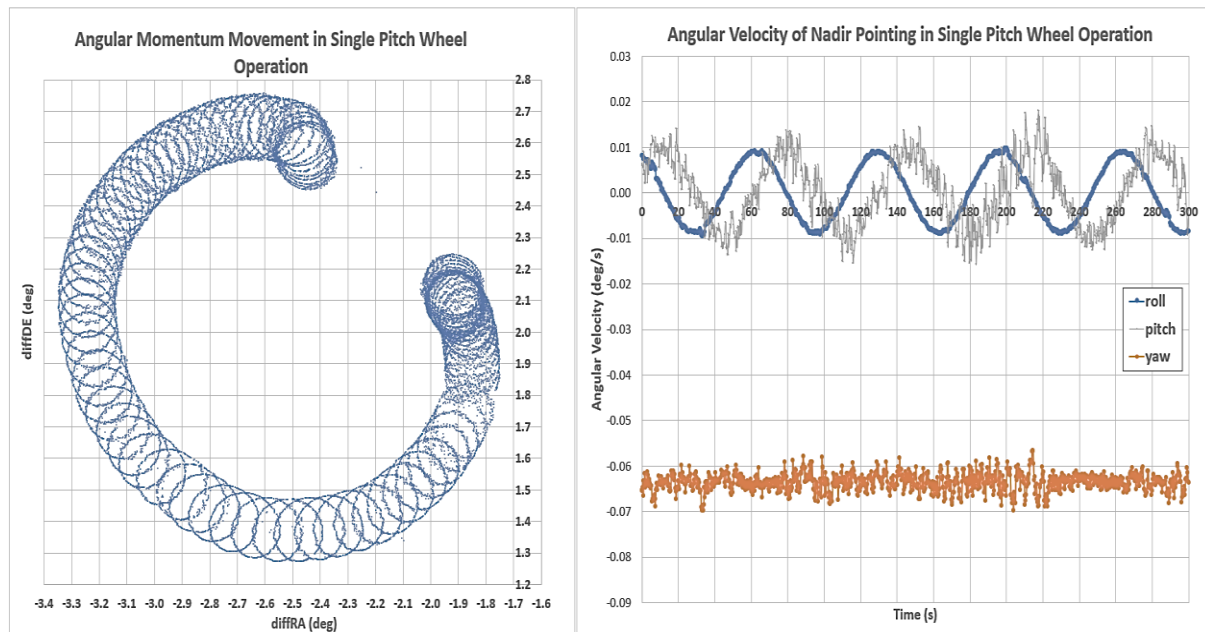


Figure 6.12: Attitude Movement in the Single Pitch Wheel Operation

To keep the spacecraft nadir pointing all the time, the precession of angular momentum has to be controlled following the precession of sun synchronous orbit as described in the section 5.1.1. Since the dominant disturbance torque is caused by a magnetic field, a perfect compensation on the residual magnetic dipole of the spacecraft would keep the angular momentum fixed in the inertial frame. Controlled precession can then be performed by overcompensate or undercompensate the residual dipole of the spacecraft by magnetic coil. In the case of polar orbiting satellite, the y coil is responsible to control the precession of angular momentum. Table 6.7 and Figure 6.13 presents the controlling angular momentum precession in the right ascension element, where ΔRA shows the deviation of the right ascension from its target.

Table 6.7: Controlling Right Ascension of Angular Momentum

| Start | ΔRA (deg) | Stop | ΔRA (deg) | Y-Coil Current (mA) | ΔRA /Orbit (deg) |
|---------------------|----------------------|---------------------|----------------------|---------------------------|-----------------------------|
| 2019/09/01 01:34:40 | -2.27 | 2019/09/01 03:07:22 | -0.33 | -25 | 2.04 |
| 2019/09/01 03:07:22 | -0.33 | 2019/09/01 14:57:58 | -1.24 | -21 | -0.12 |
| 2019/09/02 08:47:44 | -3.04 | 2019/09/02 10:20:50 | -1.33 | -27 | 1.79 |
| 2019/09/02 13:33:13 | -2.55 | 2019/09/02 15:04:58 | -0.44 | -27 | 2.24 |
| 2019/09/03 05:21:36 | -0.35 | 2019/09/03 14:45:52 | -3.1 | -21 | -0.48 |
| 2019/09/04 06:36:12 | -0.67 | 2019/09/04 14:28:21 | -2.3 | -21 | -0.34 |
| 2019/09/05 02:00:53 | -3.11 | 2019/09/05 03:29:09 | -0.01 | -27 | 3.43 |
| 2019/09/05 06:18:42 | -0.33 | 2019/09/05 14:09:49 | -1.15 | -21 | -0.17 |
| 2019/09/06 06:01:08 | 0.48 | 2019/09/06 13:54:40 | -1.98 | -21 | -0.51 |
| 2019/09/06 15:05:00 | 0.85 | 2019/09/07 01:20:32 | -2.33 | -21 | -0.50 |
| 2019/09/07 01:25:04 | -1.97 | 2019/09/07 02:53:16 | 0.28 | -27 | 2.49 |
| 2019/09/07 03:00:29 | 1.01 | 2019/09/08 01:01:19 | -1.3 | -21 | -0.17 |
| 2019/09/08 01:01:58 | -1.55 | 2019/09/08 02:35:06 | -0.1 | -25 | 1.52 |
| 2019/09/08 13:20:48 | -2.07 | 2019/09/08 14:51:28 | -1.25 | -24 | 0.88 |
| 2019/09/08 14:57:06 | -1.21 | 2019/09/09 01:54:49 | -3.82 | -21 | -0.39 |
| 2019/09/09 06:42:16 | -0.97 | 2019/09/09 12:39:50 | -0.18 | -21 | 0.22 |
| 2019/09/09 14:40:09 | -0.13 | 2019/09/10 03:13:12 | -3.12 | -21 | -0.39 |
| 2019/09/10 13:49:42 | 0.22 | 2019/09/11 01:48:47 | -2.71 | -21 | -0.40 |

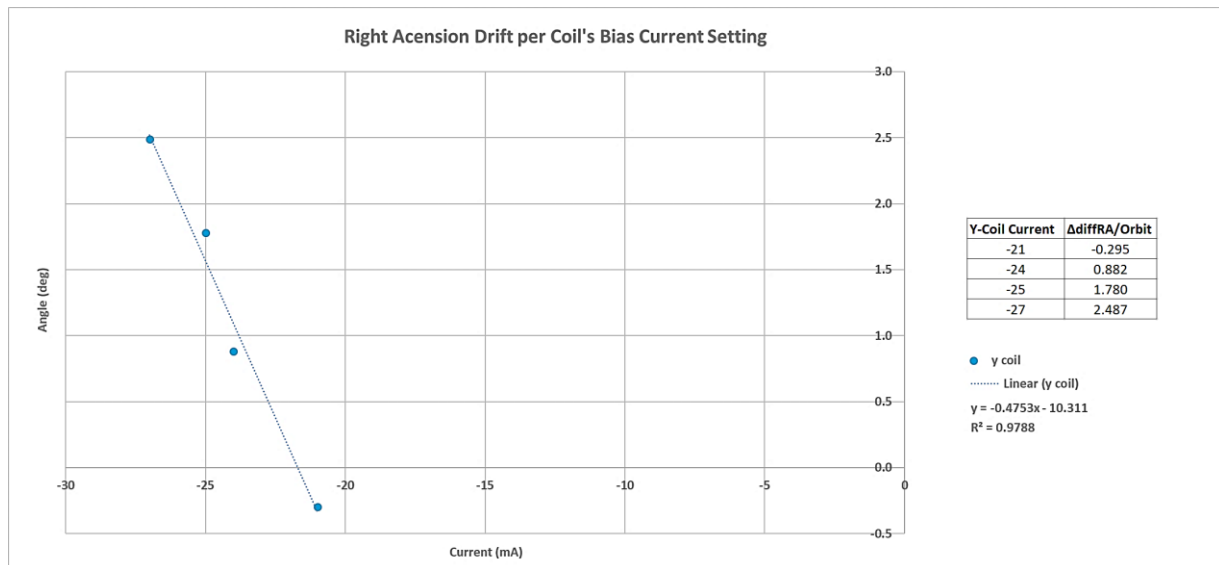
**Figure 6.13: Right Ascension Drift of Angular Momentum due to Bias Current on Y-Coil**

Figure 6.13 gives a trend of average precession of the angular momentum in right ascension element per orbital cycle. According to these table and figure, the angle of precession per orbit could be estimated by the following formula.

$$\Delta RA = -0.4753i_y - 10.311 \quad (6.2)$$

where ΔRA is the precession of right ascension expressed in degree and i_y is bias current setting of y coil in mA. This formula also found that by setting a bias current around 21.69 mA, ΔRA equals zero, so the angular momentum would follow the precession of Sun synchronous orbit.

While controlling right ascension is performed by setting a bias current to the y coil, controlled declination precession could only be performed by y coil when the local Earth's magnetic has east-west vector. This condition is possible where the spacecraft is between equator and pole, so that procedure of controlling the declination could be performed in a quarter orbit maneuver. Figure 6.14 illustrates the Earth's magnetic field dipole model and quarter orbit region definition, which denotes north-south and east-west vector of magnetic field as B_z and B_r respectively.

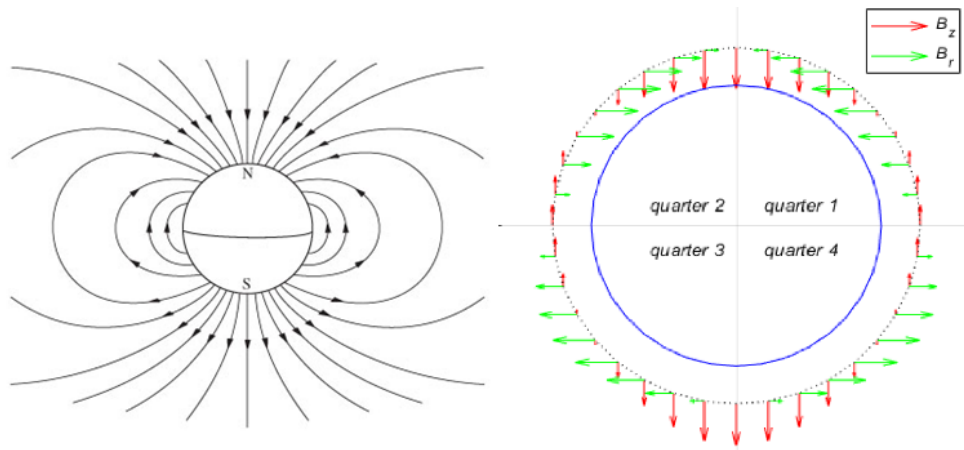


Figure 6.14: Earth's Magnetic Field Dipole Model and Quarter Orbit Region Definition [62]

The Earth's magnetic vector in east-west element, B_r , will be zero above the equator or pole and its direction becomes opposite when crossing them. If y coil interacts with B_r , then it would create a torque in north-south direction which drifts the declination. To generate the torque, the current of y coil should have a certain amount of current, Δi_y , from its bias setting 21.69 mA. Figure 6.15 shows the effect of angular momentum vector declination by applying Δi_y -29 mA and 31 mA. For both current settings, the effect to angular momentum vector declination reverse in 0 deg latitude.

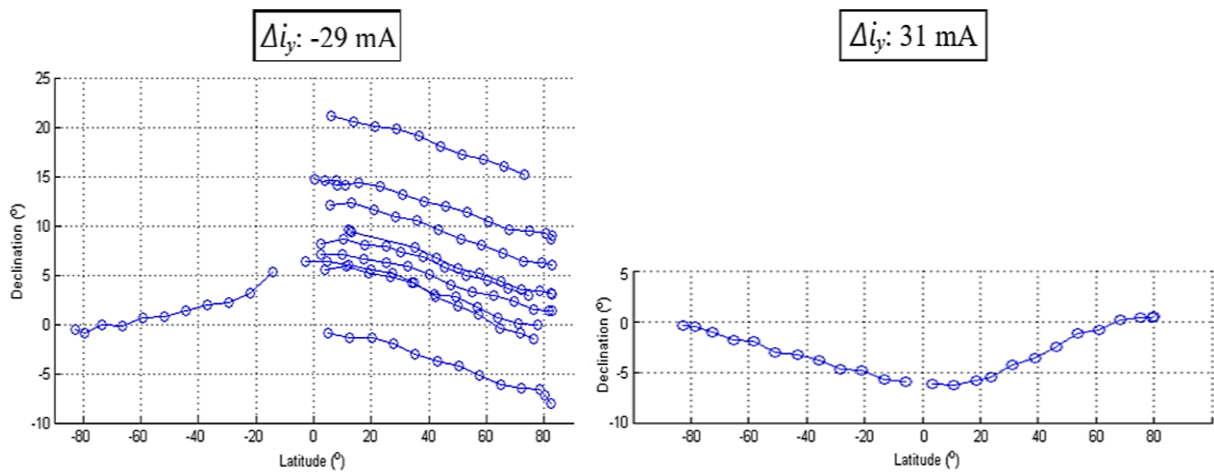


Figure 6.15: Declination Precession in A Quarter Orbit due to Deviation of Y-Coil Bias Current [62]

Figure 6.16 shows more variation of applying Δi_y in all four of quarter orbit and the declination precession resulted in a quarter orbit period (23.5 minutes). This figure shows that pairs of quarter 1 and quarter 3 have a similarity, whereas quarter 2 is similar to quarter 4. To find a relation between Δi_y and the precession of declination for a quarter orbit, the linear regressions were used. The first linear regression is for quarter 1 and quarter 2, whereas the second one is for quarter 3 and quarter 4.

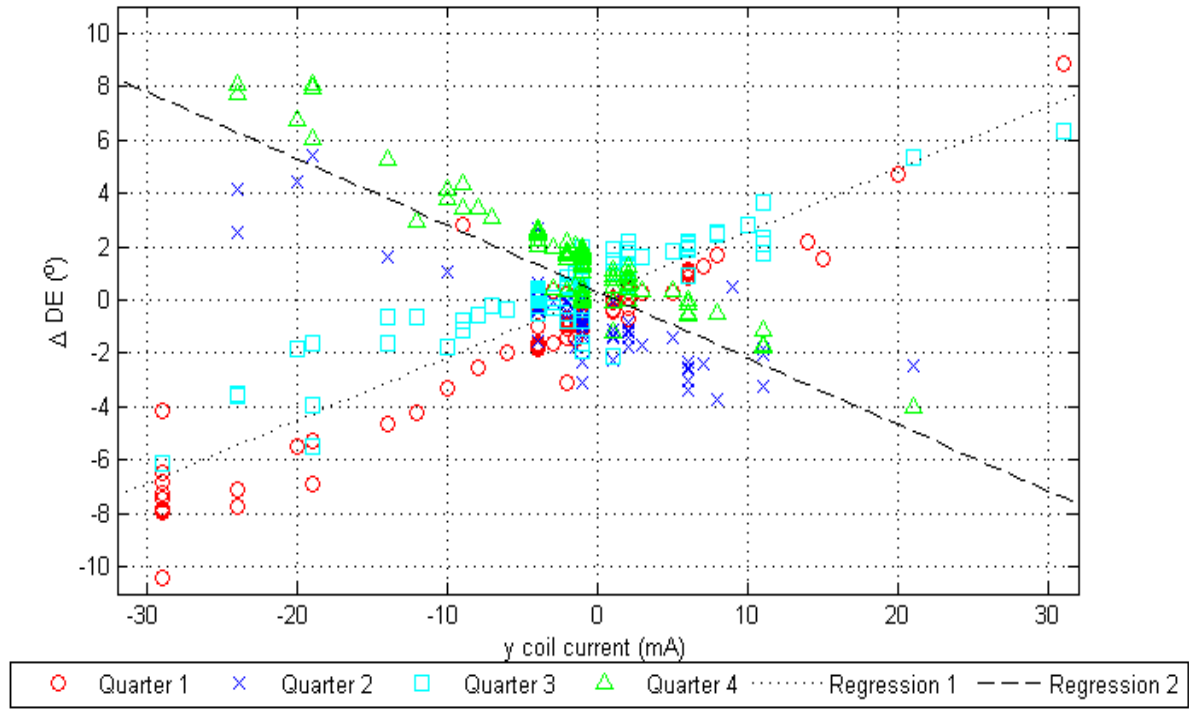


Figure 6.16: Declination Precession due to Deviation of Y-Coil Bias Current [62]

For quarter 1 and quarter 3, the declination precession will follow

$$\Delta DE = 0.2355\Delta i_y + 0.2038 \quad (6.3)$$

whereas quarter 2 and 4 give relation

$$\Delta DE = -0.2490\Delta i_y + 0.3133 \quad (6.4)$$

where ΔDE is precession of declination expressed in degree and Δi_y is the deviation of y coil current from its bias setting expressed in mA.

The formula that relates between angular momentum precession and the bias current setting of y coil as well as short maneuver have made the controlling of angular momentum direction easier for the operator. Figure 6.17 shows the achievement of pushbroom imaging mission on LAPAN-A3 satellite to cover Indonesian territory which has swath more than 5000 km using momentum bias attitude control.

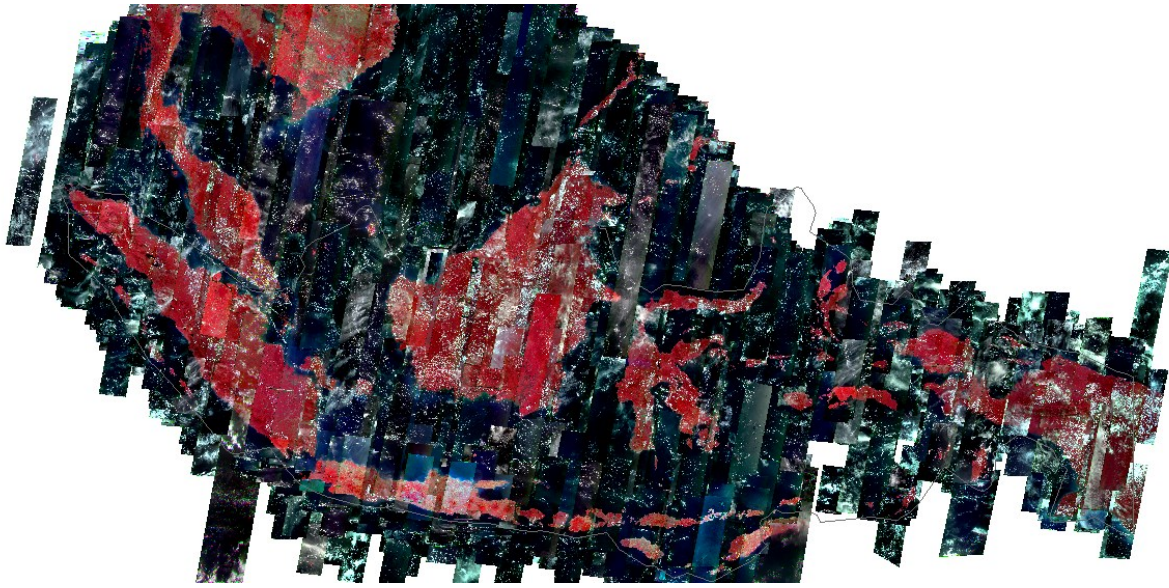


Figure 6.17: Imaging Mission over Indonesian Territory Using Momentum Bias Attitude Control

Case 2: Equatorial Orbiting Satellite

Earth's local magnetic field at the equator is only half of the polar region, meaning the disturbance torque of equatorial orbiting satellite is smaller than polar orbiting satellite. Therefore, the angular momentum precession of the equatorial satellite is lower than the polar ones as shown in the Figure 6.18.

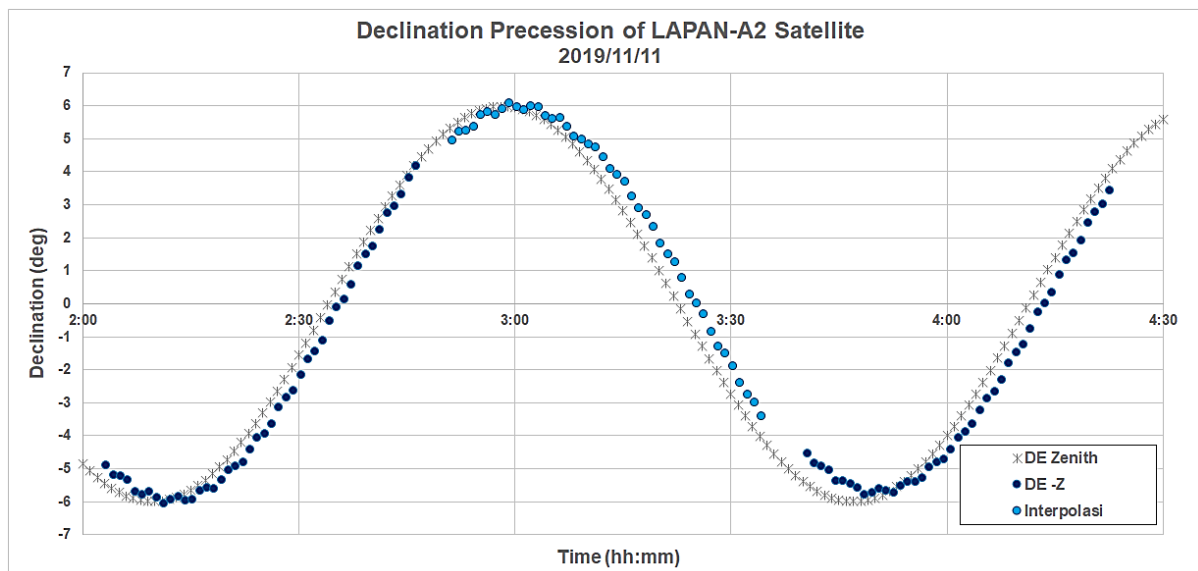


Figure 6.18: Attitude Movement of Nadir Pointing Satellite in the Equatorial Orbit

Table 6.8 shows activities to control the direction of angular momentum of the equatorial orbiting satellite, LAPAN-A2. According to the table, ΔRA , ΔDE , and ΔAZ represent the deviation of the angular momentum from the target coordinates of right ascension, declination,

and azimuth respectively. The attitude correction is needed to bring the angular momentum direction closer to the target, so that ΔRA , ΔDE , and ΔAZ are as close as possible to zero. In doing so, the pitch wheel is responsible to direct the right ascension element, x coil is controlling the declination, and z coil has to maintain the azimuth direction. However, since the Earth's magnetic field in orbit is not perfectly pointing to the north-south direction, actuating one of magnetic coil could affect in two axes. To keep the deviation below 1 deg, the attitude correction generally be conducted twice per day.

Table 6.8: Attitude Correction on LAPAN-A2 Satellite

| Initial Attitude | | | | Pitch Correction | X-Coil | | Z -Coil | | Corrected Attitude | | | |
|------------------------|----------------------|----------------------|----------------------|------------------|-----------------|-----------------|-----------------|-----------------|------------------------|----------------------|----------------------|----------------------|
| Time | ΔRA (deg) | ΔDE (deg) | ΔAZ (deg) | | Current (mA) | Duration (s) | Current (mA) | Duration (s) | Time | ΔRA (deg) | ΔDE (deg) | ΔAZ (deg) |
| 2019/11/01 14:55:05 | -0.115 | 0.055 | 0.508 | - | - | - | 50 | 48 | 2019/11/01 14:56:54 | -0.128 | 0.049 | -0.118 |
| 2019/11/02 01:19:23 | -2.176 | -1.258 | 0.170 | ✓ | -50 | 179 | 50 | 61 | 2019/11/02 01:28:46 | 0.189 | 0.111 | 0.125 |
| 2019/11/02 15:18:26 | 0.310 | -1.934 | 1.831 | - | -50 | 181 | 50 | 338 | 2019/11/02 15:27:49 | 0.365 | -0.730 | 0.247 |
| 2019/11/03 01:42:05 | 0.404 | -0.607 | 0.547 | - | -100 | 43 | 100 | 24 | 2019/11/03 01:44:12 | -0.069 | -0.797 | 0.372 |
| 2019/11/03 13:51:13 | -0.718 | -1.696 | 1.803 | ✓ | -100 | 107 | 100 | 159 | 2019/11/03 13:59:10 | 0.179 | -0.280 | 0.351 |
| 2019/11/04 14:18:58 | -0.499 | -0.982 | 0.172 | ✓ | -50 | 111 | - | - | 2019/11/04 14:23:42 | -0.103 | -0.193 | 0.224 |
| 2019/11/05 00:42:29 | -0.048 | -0.647 | 1.344 | - | -50 | 106 | 50 | 228 | 2019/11/05 00:48:49 | -0.133 | 0.002 | 0.026 |
| 2019/11/05 14:41:02 | -4.217 | -0.986 | 0.834 | ✓ | -50 | 180 | 50 | 22 | 2019/11/05 14:47:55 | 0.068 | -0.189 | 0.083 |
| 2019/11/06 01:05:21 | -1.060 | 0.332 | -0.223 | ✓ | 30 | 37 | -50 | 62 | 2019/11/06 01:10:19 | 0.098 | -0.012 | 0.052 |
| 2019/11/06 13:16:26 | -3.280 | -1.360 | 0.904 | ✓ | -30 | 456 | 30 | 381 | 2019/11/06 13:25:33 | 0.181 | -0.144 | 0.134 |
| 2019/11/07 01:29:08 | -2.077 | 0.108 | -0.283 | ✓ | - | - | -50 | 137 | 2019/11/07 01:35:58 | -0.144 | -0.063 | 0.259 |
| 2019/11/07 15:25:55 | -0.703 | -1.184 | 1.201 | - | -50 | 156 | 50 | 209 | 2019/11/07 15:33:01 | -0.721 | -0.192 | 0.331 |

6.2 Slew Mode

The slew maneuver is performed through three pairs wheel-gyro operation, so it could be any modes that operate three wheels-gyros simultaneously for Earth or inertial pointing. This mode is often referred to as off-nadir pointing mode while scanning the Earth's surface with a certain offset angle from the spacecraft ground track. To make sure the accuracy of imaging using high-resolution or narrow angle coverage payload, it is necessary to do a pointing calibration by measure the alignment between attitude sensor, spacecraft axis and payload. In particular, for off-nadir pointing mission, a misalignment between payload and spacecraft axis would multiply the pointing error from target.

6.2.1 Pointing Calibration

The pointing calibration in slew mode could be conducted by exposing satellite's camera towards celestial objects using inertial pointing. One of the interesting targets of celestial objects is the Moon. In addition of giving an absolute accuracy of pointing calibration, Moon also a good target for focusing calibration of the camera optical system. This kind of pointing calibration has been performed in LAPAN-A1 satellite which carried both of wide angle and high-resolution cameras as shown in Figure 6.19.

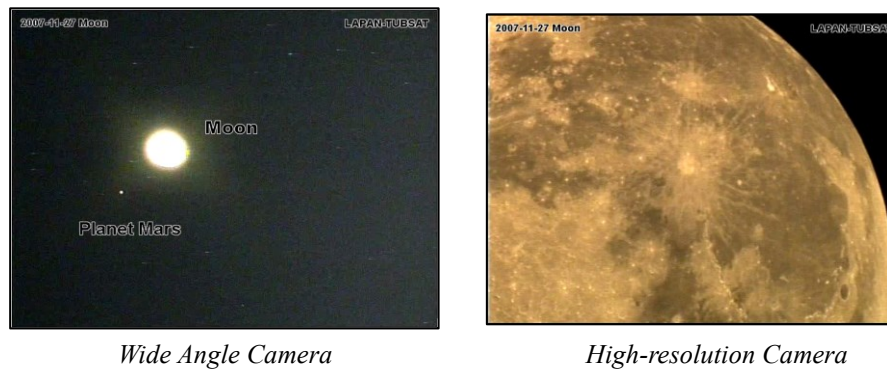


Figure 6.19: The Moon and Mars Imaging by LAPAN-A1 Satellite

In the equatorial orbiting satellite, LAPAN-A2, the acquisition of Moon image could be performed only at certain periods to enable the star sensor to find out the satellite attitude information or star reference, otherwise the star sensor would be blocked by the Earth or blinded by the Sun. The geometry of Moon imaging related to the FOV of the camera and star sensor is illustrated by Figure 6.20. The accuracy of satellite pointing should meet ≤ 0.1 deg to get the perfect full Moon imaging by its 0.7 deg FOV of high-resolution camera.

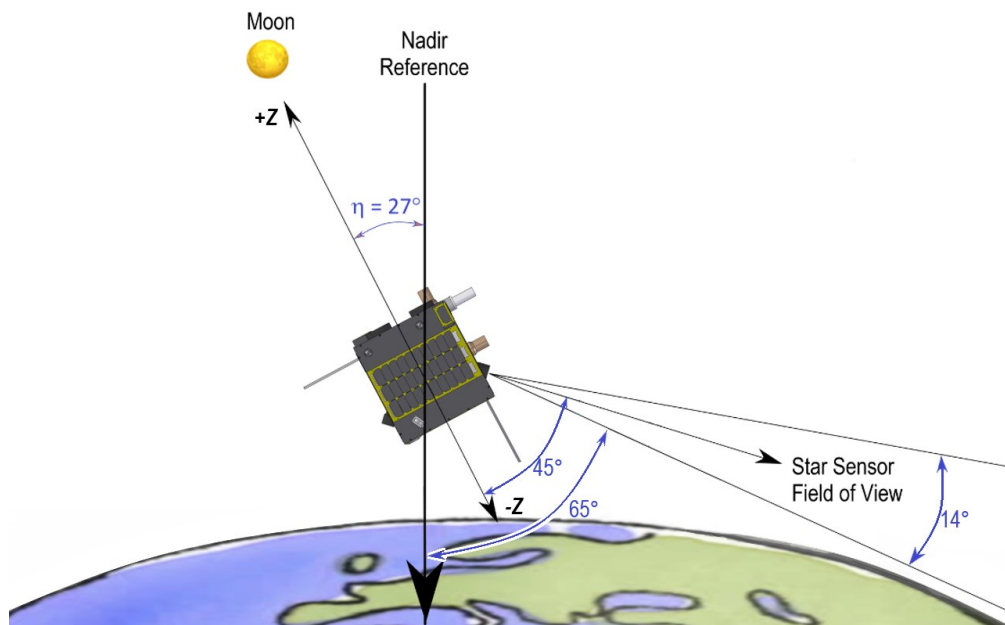


Figure 6.20: Angular Relationship between Star Sensor, Spacecraft, and Moon [50]

The Moon pointing calibration has been executed by LAPAN-A2 satellite twice. The first Moon image acquisition is used for initial measurement of the misalignment between star sensor, spacecraft axis and camera, while the second one is used to improve the accuracy of measurement. The first Moon image acquisition setup and lunar ephemeris are listed in the Table 6.9 with the results are shown in Figure 6.21.

Table 6.9: Lunar Ephemeris and the 1st Acquisition Setup [50]

| | |
|--|------------------------------------|
| Time | 2018/07/23 19:41:00 UTC |
| Spacecraft Position (Lat.; Lon.; Alt.) | 5.989868°; 105.542550°; 651.073 km |
| Spacecraft Zenith (RA; DE; AZ) | -17.7134°; 5.9899°; 89.6263° |
| Topocentric Lunar Coordinate (RA; DE) | 255.2035920°; - 18.936703° |
| Target of -z of Spacecraft (RA; DE; AZ) | 75.2036°; 18.9367°; 180° |
| Actual of -z of Spacecraft Provided by STS (RA; DE; AZ) | 74.1362°; 18.9104°; 180.198° |
| Difference between Target and Actual of -Z Side (Δ RA; Δ DE; Δ AZ) | 1.0674°; 0.0263°; -0.198° |

As shown in Figure 6.21, the Moon image in horizontal axis is located at pixel 413 to 1968 in the camera frame, so the Moon diameter consists of 1555 pixels. Since the total pixels of the image are 2048, the dark sky pixels that are not occupied by the Moon image equivalent to 493 pixels. On the vertical axis, the top pixel of the Moon is located at pixel 672. The camera placement in the spacecraft is fixed so the horizontal axis is aligned with x axis and the vertical axis is aligned to y axis of the spacecraft. Since then, the image offset at x axis and y axis can be defined by following equations.

$$x_{IO} = -\varnothing_M \times \left(\frac{1^{st} \text{ moon pixel in } x - \left(\frac{\text{dark sky pixel}}{2} \right)}{\text{total moon pixel}} \right) \quad (6.5)$$

$$y_{IO} = -\varnothing_M \times \left(\frac{1^{st} \text{ moon pixel in } y - \left(\frac{\text{dark sky pixel}}{2} \right)}{\text{total moon pixel}} \right) \quad (6.6)$$

where:

\varnothing_M = Moon's angular diameter = 0.49°

x_{IO} = image offset in x axis

y_{IO} = image offset in y axis

By applying (6.5) and (6.6) to the Moon image of Figure 6.21, the image offsets are found to be -0.052 deg on the x axis direction and -0.134 deg on the y axis direction.



Figure 6.21: 1st Acquisition Result of Moon Image [50]

Since the actual attitude in the Moon acquisition was not perfectly same as the target, then the calculation of the camera offset should accommodate the difference between actual and target of the spacecraft attitude. In the Moon imaging setup, the azimuth was arranged so rotation about x axis will change DE , and y rotation will change RA . Therefore, the camera offset on the x and y axis can be established by using equations below.

$$x_{co} = -x_{Io} - \Delta DE \quad (6.7)$$

$$\text{which } \Delta DE = DE_{target} - DE_{actual} \quad (6.8)$$

$$y_{co} = -y_{Io} - \Delta RA \quad (6.9)$$

$$\text{which } \Delta RA = RA_{target} - RA_{actual} \quad (6.10)$$

where:

x_{co} = camera offset in x axis

y_{co} = camera offset in y axis

Those equations led the first Moon imaging to find the camera offsets 0.03 deg on the x axis and -0.93 deg on the y axis. Then these values have been implemented for second Moon imaging, which has ephemeris as listed in the Table 6.10.

Table 6.10: Lunar Ephemeris and the 2nd Acquisition Setup [50]

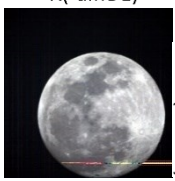
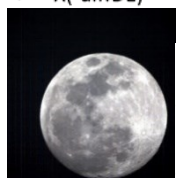
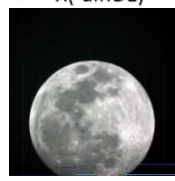
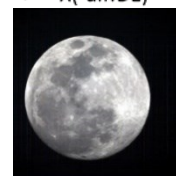
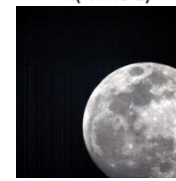
| | |
|---|------------------------------------|
| Time | 2018/07/26 22:36:00 UTC |
| Spacecraft Position (Lat.; Lon.; Alt.) | 1.013118°; 113.545953°; 646.453 km |
| Spacecraft Zenith (RA; DE; AZ) | 37.1167°; 1.0131°; 84.0840° |
| Topocentric Lunar Coordinate (RA; DE) | 294.7202970°; -20.166477° |
| Target of -z of Spacecraft (RA; DE; AZ) | 113.7803°; 20.1965°; 180.0000° |

The results of the second Moon image acquisition are displayed in the Table 6.11. According to this table, it appears that the Moon is fully captured at picture index 4. In that picture, ΔRA gives reasonable values of 0.0644 deg that is close to zero, so y_{CO} is perfectly matched. However, ΔDE in the picture 4 is still not matched so x_{CO} has to be updated. Meanwhile, in the x direction, the picture index 3 looks better since the Moon position is exactly in the center of x . Looking back at the first image obtained of the Moon (Figure 6.21), a mismatch might occur because the Moon phase in the first acquisition is not a full Moon, so the pixel measurement might not so accurately. Thus, the image offset of picture 3 should be 0 deg, and then the equation (6.5) is used with the corrected value of x_{CO} as follows.

$$\begin{aligned} \text{New } x_{CO} &= -\Delta DE_{\text{picture}_3} \\ &= 0.1232^\circ \end{aligned} \quad (6.11)$$

The updated value of the camera offset 0.1232 deg can then be verified by comparing the Moon picture in the table with the image offset on the x axis (x_{IO}) that recalculated from the equation (6.5) using the new x_{CO} .

Table 6.11: Result of the 2nd Acquisition of Moon Image [50]

| | | | | |
|---|---|---|--|---|
|  |  |  |  |  |
| picture index: 1 | picture index: 2 | picture index: 3 | picture index: 4 | picture index: 5 |
| $\Delta RA: 0.1420^\circ$ | $\Delta RA: 0.1420^\circ$ | $\Delta RA: 0.1469^\circ$ | $\Delta RA: 0.0644^\circ$ | $\Delta RA: 0.1047^\circ$ |
| $\Delta DE: -0.1025^\circ$ | $\Delta DE: -0.1025^\circ$ | $\Delta DE: -0.1232^\circ$ | $\Delta DE: -0.1442^\circ$ | $\Delta DE: 0.1456^\circ$ |
| $\Delta AZ: 1.3768^\circ$ | $\Delta AZ: 1.3768^\circ$ | $\Delta AZ: 1.3923^\circ$ | $\Delta AZ: 1.4098^\circ$ | $\Delta AZ: 1.2278^\circ$ |
| $x_{IO}: -0.0207^\circ$ | $x_{IO}: -0.0207^\circ$ | $x_{IO}: 0^\circ$ | $x_{IO}: 0.021^\circ$ | $x_{IO}: -0.2688^\circ$ |

Since the ΔDE of picture index 3 is used as reference for updating the offset on the x axis, the offset of this image should be 0 deg. The smaller image offset means the closer Moon image from the center of axis, and it has been confirmed by the Table 6.11. By these lunar pointing calibrations, the final result of the camera offsets was set up to 0.1232 deg on the x axis and -0.93 deg on the y axis that would be used for further imaging mission of LAPAN-A2 satellite

6.2.2 Off-Nadir Pointing

In the Earth imaging mission, a slew mode is usually needed for taking the images which require a crossing maneuver about the ground track. This mode also useful for testing the communication link in related to the attitude pointing [63]. The procedure for off-nadir pointing maneuver normally takes less than a minute duration. For an angle less than 10 deg, the maneuver is even shorter than 30 second.

One example of imaging mission in off nadir off-nadir pointing was capturing Mombasa Port, Kenya. This mission was conducted for research activities related to the maritime surveillance, especially comparing the images with the received ships signal by satellite *Automatic Identification System* (AIS) receiver. It has been done by LAPAN-A2 satellite when passed over Kenya, Africa, on July 17th and 18th 2018. Figure 6.22 shows the ground track when the Mombasa Port imaging mission was executed. The first ground track was 32 km north of the target, while the second ground track was 79 km south of the target.

To perform imaging over Mombasa Port, the spacecraft orientation should be rotated on roll axis about -2.7 deg and 7.1 deg for first and second imaging respectively. Figure 6.22 illustrates the distribution of angular momentum in the spacecraft axis to do roll maneuver, hence the wheel speed in the y and z axis should be set in the corresponding value. Since the target location was not in the ground station coverage, all of the procedures were uploaded on the scheduled command. However, this Mombasa imaging faces challenges in the absence of attitude information due to Sun blinding on the star sensor. This happens because the image acquisition process was carried out in the afternoon when the Sun position have already obstructed the star sensor's field of view. Here the momentum bias method shows its superiority which could not be achieved through other strategies. The attitude stability resulted by high angular momentum gives possibility to predict spacecraft orientation from a series of previous attitude information by interpolation.

For better prediction accuracy, two passes would be used to collect the attitude information, including the precession of angular momentum. For equatorial orbiting satellite, the rotation on the roll axis would change the declination coordinate of spacecraft $-z$ side of the inertial frame, hence the prediction of declination would be used as reference of roll maneuver. Figure 6.24 displays the attitude information and its interpolation acquired by recorded long term telemetry.



Figure 6.22: Ground Track of Mombasa Imaging Mission

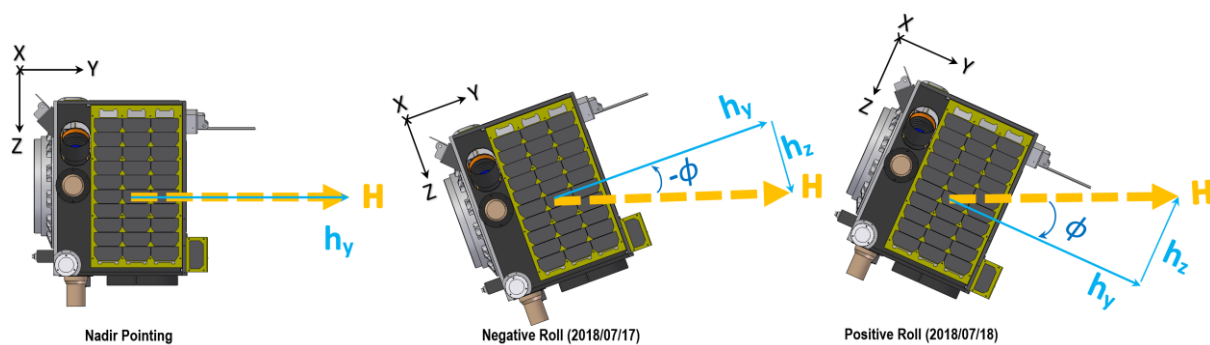


Figure 6.23: Momentum Distribution in the Off-Nadir Pointing

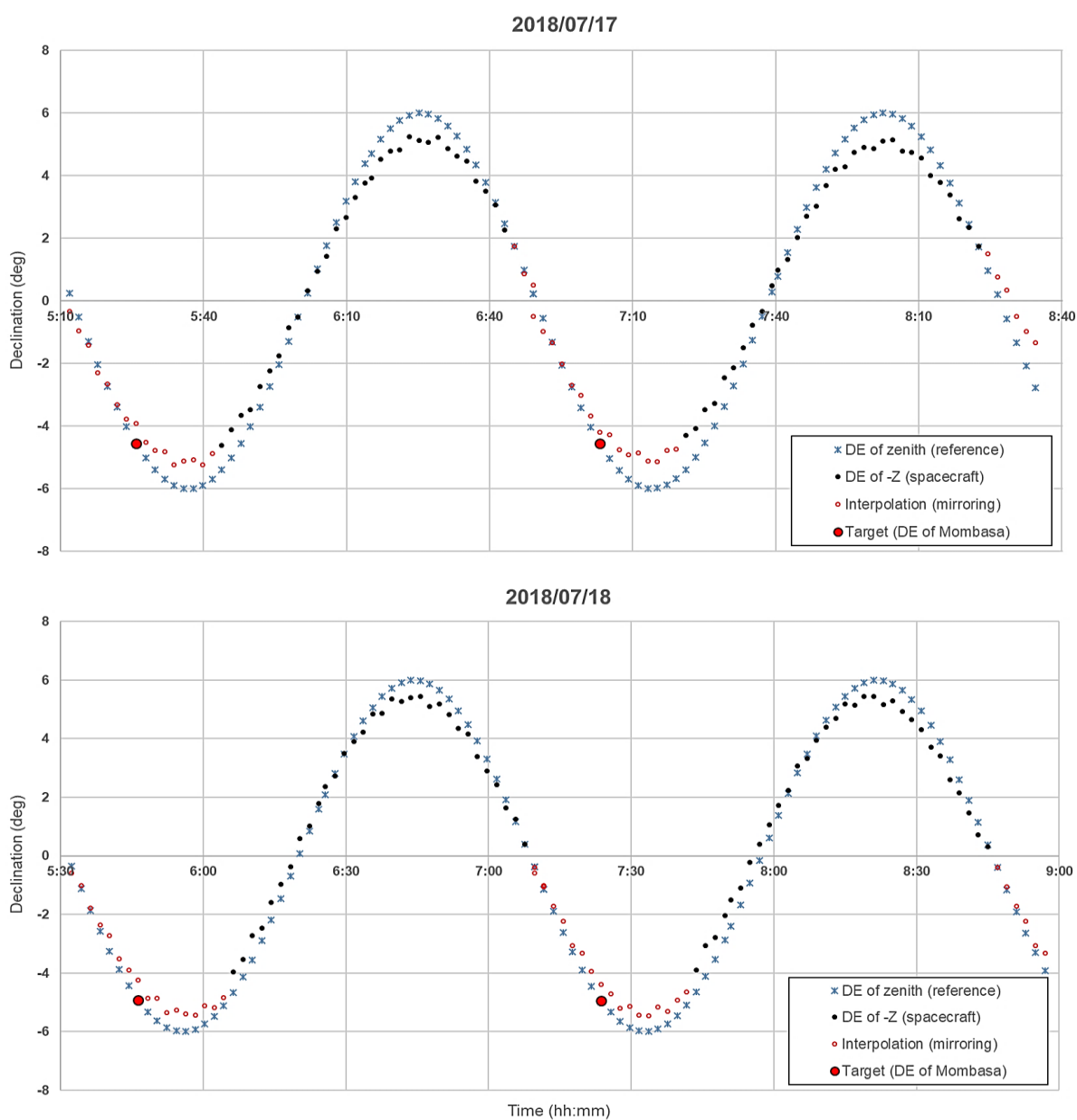


Figure 6.24: Declination (*DE*) Coordinate of LAPAN-A2 Satellite's Recorded Telemetry

In the case no attitude data at the time of imaging that require off-nadir pointing, the procedures might need about four satellite passes starting from attitude acquisition until imaging execution which could be detailed as follows:

- Observing the spacecraft attitude from recorded telemetry of two consecutive orbit period
- Predicting ΔDE , the deviation of $-z$ side spacecraft from local vertical coordinate or zenith, and angular momentum (represented in wheel speed) in the time of imaging execution as a reference for off-nadir maneuver calculation.
- Defining the required roll angle to calculate the speed of z wheel (in rpm) and angular velocity on the y axis of the spacecraft (in deg/s).
- Uploading the parameters for attitude maneuver, i.e. the speed of z wheel and the spacecraft and angular velocity on the y axis, through scheduler commands in a communication contact prior to the imaging, so that the attitude maneuver would be done 5 minutes before capturing the images

Table 6.12 presents the implementation of above steps in the imaging of Mombasa Port.

Table 6.12: Interpolation of Attitude Information for Off-Nadir Maneuver

| Parameters | Equations | 2018/07/17 | 2018/07/18 |
|---|--|-------------|-------------|
| Interpolation of attitude information: | | | |
| ΔDE of 1 st recorded telemetry | ΔDE_1 | -0.7766° | -0.688° |
| ΔDE of 2 nd recorded telemetry | ΔDE_2 | -0.8868° | -0.5368° |
| Predicted ΔDE in the imaging | $\Delta DE_{int} = \Delta DE_1 + 3(\Delta DE_2 - \Delta DE_1)$ | -1.1072° | -0.2344° |
| Speed of y wheel of 1 st telemetry | $\omega_{y-wheel1}$ | 5260 | 5169 |
| Speed of y wheel of 2 nd telemetry | $\omega_{y-wheel2}$ | 5261 | 5138 |
| Predicted RPM in the Imaging | $\omega_{y-wheel_int} = \omega_{y-wheel1} + 3(\omega_{y-wheel2} - \omega_{y-wheel1})$ | 5263 | 5076 |
| Calculation of maneuver: | | | |
| Required roll angle | ϕ | -2.78° | 7.21° |
| Actual roll angle | $\phi_{act} = \phi - \Delta DE_{int} - \text{Offset}_{cam}$ | -1.80° | 7.32° |
| Speed of z wheel | $\omega_{z-wheel} = \omega_{y-wheel_int} * \sin(\phi_{act})$ | 165 rpm | -647 rpm |
| Spacecraft angular velocity on the y axis | $\omega_{y-off_nadir} = \omega_{y-nadir} * \cos(\phi_{act})$ | -0.0626 °/s | -0.0621 °/s |

The images of Mombasa Port and the ships resulted in this off-nadir pointing is presented in the Figure 6.25.

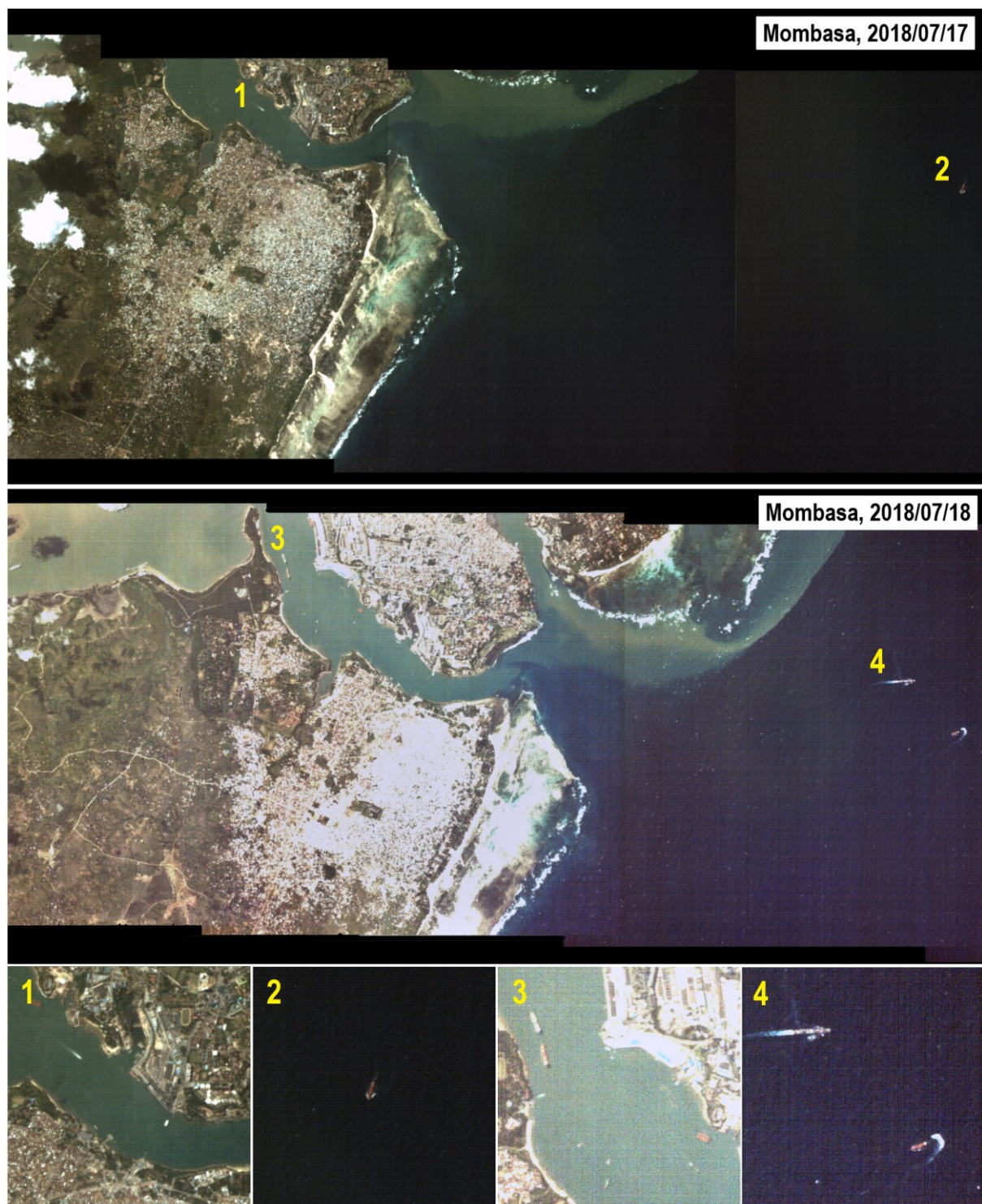


Figure 6.25: Images of Mombasa Port and Ships Resulted by Off-Nadir Pointing

However, the aforementioned steps to carry out the off-nadir pointing should be reviewed when spacecraft require a roll angle of 10 deg or more. For smaller roll maneuver, the operator could just send a small amount of speed to the z wheel. But to get a larger roll angle, z wheel requires a greater speed as well, so the acceleration is also great. Ideally, the acceleration in the z wheel

should be followed by slowing down on the y wheel to make a rotation just on the roll axis. Since those two wheels work independently in which the acceleration and deceleration between those wheels are not synchronized, the maneuver would raise unpredicted movement that is not only in the roll axis. This problem would make wandering of the pointing from the target.

To solve the problem of larger roll maneuver, the procedures should use the x wheel as main actuator by commanding a roll angle on it while the y and z wheels have to counter the rotation using an angle control. Figure 6.26 shows typical of roll maneuver using angle control mode. In this figure, the x wheel was set by -10 deg roll, while the y and z wheels were set in 0 deg to ensure that at the end of the maneuver only change in the roll axis remained. At the end of the roll maneuver, the angular momentum would distribute between y and z axes. It means the z wheel would speed up from zero to a certain rpm, while the y wheel slowed down to a value that depends on the expected roll angle. After steady state achieved, this angle mode maneuver would be inertially pointing, therefore the y wheel should be set for the corresponding off-nadir rate immediately after the x wheel finished the rotation.

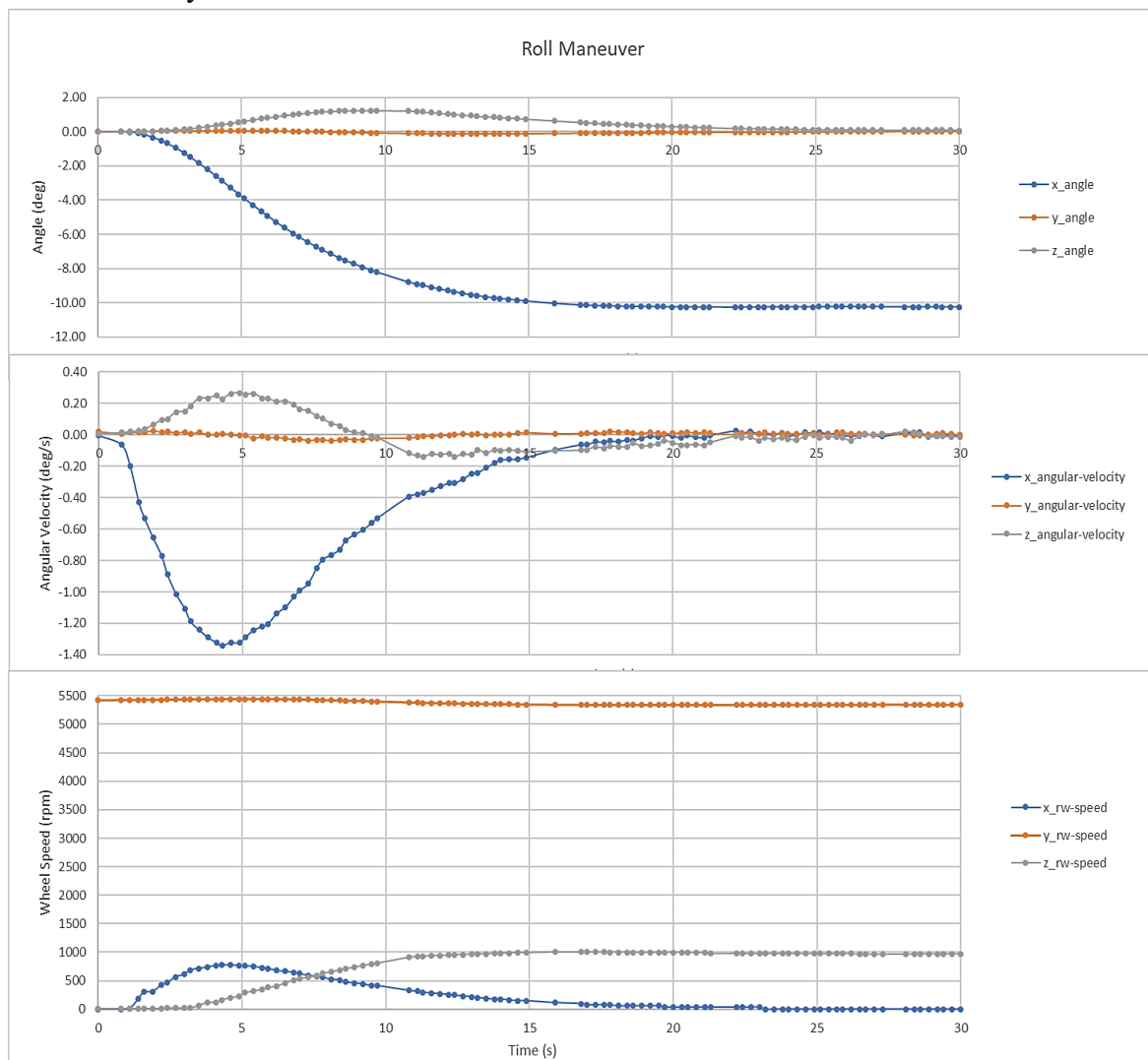


Figure 6.26: Angle Control Maneuver for Off-Nadir Pointing Mode

Oftentimes the Earth imaging with off-nadir pointing was called by disaster mitigation missions due to needs of the latest images for quick response. One sample of the missions was imaging of Mount Rinjani after Lombok earthquake. At that time, many tourists were trapped on the summit of Mount Rinjani due to avalanches when a 6.4-magnitude earthquake struck the Indonesian tourist island of Lombok on July 29th, 2018. Rescuers set off one day later to help nearly 700 trekkers and climbers who became stranded at two points on the mountain, after landslides caused by the earthquake blocked some trails off the peak [64].

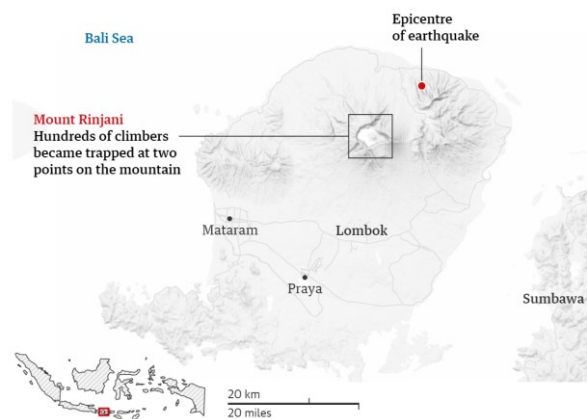


Figure 6.27: Lombok Earthquake on July 29th, 2018 [64]

LAPAN-A2 satellite had the opportunity to capture the summit of Mount Rinjani on August 2nd and 3rd, 2018, to find out if there was a deformation on the peak of the mountain after the earthquake. Figure 6.28 shows the ground track of the satellite the requires off-nadir pointing to make imaging operation. The result of high-resolution images of those two consecutive days, shown by Figure 6.29, has demonstrated a very high accuracy pointing of the LAPAN-A2 satellite.

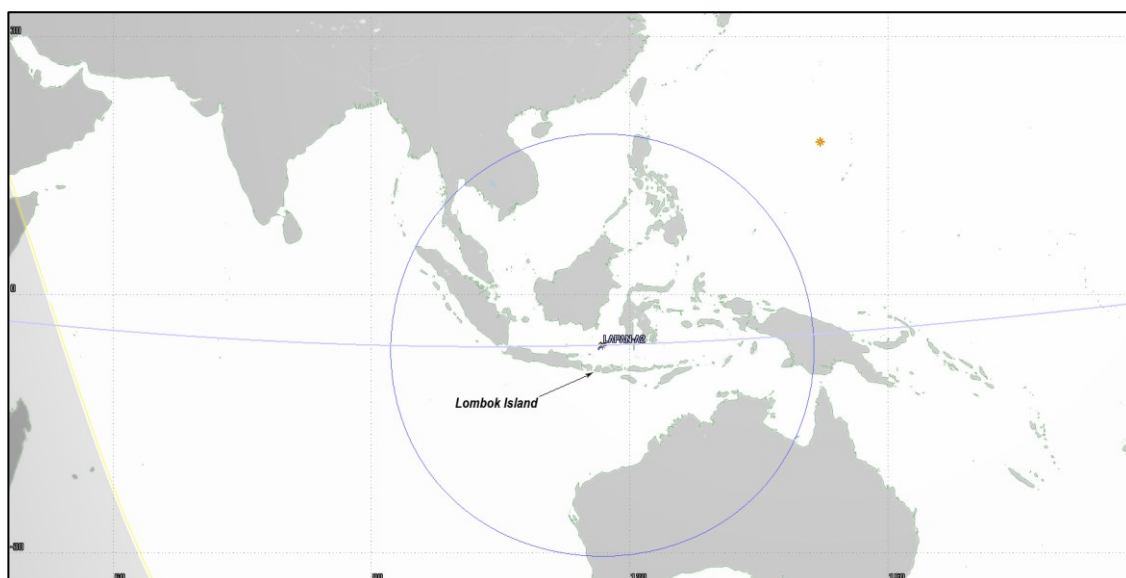


Figure 6.28: Satellite Ground Track in the Imaging of Lombok Island

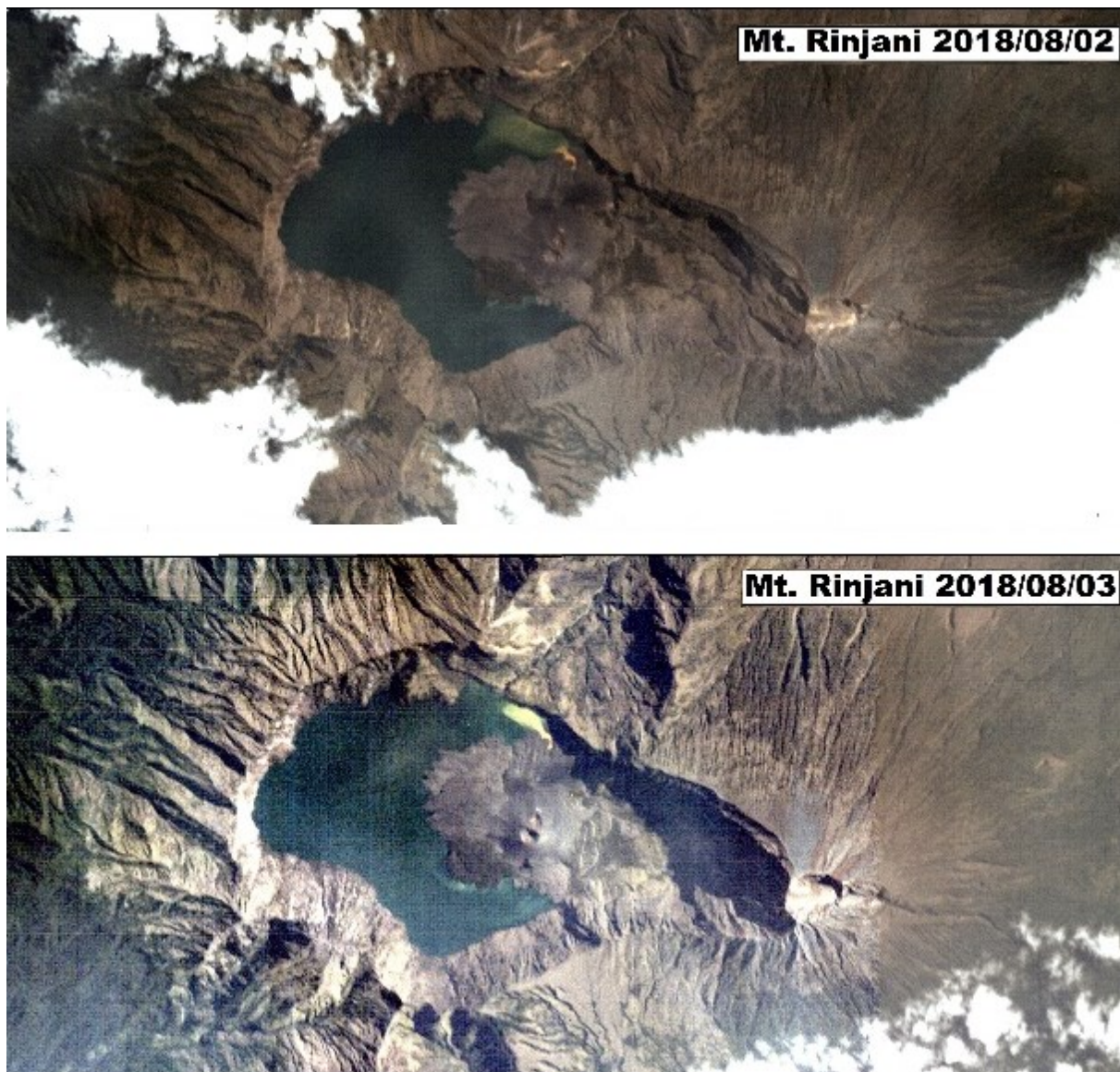


Figure 6.29: Off-Nadir Imaging of Mount Rinjani [50]

6.3 Hibernation Mode

In the hibernation mode, all devices are switched off, including the attitude control system. Instead of tumbling with uncontrolled motion, implementing momentum bias would make the spacecraft spinning in the pitch axis while the attitude control is deactivated, so the spacecraft will make a single spinner movement as applied by earlier satellite technology. The simple spinner motion would give advantages in handling the communication between spacecraft and ground station as well as performing power management. Better spin stability of the spacecraft,

which indicates by a small angle of nutation, will make it easier to wake up from hibernation, thereby faster preparation for continuing the mission.

Figure 6.30 presents the circle of cones motion resulted by LAPAN-A satellite series in the single spinner mode. While the moment of inertia of LAPAN-A satellite series have been presented in the Table 5.2, then the equation (4.48) and (4.49) are used to find the body cone and nutation angles which are presented in the Table 6.13.

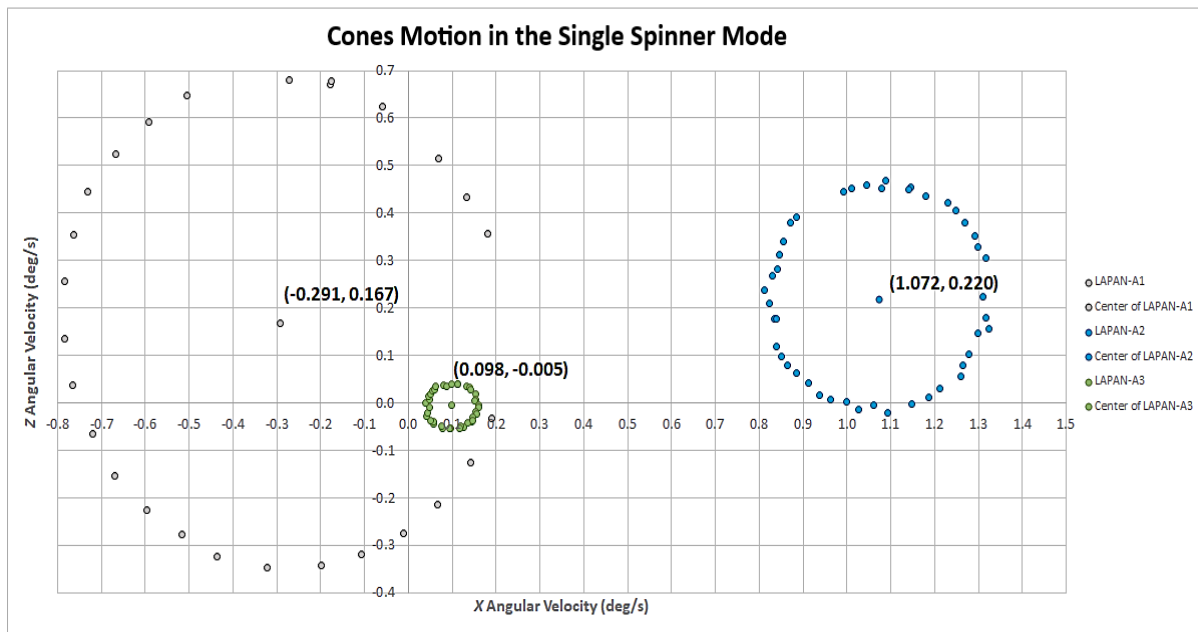


Figure 6.30: Circles of Cones Motion in the Single Spinner Mode

Table 6.13: Measurement of Body Cone and Nutation Angles in the Single Spinner Mode

| Satellite | Time | Angular Velocity | | | Body Cone Angle | Nutation Angle |
|-----------|---------------------|------------------|----------|----------|-----------------|----------------|
| | | Y Average | X Center | Z Center | | |
| LAPAN-A1 | 2007/01/23 16:01:56 | 6.953 | -0.291 | 0.167 | 2.761 | 1.875 |
| LAPAN-A2 | 2019/10/05 15:14:55 | 7.986 | 1.072 | 0.220 | 7.806 | 6.319 |
| LAPAN-A3 | 2019/12/03 10:03:50 | 4.409 | 0.098 | -0.005 | 1.278 | 1.034 |

The body cone and nutation angles in the single spinner mode presented in Figure 6.30 and Table 6.13 are highly correlated with the mass distribution of the spacecraft denoted by inertia matrix. The tensor inertia I can be expressed in the form of a diagonal matrix (I_p) by eliminating the product of inertia.

$$I_p = \begin{bmatrix} I_1 & 0 & 0 \\ 0 & I_2 & 0 \\ 0 & 0 & I_3 \end{bmatrix} \quad (6.12)$$

The diagonal matrix is known as principal moment of inertia and the corresponding axes are the principal axes. Eigenvalues are the principal moment of inertia (I_p) while eigenvectors (v) are the cosine between the reference axes x , y , and z with the principal axes 1 , 2 and 3 so that it satisfy the following equation

$$I v = v I_p \quad (6.13)$$

$$v = \begin{bmatrix} e_{1x} & e_{2x} & e_{3x} \\ e_{1y} & e_{2y} & e_{3y} \\ e_{1z} & e_{2z} & e_{3z} \end{bmatrix} \quad (6.14)$$

where, for example, e_{1x} , e_{1y} , e_{1z} are the direction cosines of the three angles between vector e_1 and the x , y , z axes, respectively. Table 6.14 presents the principal moment inertia and its direction cosines of LAPAN-A satellite series, which have inertia tensor displayed on the Table 5.2. The principal axis on the Table 6.14 put I_3 as main inertia in the major axis. Meanwhile, in this momentum bias operation, y axis is defined as the rotation axis. Therefore, to determine the angle between principal axis and the rotation axis (body cone angle), element of e_{3y} is taken as the cosine between y and the major axis 3. A good mass balancing of the spacecraft that align its pitch wheel and spacecraft rotation axis toward the major axis would diminish the body cone and nutation angles such as demonstrated by LAPAN-A3 satellites which applied layout optimization on the placement of its components [47].

Table 6.14: Principal Moments of Inertia and Its Direction Cosines Matrices

| Satellite | <i>LAPAN-A1</i> | | | <i>LAPAN-A2</i> | | | <i>LAPAN-A3</i> | | |
|--|-----------------|----------|----------|-----------------|----------|---------|-----------------|----------|----------|
| Principal moments of inertia (kg.m²) | 1.34369 | 0 | 0 | 2.81103 | 0 | 0 | 5.09439 | 0 | 0 |
| | 0 | 1.48144 | 0 | 0 | 2.92286 | 0 | 0 | 5.79719 | 0 |
| | 0 | 0 | 2.06387 | 0 | 0 | 3.63611 | 0 | 0 | 6.69542 |
| Direction cosines | -0.83935 | -0.54105 | 0.05250 | -0.13309 | 0.98321 | 0.12485 | 0.07116 | 0.99726 | 0.02031 |
| | -0.03863 | -0.03696 | -0.99857 | -0.01972 | -0.12857 | 0.99150 | 0.00481 | -0.02071 | 0.99977 |
| | -0.54222 | 0.84018 | -0.01012 | 0.99091 | 0.12950 | 0.03650 | 0.99745 | -0.07105 | -0.00627 |
| Angle between y axis and main inertia (deg) | 3.06 | | | 7.47 | | | 1.22 | | |

The other alternative to operate hibernation mode is performing a dual spinner motion. Instead of totally deactivating the attitude control system, a dual spinner spacecraft only runs the pitch wheel in the constant wheel speed. Since the spacecraft only operates one wheel without gyro in the loop, the total power of the spacecraft would still remain low. Unlike the single spinner,

even though the dual spinner hibernation mode does not involve a gyro, it could still handle the spacecraft rotation through open loop control. Thus, the spacecraft platform could spin in the lower angular velocity or even stop the rotation through an angular momentum exchange mechanism with the wheel.

Stopping the rotation when the solar panels face the Sun would be useful for faster recovery from power deficit. Meanwhile, keeping the angular velocity as close as the rate of nadir pointing through wheel speed adjustment would prevent the spacecraft communication signal from fading. But due to external disturbance torque, open loop control would not be able to prevent the spacecraft from oscillating motion. Figure 6.31 uses the same observation result as discussed in the section 6.1.1 to display the oscillating motion toward nadir reference in the constant wheel speed setting of the pitch wheel. Nevertheless, since there is no obligation to perform nadir pointing in this hibernation mode, adjusting the wheel speed a little bit higher than for nadir pointing would make the spacecraft spins in low angular velocity to minimize the effect of disturbance torque because of averaging the dipole moment by the rotation. Keeping the angular velocity lower than 0.5 deg/s would enable the spacecraft in gathering the attitude information from the star sensor as well.

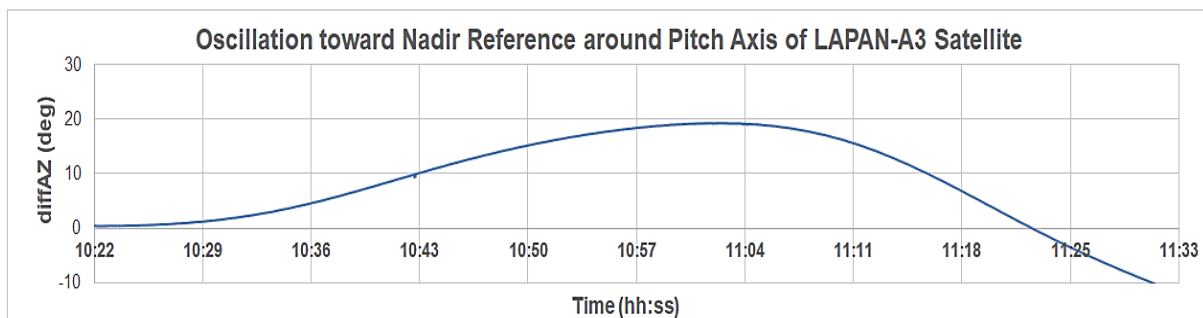


Figure 6.31: Oscillation around Pitch Axis in the Constant Wheel Speed Mode

6.4 Discussion

Although the disturbance torque has been well compensated by the magnetic coil through adjustment of the bias current, it raises the question why the compensation current among the spacecrafts differ significantly. There is important to know where the disturbance torque originated. Especially in LAPAN-A3 satellite, which has residual magnetic dipole in y axis about ten times of the other transverse axes. Meanwhile, the residual dipole of LAPAN-A2 satellite among its axes is not much different within the range 2 – 4 mA of coil current compensation. Thus, the sources of higher residual magnetic dipole on the LAPAN-A3 satellite should be found to anticipate further missions.

Where the magnetic shielding has been applied to all devices that contain permanent magnet, and the power wiring has been managed to diminish the area of the current loop, then the suspect devices that produce magnetic dipole is Li-Ion battery. Along with the increasing utilization of Li-ion batteries in the electronics industry, studies related to the application of Li-ion batteries in space have become a concern in this decade. Four orbiting satellites carrying X-band Synthetic Aperture Radar (SAR) in the constellation COSMO-SkyMed have paid much attention to the design of Li-Ion battery assembly to support space-based radar systems with high peak currents and the related challenges to overcome [59]. Even though the residual magnetic dipole on the spacecraft does not need to be zeroed, the design ingenuity needed to reduce the magnetic moment to a manageable level.

As mentioned in the Table 5.8 of the previous chapter, the compensation current of LAPAN-A3 satellite on the coil x, y, and z are -3 mA, -22 mA, and 2 mA respectively. To investigate the origin of residual magnetic dipoles on the LAPAN-A3 satellite, in particular on y axis, a measurement has been conducted in the laboratory to measure the magnetic field produced by a Li-ion battery pack. However, this procedure has been merely an approach method for estimating the strength of magnetic dipoles on LAPAN-A3 satellite batteries. The procedure used 4 Li-ion battery packs, where each package contains 4 cells. Meanwhile, the LAPAN-A3 satellite carries a large package consisting of 24 Li-ion cells.

As presented in the Figure 6.32, the procedure of batteries magnetic test starts by measuring the surrounding magnetic field that was set as a reference value. Then one by one the battery pack is placed around the magnetometer to measure the increasing magnetic field. Based on this procedure, it appears that the magnetic field on the z axis increases consistently. This procedure was carried out under environmental magnetic field conditions of 3754 nT, 42286 nT, and -20264 nT on x, y, and z axes respectively, where y axis pointed to north, z axis pointed to nadir, and x axis followed the right-hand rule.

The magnetic field magnitude of each Li-ion cell on the z axis varied from 42 nT to 146 nT, which means each cell has a maximum value about three quarters of the permanent magnet on the wheel's motor (200 nT). For LAPAN-A3 satellite, which carries 24 cells, the magnitude of the magnetic field might have ranged from 1015 nT to 3492 nT. Where the z axis of the magnetometer aligned to the -y axis of the spacecraft, this significant magnetic field produced by Li-ion batteries adds residual magnetic dipoles on the pitch axis of the spacecraft.

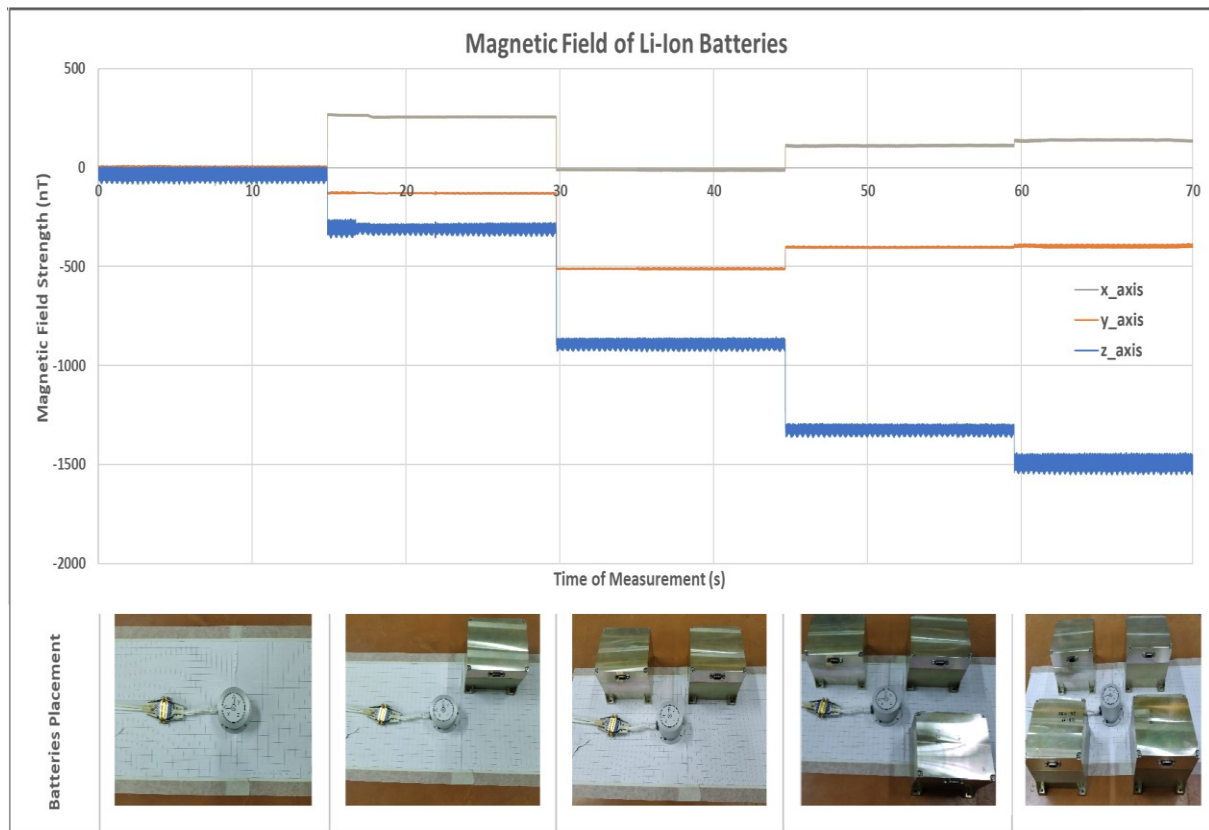


Figure 6.32: Measurement of Magnetic Field on the Li-Ion Batteries

Table 6.15: Magnetic Field Magnitude of Li-ion Batteries

| | X Axis (nT) | Y Axis (nT) | Z Axis (nT) |
|--------------------------|-------------|-------------|-------------|
| 1st battery pack | 257 | 129 | 308 |
| 2nd battery pack | 269 | 382 | 582 |
| 3rd battery pack | 122 | 108 | 434 |
| 4th battery pack | 27 | 6 | 169 |
| Range per pack (4 cells) | 27 - 269 | 6 - 382 | 169 - 582 |
| Range per cell | 7 - 67 | 2 - 95 | 42 - 146 |

7 SUMMARY AND OUTLOOK

7.1 Summary

LAPAN-A satellite series have developed and implemented a momentum bias attitude control system for small satellite missions that characterized as inexpensive, light-weight, small volume and low power consumption. Doing so, the integrated reaction wheel - gyro and the magnetic coils have been adopted as the main actuators that are supported by a star sensor for high accuracy of attitude determination. Together with the compliance of the small satellite requirements and constraints, LAPAN-A satellite series have efficiently performed the standard mode of attitude control with high precision, i.e. nadir pointing mode, slew mode, and hibernation mode.

Aiming an efficient attitude control, in the nominal of nadir pointing mode, LAPAN-A satellite series have successfully demonstrated the momentum bias attitude control method using a single pitch loop of integrated wheel-gyro system without reducing the attitude control accuracy and stability. Even though the control loops of the system are decoupled from the OBDH and require for human interference, the better knowledge and awareness about the compensation of disturbance torques lead the activities of attitude correction could be done at the convenient interval ranging from once to twice per day.

This momentum bias method has demonstrated its robustness and stability so it can bridge longer phases where no attitude information is available. Even though a gyro can also provide the attitude for a while, but the momentum bias system actually has a much lower drift. This advantage of momentum bias has freed LAPAN-A2 satellite from vulnerable to failure. Instead of implementing a momentum bias method from the beginning, LAPAN-A2 planned to operate a fully automatic attitude control system with commands for nadir pointing, target pointing, and lunar pointing. However, due to unexpected blinding of the star sensor, this automatic system which is centralized in the OBDH failed. This system failure cannot be fixed in orbit so the spacecraft often automatically deactivates its attitude control system if the star sensor fails to get an attitude reference. Deactivation of the attitude control system would lead the spacecraft tumbling in the hibernation mode.

Propitiously LAPAN-A2 satellite uses the integrated wheel-gyro system inherited from previous TUBSAT satellite series that could perform decentralized attitude control system. The decentralized system could bypass the OBDH and establish momentum bias attitude control which could tolerate temporary outages of the star sensor. In case of LAPAN-A3 satellite, which has identical system and OBDH as LAPAN-A2, the momentum bias attitude control was started right from the beginning to avoid the similar problem that happens on LAPAN-A2 satellite.

The gyroscopic stability resulted by high angular momentum gives possibility to momentum bias to perform high precision attitude control. Due to this stability, even in the absence of the attitude information, this method still could perform high accuracy pointing by interpolation of the previous data. In supporting a high precision attitude control, compensation of the disturbance torques and calibration of the pointing as well as selection of the nutation damping method are critical to the success of the mission. LAPAN-A satellite series have demonstrated an efficient and high precision attitude control through momentum bias methods that could damp the nutation angle better than 0.1 deg.

7.2 Outlook

The attitude control strategy in this study mostly conducted by human interference through software assistance on the ground station facilities. This scheme facilitates experiments and tests that mainly to get a better knowledge on the disturbance torque situation of small satellite's operation in the low Earth orbit. Nevertheless, human in the control loop is not mandatory. Once the disturbance torques have been identified and their compensation procedures have been established, then the attitude control could be performed through exact algorithm. Hereafter the human interference could be replaced by a computer program that could be installed either on the ground segment facilities or on board of the spacecraft

The development and improvement of technology in the key equipment such as well balancing wheels to avoid micro vibrations, less systematic error gyros, high-resolution star sensors or stellar-gyros, as well as effective and efficient nutation damping techniques, will directly support the formation of high precision and advanced attitude control through momentum bias. These improvements on the momentum bias attitude control would accordingly drive the advancement missions of the small satellite. Potential payloads such as a high-resolution pushbroom imager, compact or small synthetic aperture radar, and a LEO constellation of communication could be carried on the small satellite missions by implementing an efficient and high precision momentum bias attitude control.

In Indonesia, the development of a constellation of satellites in low orbit using small satellites has been initiated. The constellation of small satellites is designed for supporting a narrow band communication for the Internet of Things, the disaster early warning system as well as maritime and air traffic monitoring over Indonesian territory. The constellation consists of 9 satellites operate in the equatorial low Earth orbit within an altitude of ± 600 km and inclination of 0 deg. Consequently, the satellites will have an orbital period around 97 minutes and pass over Indonesia 14.9 times within 25 minutes duration per pass. Figure 7.1 and Figure 7.2 presents a concept of the small satellite constellation that offer real time communication for Indonesia and other equatorial region under satellites coverage. In this mission, the momentum bias attitude control would still an attractive choice because of its reliability and robustness as well as its efficiency. The high precision momentum bias attitude control would support the satellite constellation to establish a reliable communication, not only to the Earth station but also for inter satellite link communication. The efficiency of momentum bias that consume a less power become an advantage in particular for equatorial low Earth orbit that generally has less Sun illumination.

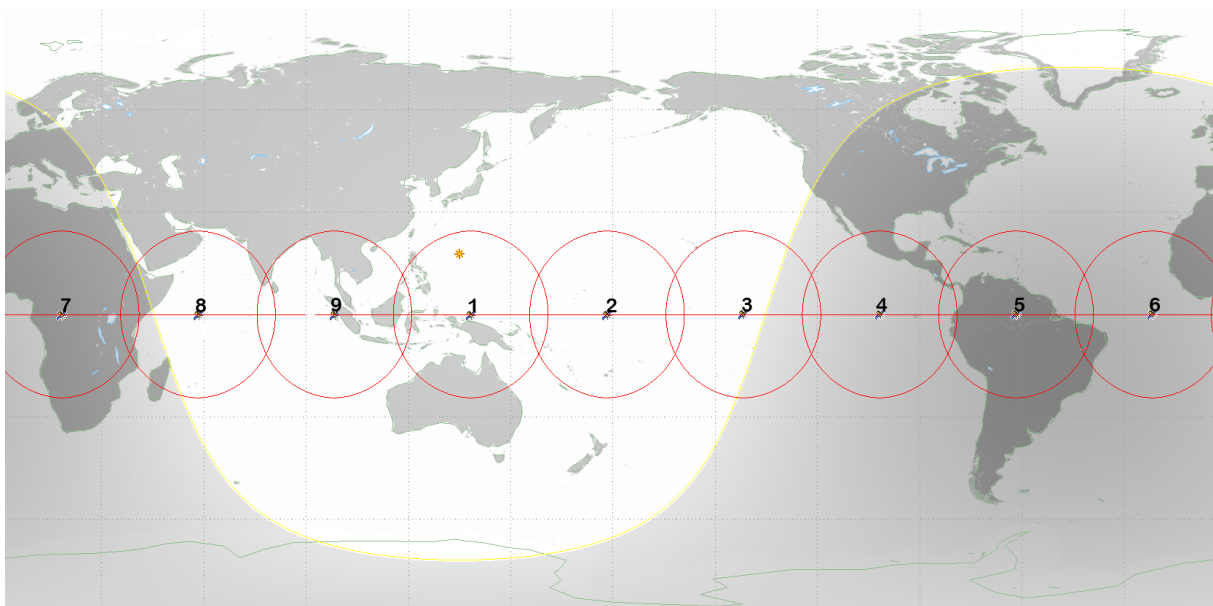


Figure 7.1: Constellation of 9 Small Satellites in Equatorial Low Earth Orbit

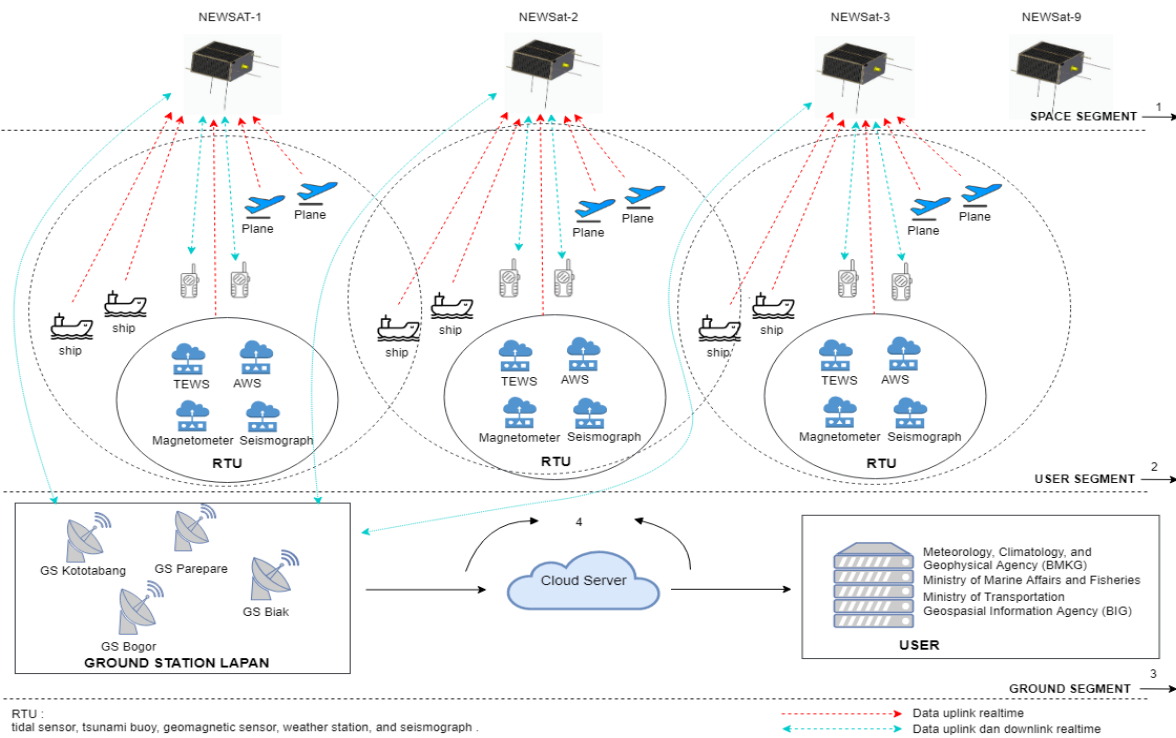


Figure 7.2: Concept of LEO Communication Satellites in Constellation

REFERENCES

- [1] UNOOSA, “Small Satellite Missions,” in *Third United Nations Conference on the Exploration and Peaceful Uses of Outer Space (UNISPACE III)*, 1998, vol. A/CONF.184, no. 26 May.
- [2] R. Sandau, K. Brieß, and M. D’Errico, “Small satellites for global coverage: Potential and limits,” *ISPRS Journal of Photogrammetry and Remote Sensing*, vol. 65, no. 6, pp. 492–504, 2010.
- [3] Ames Research Center - NASA, “Small Spacecraft Technology State of the Art,” California, 2015.
- [4] K. Murthy, M. Shearn, B. D. Smiley, A. H. Chau, J. Levine, and D. Robinson, “SkySat-1: very high-resolution imagery from a small satellite,” in *Sensors, Systems, and Next-Generation Satellites XVIII*, 2014.
- [5] S. Martin, “Modern Small Satellites - Changing the Economics of Space,” *Proceedings of the IEEE*, vol. 106, no. 3, pp. 343–361, 2018.
- [6] H. Saito *et al.*, “Compact X-band synthetic aperture radar for 100 kg class satellite,” *IEICE Transactions on Communications*, vol. E100B, no. 9, pp. 1653–1660, 2017.
- [7] Y. Hatsutori *et al.*, “Performance evaluation of Nano-JASMINE,” *EAS Publications Series*, vol. 45, no. 2010, pp. 397–400, 2011.
- [8] P. R. Hakim, W. Hasbi, and A. H. Syafrudin, “ADCS requirements of Lapan-A3 satellite based on image geometry analysis,” *Proceeding - ICARES 2014: 2014 IEEE International Conference on Aerospace Electronics and Remote Sensing Technology*, pp. 142–146, 2014.
- [9] T. Inamori, N. Sako, and S. Nakasuka, “Attitude determination and control system for the Nano-JASMINE mission,” *IFAC Proceedings Volumes*, vol. 43, no. 15, pp. 253–258, 2010.
- [10] A. Siahpush and J. Gleave, “A brief survey of attitude control systems for small satellites using momentum concepts,” in *Proceedings of the 2nd AIAA/USU Conference on Small Satellites*, 1988, pp. 18–21.
- [11] K. J. Heffernan, G. H. Fountain, B. E. Tossman, and F. F. Mobley, “the Magsat Attitude Control System,” *Johns Hopkins APL Technical Digest*, vol. 1, no. 3, pp. 188–193, 1980.
- [12] G. H. Fountain, F. W. Schenkel, T. B. Coughlin, and C. A. Wingate, “the Magsat Attitude Determination System,” *Johns Hopkins APL Technical Digest*, vol. 1, no. 3, pp. 194–

- 200, 1980.
- [13] H. J. Dougherty, K. L. Lebson, and J. J. Rodden, "Attitude Stabilization of Synchronous Communications Satellites Employing Narrow-Beam Antennas," *Journal of Spacecraft and Rockets*, vol. 8, no. 8, pp. 834–841, Aug. 1971.
 - [14] H. Mork, "Synthesis and design of a gimbaled reaction wheel attitude stabilization package (GRASP)," in *Guidance, Control and Flight Mechanics Conference*, 1971, pp. 1–12.
 - [15] S. R. Starin, "Attitude Determination and Control Systems," in *Space Mission Engineering: The New SMAD*, 1st ed., vol. 15, no. 2, J. R. Wertz, D. F. Everett, and J. J. Puschell, Eds. Microcosm Press, 2011, pp. 2017–2019.
 - [16] F. A. Leve, B. J. Hamilton, and M. A. Peck, *Spacecraft momentum control systems*. 2015.
 - [17] C. A. Markland, "Attitude and orbit control for satellite broadcasting missions," in *Proceedings of the Indian Academy of Sciences Section C: Engineering Sciences*, 1980, vol. 3, no. 1, pp. 47–65.
 - [18] M. H. Kaplan, "Modern spacecraft dynamics and control," *New York, John Wiley and Sons, Inc.*, 1976. 427 p., 1976.
 - [19] NASA Content Administrator, "The First Geosynchronous Satellite," 2008. [Online]. Available: https://www.nasa.gov/multimedia/imagegallery/image_feature_388.html. [Accessed: 03-Feb-2020].
 - [20] C. A. Markland, "A Review of The Attitude Control of Communication Satellites," in *Space Mankind's Fourth Environment*, L. G. Napolitano, Ed. Oxford · New York · Toronto · Sydney · Paris · Frankfurt: Elsevier, 1982, pp. 469–492.
 - [21] L. R. Bahor and R. M. Brooksbank, "Test of the Intelsat III Communication Spacecraft and Apogee Motor Under the Combined Effects of Simulated Altitude and Rotational Spin," Arnold Air Force Station, Tennessee, 1967.
 - [22] B. Weymiens, R. Oremus, and MSG Project ESA/ESTEC, *Meteosat second generation: The satellite development*, ESA BR-153. Noordwijk, The Netherlands: ESA Publications Division, ESTEC, 1999.
 - [23] H. R. Freeman, "Three-Axis Attitude Control for a Geostationary Satellite," *IFAC Proceedings Volumes*, vol. 9, no. 1, pp. 69–83, May 1976.
 - [24] W. Redisch, "ATS-6 Description and Performance," *IEEE Transactions on Aerospace and Electronic Systems*, vol. AES-11, no. 6, pp. 994–1003, Nov. 1975.
 - [25] J. E. Keigler, "RCA Satcom: An example of weight optimized satellite design for maximum communications capacity," *Acta Astronautica*, vol. 5, no. 3–4, pp. 219–242, 1978.
 - [26] R. J. Rusch and D. G. Dwyre, "Intelsat V spacecraft design," *Acta Astronautica*, vol. 5, no. 3–4, pp. 173–188, Mar. 1978.
 - [27] A. J. Manna, "25 years of TIROS satellites.," *Bulletin - American Meteorological Society*, vol. 66, no. 4, pp. 421–423, 1985.
 - [28] L. Muhlfelder, "Attitude control system performance of RCA Satcom," in *Guidance and Control Conference 16 August 1976 - 18 August 1976*, 1976, pp. 111–121.

-
- [29] W. P. Manger, "Attitude Control for the Tiros Weather Satellites," *IFAC Proceedings Volumes*, vol. 2, no. 1, pp. 219–233, Jun. 1965.
 - [30] H. Perkel, "Stabilite -- A Three-Axis Attitude Control System Utilizing a Single Reaction Wheel," in *Communication Satellite Systems Technology*, New York: American Institute of Aeronautics and Astronautics, 1966, pp. 375–400.
 - [31] J. J. Rodden, "Attitude Control Using Momentum Wheels," *IFAC Proceedings Volumes*, vol. 14, no. 2, pp. 2197–2202, Aug. 1981.
 - [32] R. Weiss, J. J. Rodden, and R. J. Hendricks, "SEASAT-A attitude control system," *AIAA Journal of Guidance and Control*, vol. 1, no. 1, pp. 146–154, 1978.
 - [33] M. N. Sweeting and S. Pookyaudom, "TMSAT: Thailand's first microsatellite for communications and Earth observation," *Acta Astronautica*, vol. 40, no. 2–8, pp. 423–427, 1997.
 - [34] W. Steyn and Y. Hashida, "An Attitude Control System for a Low-Cost Earth Observation Satellite with Orbit Maintenance Capability," *13th AIAA/USU Conference on Small Satellites*, pp. 1–13, 1999.
 - [35] A. M. Si Mohammed, M. Benyettou, Y. Bentoutou, A. Boudjemai, Y. Hashida, and M. N. Sweeting, "Three-axis active control system for gravity gradient stabilised microsatellite," *Acta Astronautica*, vol. 64, no. 7–8, pp. 796–809, Apr. 2009.
 - [36] M. N. Sweeting, *Space at surrey: Microsatellites & minisatellites for affordable access to space*, vol. 10, no. C. Elsevier Masson SAS, 1999.
 - [37] W. H. Steyn and Y. Hashida, "In-orbit Attitude and Orbit Control Commissioning of UoSAT-12," in *Spacecraft Guidance, Navigation and Control Systems, Proceedings of the 4th ESA International Conference 1999. ESTEC*, 1999, pp. 95–101.
 - [38] U. Renner, B. Lubke-Ossenbeck, and P. Butz, "TUBSAT, Low cost access to space technology," in *CNES, Small Satellites Systems and Services*, 1993, pp. 601–610.
 - [39] M. Steckling, U. Renner, and H.-P. Röser, "DLR-TUBSAT, qualification of high precision attitude control in orbit," *Acta Astronautica*, vol. 39, no. 9–12, pp. 951–960, Nov. 1996.
 - [40] S. Schulz and U. Renner, "DLR-TUBSAT: a microsatellite for interactive Earth observation," in *Small Satellites Systems and Services, 5th International Symposium*, 2000.
 - [41] S. Roemer, "Flight Experience with the Micro Satellite Maroc-Tubsat," in *54th International Astronautical Congress of the International Astronautical Federation, the International Academy of Astronautics, and the International Institute of Space Law*, 2003, no. October, pp. 3–5.
 - [42] M. Buhl and U. Renner, "Star Sensor Development Based on the TUBSAT Experience," in *Small Satellite Missions for Earth Observation*, Berlin, Heidelberg: Springer Berlin Heidelberg, 2010, pp. 379–390.
 - [43] B. Kim, H. Lee, and S. Choi, "Three-axis reaction wheel attitude control system for KITSAT-3 Microsatellite," *Pergamon, Space Technology*, vol. 16, no. No 5/6, pp. 291–296, 1996.

-
- [44] T. Inamori, "Attitude control system for arc-second stabilization of 30-kg Micro Astronomy Satellite," in *1st Interplanetary CubeSat Workshop Massachusetts, USA, 29-30 May 2012*, 2012.
 - [45] M. Mukhayadi, R. Madina, and U. Renner, "Attitude control of bias momentum micro satellite using magnetic and gravity gradient torque," in *2014 IEEE International Conference on Aerospace Electronics and Remote Sensing Technology*, 2014, pp. 132–136.
 - [46] M. A. Saifudin and M. Mukhayadi, "LAPAN-A2 Attitude Control Strategy for Equatorial Surveillance Mission," in *Proc. of the 9th IAA Symposium on Small Satellites for Earth Observation*, 2013.
 - [47] M. Mukhayadi, I. Hermadi, and S. Hardhienata, "Layout optimization of microsatellite components using genetic algorithm," *Telkomnika (Telecommunication Computing Electronics and Control)*, 2017.
 - [48] E. Zapata and C. McCleskey, "An analysis and review of measures and relationships in space transportation affordability," in *50th AIAA/ASME/SAE/ASEE Joint Propulsion Conference 2014*, 2014, pp. 1–14.
 - [49] D. Headrick, "Momentum and Reaction Wheels," in *Spacecraft Attitude Determination and Control*, 11th ed., J. Wertz, Ed. Dordrecht: Kluwer Academic Publishers, 1978, pp. 600–604.
 - [50] R. Madina, A. P. S. Jayani, A. Sarah, and M. Mukhayadi, "Moon Image Acquisition for Pointing Calibration of LAPAN-A2 Satellite's High Resolution Camera," *Proceedings of the 2019 IEEE International Conference on Aerospace Electronics and Remote Sensing Technology, ICARES 2019*, pp. 1–6, 2019.
 - [51] J. R. Wertz, "Space Mission Geometry," in *Space Mission Analysis and Design*, 7th ed., W. J. Larson and J. R. Wertz, Eds. El Segundo, California: Microcosm Press & Kluwer Academic Publisher, 1999, pp. 95–130.
 - [52] J. R. Wertz, "Attitude Geometry," in *Spacecraft Attitude Determination and Control*, 11th ed., J. R. Wertz, Ed. Dordrecht: Kluwer Academic Publishers, 1978, pp. 22–35.
 - [53] T. S. Kelso, "Orbital Coordinate Systems, Part I," 2019. [Online]. Available: <https://celestrak.com/columns/v02n01/>. [Accessed: 06-Jan-2020].
 - [54] G. H. Bryan, *Stability in aviation; an introduction to dynamical stability as applied to the motions of aeroplanes*. London, Macmillan and Co., limited, 1911.
 - [55] D. G. Boden, "Introduction to Astrodynamics," in *Space Mission Analysis and Design*, 7th ed., W. J. Larson and J. R. Wertz, Eds. El Segundo, California: Microcosm Press & Kluwer Academic Publisher, 1999, pp. 131–158.
 - [56] J. Wertz, "Summary of Orbit Properties and Terminology," in *Spacecraft Attitude Determination and Control*, 11th ed., J. R. Wertz, Ed. Dordrecht: Kluwer Academic Publishers, 1978, pp. 36–81.
 - [57] R. H. Triharjanto, W. Hasbi, A. Widipaminto, M. Mukhayadi, and U. Renner, "LAPAN-TUBSAT: Micro-satellite platform for surveillance & remote sensing," in *European Space Agency, (Special Publication) ESA SP*, 2004, no. 571, pp. 277–283.

-
- [58] V. H. Selby, "Modular Attitude Determination and Control System for Small Satellites," in *4th Annual AIAA/USU Conference on Small Satellites*, 1990, pp. 1–13.
 - [59] A. Csizmar, L. Richards, E. Scorzafova, and G. Perrone, "Cosmo-skymed first lithium ion battery for space based radar," in *Proceedings of the 7th European Space Power Conference, Stresa, Italy (ESA SP-589, May 2005)*, 2005.
 - [60] S. Schulz, "Interaktive Lageregelung zur Erdbeobachtung mit Mikrosatelliten am Beispiel DLR-TUBSAT," Technischen Universität Berlin, 2001.
 - [61] S. Utama, M. A. Saifudin, and M. Mukhayadi, "Momentum Biased Performance of LAPAN-A3 Satellite for Multispectral Pushbroom Imager Operation," *IOP Conference Series: Earth and Environmental Science*, vol. 149, no. 1, 2018.
 - [62] S. Utama, P. R. Hakim, and M. Mukhayadi, "Quarter orbit maneuver using magnetorquer to maintain spacecraft angular momentum," *IOP Conference Series: Earth and Environmental Science*, vol. 284, no. 1, 2019.
 - [63] W. Hasbi, Kamirul, M. Mukhayadi, and U. Renner, "The impact of space-based AIS antenna orientation on in-orbit AIS detection performance," *Applied Sciences (Switzerland)*, 2019.
 - [64] K. Lamb, "Lombok Earthquake: 500 Trapped Climbers Make Way Down Indonesian Peak," *The Guardian*, 30-Jul-2018.

APPENDIX



Appendix 1: Picture of LAPAN-A1 (LAPAN-TUBSAT) satellite, the first research satellite of Indonesia based on the existing TUBSAT program heritage. LAPAN-A1 is a video surveillance microsatellite within 5 meters of ground resolution from 630 km altitude. It was launched on a PSLV launcher on January 10th, 2007 from the Indian space center in Sriharikota.



Appendix 2: Picture of LAPAN-A2 (LAPAN-ORARI/IO-86) satellite, a successor mission of the LAPAN-A1 microsatellite that is also the first indigenous satellite design and development in Indonesia. The mission objectives of LAPAN-A2 are to use the microsatellite for disaster mitigation and Earth observation as well as maritime surveillance. It brings several mission payloads that are Digital Space Camera that provides a swath width of 9 km within a resolution of 4 m, an amateur radio APRS (Automatic Packet Reporting System) and voice repeater functions for disaster mitigation communications, and an AIS (Automatic Identification System) payload for the provision of maritime monitoring in the equatorial region. It was launched on September 28th, 2015 by PSLV-C30.



Appendix 3: Picture of LAPAN-A3 (LAPAN-IPB) satellite, the third satellite of LAPAN. It was developed based on the LAPAN-A2 satellite bus with several enhancements to accommodate the linear imager payload. The objective of the demonstration mission is to monitor food resources in Indonesia and to provide environmental monitoring. To perform such a mission, LAPAN-A3/IPB carries a medium resolution multispectral (4-band) imager and a digital camera. LAPAN-A3 satellite was launched on June 22nd, 2016 by PSLV-C34.